STERICALLY HINDERED CHIRAL ORGANOMETALLIC COMPLEXES: AN X-RAY CRYSTALLOGRAPHIC, NMR SPECTROSCOPIC AND EHMO STUDY

by

KRISZTINA LAURA MALISZA, B.Sc.

A thesis

Submitted to the Faculty of Graduate Studies

In Partial Fulfilment of the Requirements

for the Degree

Doctor of Philosophy

McMaster University

August, 1992

STERICALLY HINDERED CHIRAL ORGANOMETALLIC COMPLEXES

DOCTOR OF PHILOSOPHY (1992) McMASTER UNIVERSITY

(Chemistry) Hamilton, Ontario

TITLE: Sterically Hindered Chiral Organometallic Complexes:
An X-ray Crystallographic, NMR Spectroscopic and EHMO Study

AUTHOR: Krisztina Laura Malisza, B.Sc. (McMaster University)

SUPERVISOR: Professor M.J. McGlinchey

NUMBER OF PAGES: xvii, 242

ABSTRACT

Sterically crowded organometallic complexes present fascinating problems of structure and molecular dynamics. Tetrahedral clusters such as (RC≡CR')-$(C_5H_5)_2M_2(CO)_4$, where M = Mo or W, crystallize in conformations possessing three terminal carbonyls while the fourth is semi-bridging. However, these ligands undergo a rapid exchange process which can be followed by variable-temperature NMR spectroscopy. When the R substituent is derived from a chiral natural product, the low temperature NMR spectra reveal the presence of diastereomers which are interconvertible via rotations of the organometallic vertices.

The fluxional behaviour of tetrahedral clusters containing such vertices as $Co(CO)_3$, $Fe(CO)_3$ or $(C_5H_5)Mo(CO)_2$ can be rationalized by means of molecular orbital calculations at the extended Hückel level of approximation. These studies show that the barriers to vertex rotation can usually be traced to one principal orbital interaction in each case. However, in $(C_5H_5)_2Mo_2(CO)_4$(R-C≡C-R) clusters, the barriers are primarily steric in character.

The ability of transition metal clusters to delocalize electronic charge is well known and, in principle, could be used to stabilize intermediates of biochemical significance. Treatment of 2-methylcyclopentanone with an alkyne anion was carried out in order to generate 1-alkynyl-2-methylcyclopentanols in which the

methyl and alkynyl groups are trans diaxial; the aim was to mimic the "D"-ring of the steroidal contraceptive mestranol. In fact, the major epimer was the one in which the methyl and alkynyl substituents were disposed in a cis manner. The conformation of 2-methyl-1-phenylethynylcyclopentanol **47** was elucidated by two-dimensional NMR techniques. Moreover, the structure of **47** and also of its $Co_2(CO)_6$ derivative have been determined crystallographically. Protonation of the dicobalt or dimolybdenum complexes of **47** lead to stable cations; treatment of these cations with nucleophiles results in elimination of water to yield 2-methylcyclopentene derivatives of which the dimolybdenum cluster has been characterized by x-ray crystallography.

The sterically crowded complexes $(C_6H_5)_3SiOH[Cr(CO)_3]_n$, where n = 1,2,3, have also been characterized X-ray crystallographically and all three have propellor-type geometries. The question of whether the phenyl ring rotations are correlated has been studied by variable-temperature NMR spectroscopy. These systems do not yield stable silicenium cations, but the analogous $Cr(CO)_3$ complex of triphenylcarbinol not only shows fluxional behaviour but also yields a metal-stablized cation. The pathway for phenyl rotations in such systems can be followed via a Dunitz-type trajectory approach in which a number of x-ray structures were analyzed.

ACKNOWLEDGEMENTS

I would like to express my sincere thanks to my supervisor, Dr. McGlinchey, who has been an inspiration to me as a chemist. I am grateful for his guidance, patience and friendship. He would always make time for me, even when I didn't want it. I would also like to express my appreciation to the members of my supervisory committee, Dr. Lock and Dr. Stover, for all their help throughout this project.

For all their help in my research, I thank Brian Sayer and Don Hughes in the NMR facility, Richard Smith in the MS facility and Jim Britten for his help with the crystal structures.

I would also like to thank my lab mates throughout the years, Karen, Debbie, Richard, Bavani, Mike, Patty, Andreas, Lijuan and Lisa, as well as all the fourth year thesis students who have made ABB 357 a warm and fun place to be! I would especially like to thank Karen who took me under her wing as an undergraduate and taught me the ropes. I will always remember her kindness and smiling face in the back of the crowd at my talks. Andreas.....I will now pay you the greatest compliment I can think of..... . I would also like to thank Lijuan for her chemical expertise, she was always able to help me if I asked. I am very grateful to Patty for her friendship and help, especially on the late night NMR nightmarishtype experiences. She has shown me patience, kindness, and a friendship that I cherish. I am glad that I had the opportunity to become friends with Lisa, who not only puts up with Andreas but can spend the next few years showing him what humility means.

A note of thanks also goes out to my good friend Liz who I turned to now and then for advice in organic synthesis.

I would like to thank my parents for their love and encouragement throughout the years.

Finally, I wish to thank Laurel who has put up with me throughout my foul moods as I wrote this. Her encouragement, honesty, patience and love have meant a great deal to me.

TABLE OF CONTENTS

		PAGE
CHAPTER 1: INTRODUCTION		
1.1	General Introduction	1
1.2	Background on Steroids	1
1.3	Organometallic Complexes of Steroids	16
1.4	Biological Importance	20
1.5	Organometallic Clusters	24
1.6	Alkynyl and Carbynyl Clusters	26
1.6.1	Chirality and NMR	30
1.7	Cluster Stabilized Cations	31
1.8	History of Chromium Complexes	34
1.9	Reactions of Chromium Complexes	40
1.9.1	Activation of Aromatic Rings to Nucleophilic Attack and Enhancement of Aryl-H Acidities	41
1.9.2	Steric Effects	42
1.9.3	Stability of Benzylic Cations and Anions	49

PAGE

CHAPTER 2: VERTEX ROTATIONS

2.1 Introduction 51

2.1.1 Dimetallic Tetrahedral Clusters 51

2.2 Statement of the Problem 54

2.3 Results and Discussion 55

CHAPTER 3: VERTEX ROTATIONS IN METAL CLUSTERS - AN EHMO STUDY

3.1 Introduction 67

3.1.1 Trimetallic Tetrahedral Clusters 67

3.2 Statement of the Problem 72

3.3 Results and Discussion 74

3.3.1 $M(CO)_3$ Rotation in $FeCo_2(CO)_9S$ 74

3.3.2 $(C_5H_5)Mo(CO)_2$ Rotation in $(C_5H_5)MoCo_2(CO)_8CR$ Clusters 82

3.3.3 $(C_5H_5)Mo(CO)_2$ Rotation in $[(C_5H_5)Mo(CO)_2]_2(C_2H_2)$ and $[(C_5H_5)Mo(CO)_2]_2As_2$ 88

3.3.4 The Structural Dynamics of $[(C_5H_5)Mo(CO)_2]_2(A\equiv B)$ Systems: A Bürgi-Dunitz Approach 96

3.4 Future Work 104

PAGE

CHAPTER 4: A MODEL FOR THE STEROIDAL D-RING OF MESTRANOL

4.1 Introduction 105

4.2 Synthesis and Reactions of 2-methyl-1-phenylethynylcyclopentanol, **47** 108

4.3 Future Work 132

CHAPTER 5: HINDERED ROTATIONS

5.1 Introduction 160

5.1.1 Statement of the Problem 162

5.2 Results and Discussion 162

5.2.1 The Significance of Torsion Angles 186

5.2.2 Chromium-Stabilized Benzylic Cations 189

5.3 Future Work 192

CHAPTER 6: EXPERIMENTAL

6.1 General Procedures 217

6.2 Experimental Procedures 218

REFERENCES 224

LIST OF TABLES

Table 1.1	Dipole Moments of Selected (Arene)$Cr(CO)_3$ Complexes.
Table 3.1	Selected bond angles from a number of X-ray crystal structures of the type $[C_5H_5M(CO)_2]_2(A{\equiv}B)$.
Table 4.1	^{13}C NMR data for methylcyclopentanols and related metal complexes.
Table 4.2	Structure Determination Summary for 2-methylphenylethynyl-cyclopentanol, **47**.
Table 4.3	Atomic coordinates ($x10^4$) and equivalent isotropic displacement coefficients ($Å^2x10^3$) for complex **47**.
Table 4.4	Bond lengths (Å) for complex **47**.
Table 4.5	Bond angles (°) for complex **47**.
Table 4.6	Anisotropic displacement coefficients ($Å^2x10^3$) for complex **47**.
Table 4.7	H-Atom coordinates ($x10^4$) and isotropic displacement coefficients ($Å^2x10^3$) for complex **47**.
Table 4.8	Structure Determination Summary for 2- methylphenylethynyl-cyclopentanol $(Co_2(CO)_6)$, **48**.
Table 4.9	Atomic coordinates ($x10^4$) and equivalent isotropic displacements coefficients ($Å^2x10^3$) for complex **48**.
Table 4.10	Bond lengths (Å) for complex **48**.
Table 4.11	Bond angles (°) for complex **48**.
Table 4.12	Anisotropic displacement coefficients ($Å^2x10^3$) for complex **48**.
Table 4.13	H-Atom coordinates ($x10^4$) and isotropic displacement coefficients ($Å^2x10^3$) for complex **48**.

Table 4.14	Structure Determination Summary for 2-methylphenylethynyl-cyclopentene ($Cp_2Mo_2(CO)_4$), **51**.
Table 4.15	Atomic coordinates ($x10^4$) and equivalent isotropic displacement coefficients ($Å^2x10^3$) for **51**.
Table 4.16	Bond lengths (Å) for **51**.
Table 4.17	Bond angles (°) for **51**.
Table 4.18	Anisotropic displacement coefficients ($Å^2x10^3$) for **51**.
Table 4.19	H-Atom coordinates ($x10^4$) and isotropic displacement coefficients ($Å^2x10^3$) for **51**.
Table 5.1	List of NMR data for complexes **66**, **67** and **68**.
Table 5.2	X-ray crystallographic and NMR spectroscopic data of selected Ph_3SiO-X systems.
Table 5.4	Structure Determination Summary for triphenylsilanol ($Cr(CO)_3$), **66**.
Table 5.5	Atomic coordinates ($x10^4$) and equivalent isotropic displacement coefficients ($Å^2x10^3$) for **66**.
Table 5.6	Bond lengths (Å) for **66**.
Table 5.7	Bond angles (°) for **66**.
Table 5.8	Anisotropic displacement coefficients ($Å^2x10^3$) for **66**.
Table 5.9	H-Atom coordinates ($x10^4$) and isotropic displacement coefficients ($Å^2x10^3$) for **66**.
Table 5.10	Structure Determination Summary for triphenylsilanol

$(Cr(CO)_3)_2$, **67**.

Table 5.11 Atomic coordinates ($x10^4$) and equivalent isotropic displacement coefficients ($Å^2x10^3$) for **67**.

Table 5.12 Bond lengths (Å) for **67**.

Table 5.13 Bond angles (°) for **67**.

Table 5.14 Anisotropic displacement coefficients ($Å^2x10^3$) for **67**.

Table 5.15 H-Atom coordinates ($x10^4$) and isotropic displacement coefficients ($Å^2x10^3$) for **67**.

Table 5.16 Structure Determination Summary for triphenylsilanol $(Cr(CO)_3)_3$, **68**.

Table 5.17 Atomic coordinates ($x10^4$) and equivalent isotropic displacement coefficients ($Å^2x10^3$) for **68**.

Table 5.18 Bond lengths (Å) for **68**.

Table 5.19 Bond angles (°) for **68**.

Table 5.20 Anisotropic displacement coefficients ($Å^2x10^3$) for **68**.

Table 5.21 H-Atom coordinates ($x10^4$) and isotropic displacement coefficients ($Å^2x10^3$) for **68**.

LIST OF FIGURES

Figure 3.1 Frontier orbitals of $M_3(CO)_9$ fragments.

Figure 3.2 Frontier orbital interactions in $Co_3(CO)_9S$ and $FeCo_2(CO)_9S$.

Figure 3.3 Energy profile resulting from rotation of the $M(CO)_3$ fragment in $SFeCo_2(CO)_9$, **33**.

Figure 3.4 The effect on the *1a* frontier orbital in $SFeCo_2(CO)_9$ of rotating the $Fe(CO)_3$ group through 60°.

Figure 3.5 Calculation of the point "**X**" in $CpMo(CO)_2Co_2(CO)_6CH$.

Figure 3.6 Walsh diagram showing orbital energy changes as a result of rotation of the $CpMo(CO)_2$ vertex in $CpMo(CO)_2Co_2(CO)_6CH$. The dotted line represents the change in total energy and is drawn to a different scale, see text.

Figure 3.7 The effect on the *1a* frontier orbital in $CpMo(CO)_2Co_2(CO)_6CH$ of rotating the $CpMo(CO)_2$ group.

Figure 3.8 The effect on the *1s* frontier orbital in $CpMo(CO)_2Co_2(CO)_6CH$ of rotating the $CpMo(CO)_2$ group.

Figure 3.9 Calculated energy profile resulting from synchronous swivelling of both molybdenum vertices to generate ultimately a molecule of pseudo-C_{2v} symmetry.

Figure 3.10	Calculated energy profiles corresponding to rotation through θ of only 1 molybdenum vertex while the other is kept constant with ϕ = 120, 130, 140, 150°.
Figure 3.11	Calculation of the point **"X"** in $[CpMo(CO)_2]_2(A{\equiv}B)$ systems.
Figure 3.12	Comparison of calculated Cp-Mo-Mo angles vs twist angles with data from Table 3.1. [**X** - calculated; □ - X-ray crystal structures].
Figure 3.13	Comparison of X-ray structures with energy profile shown in Figure 3.10.
Figure 4.1	^1H-^1H COSY spectrum of **47**.
Figure 4.2	^1H-^{13}C shift-correlated spectrum of **47**.
Figure 4.3	View of 2-methyl-1-phenylethynylcyclopentanol, **47**.
Figure 4.4	View of **47**.
Figure 4.5	Unit cell diagram of **47**.
Figure 4.6	Hydrogen bonding of the hydroxy groups in **47**.
Figure 4.7	View of the cobalt complex, **48**.
Figure 4.8	View of **48**.
Figure 4.9	Unit cell diagram of **48**.
Figure 4.10	Antarafacial shift process.
Figure 4.11	View of the molybdenum complex **51**.

Figure 4.12 View of **51**.

Figure 4.13 Unit cell diagram of **51**.

Figure 5.1 View of triphenylsilanol chromiumtricarbonyl, **66**.

Figure 5.2 View of **66**.

Figure 5.3 Unit cell of **66**.

Figure 5.4 View of bis(chromiumtricarbonyl)triphenylsilanol, **67**.

Figure 5.5 View of **67**.

Figure 5.6 Unit cell diagram of **67**.

Figure 5.7 View of tris(chromiumtricarbonyl)triphenylsilanol, **68**.

Figure 5.8 View of **68**.

Figure 5.9 Unit cell diagram of **68**.

Figure 5.10 ^{1}H NMR spectra of complexes **66**, **67** and **68**.

Figure 5.11 ^{13}C NMR spectra of complexes **66**, **67** and **68**.

Figure 5.12 Highest available symmetry of complexes **66**, **67** and **68**.

Figure 5.13 Selected variable-temperature 500 MHz ^{1}H NMR spectra of **69** in the non-complexed phenyl ring region.

Figure 5.14 Sections of the ^{1}H and ^{13}C NMR for triphenylmethyl chromium tricarbonyl cation, **70**. The dots mark signals attributable to $[Ph_3C]^+$, and "s" is the flourine-coupled quartet from CF_3SO_3H.

LIST OF SCHEMES

Scheme 1.1	Regioselectivity and Stereoselectivity of α-carbanion formation in $Cr(CO)_3$ complexes of estradiol derivatives.
Scheme 1.2	General procedure for the preparation of organometallic clusters with alkynyl or carbynyl moieties.
Scheme 1.3	A general route to tetrahedral dicobalt μ-alkyne clusters.
Scheme 1.4	Establishment of the link between σ and π-bonded complexes.
Scheme 1.5	Stereospecific *exo* nucleophilic attack in indanone derivatives.
Scheme 1.6	Preparation of optically active indanols.
Scheme 1.7	Synthesis of optically pure 2-methylindanone.
Scheme 1.8	Introduction of a second alkyl group onto the disubstituted indanone.
Scheme 1.9	Base-catalyzed stereoselective hydrogen-deuterium exchange of benzylic protons of alkylbenzene chromiumtricarbonyl complexes.
Scheme 1.10	Selected reactions of substituted phenylchromiumtricarbonyl complexes.
Scheme 2.1	Exchange process which interconverts carbonyl ligands in semi-bridging and in terminal environments.

Scheme 2.2 Synthetic routes to chiral clusters.

Scheme 2.3 Proposed mechanism of interconversion of enantiomeric clusters *via* C_s rather than C_{2v} intermediates.

Scheme 3.1 Rotation of a $CpMo(CO)_2$ vertex relative to a triangular face.

Scheme 4.1 Synthesis and complexation of the 17α-ethynyl derivative of 3-methoxyestrone.

Scheme 4.2 Fluxional processes illustrating interconversion of stereoisomers.

Scheme 5.1 Preparation of triphenylsilanol complexes **66**, **67** and **68**.

CHAPTER 1

INTRODUCTION

1.1 General Introduction.

This thesis describes the synthesis and molecular dynamics of two types of organometallic complexes: the first type involves the interactions of cobalt or molybdenum multiple-bonded systems with steroidal or terpenoid alkynes. These cluster complexes yield isolable cationic derivatives. Cations can also be stabilized by chromium tricarbonyl moieties and a series of such compounds has been prepared. Therefore, introductory material is presented on steroids, on organometallic clusters and on chromium tricarbonyl complexes.

1.2 Background on Steroids.

Steroids are important biological regulators and almost always show dramatic physiological effects when they are administered to living organisms. Steroids are derived from the perhydrocyclopentanophenanthrene ring system shown below.[1]

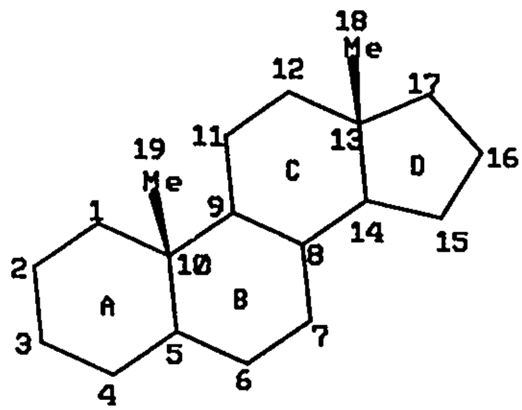

Conventionally, other groups which lie on the same face of the molecule as the "angular methyl groups" are referred to as β-substituents; those on the lower face, i.e., opposite to the angular methyl groups are designated as α-substituents. The following gallery of steroids shows various important steroids.[2]

Steroids encompass a very large range of compounds and have been one of the most extensively studied chemical systems. Numerous books and journals have been published documenting their chemistry and biochemistry.[1,2,3,4] Cholesterol was the first steroid to be isolated, it was purified as early as 1812, and thus became readily available as it is a main constituent in brain and nervous tissues. The x-ray crystal structure of cholesterol was accurately determined in 1932 by physicist J.D. Bernal.[2] From this point forward, research rapidly expanded in the general field of steroid chemistry.

A GALLERY OF STEROIDS

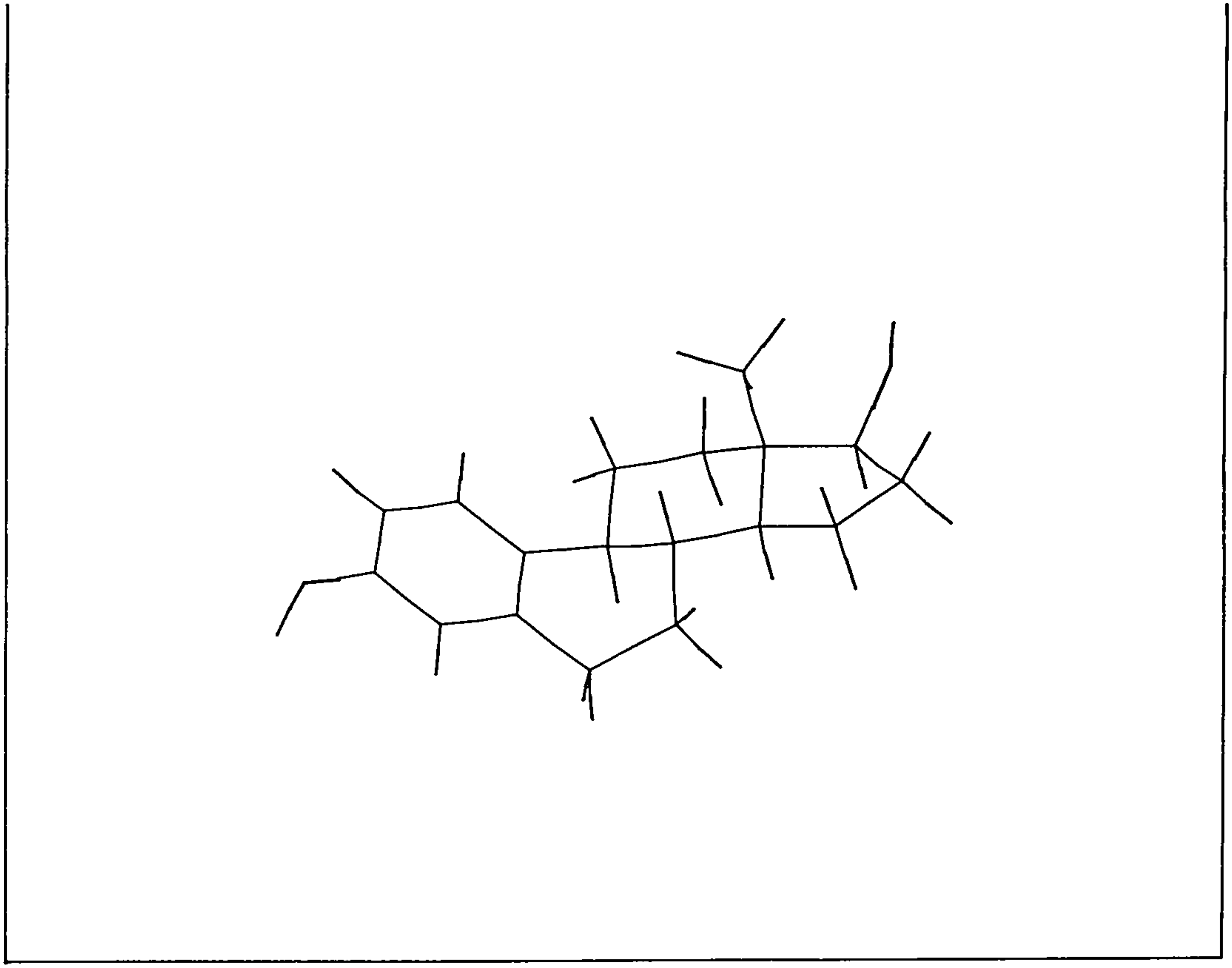

ESTRADIOL

Alchemy II
TRIPOS Associates
St. Louis. Mo.

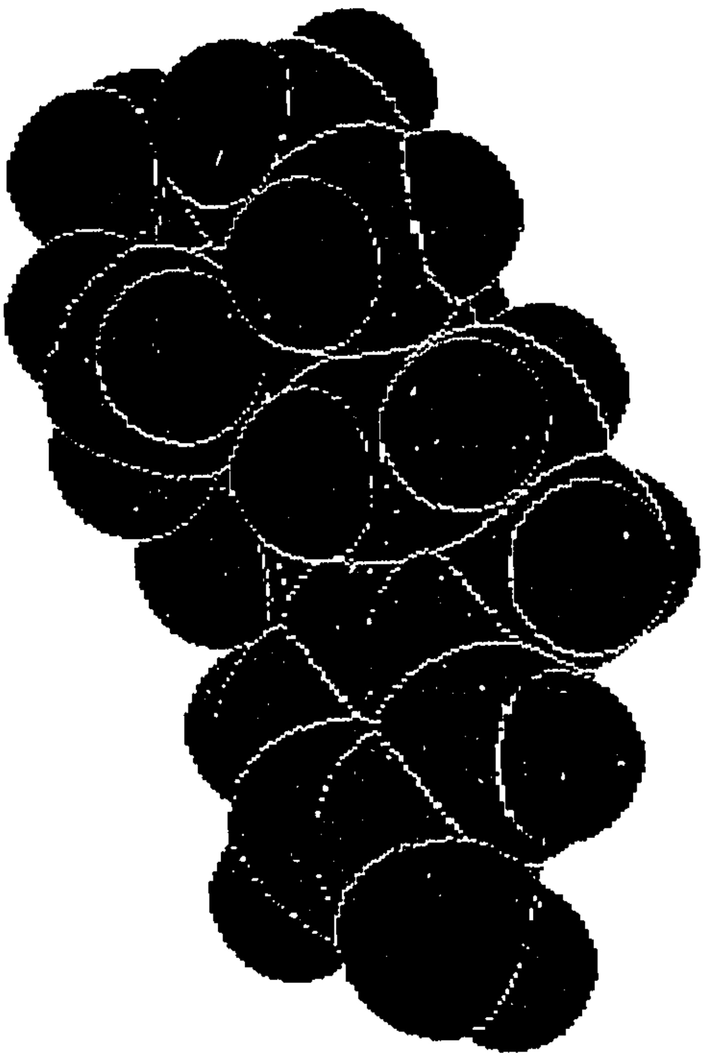

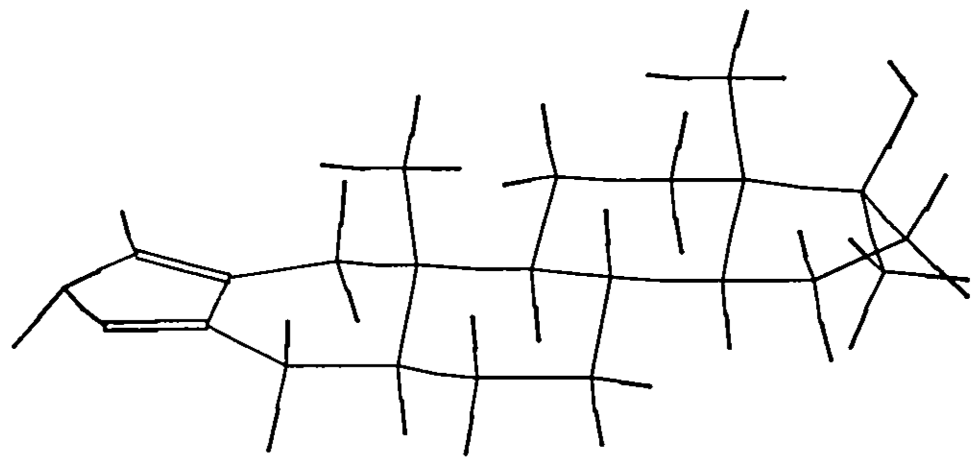

Alchemy II
TRIPOS Associates
St. Louis. Mo.

STANAZOLOL

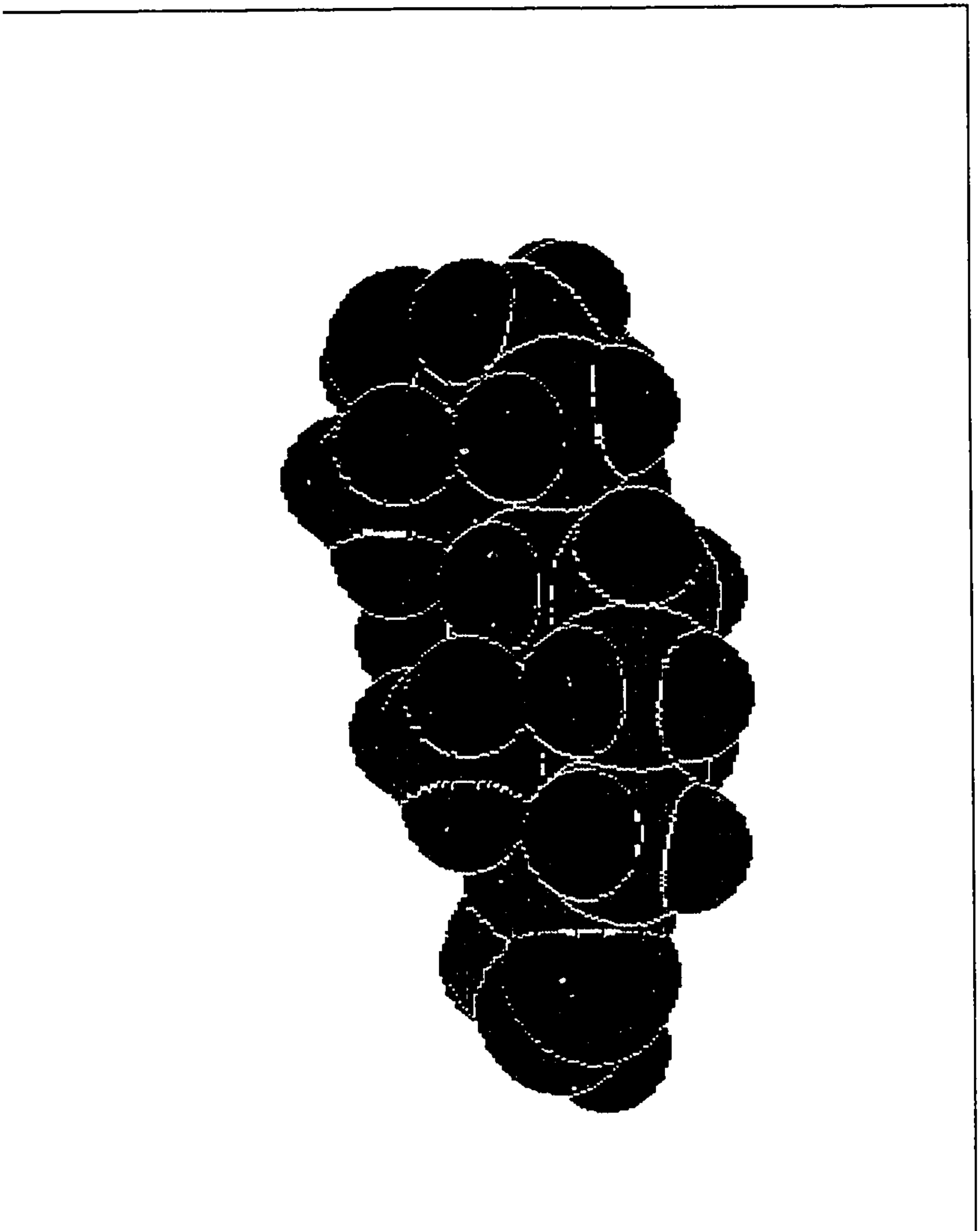

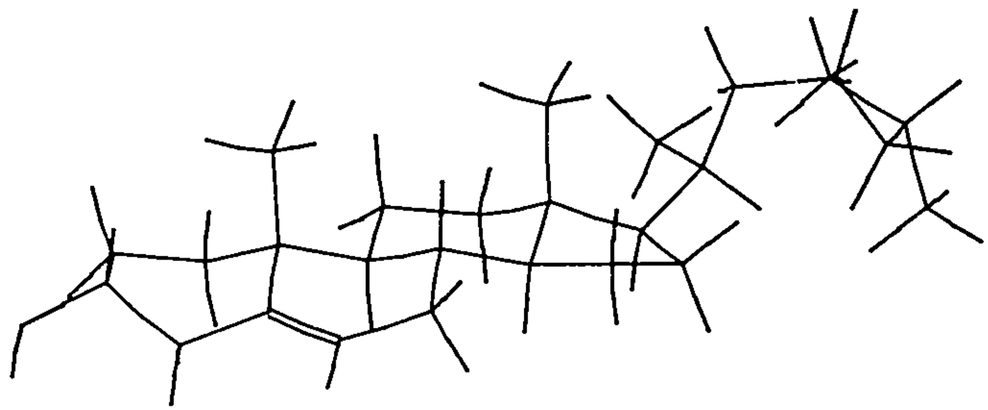

CHOLESTEROL

Alchemy II
TRIPOS Associates
St. Louis. Mo.

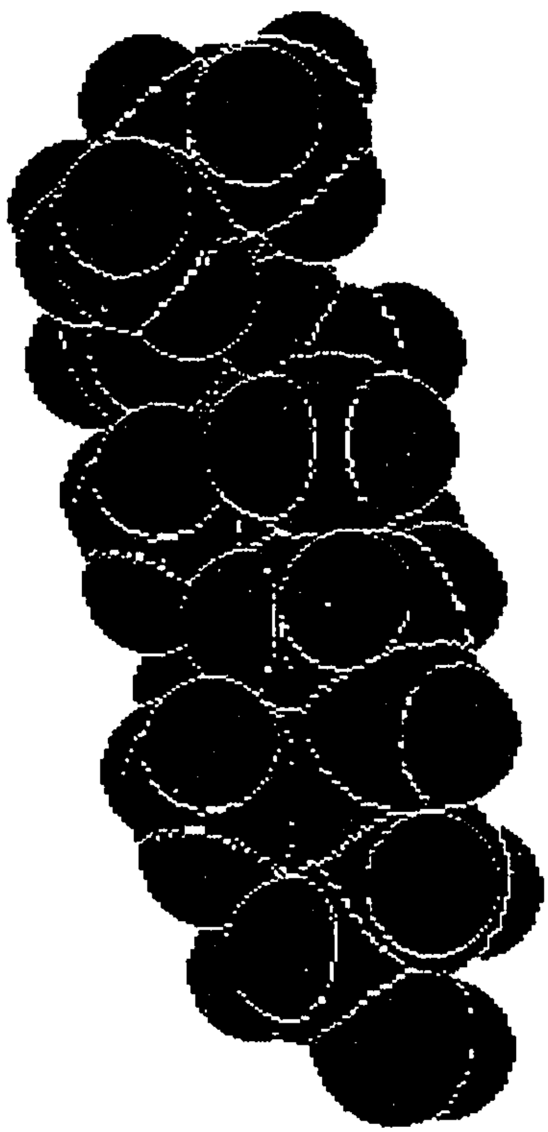

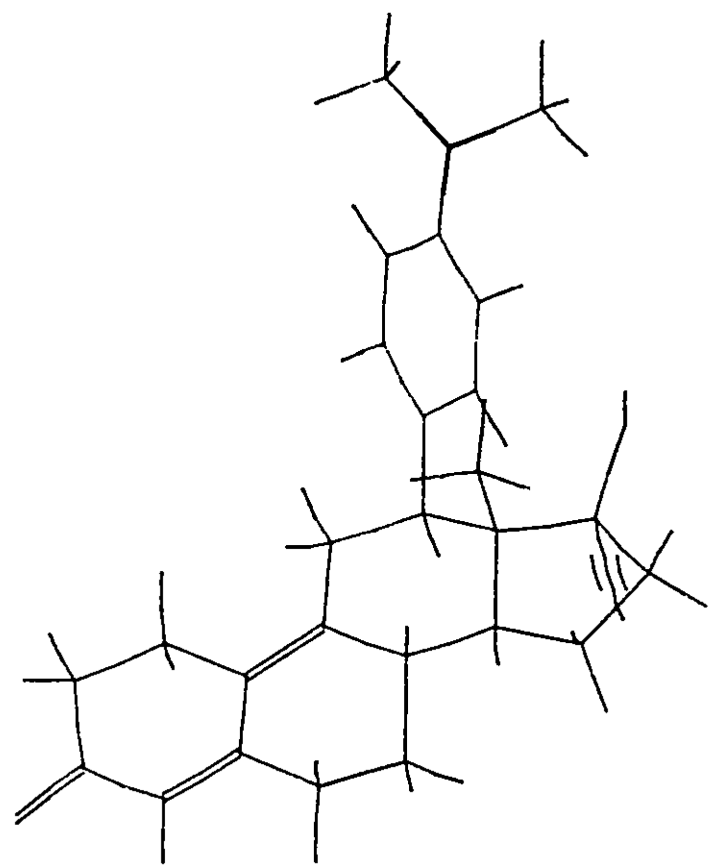

RU486

Alchemy II
TRIPOS Associates
St. Louis. Mo.

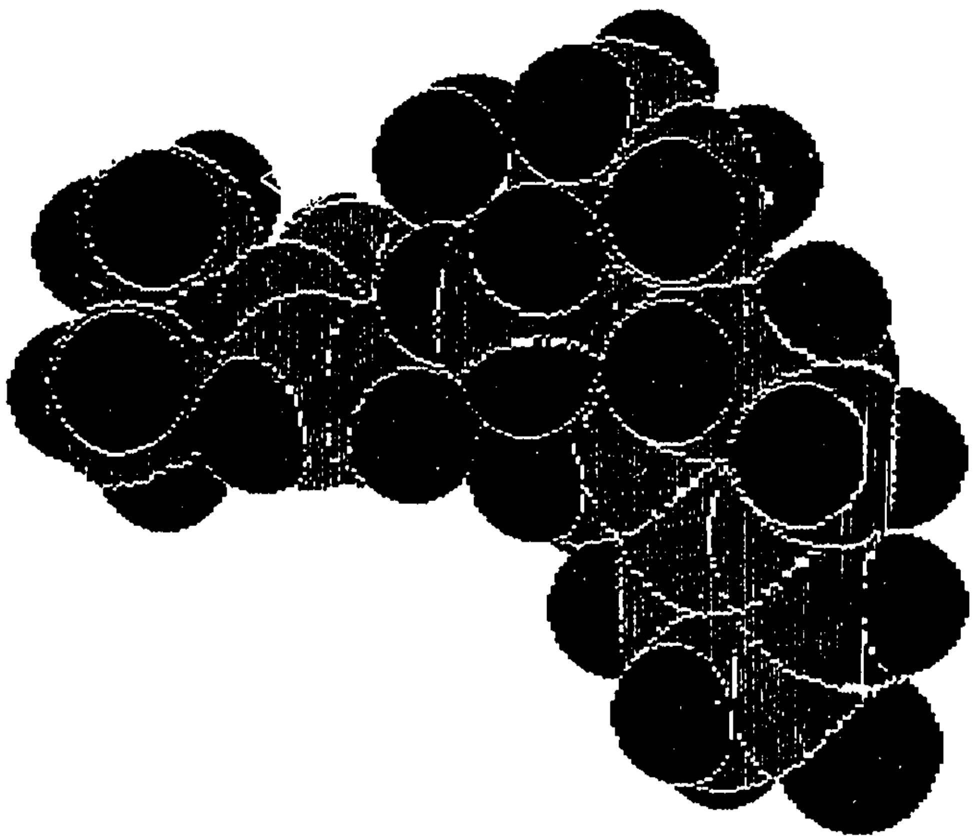

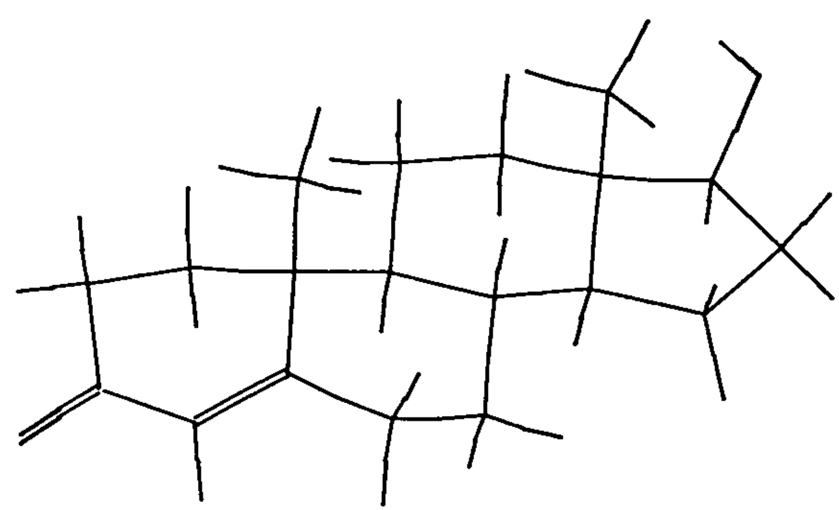

Alchemy II
TRIPOS Associates
St. Louis. Mo.

TESTOSTERONE

13

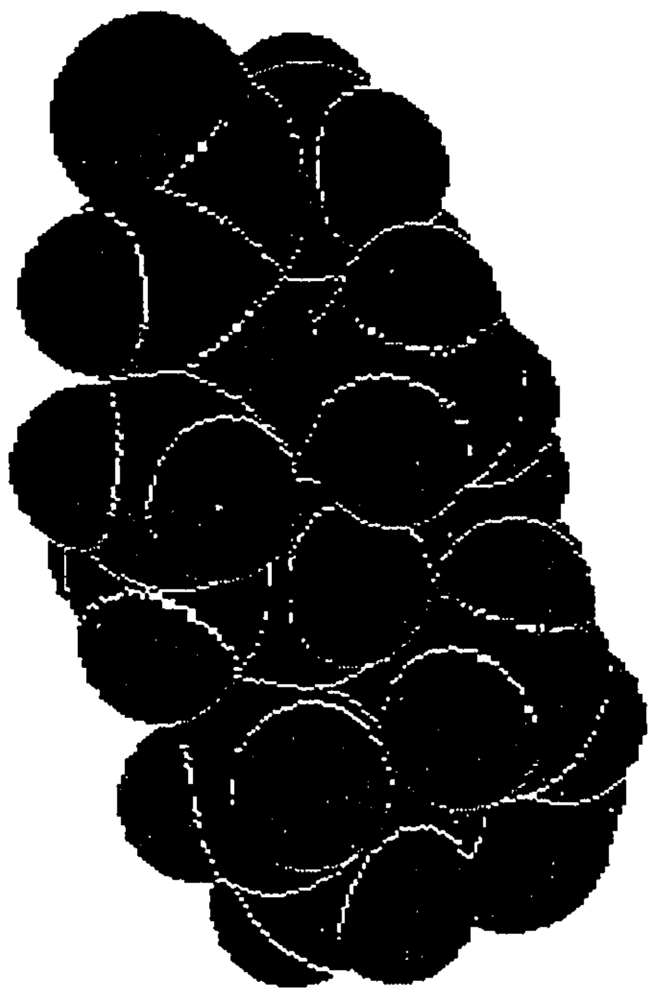

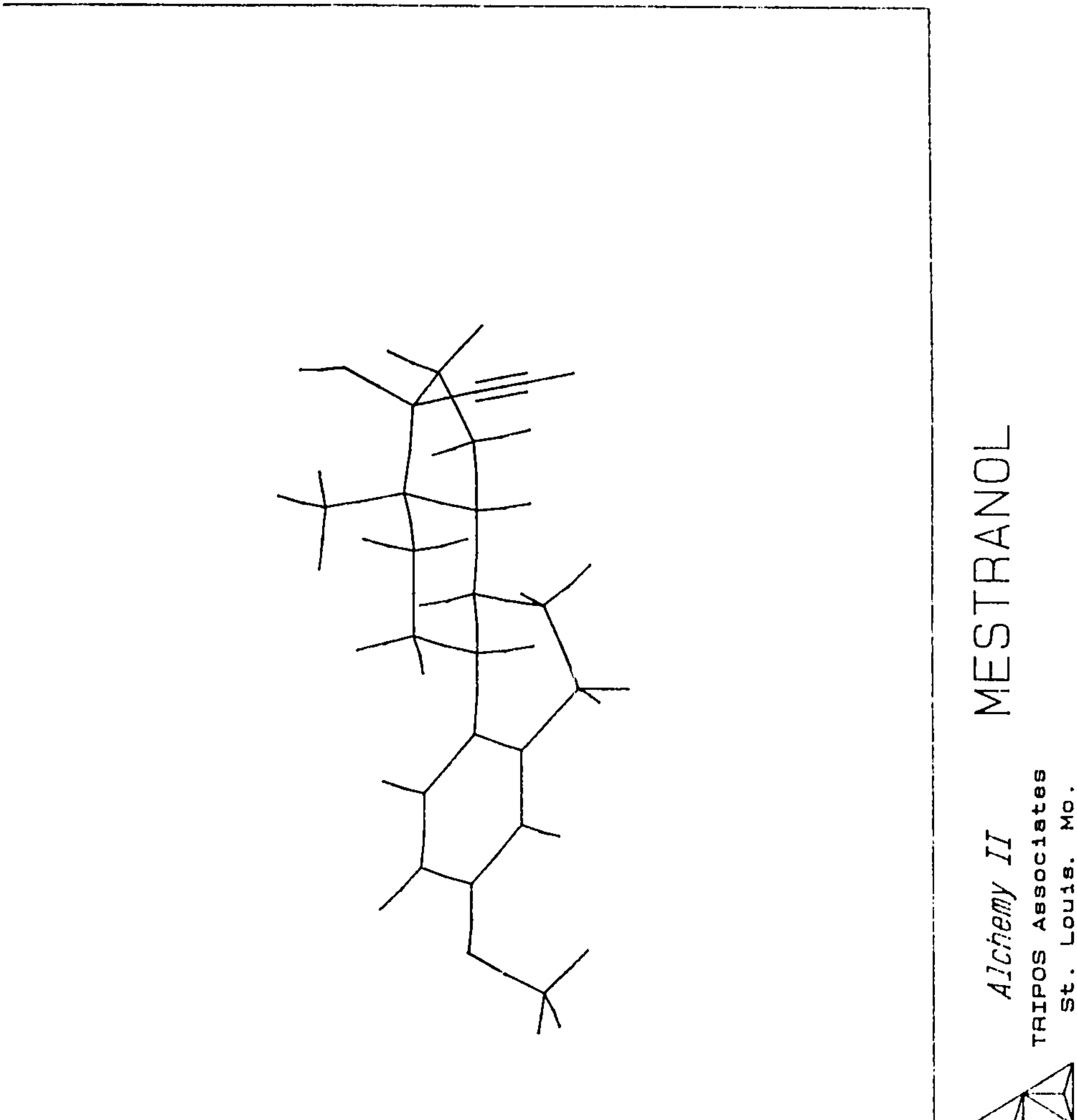
MESTRANOL
Alchemy II
TRIPOS Associates
St. Louis. Mo.

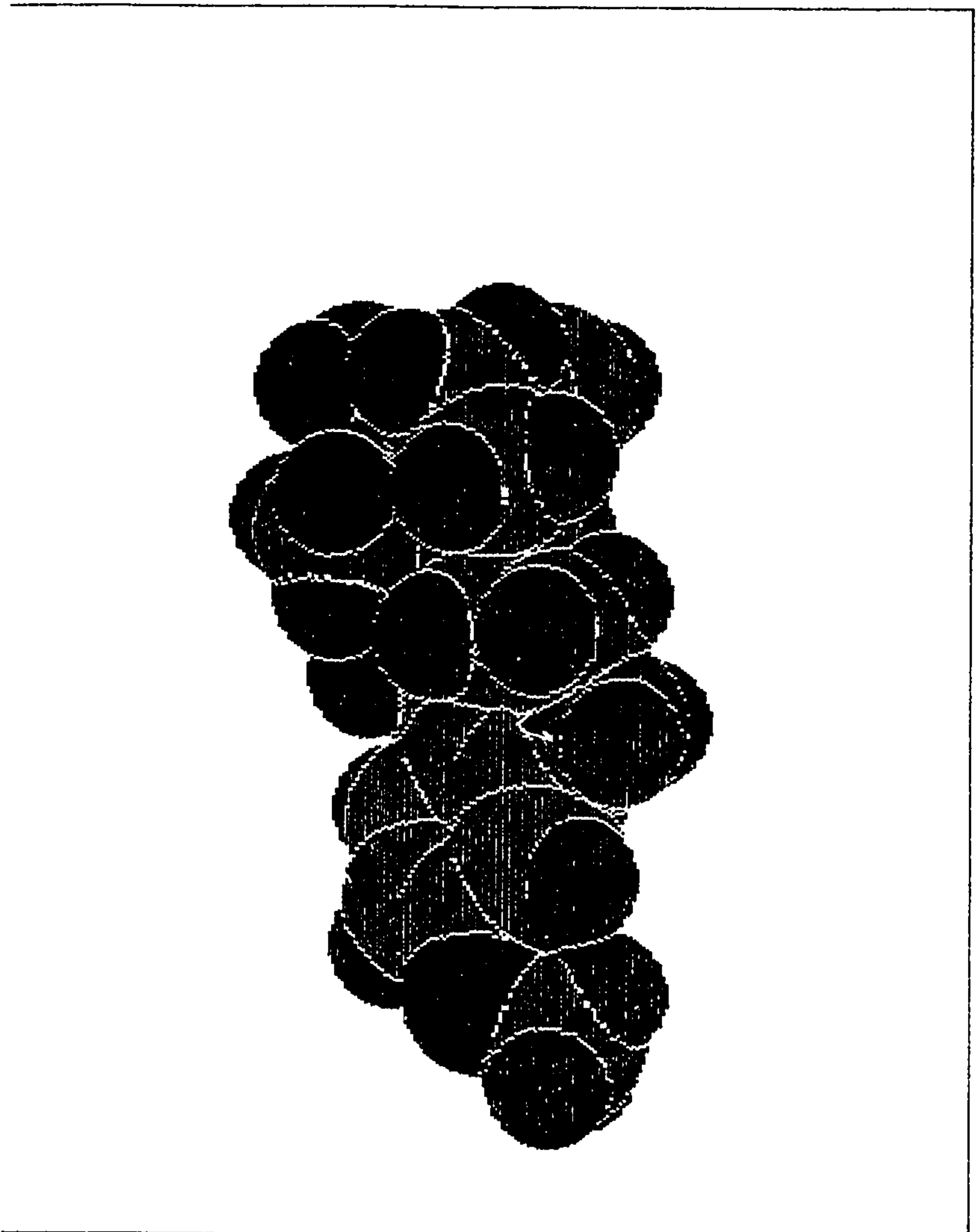

1.3 Organometallic Complexes of Steroids.

The incorporation of transition metals into the steroid framework has been an area which in recent years has increased tremendously. Various transition metal complexes have been formed by coordination to steroidal rings. The first of these complexes were prepared as early as 1963 by Nakamura in which the A-ring of estrone was complexed by $Cr(CO)_3$ and the B-ring of ergosterol acetate by $Fe(CO)_3$.[5,6] They were unable, however, to determine whether the metal fragments were bound to the α or β face. These and related systems have recently been characterized x-ray crystallographically. Crystal stuctures of β-[CpRu(estrone 3-methyl ether]$^+PF_6^-$ and α-[3-dimethyl-tert-butylsiloxy-17β-estradiol]$Cr(CO)_2CS$ have been recently elucidated.[6a,6b] This work led the way to organometallic complexes of steroids as intermediates in the preparation of new steroidal derivatives which would have been difficult to isolate via conventional organic means.

Steroidal organometallics have been utilized in many ways. For example, they can be used as protecting agents, in bond rearrangements, in nucleophilic and electrophilic additions as well as in steroid synthesis. The $Fe(CO)_3$ group may be used as a temporary protecting group[7,8] as shown by Barton *et al.*, who used the iron tricarbonyl group to protect the C-5/C-7 diene in ergosterol acetate; meanwhile they were able to manipulate the C-22/C-23 exocyclic bond by means of various electrophilic reactions. Once the reactions were complete, the iron tricarbonyl was removed by using ferric chloride to yield various substituted ergosterols. Barton and coworkers also showed that $Fe(CO)_3$ complexes of ergosterol and its esters, which are easily made from $Fe(CO)_5$, $Fe_2(CO)_9$ or from (benzylideneacetone)$Fe(CO)_3$ precursors, can be used as intermediates in the preparation of new ergosterol derivatives.[9]

Protection of a triple bond may also be accomplished via transition metal carbonyls. As will be discussed in greater detail in section 1.5, Nicholas[9a] and his coworkers took advantage of this concept to protect the alkynyl group in 17-ethynyl-$\delta^{5,6}$-dehydroisoandosterol with $Co_2(CO)_6$, **2**.

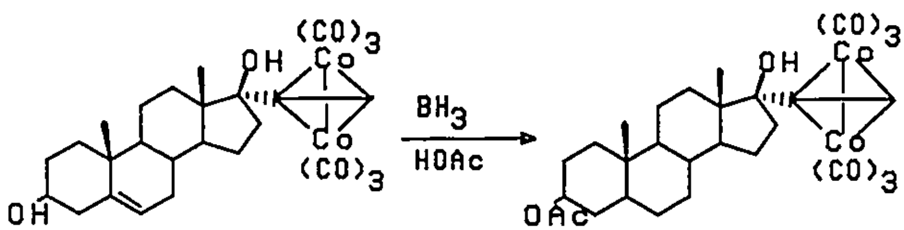

2 **3**

Bond rearrangements may also be performed via organometallic complexes of steroids. $Fe(CO)_3$ complexes have been used to convert steroidal trans diens to their cis isomers[10] by means of selective bond migrations. Conversely, Barton *et al.* illustrated that the reverse reaction is also possible[11,12] and that $Cr(CO)_3$ is a much more efficient reagent to accomplish cis to trans isomerizations.[13]

By far the most thoroughly studied types of reactions to be performed on organometallic complexes have been nucleophilic and electrophilic additions.

Indeed, the main reason for attaching an organometallic unit into a steroidal framework lies in the fact that organometallic groups provide sites for the ready formation of new C-C bonds. The coordination of a functional group by a transition element often activates this functionality towards nucleophilic or electrophilic attack.[14]

Jaouen *et al.* has beautifully illustrated that the benzylic protons become more acidic and the reactivity of an arene is increased when complexed by $Cr(CO)_3$.[15] He and his coworkers were able to selectively generate α-carbanions in substituted $Cr(CO)_3$ complexes and form a series of new estradiol derivatives in a stereospecific manner with a high degree of regioselectivity (see Scheme 1.1).[15] They demonstrated that treating the α or β estradiol $Cr(CO)_3$ derivatives with $(Me_3Si)_2NNa$ generates an anion at position 6 which when treated with p-formaldehyde yielded products with a hydroxy methyl substituent at position 6. The 6β-CH_2OH product was formed from the α-$Cr(CO)_3$ complex and the 6α-CH_2OH product was formed from the β-$Cr(CO)_3$ complex. Thus, the alcohol functionality was shown to be anti to the transition metal in all cases; this illustrates the stereospecificity of the process. Furthermore, despite the availability of two benzylic positions (6 and 9) for proton abstraction, only attack at the 6 position was observed.[16]

Jaouen also utilized these new alkylated steroidal organometallic derivatives in receptor binding assays which will be discussed further in the following section.[16]

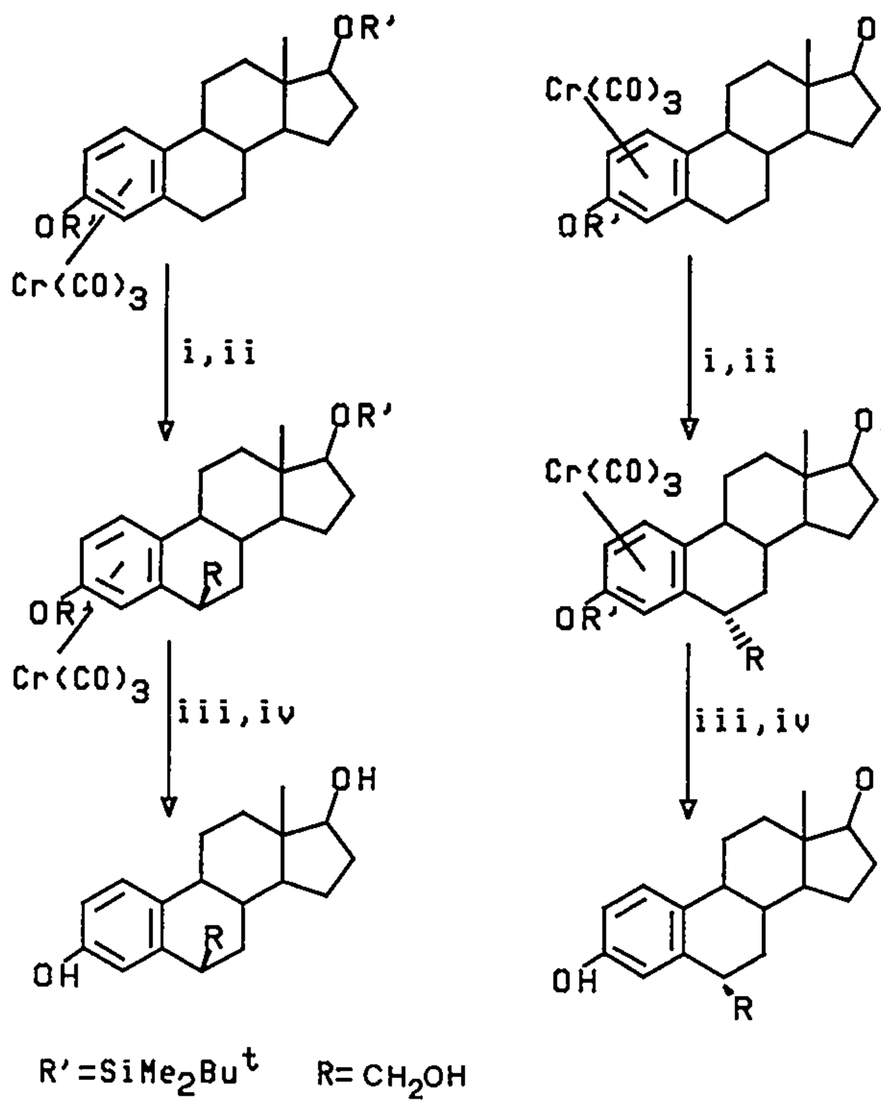

Scheme 1.1: i, $(Me_3Si)_2NNa$; ii, CH_2O; iii, $h\upsilon$=O_2; iv, $Bu^n{}_4NF$.
Regioselectivity and Stereoselectivity of α-carbanion formation in $Cr(CO)_3$ complexes of estradiol derivatives.

Clearly, the chemistry in this area is so extensive that only a mere fraction of it has been mentioned here. Significant contributions have also been made concerning η^3-π-allyl palladium chemistry at the junction between the A and B rings[17-21] as well as in the A-ring itself.[22,23]

1.4 Biological Importance.

Metalloimmunoassay, developed by Cais and coworkers[24-27] used metals in the form of their organometallic or coordination complexes as non-radioactive agents in the study of antigen-antibody interactions. By definition, an antigen is a substance which when introduced into an animal's body triggers the formation of antibodies and reacts with them. Antibodies are glucoproteins formed in pertinent cells of the organism on intrusion of antigens.[28] Simply put, antibodies (Ab) specifically recognize and bind to antigens (Ag) forming a complex (Ab-Ag). If the antigen is replaced by a metal-labelled antigen (Ag-M) and the presence of the metal does not cause the binding to the antibody to be disturbed, then a competitive reaction develops when both types of antigen react with a limited quantity of antibody.

Once the reaction is complete, these antigen-antibody complexes (Ab-Ag, Ab-Ag-M) are separated from the unbound antigen (Ag, Ag-M) and the amount of metal present is determined by selective analytical techniques such as atomic

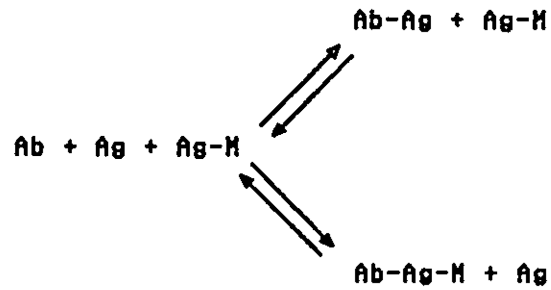

absorption spectrometry, emission and fluorescence spectrometry, electrochemical methods and neutron activation. The amount of antibodies present in an unknown sample can then be counted by plotting the amount of metal isolated on calibration curves for standard amounts of antigens and metalloantigens.[28]

Analogously, Jaouen utilized steroidal hormones labelled with metal carbonyls for the purpose of studying the interactions of such hormones with high affinity binding proteins known as receptors, found in target cells.[29] The interactions of hormones with their receptors is highly stereospecific, however, and even slight alterations in the hormonal structure will often affect the relative binding affinity (RBA) of the receptor and thus will lower the biological activity. Variations in the concentrations of certain hormone receptors have been clearly linked to such malignancies as breast cancer.[29] Although utilizing radiolabelled hormones as a method of assaying provides excellent detection, there are adverse effects such as health hazards, limited variety of useable isotopes and biochemical radiolysis. The use of organometallic markers was recognized as an excellent alternative to isotopic procedures for receptor assay. There are two reasons these complexes are such good markers. First, a spectral window occurs in the IR spectra of proteins, and second, metal carbonyls absorb very strongly in the region where this window occurs, 2100-1850 cm^{-1}.[29] Furthermore, the sensitivity of FT-IR is such that it can detect even at the level of femtomoles/mg protein, which corresponds to that commonly found in biological systems, and could therefore be used to monitor hormone dependence of breast cancer.[30]

As illustrated earlier, Jaouen's initial studies utilized α- and β-$Cr(CO)_3$ complexes of derivatized estradiol. The relative binding affinity studies showed the α-complex (28%) was similar to the uncomplexed silyl derivative (35%) while the β-complex was much lower (1.8%) due to steric hindrance of the $Cr(CO)_3$ moiety. The specific binding of the α-complex was confirmed by the observation of two carbonyl absorptions in the FT-IR after incubation in lamb uterine cytosol.[29]

The problem encountered in using $Cr(CO)_3$ complexes was their photosensitivity which prevented their use in routine clinical studies. Another position which can be labelled with an organometallic unit is the 17α alkynyl group in 17β-estradiol, which when modified, will not greatly affect the RBA of the hormone. This alkyne readily reacts with $Co_2(CO)_8$ and $Cp_2Mo_2(CO)_6$, as will be illustrated in section 1.5, to form the Co and Mo complexes, respectively.[31] After incubation, the molybdenum complex showed 3 of 4 υ_{CO} absorptions. This was the first direct measure of an organometallic steroid bonding to the estradiol receptor site.

The controversial steroid mifepristone, **4**, also known as RU486, the "morning after pill", which is currently marketed in France and China, has high affinity for the progesterone and glucocorticoid receptor sites and has potent antiprogestin and antiglucocorticoid activity both in *vitro* and in *vivo*.[32] RU486 has two obvious sites for complexation, the 17α-alkynyl and 11β-aryl ring positions. The arene-$Cr(CO)_3$ complex and the cobalt and molybdenum alkyne complexes were synthesized and the relative binding affinities measured. The $Cr(CO)_3$ complex had a smaller RBA than the 17α complexes, presumably due to steric hindrance of the metal with a receptor site. After incubation, the Co-complex showed the highest RBA and two carbonyl absorptions were observed in the IR to confirm binding to the receptor site.

Other than immunoassay approaches, several investigations have been carried out based on the potential of steroidal organometallics as antitumor agents. Several Pt[33], Pd[34], and Sn[35,36] complexes have also been synthesized for this purpose.

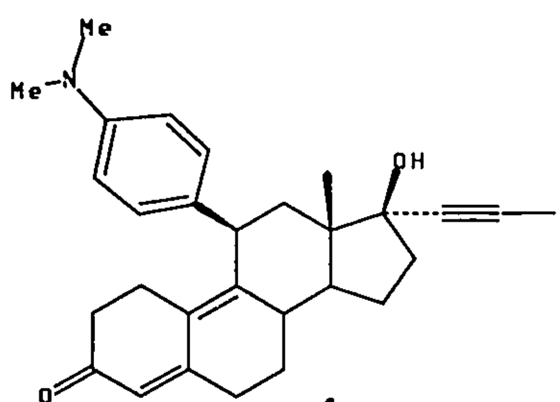

4

1.5 Organometallic Clusters.

Organometallic chemistry is the study of complexes which contain metal-carbon bonds[37]. Metal-Ligand bonding in a complex can be easily described by the Dewer, Chatt and Duncanson model.[39] Theoretically, the organic molecule donates π electron density from its occupied p-π molecular orbitals into the metal's valence shell. Concomitantly, the metal back-donates electron density from its d valence shell into the empty p-π* molecular orbitals in the organic molecule.[40]

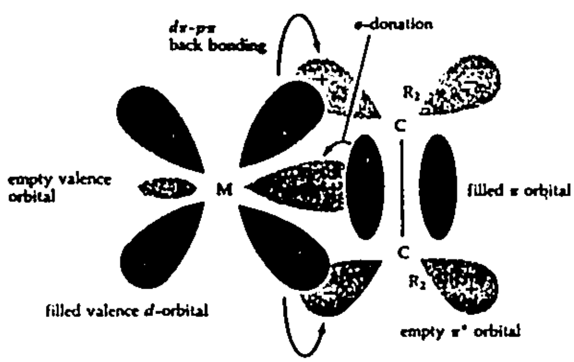

The degree of back-donation to an unsaturated organic molecule depends on the "chemical accessibility" of the d-electron density of the transition metal. If the metal is in a relatively high oxidation state, then the back-donation to the ligand is insignificant, and the complex may be very unstable. When there is significant back-donation from the metal to the ligand, the metal-ligand bond is strengthened and the amount of negative charge on the metal, which is viewed as arising from ligand donation of electron density, is reduced. Therefore, metal-to-ligand back-donation stabilizes low oxidation states of transition metals.[40]

The donation of electron density from the ligand to the metal varies according to the ligand's nature. NH_3 is a strong σ-donor, but cannot act as a π-acceptor since the nitrogen atom does not have an empty d-orbital in its valence shell to accept electron back-donation. Et_3P is a moderately strong σ-donor as well as π-acceptor since the phosphorus has empty 3d orbitals in its valence shell into which electrons can be back-donated.

In the light of this model of metal-ligand bonding, let us now focus on concepts which may help us to predict the outcome of reactions, and which molecular formulas may represent realistic stable complexes. The Effective Atomic Number (EAN) rule, also known as the 18 electron rule, is a useful tool in predicting the stability and structures of small organometallic complexes.[39] A transition metal has an inner core electron configuration identical to that of the next lighter noble gas atom and a valence shell consisting of 5 d-orbitals, 1 s-orbital and 3 p-orbitals. Transition metals accept electron density from ligands in order to fill their valence shells. The 18 valence electrons are the sum of the number of electrons initially possessed by the metal itself and the electrons acquired from the ligands.[40] The simplest way to calculate the total number of valence electrons in an organometallic molecule is via the covalent model in which both the metal atom and the ligands are assumed to be neutral. The number of electrons contributed from the metal is the number of d-electrons in its zero oxidation state.[40]

Stable transition metal clusters tend to have the greatest number of metal-

metal bonds possible since the individual fragments which make up the cluster are electron deficient.[37] Now, the electrons can be delocalized over the entire cluster. Assuming the cluster obeys the EAN rule, and knowing the number of metal atoms, (a shared M-M bond counts as a shared pair of electrons, each metal contributing one electron), and counting the number of electrons, the number of metal-metal bonds present in a polymetallic system can be predicted.[39] Once the clusters contain more than 5 or 6 metal atoms, the EAN rule is no longer adequate to predict the stability of molecules, and one must usually apply the Wade-Mingos electron-counting rules.

1.6 Alkynyl and Carbynyl Clusters.

Organometallic clusters with alkynyl or carbynyl moieties can be readily prepared by adding a metal-metal bond to either a metal-carbon multiple bond, as in Scheme 1.2, or a carbon-carbon multiple bond.[41] In fact, an easy way of preparing tetrahedral dicobalt μ-alkyne clusters is to simply add an alkyne, such as acetylene, to $Co_2(CO)_8$ as shown in Scheme 1.3. These dicobalt μ-alkyne clusters are also very useful starting materials for the synthesis of other clusters. Interestingly, protonation of the dicobalt complex with sulphuric acid gives the tricobalt complex, **5**.[42] This complex was also the first tricobalt-carbon complex to be examined crystallographically.[43] This synthetic route was found to be a

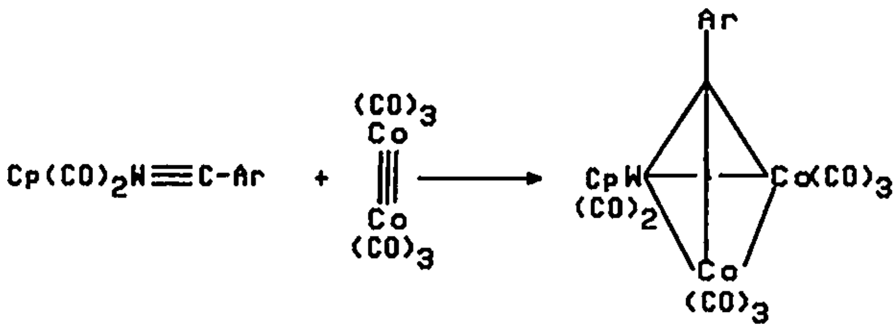

Scheme 1.2: General procedure for the preparation of organometallic clusters with alkynyl or carbynyl moieties.

general one to tricobalt clusters, albeit limiting since there will always be a CH_2 in the α position, since the alkyne must possess at least one terminal hydrogen.

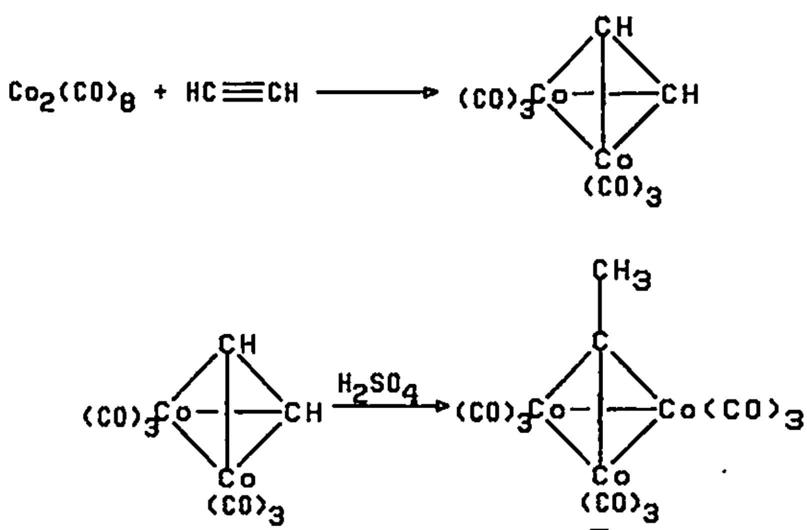

5

Scheme 1.3: A general route to tetrahedral dicobalt μ-alkyne clusters.

An even more general approach to tricobalt clusters was found shortly thereafter in which a substituted α,α,α-trihalomethane was treated with $Co_2(CO)_8$. This procedure allows the formation of clusters with a wide variety of apical substituents.[44,45]

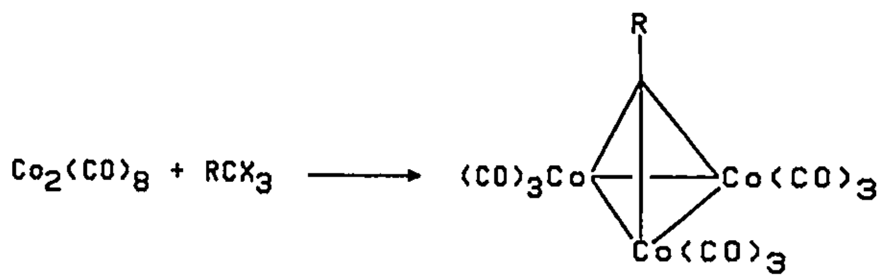

Jaouen introduced a simple route to the square-based pyramidal trimetallic cluster, **6**, by the reaction of a tetrahedral bimetallic alkyne cluster with metal fragments.[46]

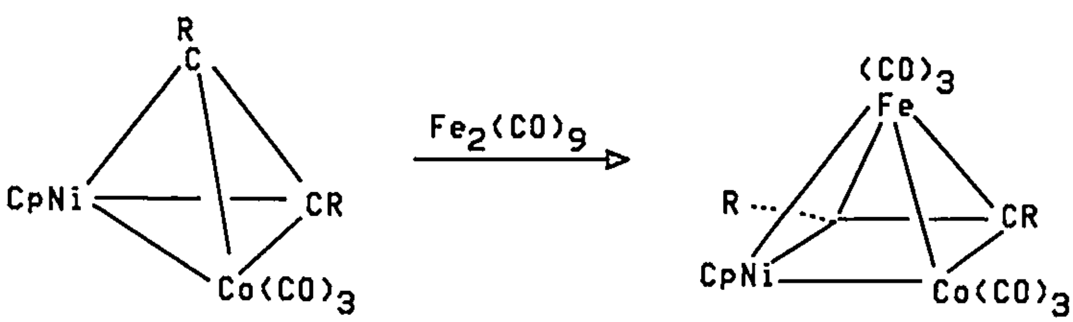

6

The concept of isolobality developed by Roald Hoffmann[47] is an essential tool required by the organometallic chemist in order to compare molecular fragments with one another. The use of this concept has greatly extended this field of research by allowing the replacement of isolobal units with one another thus leading to a greater range of complexes. Two molecular fragments are isolobal if the "number, symmetry properties, approximate energy and shape of the frontier orbitals and the number of electrons in them are similar".[40] The symbol used to show two isolobal ligands is a double headed arrow with half an orbital lobe.

$$Mn(CO)_5 \longleftrightarrow CH_3$$

If $Mn(CO)_5$ is isolobal with CH_3, then so are $Tc(CO)_5$, $Re(CO)_5$ and $Fe(CO)_5^+$. Also, if this relationship holds, then $Cr(CO)_5$, $Mo(CO)_5$ and $W(CO)_5$ are isolobal with CH_3^+ and $Fe(CO)_5$ is isolobal with CH_3^-.[39]

Consider $Mn(CO)_5$ (where Mn is d^7). This molecule has a single electron in a hybrid orbital pointing away from the ML_5 fragment and above the 3 lone pairs originating from the t_{2g} set. This is similar to the methyl radical in that the methyl also has a single electron in its frontier orbital. Consequently, the two should behave similarly, and they do! To illustrate this one should think of what the methyl radical does...it dimerizes to ethane and starts radical chain reactions. Similarly, $Mn(CO)_5$

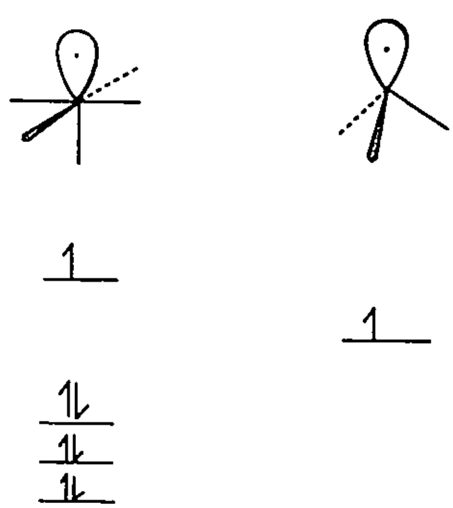

d^7-ML_5 CH_3

dimerizes to $Mn(CO)_{10}$ and has a rich radical-type chemistry.[47] In fact in accord with this relationship, the inorganic and organic fragments can combine to form $(CO)_5MnCH_3$.

Based on this theory of isolobality a number of syntheses have been carried out on a wide variety of clusters.[48-50] One metal vertex in a cluster can be replaced by another metal fragment which is isolobal to it. This may be illustrated with a tricobalt tetrahedral complex in which each $Co(CO)_3$ vertex may be replaced by an isolobal fragment. For instance, one vertex may be replaced with $CpW(CO)_2$ and another $Co(CO)_3$ vertex may be replaced with CpNi.

1.6.1 Chirality and NMR.

Since the majority of work deals with chiral complexes, the phenomenon of diastereotopic nuclei should be clarified. In a molecule of C_1 symmetry all magnetically active nuclei are in different environments and should resonate at different frequencies. If two or more nuclei are interconverted via an inter-conversion or rearrangement then, eventually, they will become magnetically equivalent at some temperature where the activation energy is overcome. This may be exemplified by a chiral ethane, **7**. The methyls are magnetically different, but rotation about the carbon-carbon bond results in the methyl hydrogens being brought into equivalent positions and a single peak is seen in the NMR spectrum.

If one of the hydrogens is replaced by another atom or group, as shown in **8**, the two remaining hydrogens will always be different and the proton NMR will show two doublets, one for each of the diastereotopic nuclei.

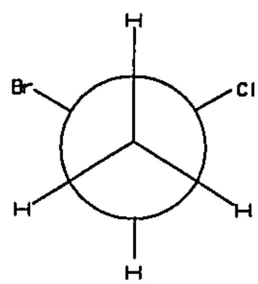

7

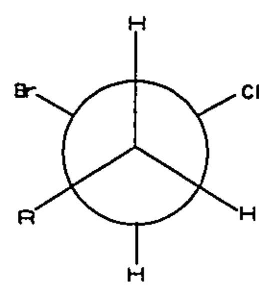

8

1.7 Cluster Stabilized Cations.

Seyferth has established the ability of vinylidene and ketenylidene tricobalt-carbyne clusters to stabilize a positive charge at the α position to their tetrahedral cores.[44] The stability of these complexes may be explained by charge density delocalization onto the carbonyls via direct interaction with a metal centre. Extended Hückel Molecular Orbital, EHMO, calculations performed by Schilling and Hoffmann[55] on $[Co_3(CO)_9C\text{-}CH_2]^+$ predicted the capping group to be preferentially located over the metal vertex as in **9a**, while **9b** in which the methylene bisects the Co-Co vector may provide a pathway in which the capping group could move around the basal triangle, and both of these are more stable than **9c**. The conformation that the structure in solution was **9a** was experimentally proven when

Mislow *et al.* showed the ^{13}C NMR of $[Co_3(CO)_9CCH(CHMe_2)]^+$ to have a single peak for the isopropyl methyls at high temperature but two at low temperature (-65°C). Hence, the methyls must be diastereotopic and the molecule is chiral.[56] The coalescence of the methyls at higher temperature ($\Delta G^{\ddagger}_{221K}$ = 10.5 kcal/mol) reflects the barrier to enantiomerization of the cluster via transition state **9b**.

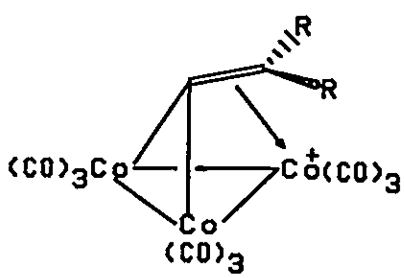

9a

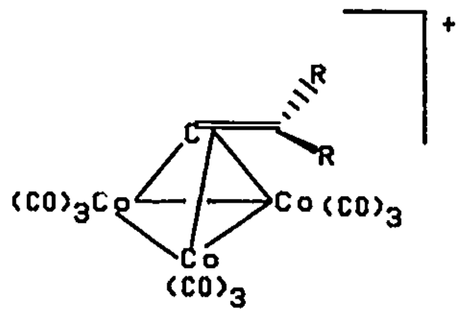

9b

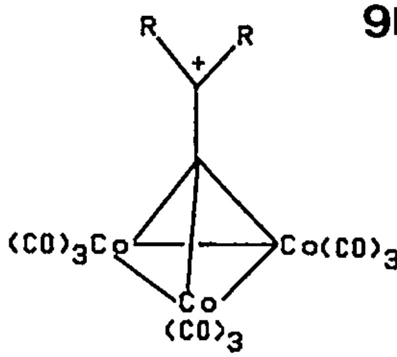

9c

For clusters in which the apical group is a ketenylidene, such as $[Co_3(CO)_9C{=}C{=}O]^+$, the three possible conformations have different symmetries which would impose different splittings in degeneracy in the metals and the carbonyls. The ^{13}CO enriched ^{13}C NMR showed a 6:3 splitting at low temperature indicating either structure **10a** which has C_{3v} symmetry and slowed axial-equatorial exchange or **10b** or **10c** which have C_s symmetry.[57] Since it is unlikely that axial-equatorial exchange would stop, as all evidence points to the barrier to tripodal rotation being very low, the proposed structure is one with bent geometry with the ketenylidene leaning towards one vertex or over the middle of the Co-Co vector. Unfortunately, it is not known for certain which is the predominant conformation in solution, unlike the case of the vinylidene cation.

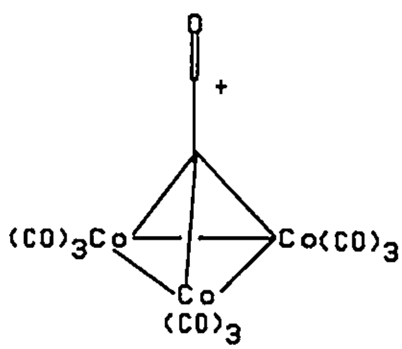

10a

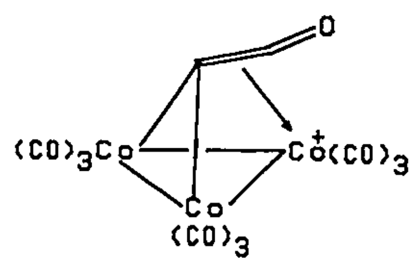

10b

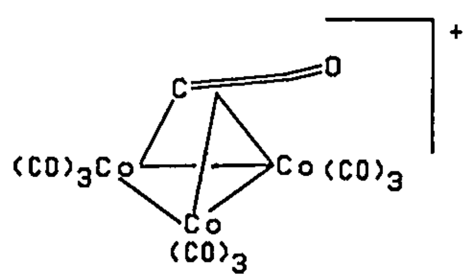

10c

1.8 History of Chromium Complexes.

It was not until 1957 that Anet and Leblanc[58] successfully prepared the first solution of a pure σ-bonded organochromium complex. Hein, however, reported the synthesis of a benzene chromium complex in 1919[59], which later turned out to be the π-complex bis(benzene)chromium, **11**, shown in reaction "a" below.[60,61]

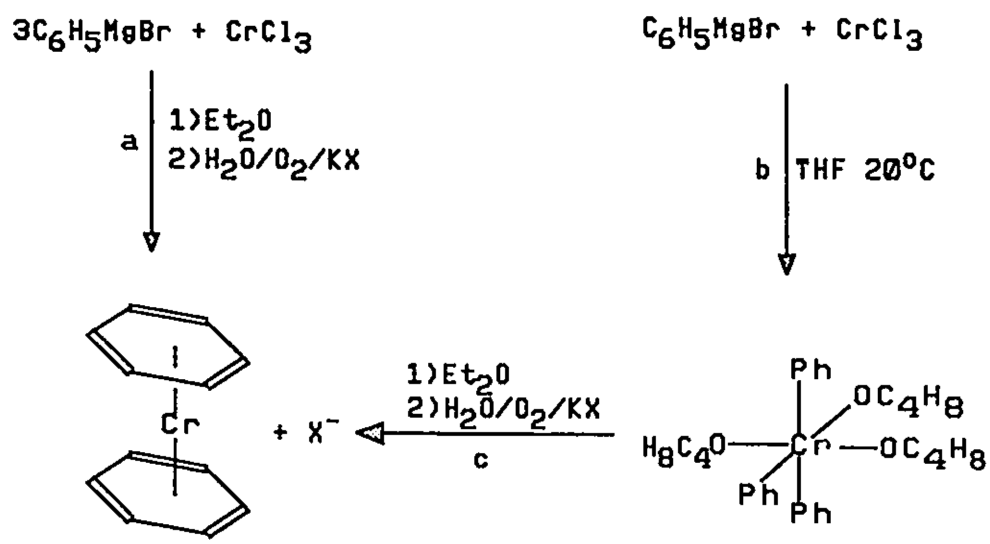

11

Scheme 1.4: Establishment of the link between σ and π-bonded complexes.

Herwig and Zeiss showed that the Grignard reaction described by Leblanc could proceed under milder conditions in THF to yield the σ-bonded tris(phenyl)chromium complex illustrated in reaction "b",[62] from which Zeiss subsequently established a link to the π-complexes (reaction "c").[63,64]

These findings and the synthesis of bis(benzene)chromium by Fischer[65], led the way to organochromium chemistry.

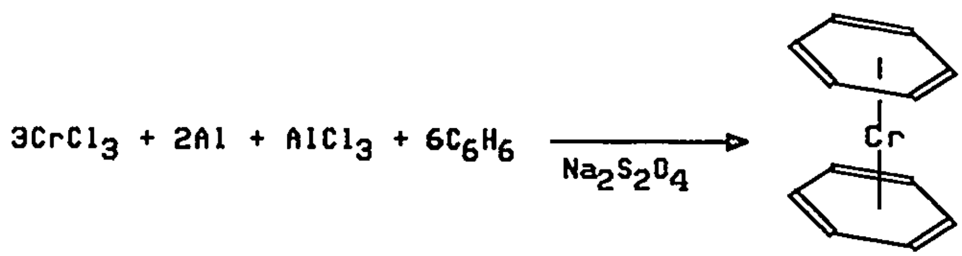

The main focus of this work deals with tricarbonylchromium π-complexes. Nicholls and Whiting[66] found that heating aromatic compounds with $Cr(CO)_6$ under anaerobic conditions in an inert solvent led to the formation of π-(arene)$Cr(CO)_3$ compounds in good yield.

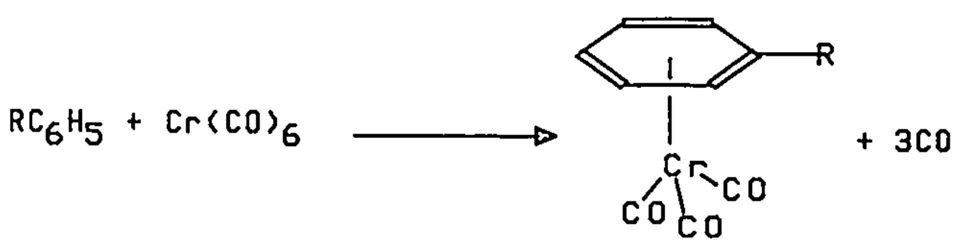

The problem encountered with this synthesis is the volatility of $Cr(CO)_6$ which continuously needs to be replaced in the reaction vessel. The "closed-cycle" apparatus designed by Strohmeier alleviated this difficulty by returning the volatilized $Cr(CO)_6$ back into the reaction vessel.[67]

Studies have shown that a 10:1 solution of n-butyl ether:THF was the most suitable solvent medium for a number of tricarbonylchromium reactions.[68,69] This also eliminates the problem of volatility of the chromium hexacarbonyl since it is soluble in THF. These reactions are, however, limited by the substituents on the arene. It has been shown that the conditions are too drastic to allow π-arene complexes with strong electron-withdrawing groups such as NO_2, COOH, $CH=CH_2$, CHO or CN, to be isolated.[66,70] Chromium complexes bearing some of these subtituents may be formed by combining the substituted arene with $L_nCr(CO)_{c-n}$ (n=1-3) rather than with $Cr(CO)_6$ which requires more energy to remove the carbonyl ligands. Reactions have been carried out using ligands such as picoline[71], pyridine[72] or most often NH_3[73] or CH_3CN[74,75]. These ligands are better leaving groups than CO and are readily replaced by arenes in THF at lower temperatures than required before.

As discussed in the previous section, the ligand donates electrons to the metal which then back-donates electron density into the ligand's π* orbital. The M-CO bonding is "synergic" in that the metal is now slightly more positive because of the loss of some electron density and the metal ligand bond becomes stronger because of the metal's ability to attract the original ligands electrons.[40,76] The arene π electrons donated to the chromium can assist in the back-donation into the π* of the CO ligands.

Infra-red spectroscopy of substituted and non-substituted benzene $Cr(CO)_3$ complexes can be used to illustrate the inductive effect of the $Cr(CO)_3$ on the arene. If the complex has local C_{3v} symmetry, as in most chromiumtricarbonyl complexes, two IR stretches are observed for the CO's, one at 1900-1950 cm^{-1} (doubly degenerate asymmetric vibration (E)) and one at 1970-2000 cm^{-1} (non-degenerate symmetric vibration (A_1)).[77]

In cases where the arene is unsymmetrically substituted, there is a splitting in the IR of the degenerate band, indicating that the local C_{3v} symmetry is restricted. As electron density is back-donated into the CO π^* the C-O bond is weakened and lengthened resulting in a decrease of the IR stretching frequency (υ_{CO}), while the σ bond between the metal and the carbonyl is shortened and strengthened.

The degree of back-donation and IR absorptions are of course sensitive to the electronic effect of the substituent on the arene ring.[78] An electron-donating substituent increases the flow of electron density towards the metal thereby enhancing back-donation to the antibonding orbital while electron-withdrawing groups reduce back-donation.

The π-bound $Cr(CO)_3$ group can withdraw electrons to a similar degree as a para-nitro substituent (pKa values of $C_6H_5CO_2H$ and p-NO_2-$C_6H_4CO_2H$ are approximately the same). The dipole moments of several $Cr(CO)_3$ complexes have been measured and illustrate the re-allocation of electron density. The positive end of the dipole points towards the benzene ring along the C_3 axis and increases with increasing electron-donating substituents.[79,80]

Arene	D
C_6H_6	5.08
C_6H_5Me	5.26
$p\text{-}C_6H_4(Me)_2$	5.52
C_6Me_6	6.48

Table 1.1: Dipole Moments of Selected (Arene)$Cr(CO)_3$ Complexes.

In the proton NMR spectrum, there is an upfield shift of approximately 2 ppm observed for aromatic protons and protons on adjacent alkyl substituents show a shift of 0.2 ppm.[81,82] The ^{13}C NMR also shows a significant shift, the aromatic carbons move upfield 30 to 40 ppm and the CO shifts downfield with respect to the uncomplexed carbonyl case.[83-86]

X-ray studies on π-(arene)$Cr(CO)_3$ complexes show a "piano stool" arrangement of the carbonyls with the $Cr(CO)_3$ directly below the arene ring and the chromium equidistant from each aromatic carbon.[87-89] The Cr-C_{CO} bond distances (1.76-1.85 Å) are always shorter than in $Cr(CO)_6$ (1.92 Å), which is consistent with the arene being a weaker π acceptor than CO. Variability in bond lengths reflects relative electron-donating or electron-withdrawing ability of the substituents on the arene ring. If the substituent is an electron-donating group, electrons are pushed into the π^* orbital of the C=O which lengthens the C-O bond and shortens the M-CO bond. Conversely, for an electron-withdrawing group there is more double bond character in the C=O bond due to less back bonding and subsequently a longer M-CO bond. The arene ring is planar with the hydrogens bent 1.6° out of the plane towards the metal making for better overlap of the carbon 2p orbital with the chromium. The M-C(arene) bond lengths (2.20-2.25 Å) are independent of the electronic nature of the arene substituents.

There are several conformations which can be adopted by the piano stool arrangement of the chromiumtricarbonyl unit. These conformations can be divided up into two main categories, staggered, **12**, which bisects the C-C bond, or eclipsed, **13**, in which the projection of the CO's are directly beneath the aromatic carbons. The unsubstituted (C_6H_6) and fully substituted (C_6R_6, R=Me, Et) arene complexes adopt the staggered conformation. For the mono-substituted benzene complexes, the syn-eclipsed, **14**, and anti-eclipsed, **15**, orientations are favoured depending on the electronic factors of the substituent. If the substituent is electron-donating then conformation **14** is favoured in the solid state; in contrast for electron-withdrawing substituents, **15** is favoured.[87,90,91]

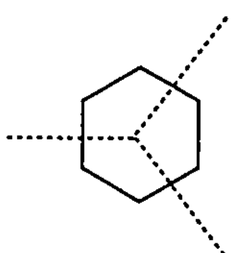

12

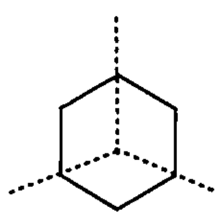

13

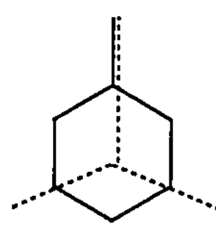

14

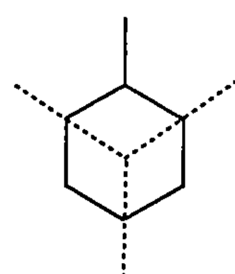

15

In the case of electron-donating groups, the π electron density resides mainly on the ortho and para carbons, the chromium retains its octahedral environment by forming stronger Cr-C bonds to these electron rich positions forcing the CO's to lie directly underneath the substituent.[92] Electron-withdrawing groups on the ring are meta directors which causes the (arene)$Cr(CO)_3$ to adopt a staggered geometry.

The geometry of the disubstituted (arene)Cr complexes also depends on the electron-donating character of the substituents.[93] This case is more complicated because there are three possibilities, ortho, meta and para. Illustrating with the ortho-substitution, three arrangements are preferred, **16**, **17** and **18** in which the eclipsed conformation is the sterically favoured one in which the less bulky group is eclipsed.[93]

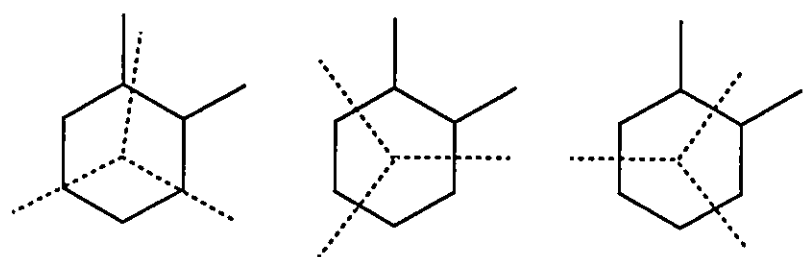

16 **17** **18**

1.9 Reactions of Cr-complexes.

In general, attachment of a metal carbonyl unit to an aromatic compound can have several effects; activation of an aromatic ring to nucleophilic attack, enhancement of the aryl-H acidities, steric inhibition of attack on functional groups from the same side as the metal tricarbonyl and finally, stabilization of negative or or positive charge on the carbon atoms which are α and β to the arene metal moiety.[94,95]

1.9.1 Activation of Aromatic Ring to Nucleophilic Attack and Enhancement of Aryl-H Acidities.

The problems of introducing and later displacing activating groups are not easily solved in organic chemistry. Consequently, fixation of carbon substituents in the synthesis of aromatic natural products by nucleophilic additions are rare. It is possible, however, to obtain the desired product by the combination of a stabilized carbanion with an aromatic moiety and since the addition and removal of $Cr(CO)_3$ is quite facile, it is the reagent of choice.[96] When complexed, the benzene supports a slight positive charge while the $Cr(CO)_3$ group has a negative charge associated with it, thereby leaving the benzene susceptible to nucleophilic attack. Halobenzenes readily undergo nucleophilic substitutions[97,98] due to the electron-withdrawing ability of the $Cr(CO)_3$ moiety which stabilizes the intermediate in an addition-elimination mechanism.[98-100]

As has been shown in Table 1.1, the $Cr(CO)_3$ group has the ability to attract electrons similar to that of a p-nitro group, making the complexed arene much more electron-withdrawing than the uncomplexed arene.

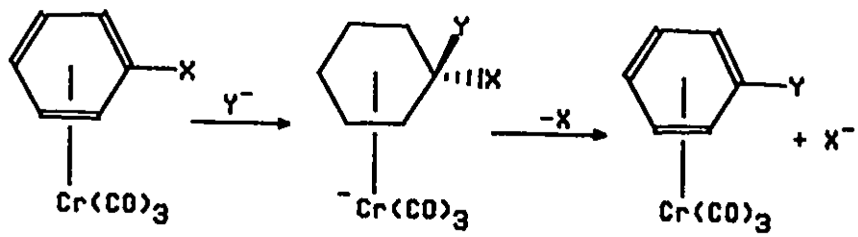

Temporary complexation of the organic moiety also favours proton abstraction from the carbon chain in basic media, which permits alkylation of substrates whose free ligands have little or no reactivity.

1.9.2 Steric Effects.

The first stereochemical consequence of complexation is illustrated below.[101] Arenes that contain different ortho or meta substituents are prochiral. "Metal π-complexes formed from prochiral ligands comprise a planar chiral element which is capable of demonstrating very high chemical differentiation between the two faces of the plane in the ligand."[102]

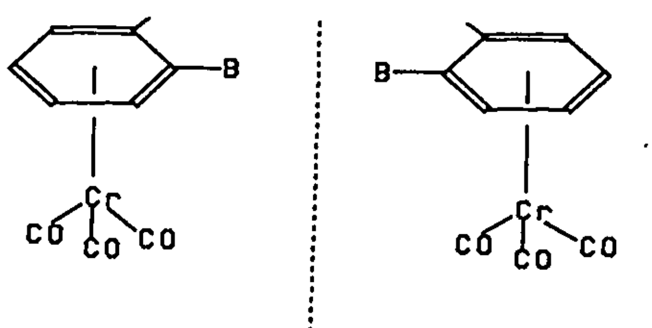

The second consequence of complexation of an organometallic moiety is the possibility of two modes of attack for the reagent, whether from the same side (endo) or opposite (exo) face of the chromium tricarbonyl unit. Due to the bulkiness of the chromium tricarbonyl group, there are some interesting consequences regarding reactions of proximal functional groups in conformationally rigid or cyclic systems. The attack by nucleophiles in cationic arene complexes occurs stereospecifically in an *exo* fashion.

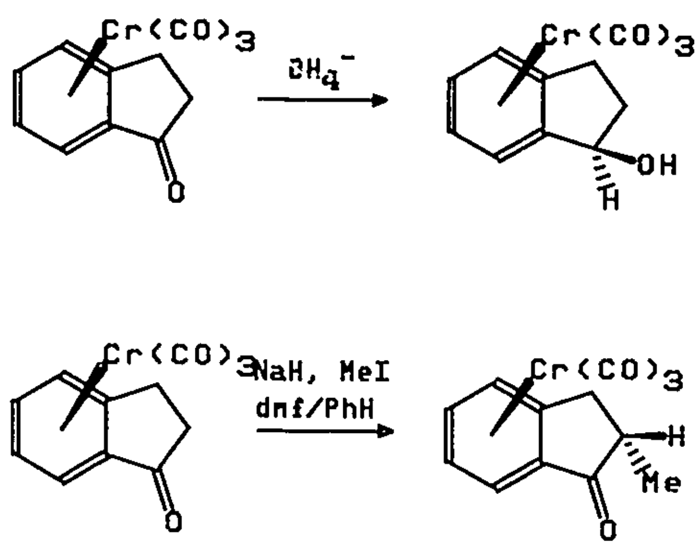

Scheme 1.5: Stereospecific *exo* nucleophilic attack in indanone derivatives.

The stereospecificity of exo attack is shown in indanone derivatives where only the *endo* isomer is obtained.[76,94] The stereospecific nature has been interpreted as a phenomenon of steric control due to the bulky chromium tricarbonyl group, yet, electronic factors cannot be ruled out.[103] The powerful withdrawal of electron density from the aromatic ring has been noted by several authors.[101,104,105] This appears to be responsible for the significant enhancement of acidity of benzylic hydrogens in η^6-(alkylarene) metal complexes observed for the $Cr(CO)_3$ series.

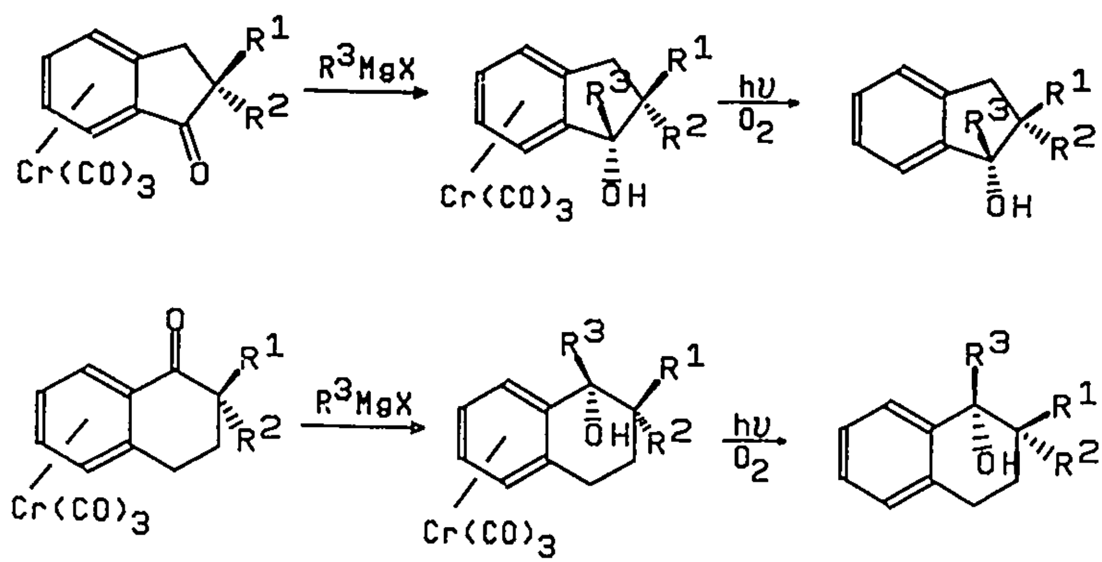

Scheme 1.6: Preparation of optically active indanols.

In the reduction of indanones, the alcohols are always cis to the chromium tricarbonyl unit. Thus, decomplexation leads quantitatively to indanols of well-defined configuration and as a result optically active indanols may be prepared. The first example of optically pure indanol was that of 3-methyl-1-indanols.[106] Since then, several optically pure indanols have been prepared.[40,107,108] Even in cases where there are alkyl substituents in the position α to the indane carbonyl, attack occurs from the opposite side of the metal tricarbonyl unit as shown in Scheme 1.6. The preparation of optically active ketones has always been tedious and rather difficult. Indanones readily undergo substitution at the carbon alpha to the ketonic group to produce mono- and di-alkyl derivatives. The preparation of optically active ketones becomes even more troublesome when the asymmetric centre alpha to the carbonyl group possesses a hydrogen atom which, potentially, can racemize. The use of chromium tricarbonyl derivatives can overcome this difficulty and mono-methylation occurs stereospecifically in an exo manner. Scheme 1.7 illustrates the stereospecific exo attack to produce the optically pure 2-methyl-indanone complex.[40] These complexes readily and quantitatively decomplex with sunlight in air which destroys the planar chirality leaving the enantiomerically pure aromatic ligand.

The second methyl attack to form the dimethylated species also occurs in an exo fashion and only on the endo isomer which is present in the basic medium by an equilibrium through the enolic form. Thus, it is not necessary to use the pure isomer, an exo/endo mixture may be used and its enantiomer may be formed simply by changing the introduction of substituents. Scheme 1.8 shows the introduction of the second alkyl group onto the disubstituted species.[101]

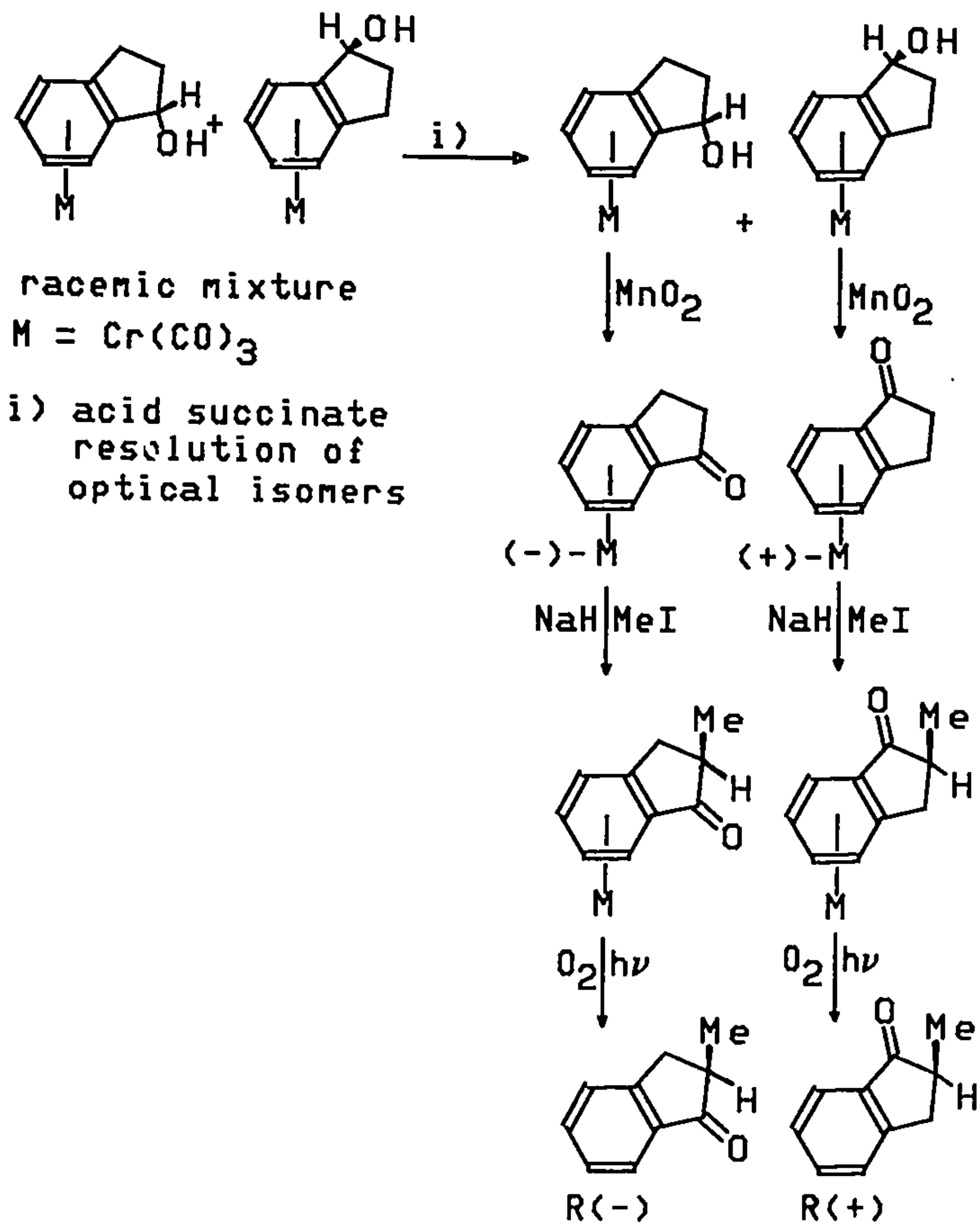

Scheme 1.7: Synthesis of optically pure 2-methylindanone.

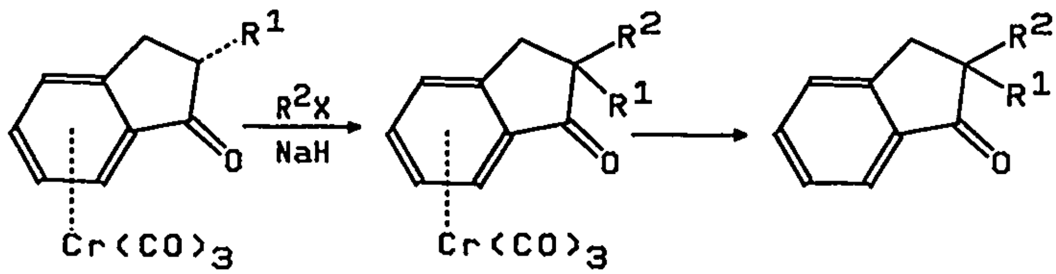

Scheme 1.8: Introduction of a second alkyl group onto the disub' ituted indanone.

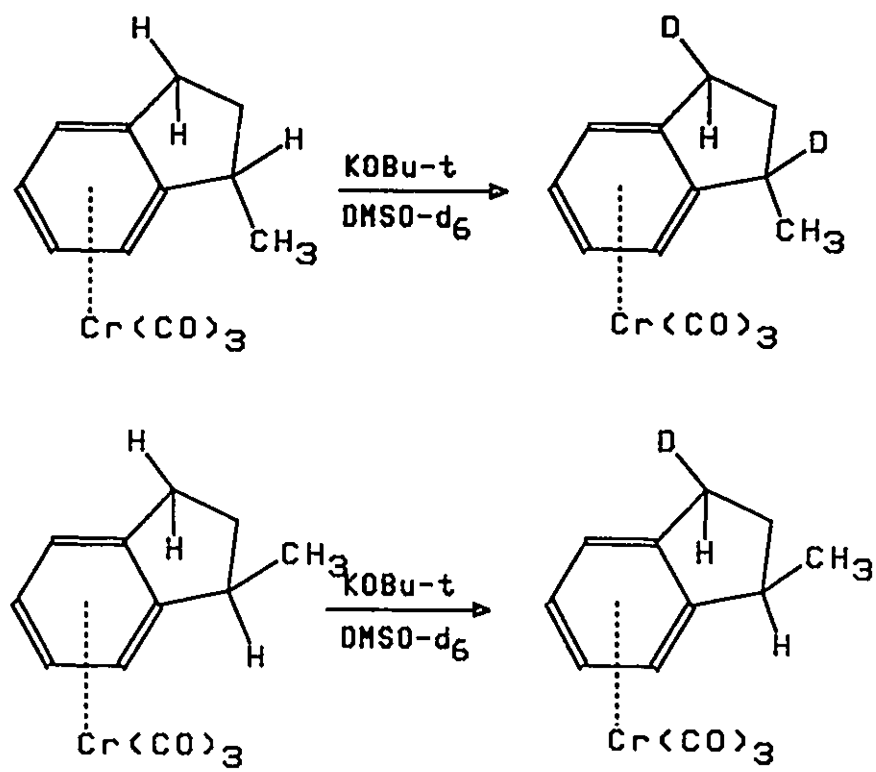

Scheme 1.9: Base-catalyzed stereoselective hydrogen-deuterium exchange of benzylic protons of alkylbenzene chromiumtricarbonyl complexes.

Similarly, base-catalyzed stereoselective hydrogen-deuterium exchange of benzylic protons of chromium tricarbonyl complexes of alkylbenzenes has been accomplished. Only benzylic protons which are anti to the metal atom of syn-methyl and anti-methyl isomers undergo exchange, once again illustrating the stereochemical effect of the chromium tricarbonyl moiety.[109]

Jaouen who pioneered much of this work, had also looked at annulation reactions of chromium tricarbonyl complexes of indanone and tetralone derivatives.[110] These reactions were found to occur in a stereospecific manner as well.

The use of chromium tricarbonyl as a blocking substituent to direct attack on a particular side of a molecule has been illustrated by indanol and indanone derivatives. Since removal of the metal results in the loss of planar chirality, the result would be of no interest to the organic chemist unless a second chiral centre is present or the original complex is optically active. Since biological processes often involve chiral reactions, the potential use of asymmetric reagents modeled on enzyme systems is apparent.[111]

The most useful enzymes are those which can accept a broad range of substituents while maintaining their stereospecificity under mild conditions.[112] Thus, combining the higher efficiency enzymatic catalysis with the features of planar chiral complexes to give optically active organometallic synthons may be of interest. Much of this was demonstrated in section 1.1 on steroidal derivatives.

1.9.3 Stability of Benzylic Cations and Anions.

The ability of $Cr(CO)_3$ to stabilize anions,[113-120] and cations[121-126] at benzylic positions has been studied by several workers.

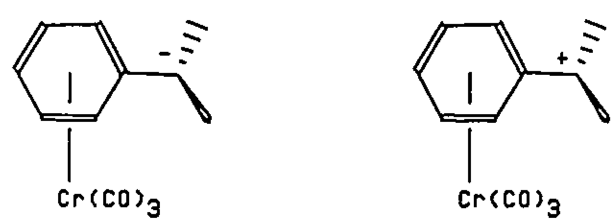

Attaching an electron-withdrawing $Cr(CO)_3$ group to the aromatic ring increases its susceptibility to proton abstraction from the exocyclic carbon chain. The increased ability to form anions allows electrophilic attack of arene complexes towards which the free arene has little or no reactivity. The reaction of (diphenylmethane)-$Cr_2(CO)_6$ with NaH in DMSO to form the more stable α-anion is shown below.[120]

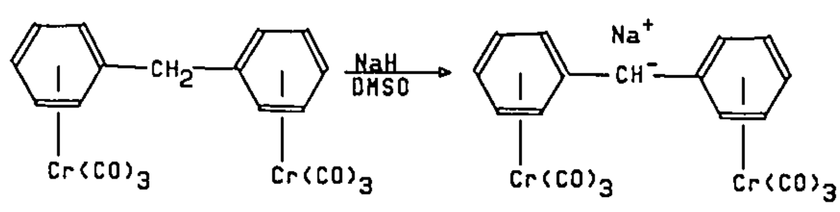

The ability of metal carbonyls to stabilize benzylic carbocations is also useful for synthetic purposes. Carbocations such as **20** can be formed by treating their corresponding alcohols, **19**, with HPF_6/CH_2Cl_2 (Scheme 1.10).[127,128]

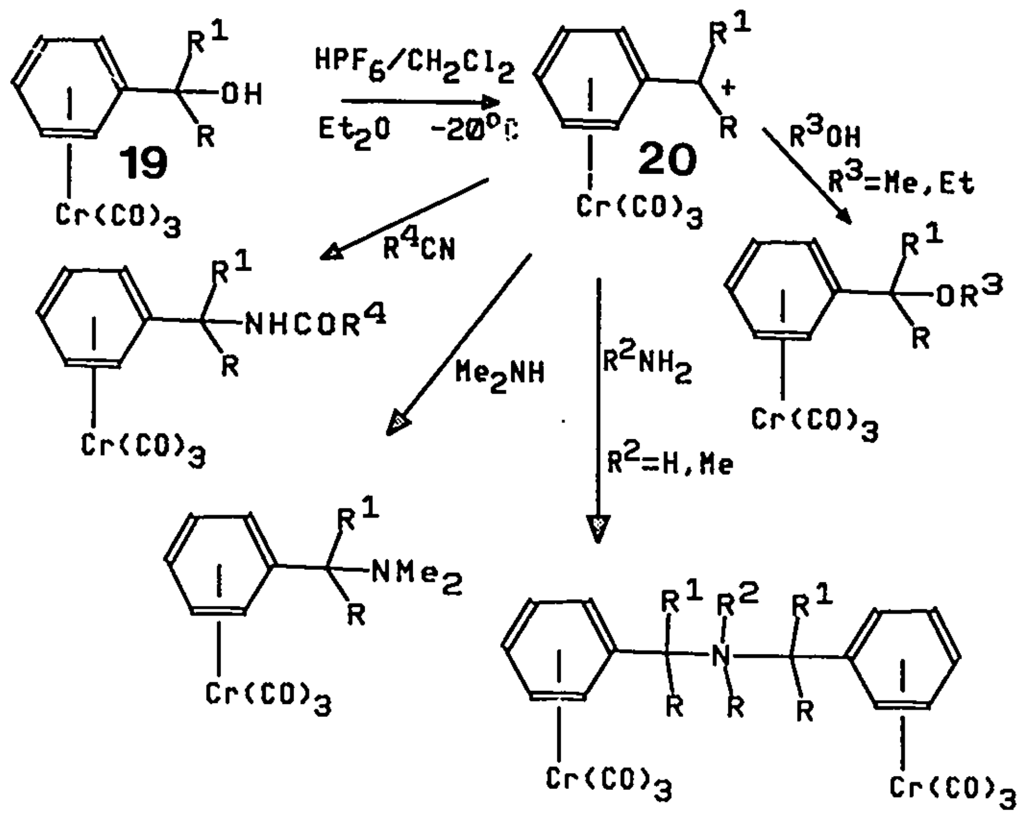

Scheme 1.10: Selected reactions of substituted phenylchromiumtricarbonyl complexes.

CHAPTER 2

VERTEX ROTATIONS

2.1 Introduction.

2.1.1 Dimetallic Tetrahedral Clusters.

The molecular structures and fluxional behaviour of the type $Cp_2(CO)_4M_2(RC{\equiv}CR')$, where M = Mo or W, were first described by Cotton et al.[51] The crystal structure revealed the presence of a semi-bridging carbonyl unit[51], which was also confirmed by ^{13}C NMR. General routes to the synthesis of tetrahedral clusters have already been outlined in section 1.5. A series of clusters of the general type $[(C_5Me_xH_{5-x})M(CO)_2]_2[RC{\equiv}CR']$ where M=Mo or W, and x=0,1, or 5, were prepared by McGlinchey and coworkers and the variable-temperature NMR spectra recorded.[51,52] The ^{13}C NMR of the analogous cluster with R=H,R'=Ph also revealed three terminal and one semi-bridging CO environments. At low temperature, the ^{13}C NMR also showed the cyclopentadienyl units of these two clusters to be magnetically non-equivalent. As the temperature was increased, exchange between terminal and semi-bridging CO's was observed.

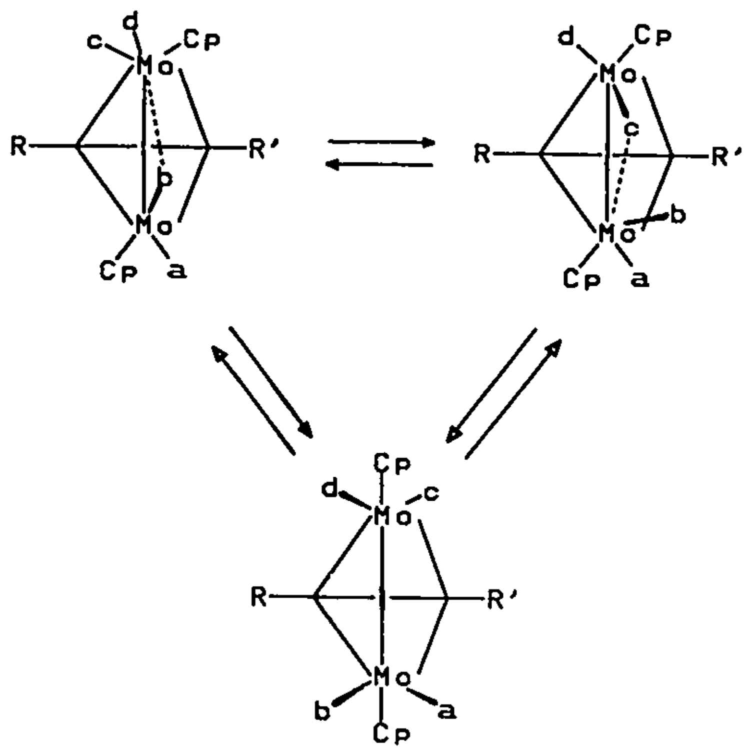

Scheme 2.1 Exchange process which interconverts carbonyl ligands in semi-bridging and in terminal environments.

The fluxional process illustrated above can be considered to have time-averaged C_{2v} symmetry for symmetrical alkynes (i.e. R=R') (1 CO environment, 1 Cp environment) and C_s symmetry for the asymmetric alkyne (2 CO environments (b=d,a=c), 1 Cp environment). Analogous studies have shown that all clusters of a series of methyl-substituted cyclopentadienylmolybdenum complexes exhibit the same fluxional behaviour.[52] Studies carried out on similar W complexes containing symmetrical and asymmetrical alkynes only showed 1 CO and 1 Cp environment even at -100°C on a 400 MHz NMR spectrometer. The IR data, however, were able to show the presence of semi-bridging carbonyl, indicating a much lower fluxional barrier in the tungsten complex than the molybdenum complex. Clearly, the ability to detect the semi-bridging carbonyl on the IR spectrometer and not on the NMR spectrometer depends on the time scale of the spectroscopic technique being utilized (IR $\approx 10^{-13}$ sec and NMR $\approx 10^{-1}$-10^{-9} sec).[53]

There are two exchange processes which have been characterized for the R=R' case. The first has an activation energy of approximately 8 kcal mol^{-1}. This was suggested to involve a twitching motion by which a semi-bridging carbonyl on one molybdenum and a terminal carbonyl ligand on the other molybdenum are equilibrated; the effective symmetry would then be C_2 rather than C_1 and this process would also interconvert the two cyclopentadienyl environments as shown in Scheme 2.1. The observation of a single ^{13}CO peak requires that the time averaged symmetry be raised to C_{2v} as would be the case if partial rotation of the $CpMo(CO)_2$ group were to occur; this barrier ranges from 9.5 - 12.5 kcal mol^{-1} depending on the steric bulk of the substituents borne by the cyclopentadienyl ligand.[52,54] It is apparent that if R $\neq$ R', the maximum symmetry attainable is C_s and four ^{13}CO resonances will be observed at low temperature and at best two resonances would be observed even when the fluxional processes are fast at high temperature. If one of the alkyne substituents is chiral, the four carbonyls are always non-equivalent. Likewise in a molecule such as **21**, where the alkyne bears a hormonal steroid as one of the substituents, the Cp group will also retain its chemical shift difference.

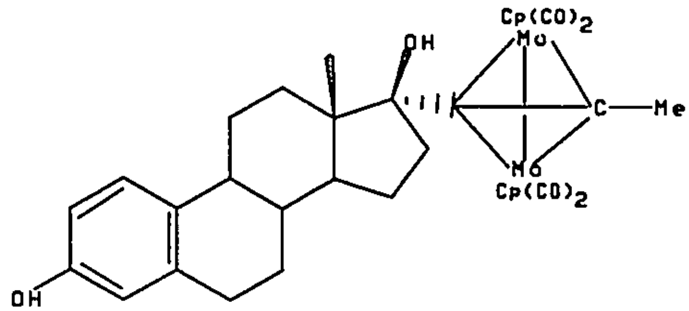

21

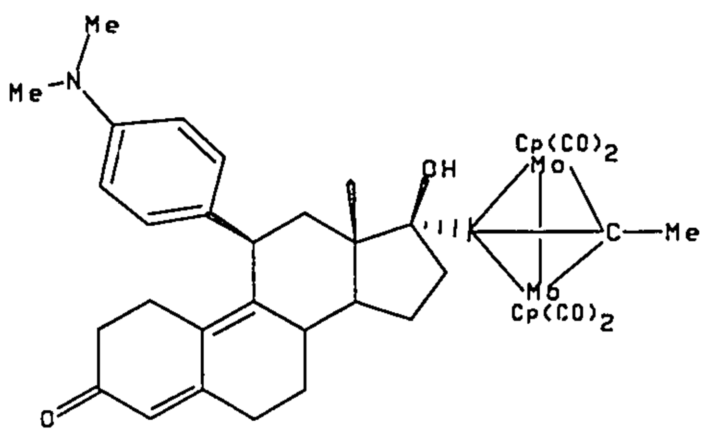

22

2.2 Statement of the Problem.

Carbon-13 NMR has been used to study $(\eta^5\text{-}C_5H_5)_2Mo_2(CO)_4$ complexes of chiral alkynes derived from a terpene or hormonal steroid. At low temperature, the interconversion of diastereomers arising from the different orientations of the semi-bridging carbonyl ligand can be slowed on the NMR time-scale. The barrier to diastereomer interchange has been determined for the terpenoid cluster and the mechanism of this process is discussed.

The diastereotopic character of the metal centres is reflected in the NMR spectra of molecules **21** and **22** each of which gives rise to two cyclopentadienyl resonances in both the ^{1}H and ^{13}C regimes.[129] We were particularly intrigued by the observation that these pairs of Cp peaks were further split on cooling thus indicating the presence of more than one diastereomer. The following is a variable-temperature NMR study carried out to clarify and extend these observations.

2.3 Results and Discussion.

As shown in Figure 2.1, the ^{1}H NMR spectrum of **22**[130] in the cyclopentadienyl region changes quite noticeably upon lowering the temperature from 20°C to -40°C. The low temperature spectrum clearly shows the presence of two molecular species in an 80:20 ratio. Upon increasing the temperature, these two species are equilibrated and the four cyclopentadienyl resonances coalesce to yield only two peaks.

As shown in Figure 2.2, the ^{13}C NMR spectrum of **22**[130] recorded at -40°C

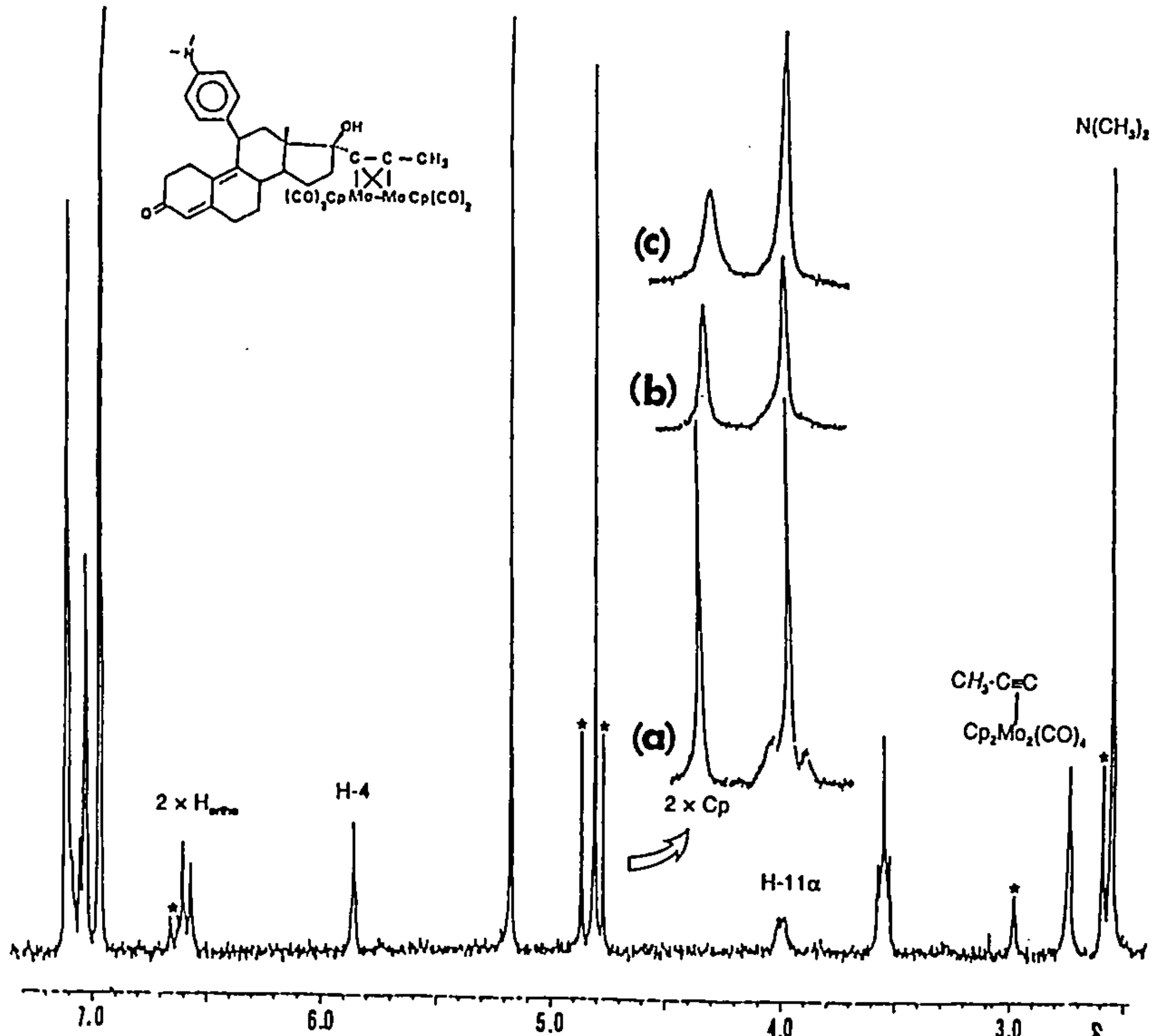

Figure 2.1 Section of the ^{1}H NMR spectrum of **22** at -40°C, (a) at 2°, (b) at 10° and (c) at 20°

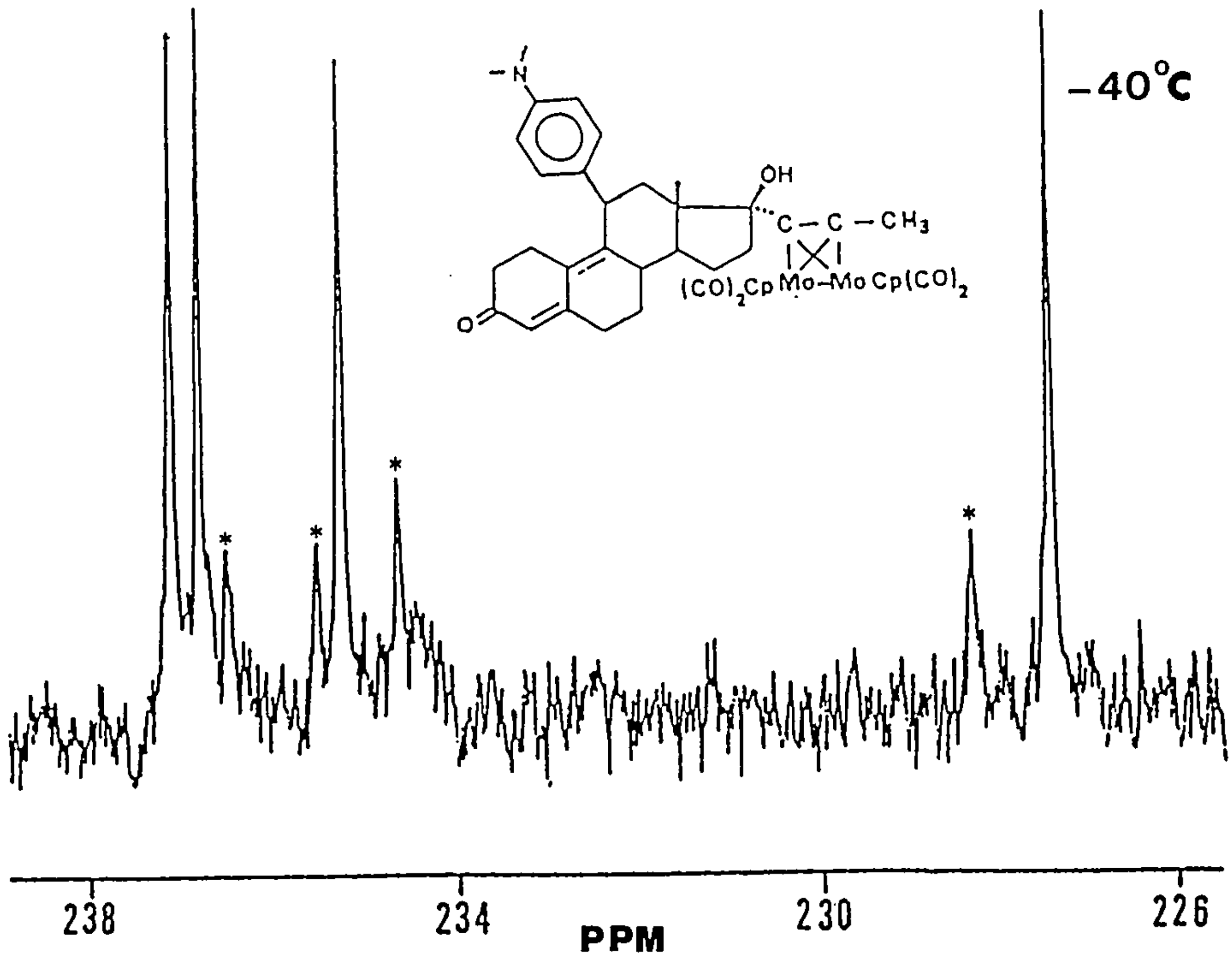

Figure 2.2 Carbonyl region of the ^{13}C NMR spectrum of **22**. The asterisks refer to the minor diastereomer.

reveals the anticipated eight resonances in the metal carbonyl region; four of these ^{13}CO peaks are assigned to the major diastereomer and the other four to its less abundant partner. Further examination of the ^{1}H spectra reveals that one of the C_5H_5 rings in the major diastereomer is markedly deshielded from the remaining cyclopentadienyl protons; one is led to the suspicion that this particular Cp ring may be situated near the edge of the aromatic ring attached to C-11 of the steroid and so lies in the deshielding region of the diamagnetic anisotropy associated with the arene. This idea is buttressed by the observation that the resonances attributable to the Me_2N group and also the ring protons *ortho* to this substituent are clearly separated in the two diastereomers. Furthermore, these chemical shift differences are detectable not only for the methyl groups situated at C-13 but also for the CH_3's attached to the alkyne which are likewise split in a 4:1 ratio at low temperature. Clearly, X-ray crystallographic data would be valuable in elucidating the detailed structures of these diastereomers. These observations are relevant to the recent report describing the variable-temperature NMR spectra of the alkyne cluster $[(C_5H_5)_2Mo_2(CO)_4(HC{\equiv}CR)]^{+}$, where R is a cationic steroidal substituent.[131] In this cation there are intimations of a very low energy fluxional process in which extra cyclopentadienyl resonances are observed. Subsequently, there has been speculation about the possibility of evaluating the barrier to rotation of the $(C_5H_5)Mo(CO)_2$ vertices.[132]

The results of these variable-temperature NMR experiments prompted

McGlinchey and coworkers to look in more detail at another di-molybdenum cluster in which the alkyne possessed a chiral substituent. D'Agostino et al. have recently described convenient routes to a variety of chiral di-cobalt, di-molybdenum or di-tungsten clusters as well as those containing Co-Mo or Co-W units.[133,134] Molecules such as **23** or **24** are obtainable in multigram quantities by reaction of the appropriate organometallic precursor with 2-propynylborneol, as in Scheme 2.2. Furthermore, ^{13}CO enrichment of **23** is a straighttorward process and greatly facilitates the acquisition of the variable-temperature spectra.

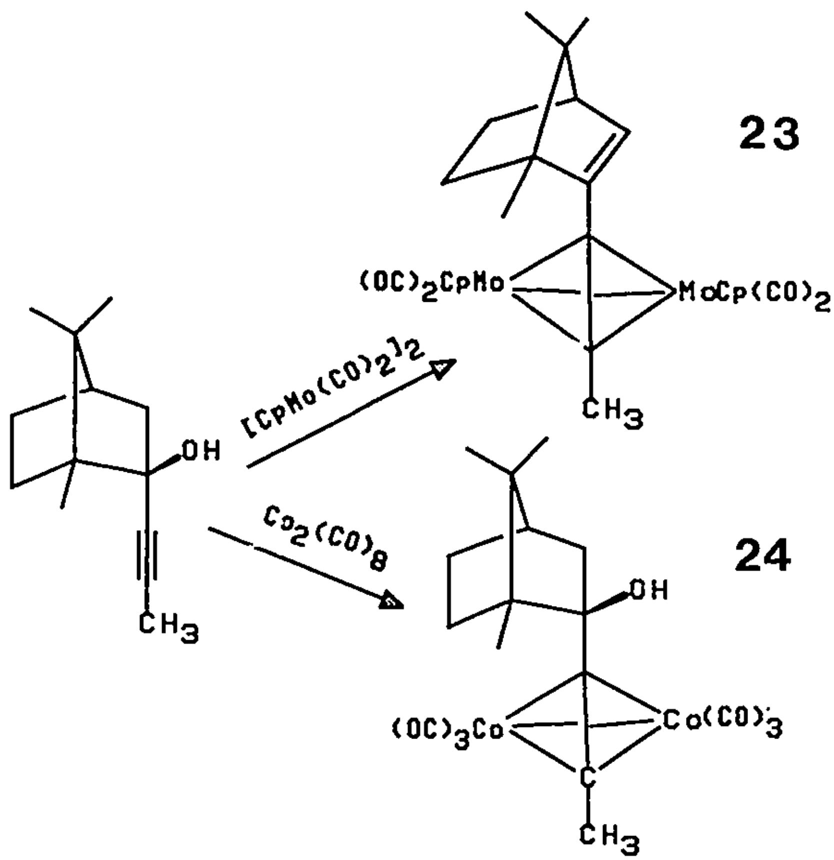

Scheme 2.2 Synthetic routes to chiral clusters.

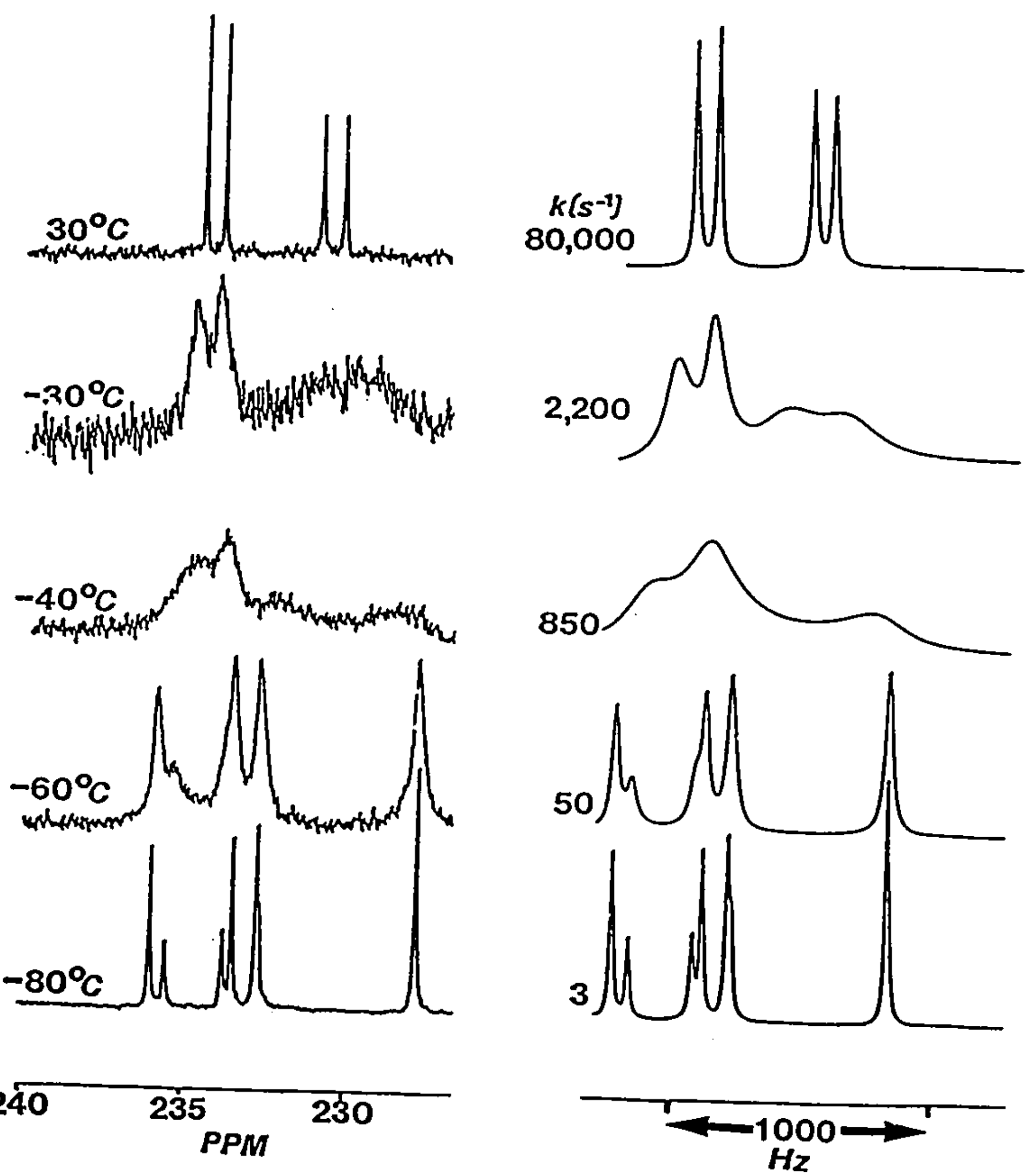

Figure 2.3 Variable-temperature ^{13}C NMR spectra and simulated spectra of **23**.

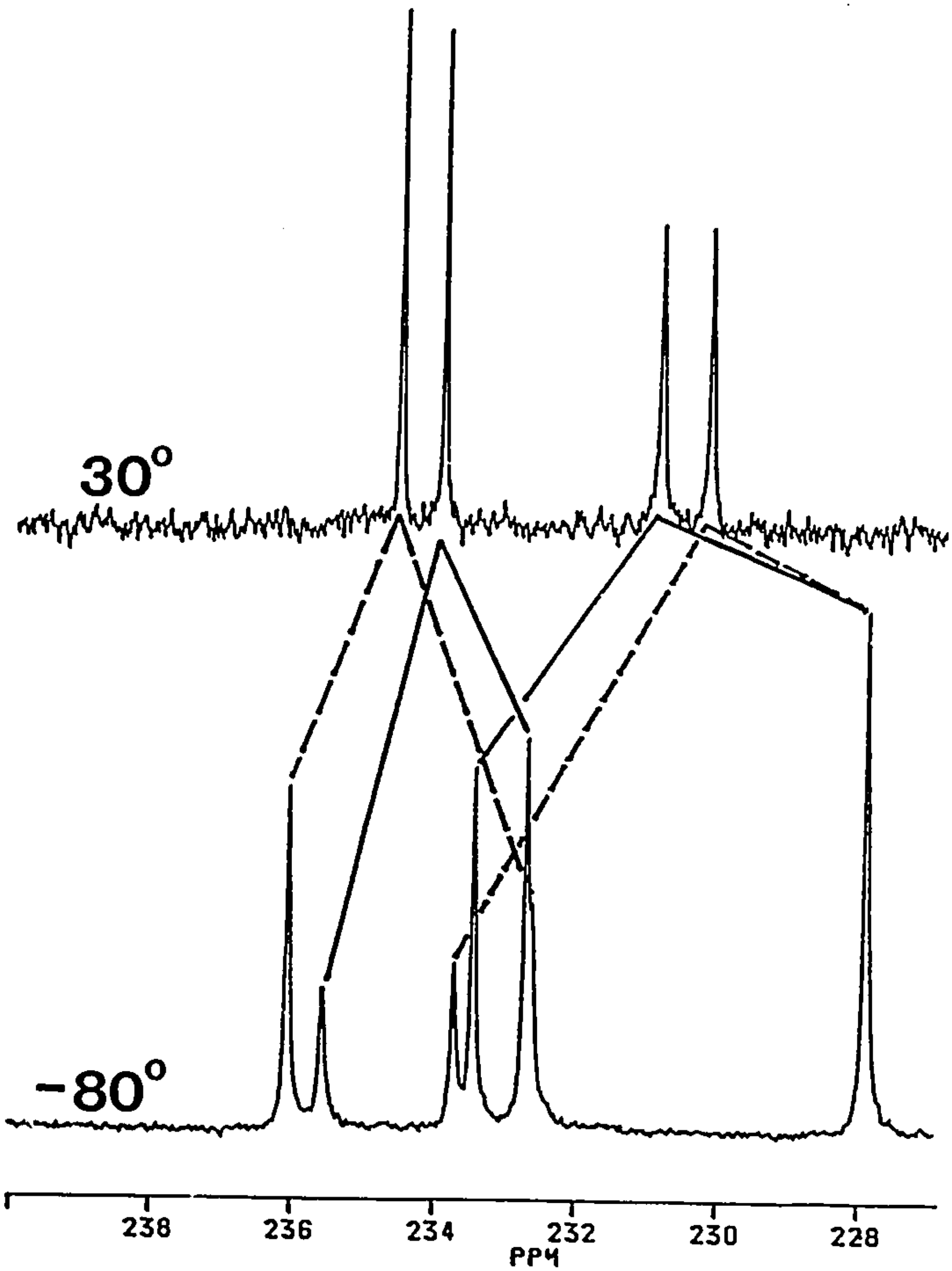

Figure 2.4 Interchange of ^{13}CO resonances in different environments of **23**.

The ^{13}C NMR spectrum of **23** has been recorded over the temperature range +30°C to -80°C and a selection of these spectra appear in Figure 2.3, together with those simulated by using the program EXCHANGE. There is a coalescence phenomenon which interchanges pairs of ^{13}CO resonances in quite different environments (see Figure 2.4). This is in complete accord with Cotton's original proposal in which a semi-bridging carbonyl on one metal exchanges with a terminal CO ligand on the other metal. The X-ray crystal structure of **23** appears as Figure 2.5 and reveals that the three terminal carbonyl ligands are oriented very differently with respect to the terpenoid substituent[132] and so would be expected to have noticeably different chemical shifts. The crystallographically characterized molecule is presumably the major diastereomer and the minor isomer can arise simply by invoking semi-bridging of a different carbonyl ligand. The activation energy barrier for this fluxional process (obtained from a knowledge of the experimental temperatures and the rate constants given by the spectral simulations) is 11.2 ± 0.4 kcal mol^{-1} and is in the range found for other systems with modestly large steric requirements.[52]

In this case the simulation is non-trivial since the relative populations of major and minor diastereomers change with temperature; that is, the simulation requires a knowledge not only of the rate constant but also of the equilibrium constant at each temperature for which the experimental data are available. The ratio at the low temperature limit is of course directly measurable from peak

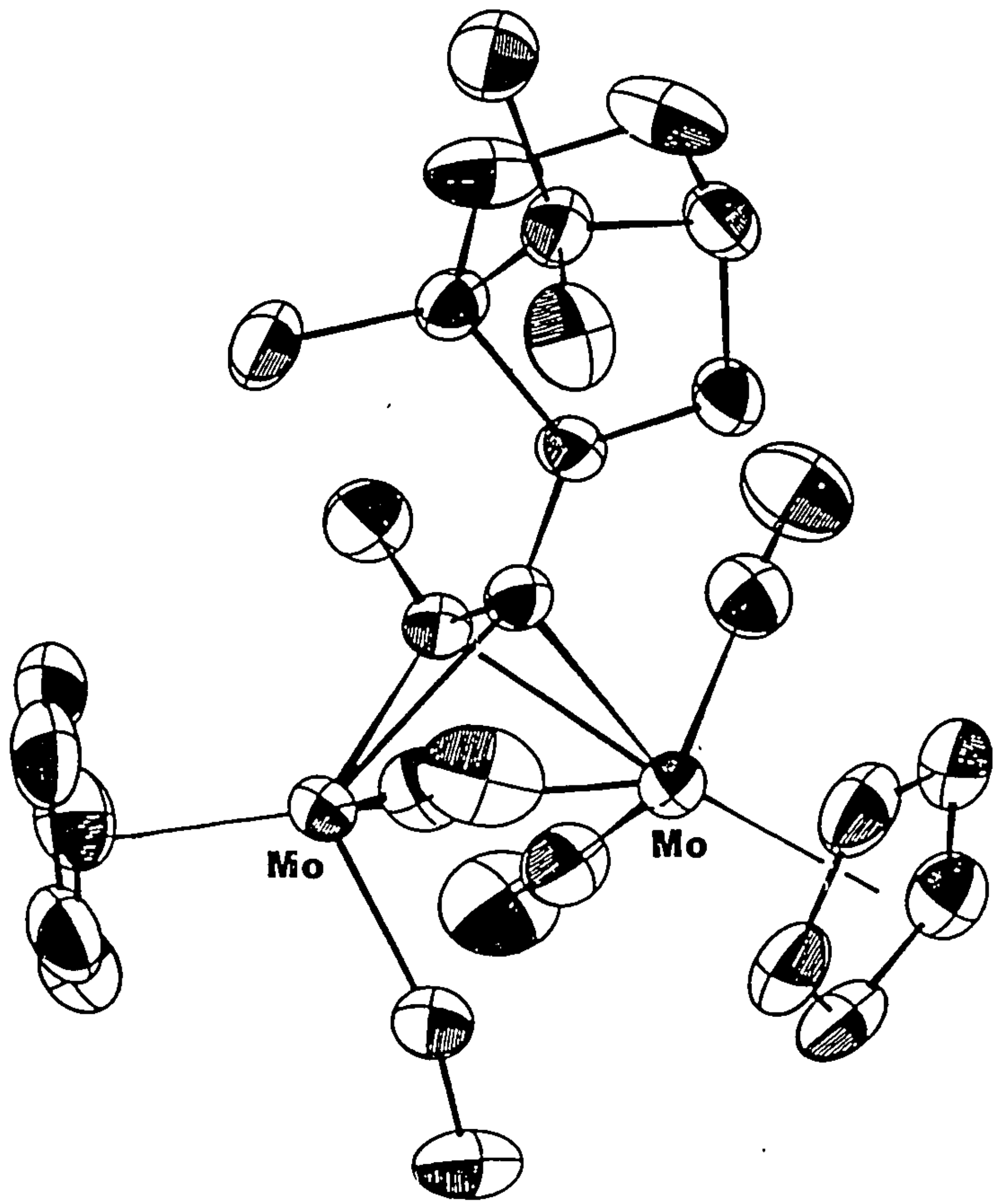

Figure 2.5 X-ray crystal structure of **23**.

intensities; the diastereomer ratio at +30°C is calculable from the peak positions which reflect the weighted average of the chemical shifts of the individual molecules. The equilibrium constants for the intermediate temperatures were obtained by interpolation of the measured values at -80°C and 30°C; these data allowed the simulation of the variable-temperature NMR spectra, shown in Figure 2.3, and yielded the above-mentioned activation energy of 11.2±0.4 kcal mol^{-1}. The variation of K_{eq} with temperature corresponds to a preferential stabilization of one of the two diastereomers by ≈ 0.2 kcal mol^{-1}.

As noted already, this chemical exchange process involves not merely the carbonyl ligands but also requires the swivelling of the $CpMo(CO)_2$ fragments so as to interconvert enantiomers (when $R^1 = R^2$) or diastereomers (when one of the R groups is chiral, as in the present case). The more fundamental question perhaps concerns the course of the molecular rearrangement which interconverts the rotamers **A** and **B** in Scheme 2.3. The low energy twitching process generates a pair of molecules each of which has effective C_2 symmetry; that is, when $R^1 = R^2$ we have an enantiomeric pair which must be equilibrated by the high energy process. Thus when both processes have high rate constants the time-averaged symmetry is C_{2v}. However, this does not mandate that the molecule actually adopt the C_{2v} geometry during the course of the rearrangement. Indeed, such a transition state would be disfavoured on entropic grounds since this would require a synchronous swivelling motion of both $CpMo(CO)_2$ groups about imaginary axes joining each molybdenum to the tetrahedral center. One possible technique is to use the Bürgi—Dunitz approach in which the crystal structures of a large number of closely related molecules are analyzed.[135] By this means one can obtain a profile of the reaction pathway whereby a suitably arranged series of structures maps out the trajectory followed by the interacting species. This method has been adopted by Crabtree and Lavin who showed that there is a gradual bending of a carbonyl ligand (*i.e.* a decrease in the M=C=O bond angle) as it migrates from a terminal to a bridging environment.[136] While the detailed analysis of more than a dozen crystal structures is deferred to the following section, we note that the published data on molecules of the type $[CpM(CO)_2]_2(X{\equiv}Y)$, where M = Mo or W, and X≡Y can be RC≡CR, $RC{\equiv}ML_n$, As≡As, P≡P, RN≡C, etc., are of the C_2 or C_S types rather than the C_{2V} structures (see Scheme 2.3).

One might conclude that the reaction proceeds *via* successive rotations of single $CpM(CO)_2$ vertices rather than by concerted motion of both. These conclusions are supported by EHMO calculations which are discussed in the following chapter.

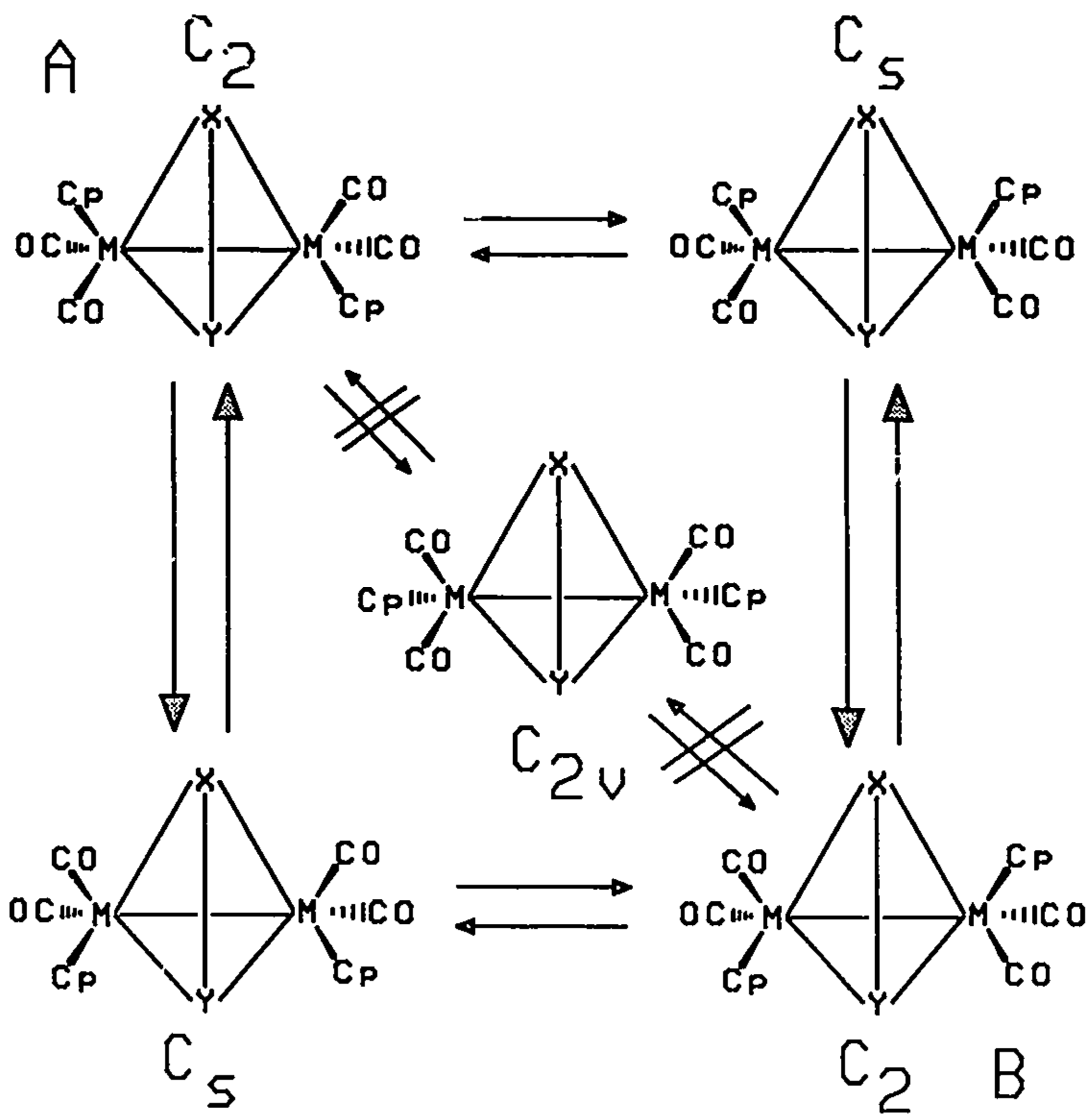

Scheme 2.3 Proposed mechanism of interconversion of enantiomeric clusters *via* C_s rather than C_{2v} intermediates.

CHAPTER 3

VERTEX ROTATIONS IN METAL CLUSTERS - AN EHMO STUDY

3.1 Introduction.

3.1.1 Trimetallic Tetrahedral Clusters

A large number of methynyltricobalt enneacarbonyls of the type $XCCo_3(CO)_9$, (where X=halogen, alkyl, aryl, acyl, etc.), and which have a tetrahedral core possessing the Co_3C unit, have been prepared since 1958.[42] The crystal structure of this type of complex, which was first solved eight years later, showed that 3 CO's were axial while the rest were equatorial and bent out of the plane of the metals towards X.[137]

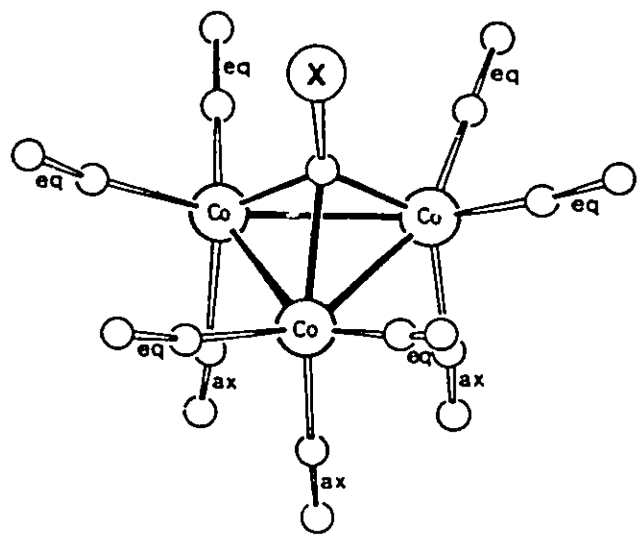

Stone[138] and Vahrenkamp[139] reported the crystal structures of trimetallic tetrahedral clusters in which one of the $Co(CO)_3$ vertices in the tetrahedron had been replaced by an $M(CO)_2(C_5H_5)$ unit where M is either Mo or W; this illustrates the concept of isolobality. In each of these first two structures, $(C_5H_5)W(CO)_2$-$Co_2(CO)_6C(4\text{-}CH_3C_6H_4)$, **25a**, and $(C_5H_5)Mo(CO)_2Co_2(CO)_6C\text{-}C_6H_5$, **25b**, the Cp ring is pseudo axial, and below the plane of the metals, and the alkynyl group caps the tetrahedron. The authors, however, saw too many carbonyl stretching vibrations in the IR spectra for just a single isomer and hypothesized that there may be rotational isomers in which the Cp ring adopts either a proximal ("up") or distal ("down") position. The crystal structure of $Rh_2W(\mu_3\text{-}CC_6H_4Me\text{-}4)(acac)_2(\mu\text{-}CO)$-$(CO)_2(\eta\text{-}C_5H_5)$, **26**, showed the Cp group to be proximal with respect to the capping group.[138] It was apparent that the Cp group could adopt other orientations. Subsequently, Stone prepared an iron-tungsten complex, **27**, in which the Cp ring occupied an equatorial position.[140] Farrugia et al. described the crystal structure of $Fe_3(CO)_6(\mu\text{-}CO)_2\text{-}(\eta\text{-}C_5H_5)C\text{-}OCH_3$, **28**, which possesses approximate mirror symmetry with respect to the Fe_3C skeleton, CO's and the Cp ring. In this case the Cp ring makes an angle of 21.1° from the Cp-centroid to the Fe_3 plane.[141]

In 1987, Sutin *et al.* reported that the low temperature ^{13}C NMR spectrum of $(C_5H_5)MoCo_2(CO)_8C\text{-}CO_2{}^iPr$, **29**, revealed the presence of two species which were assigned as those rotamers in which the cyclopentadienyl ring was sited (i) below the trimetallic plane, as in **30a**, and (ii) above the metal triangle and

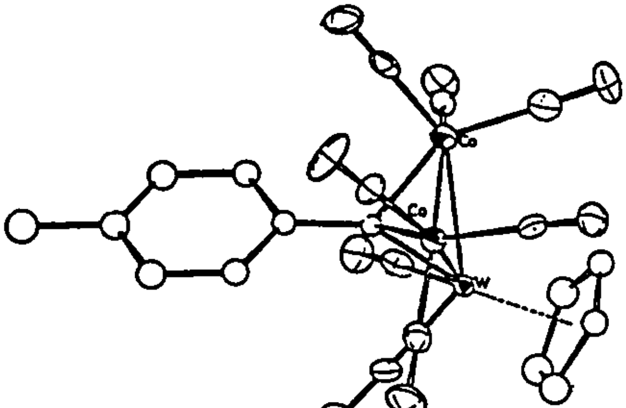

25a

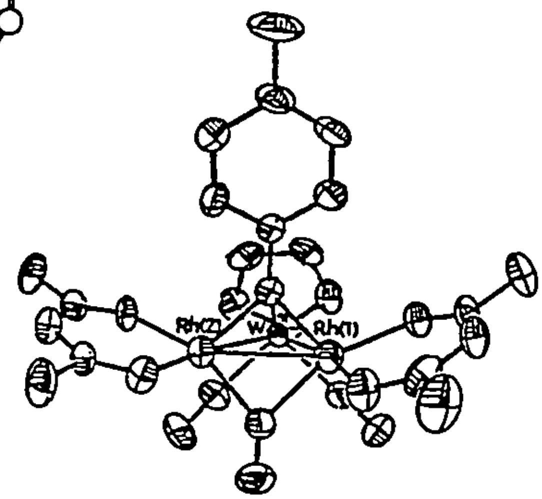

26

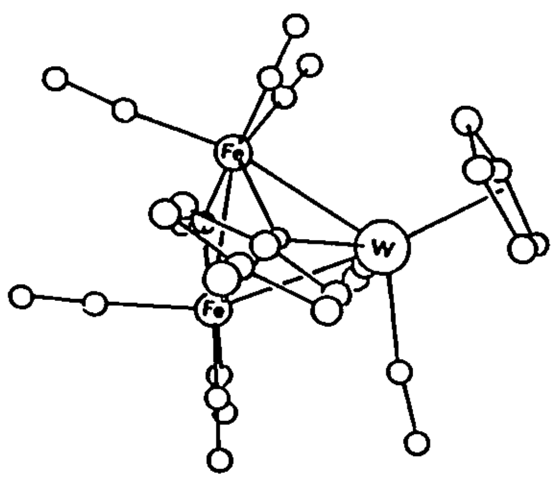

27

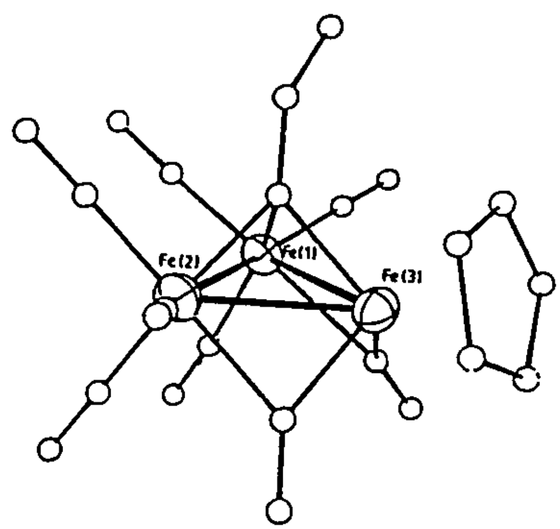

28

proximal to the carbynyl capping group, as in **30b**.[142] The rotational barrier for the interconversion of rotamers **30a** and **30b** is approximately 8.5 - 10 kcal mol^{-1} depending on the nature of the substituents at the carbynyl capping position and within the cyclopentadienyl ring.[143]

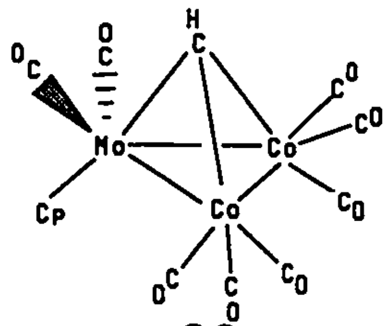

30a

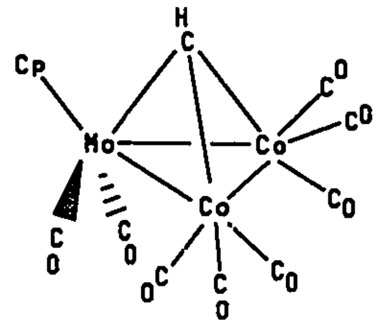

30b

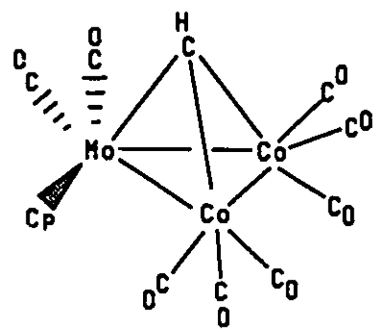

30c

At ambient temperatures, there was a single peak in the CO region of the ^{13}C NMR. At lower temperatures, intermetal exchange has stopped and the CO's are localized. The chemical shift of cobalt carbonyls is approximately 200 ppm, while for molybdenum or tungsten it is between 220 and 240 ppm. There are also two isomers present in the limiting ^{13}C NMR spectrum; a major and a minor isomer in a ratio of 3:1 in the region Mo or W : Co. Since only one peak is present at higher temperatures, the two isomers must be interconvertible. The most reasonable explanation for this behaviour involves different orientations of the CP [where CP = C_5H_5, $C_5H_4CH_3$, $C_5(CH_3)_5$] rings relative to the Co_2M trimetallic plane. This was rationalized by interconversion via rotation of the $(CP)M(CO)_2$ vertex relative to the Co_2C triangle in which an energy barrier must be overcome where the ligands pass through regions of increased interaction with the rest of the molecule.[143] See Scheme 3.1.

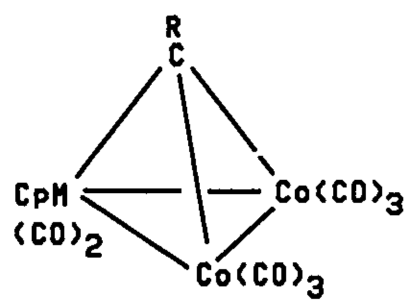

25a R = Ph, M = Mo
25b R = tolyl, M = W

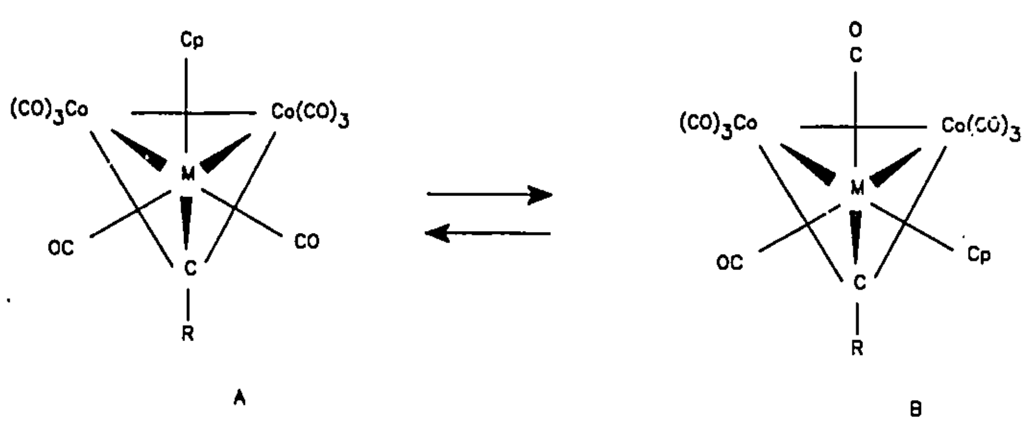

Scheme 3.1 Rotation of a $CpMo(CO)_2$ vertex relative to a triangular face.

As noted above, the clusters **25a** and **25b** reported by Vahrenkamp[139] and by Stone[138] adopt structure **30a** while the latter rotamer, *viz* **30b**, has been characterized X-ray crystallographically for the particular case of $(C_5Me_5)MoCo_2(CO)_8C\text{-}CO_2{}^iPr$, **29**.[144]

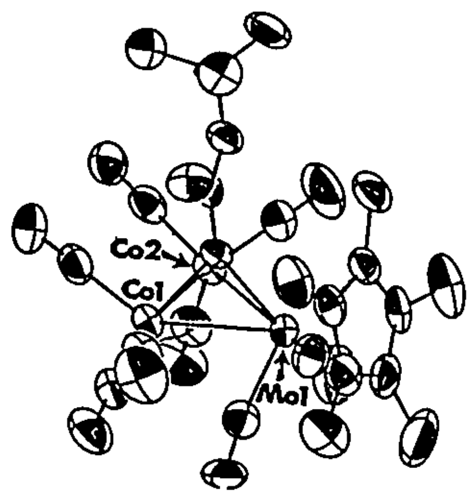

29

3.2 Statement of the Problem.

Molecular orbital calculations at the Extended Hückel level have proven invaluable in gaining an understanding of the structure and reactivity of organotransition metal clusters. In particular the fragment approach pioneered by Hoffmann and his colleagues[145] lends itself beautifully to this chemistry since it allows us to take advantage of the picturesque symmetry of these systems. In recent years, we have used these concepts to rationalize the structures of a number of clusters, many of which exhibit stereochemical non-rigidity on the NMR time-scale.[57,134] Since these simple EHMO methods could be successfully used to account for the fluxional character of five-vertex square-based pyramidal molecules such as **6**, shown in chapter 1,[46] we chose to extend them to encompass the phenomenon of metal vertex rotations in tetrahedral di- and tri-metallic clusters **30** through **33**. We have selected three systems for which reliable experimental data are available: (a) the interchange of axial and equatorial carbonyl ligands within the $Fe(CO)_3$ and $Co(CO)_3$ vertices of $FeCo_2(CO)_9S$, **33**, (b) rotation of the $(C_5H_5)Mo(CO)_2$ fragment in $(C_5H_5)MoCo_2(CO)_8CH$, **30**, and (c) the fluxional behaviour of the $(C_5H_5)Mo(CO)_2$ moiety in clusters of the type $[(C_5H_5)Mo(CO)_2]_2E_2$, where E = As, **31**, or CH, **32**.

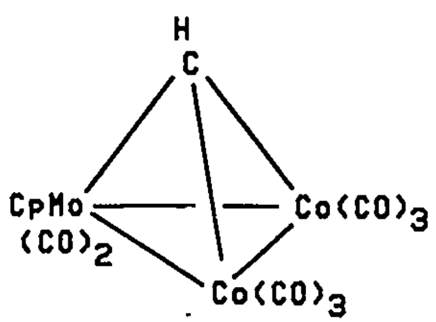

30

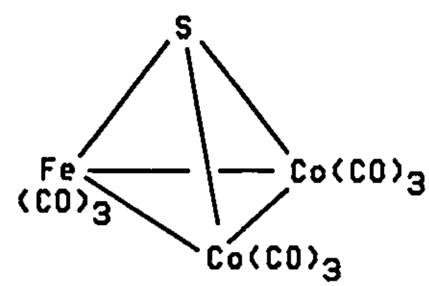

33

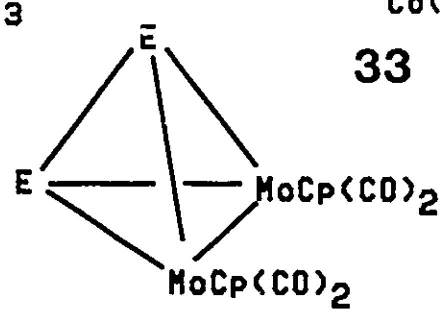

31 E = As
32 E = CH

3.3 Results and Discussion.

3.3.1 $M(CO)_3$ Rotation in $FeCo_2(CO)_9S$.

As shown in Figure 3.1, metal triangles such as $[Co_3(CO)_9]^{3+}$, **34**, or $[Fe_3(CO)_9]^{2+}$, **35**, give rise to a low-lying set of three filled orbitals (*1s, 2s, 1a*) and, at somewhat higher energy, a set of three vacant orbitals (*2a, 3s, 4s*) which serve to accept electron density from capping ligands.[55] There is also a *3a* orbital (made up primarily of out-of-phase d_{xy} orbitals) which is metal-metal anti-bonding in character. In $Co_3(CO)_9S$, this *3a* orbital does not find a symmetry match with the frontier orbitals of the sulfur cap and is singly occupied in the cluster, as shown in Figure 3.2. Replacement of a $Co(CO)_3$ vertex in the tricobaltnonacarbonyl triangle by a different metal fragment such as $(C_5H_5)Mo(CO)_2$ or $Fe(CO)_3$ lowers the symmetry from C_{3v} to C_s and splits the degeneracies of the *1a/2s* and *2a/3s* orbital pairs. Thus the localization of the frontier orbitals on the three metal vertices can change quite markedly. Saillard et al. have previously used this premise to rationalize the orientations of alkyne moieties in heterometallic M_3C_2 clusters, **6**.[46]

Compared to the situation in $[Co_3(CO)_9]^{3+}$, **34**, the localization of the acceptor set of frontier orbitals in the heterometallic fragment $[FeCo_2(CO)_9]^{2+}$, **36**, is much more heavily weighted towards the iron atom than to its cobalt partners. Typically, in the *3a* orbital, which has 22.5% localization on each cobalt in **34**, the distribution in **36** is calculated to be 28% on Fe and only 19% on each cobalt.

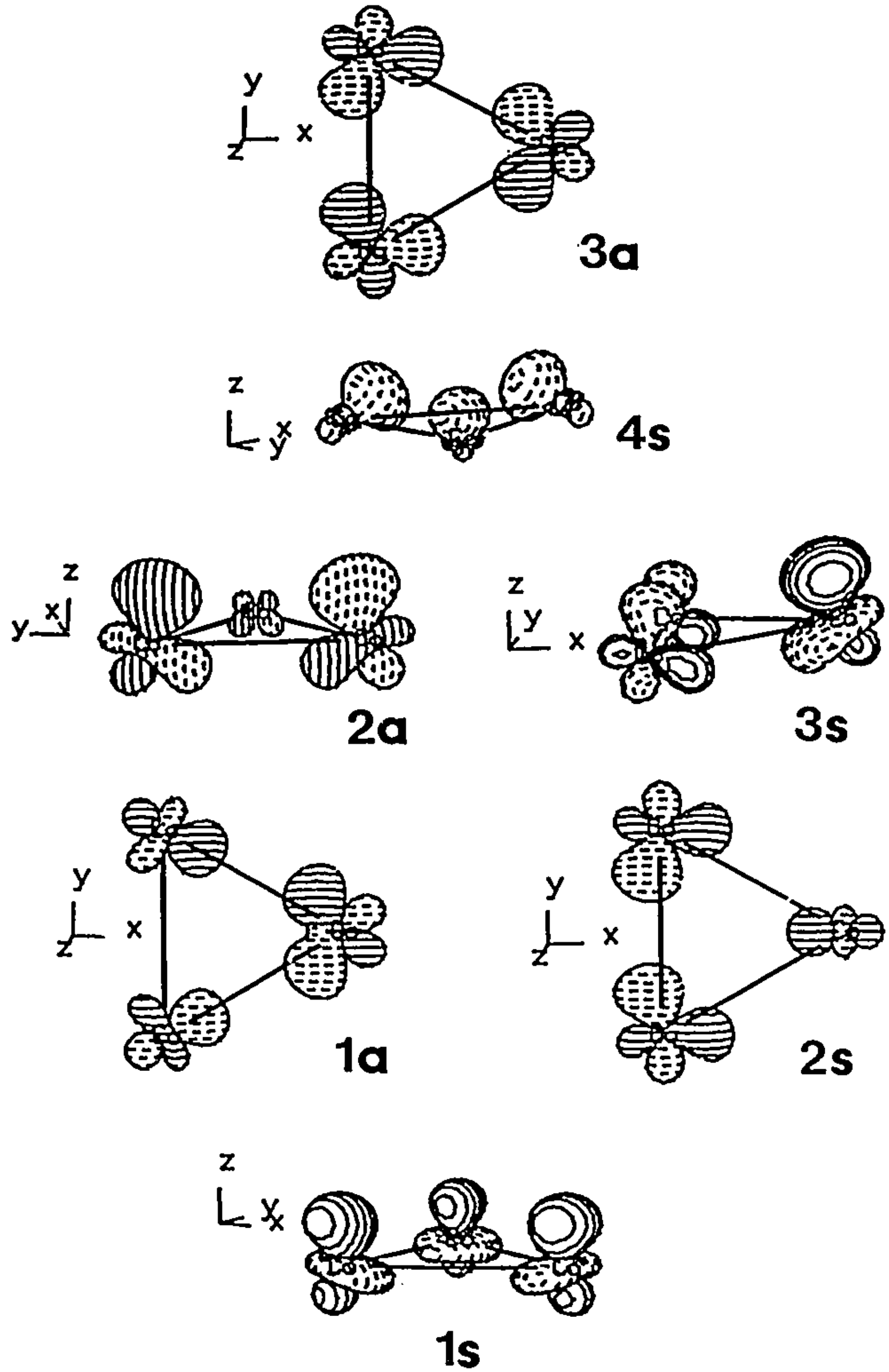

Figure 3.1 Frontier orbitals of $M_3(CO)_9$ fragments.

More importantly, the *3s* orbital in **36** (which is poised to accept electron density from the p_x orbital of the capping moiety) is now 51% localized on Fe with less than 10% on each cobalt; this is considerably perturbed from that found in the tricobalt fragment **34** which has 42% localization on Co(1) and 13% on each of Co(2) and Co(3). In contrast, the *2a* orbital, which interacts with the p_y donor orbital from the capping sulfur, has only a negligible contribution from Co(1) in **34** (or from Fe in **36**) and so remains almost unchanged. Concomitantly, the filled orbital set arising from the metal triangle is correspondingly more heavily weighted towards the cobalt vertices in **36**.

We see in Figure 3.2 not merely that the orbital degeneracies present in $Co_3(CO)_9S$ have been lifted in $FeCo_2(CO)_9S$, **33**, but also that the major π-type interactions, *viz* sulfur p_x with *3s* and sulfur p_y with *2a*, are now different in magnitude. This enhanced splitting of the symmetric component of the π interaction is attributable to the greater contribution of the iron atom to the *3s* acceptor orbital.

To summarize, the interactions of the *2s*, *1a* and *1s* filled orbital set with p_x, p_y and p_z, respectively, of sulfur are rather small since the overlaps are poor. The principal differences in bonding between the tricobalt and iron-dicobalt clusters can be traced to the preferential localization of the *3s* orbital of the metal triangle on Fe. In effect, it is not a gross over-simplification to draw a structure **37** in which the sulfur donates an electron pair to iron which thereby achieves an 18-electron

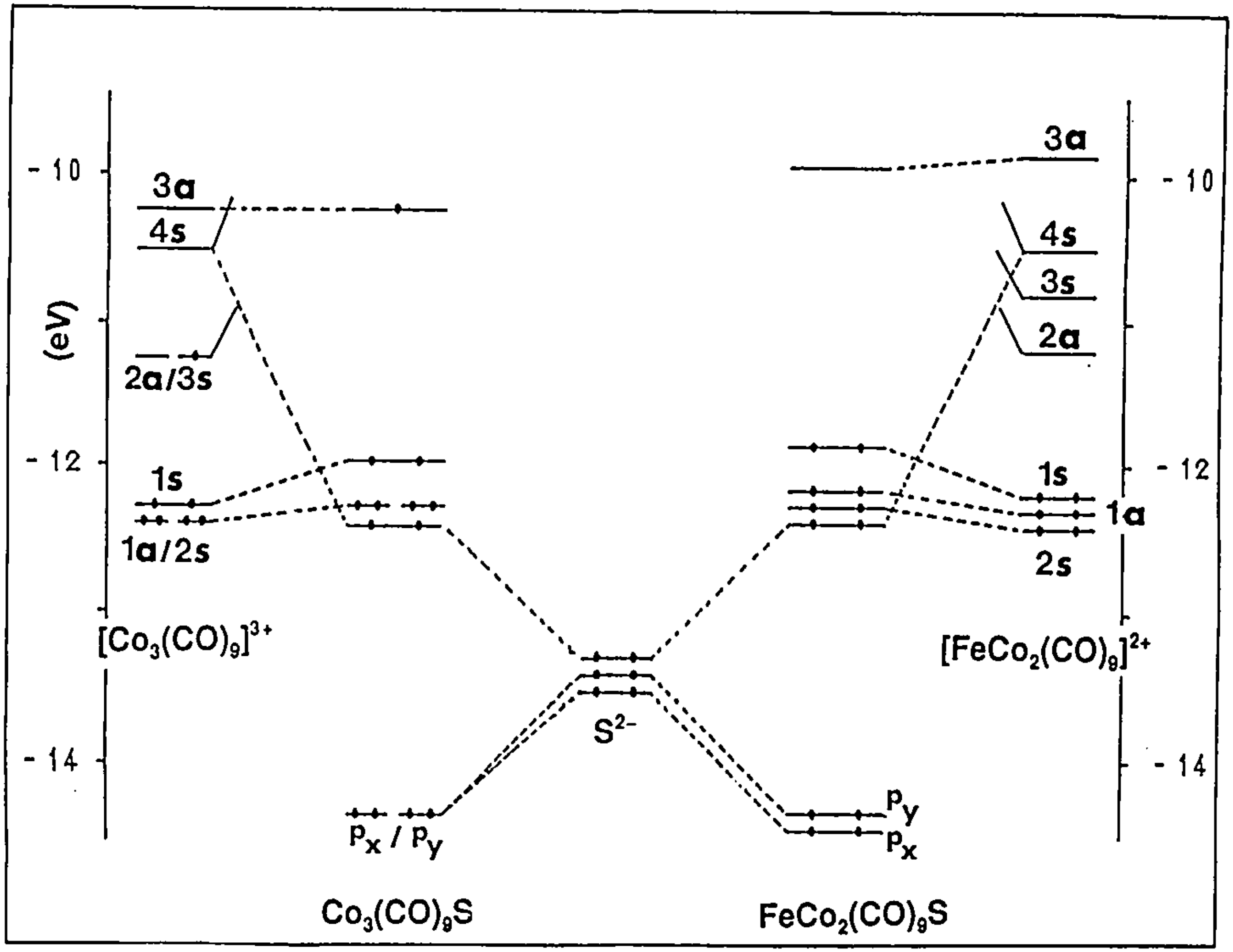

Figure 3.2 Frontier orbital interactions in $Co_3(CO)_9S$ and $FeCo_2(CO)_9S$.

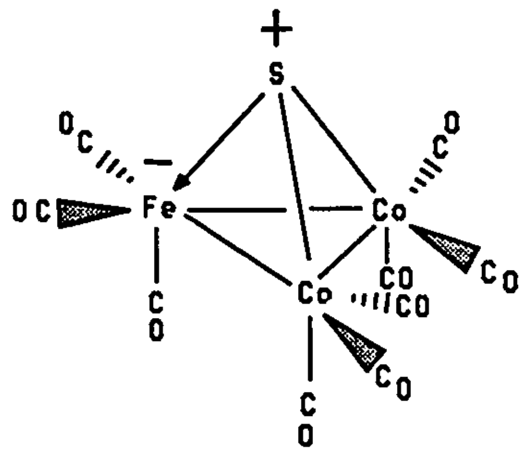

37

configuration. To the extent that we choose to believe the charge distribution given by the EHMO calculation, we gain some support for a structure such as **37** when we note that the $Fe(CO)_3$ fragment is more negative than each of the $Co(CO)_3$ units by almost 0.5 electrons. This model focuses charge along the sulfur-iron vector and places the metal in a pseudo-octahedral environment, as in **38a**. Now, if we allow local rotation of the $Fe(CO)_3$ vertex so as to interchange the axial and equatorial carbonyl ligands, this must proceed via the trigonal-prismatic geometry **38b**. (To simplify the problem, and to take maximum advantage of symmetry, the starting molecular geometry for $Co_3(CO)_9S$ (and for $FeCo_2(CO)_9S$) is an idealized version of the crystallographically determined structure.[146] Thus, the experimentally observed OC-Co-CO angles differ by only ≈ 2° and so we have imposed local C_{3v} symmetry on each $M(CO)_3$ vertex.)

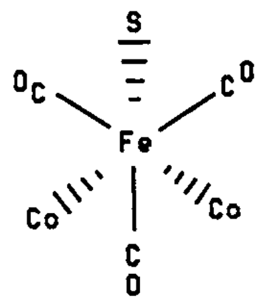

38a

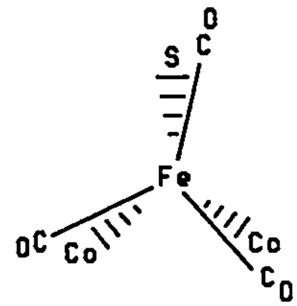

38b

In Figure 3.3 we show the result of rotating through 60° either of the $M(CO)_3$ fragments in $FeCo_2(CO)_9S$, **33**, so as to orient the axial ligand *proximal* with respect to the sulfur cap while the two equatorial ligands are now in *distal* positions. It is apparent that the greater barrier must be surmounted when rotating the $Fe(CO)_3$ vertex from the pseudo-octahedral to the trigonal-prismatic geometry. Figure 3.3 also reveals that this barrier can be traced primarily to the behaviour of the *1a* orbital which is destabilized by the rotation process. The remaining orbitals are but little affected since either they lie along the rotation axis (*4s*), can rehybridize to generate essentially the same orbital (*1s*, *3s*) or have almost no contribution from the vertex undergoing rotation (*2a*, *2s*, *3a*). In contrast, the *1a* orbital which was originally a d_{xy} orbital on iron is transformed during the rotation into a hybrid with predominant d_{yz} character. One can see from Figure 3.4 that this results in a markedly diminished interaction between the iron and the two cobalt atoms; consequently there is a loss of metal-metal bonding in the plane of the metal triangle. Overall, the EHMO calculations support the idea of a sizeable

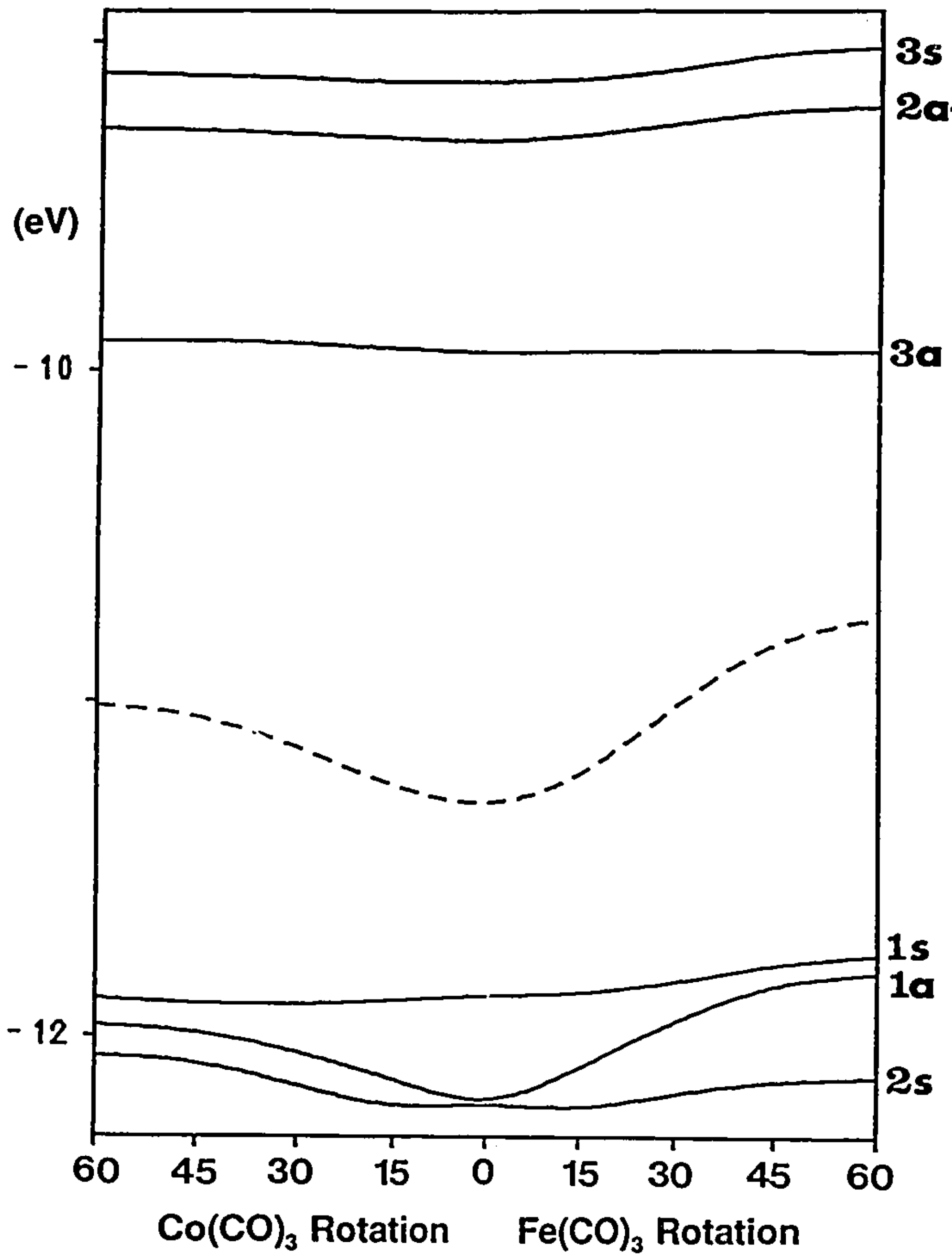

Figure 3.3 Energy profile resulting from rotation of the $M(CO)_3$ fragment in $SFeCo_2(CO)_9$, **33**.

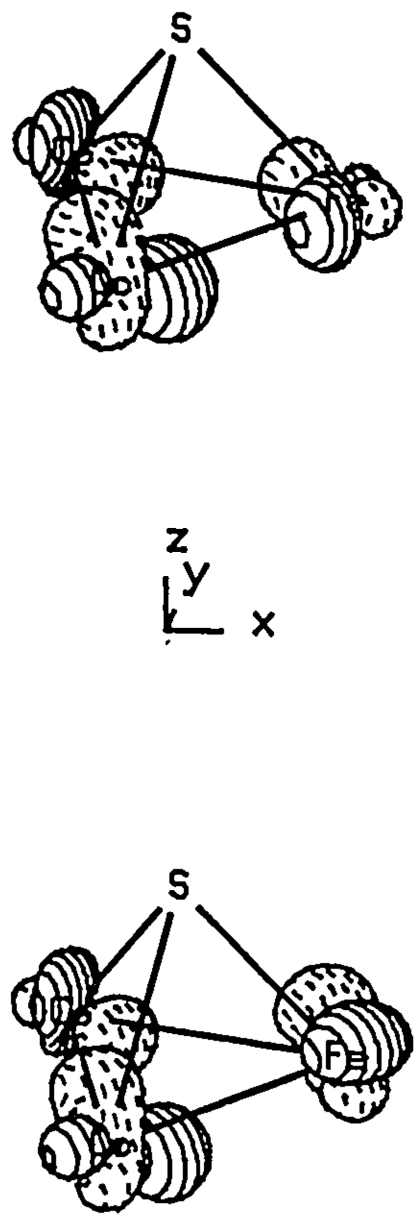

Figure 3.4 The effect on the *1a* frontier orbital in $SFeCo_2(CO)_9$ of rotating the $Fe(CO)_3$ group through 60°.

barrier to $Fe(CO)_3$ rotation (9 kcal mol^{-1}) and a somewhat more modest energetic requirement (5 kcal mol^{-1}) for the $Co(CO)_3$ vertex to spin about its three-fold axis.

Experimental data describing the fluxional behaviour of $FeCo_2(CO)_9S$, **33**, have been furnished by Aime[147] who showed that the initial ^{13}CO singlet (at +30°C) exhibits a 6:3 splitting at -80°C. Clearly, intermetal exchange of the carbonyls has slowed and one sees the six equivalent ligands on cobalt and three bonded to iron. At -100°C the $Fe(CO)_3$ resonance shows a well-resolved 2:1 pattern demonstrating unequivocally that local rotation of the tricarbonyliron fragment has a sufficiently large barrier to slow this process on the NMR time-scale. In contrast, the cobalt carbonyl resonance remains a sharp singlet at all accessible temperatures. These results are in excellent accord with the energy barriers derived from the EHMO calculations.

3.3.2 $(C_5H_5)Mo(CO)_2$ Rotation in $(C_5H_5)MoCo_2(CO)_8CR$ Clusters.

Let us turn now to the question of rotation of the $(C_5H_5)M(CO)_2$ vertex [M = Mo or W] in trimetallic clusters such as $(C_5H_5)MoCo_2(CO)_8CH$, **30**, described in the introduction to this section. Before attempting to calculate the relative energies of the various rotameric structures on the $(C_5H_5)MoCo_2(CO)_8CH$ hypersurface, one must select a viable rotation axis about which to spin the $(C_5H_5)Mo(CO)_2$ fragment. We were guided in this problem by the powerful concepts developed by Dunitz and

Bürgi who have shown that a succession of static X-ray structures can give information about the dynamics of a reaction.[135] In their now classic studies they demonstrated, for example, that a series of crystal structures of systems containing both a nucleophile and an organic carbonyl group could be used to obtain the trajectory of approach of the two reagents. It is clear from these data not only that the nucleophile attacks along a line making an angle of approximately 105° to the C=O bond but also that the trigonal planar sp^2 carbon atom is gradually transformed into a tetrahedral centre.[135] These ideas have been elegantly extended into the organometallic arena by Crabtree and Lavin; in their study it was shown that carbonyl migration between two metal atoms proceeds *via* a trajectory in which a linear terminal ligand proceeds through a series of increasingly more bent semi-bridging situation to a symmetrically bridging situation.[136]

We therefore required several crystal structures in which the $CpM(CO)_2$ unit was oriented differently with respect to the trimetallic plane. As mentioned previously, two essentially identical X-ray structures of type **30a** have been reported[138,139] and also one of type **30b**. Another molecule closely analogous to **29** is the $Fe_3(CO)_8C$-OMe cluster **28** reported by Farrugia.[141] Finally, we were aware of the structure of the $(C_5H_5)WFe_2(CO)_9C$-tolyl cluster **27** in which the tungsten-to-cyclopentadienyl vector is almost exactly in the plane of the metals, as in **30c**.[140] The crucial parameter to note here is the angle made by the Cp-centroid—metal axis with a line joining the metal to the centre of the cobalt-cobalt (or iron-iron) vector. This angle is 125.5° in **25**, it becomes 141° in **27** and opens up to 156°(160°) in **29**(**28**). These values are consonant only with rotation of the $CpM(CO)_2$ fragment about an imaginary line connecting the metal atom to a point **X** within the cluster.

To be more precise, **X** is located as follows: we see from Figure 3.5 that, assuming the $CpMo(CO)_2$ vertex executes a simple rotation about the axis defined by the line **X**—Mo, the locus of the centroid of the cyclopentadienyl ring will define a circle. The lowest point "Cp_a" corresponds to structure **30a** for which the angle Cp_a-Mo-**Y** is 125.5° (in **25a** and **25b**), where "**Y**" is the midpoint of the cobalt-cobalt bond. The highest point "Cp_b" corresponds to structure **30b** for which the angle Cp_b-Mo-**Y** is 156° (in **29**). Since these two positions Cp_a and Cp_b are diametrically opposed then $(24 + \theta) = (54.5 - \theta)$; the angle θ in Figure 3.5 can thus be evaluated as 15.25°, and the point **X** can be located vertically below the capping carbon atom.

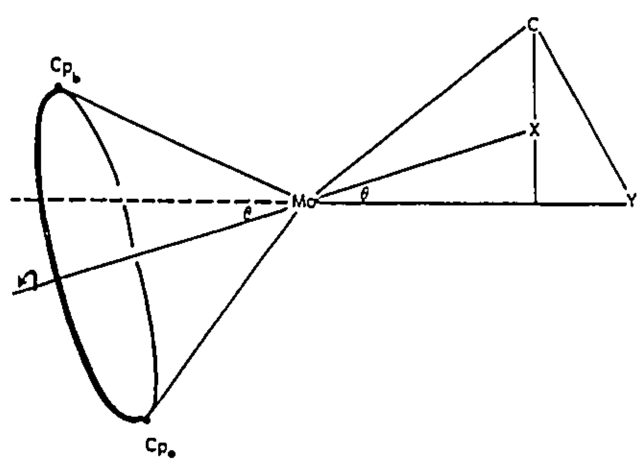

Figure 3.5 Calculation of the point "**X**" in $CpMo(CO)_2Co_2(CO)_6CH$.

Such a scenario provides support to the Wade-Mingos delocalized model of cluster bonding[148-150] rather than one in which there is localized bonding along the edges of the tetrahedron. Indeed, some years ago, the photoelectron spectra of a series of $Co_3(CO)_9CR$ clusters were interpreted in terms of a carbyne ligand bridging a triangle of metals.[151]

As a consequence of this analysis, the energies of the rotamers derived by following the trajectory depicted in Figure 3.5, *i.e.* from **30a** to **30b**, were evaluated by using the EHMO method. A simple rotation of the $(C_5H_5)Mo(CO)_2$ vertex while holding the rest of the molecular geometry constant yields a barrier of more than 40 kcal mol^{-1}; this value arises as a result of unfavourable steric interactions between the cyclopentadienyl and carbonyl ligands on the molybdenum with the carbonyls attached to cobalt. However, one must recall that, while the barrier to $CpMo(CO)_2$ rotation was sufficiently large that the process could be slowed on the NMR time-scale, local rotation of the $Co(CO)_3$ vertices continued unabated. Therefore, rotation of the $CpMo(CO)_2$ vertex was carried out in 15° increments, and the tricarbonylcobalt fragments were each rotated independently so as to give the minimum energy conformation for each point on the curve. At this juncture, the calculated barrier plummeted to 13.1 kcal mol^{-1} — a value more in line with the experimental result.[143] The changes in orbital energy levels and also of the total energy are shown in Figure 3.6.

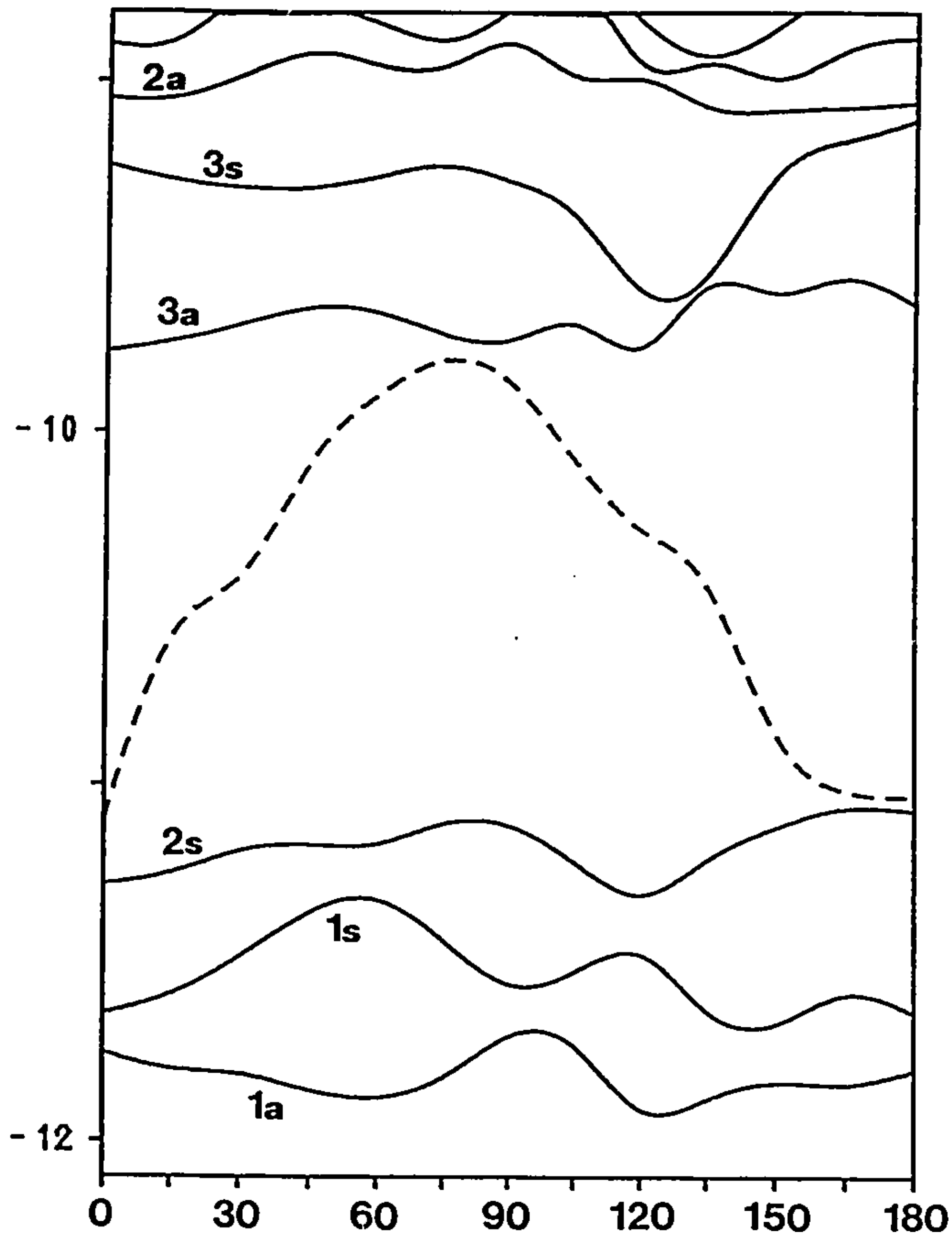

Figure 3.6 Walsh diagram showing orbital energy changes as a result of rotation of the $CpMo(CO)_2$ vertex in $CpMo(CO)_2Co_2(CO)_6CH$. The dotted line represents the change in total energy and is drawn to a different scale, see text.

It is clear that there is a substantial barrier to rotation of the molybdenum vertex through approximately 75° from structure **30a** towards rotamer **30b**; this must be primarily an electronic effect since any potential steric problems can be alleviated *via* facile rotation of the cobalt carbonyl fragments. Finally, we note that as the rotation angle of the molybdenum vertex approaches 180°, *i.e.*, towards structure **30b**, it is energetically favourable to allow the molybdenum carbonyls to become semi-bridging as has been found crystallographically for **29**.[143]

The frontier orbitals of the $(C_5H_5)Mo(CO)_2$ moiety have been described by Hoffmann, Schilling and Lichtenberger[152]. As with the trimetallic fragments $[Co_3(CO)_9]^{3+}$, **34**, and $[FeCo_2(CO)_9]^{2+}$, **36**, discussed already, the $[(C_5H_5)Mo(CO)_2$-$Co_2(CO)_6]^{3+}$ unit gives rise to a set of three low-lying filled frontier orbitals and also three vacant orbitals which can readily form one sigma and two pi bonds with the capping carbyne moiety. Once again, the barrier to vertex rotation can be traced primarily to a marked destabilization of one of the filled frontier orbitals of the metal triangle. However, in the $MoCo_2$ system, it is not the in-plane *1a* orbital which causes the problem; indeed, as shown in Figures 3.6, rotation actually stabilizes this orbital slightly. The effect on the 1*a* orbital of rotating the $CpMo(CO)_2$ vertex through 60° is shown pictorially in Figure 3.7; it is apparent that the orbital component on molybdenum can readily re-hybridize so as to retain the in-plane metal-metal bonding interactions. The culprit in this case is the *1s* orbital in which the large d_{z^2} orbital on molybdenum not only forms a strong bond with the p_x

orbital of the capping carbon but also overlaps very well with its cobalt neighbours to enhance the bonding within the metal triangle. We see in Figure 3.8 that rotation of the molybdenum vertex through 60° is detrimental to both of these bonding interactions; however, the favourable orbital overlaps are mostly recovered upon rotation through 90°.

In summary, there are two strongly favoured rotamers of $(C_5H_5)Mo(CO)_2$-$Co_2(CO)_6CH$, both of which possess mirror symmetry: the molybdenum vertex may be oriented with the cyclopentadienyl group below the trimetallic plane, as in **30a**, or above and *proximal* to the carbyne as in **30b**. In the latter case, the molybdenum carbonyls adopt semi-bridging postures and this rotamer is favoured when the cyclopentadienyl group is strongly electron-donating, as shown by Sutin for $(C_5Me_5)Mo(CO)_2Co_2(CO)_6CR$. There is an example of a molecule — the $(C_5H_5)WFe_2(CO)_9C$-tolyl cluster **27** — in which the vertex is rotated through 90°, but the two $Fe(CO)_3$ units are linked by a bridging carbonyl.[1,0] This molecule would be an interesting candidate for a detailed variable-temperature NMR study.

3.3.3 $(C_5H_5)Mo(CO)_2$ Rotation in $[(C_5H_5)Mo(CO)_2]_2(C_2H_2)$ and $[(C_5H_5)Mo(CO)_2]_2As_2$.

Since the original report of the structure and fluxionality of $[(C_5H_5)Mo(CO)_2]_2$-$(HC{\equiv}CH)$, **32**, by Cotton in 1978,[51] there have been more than twenty crystallo-

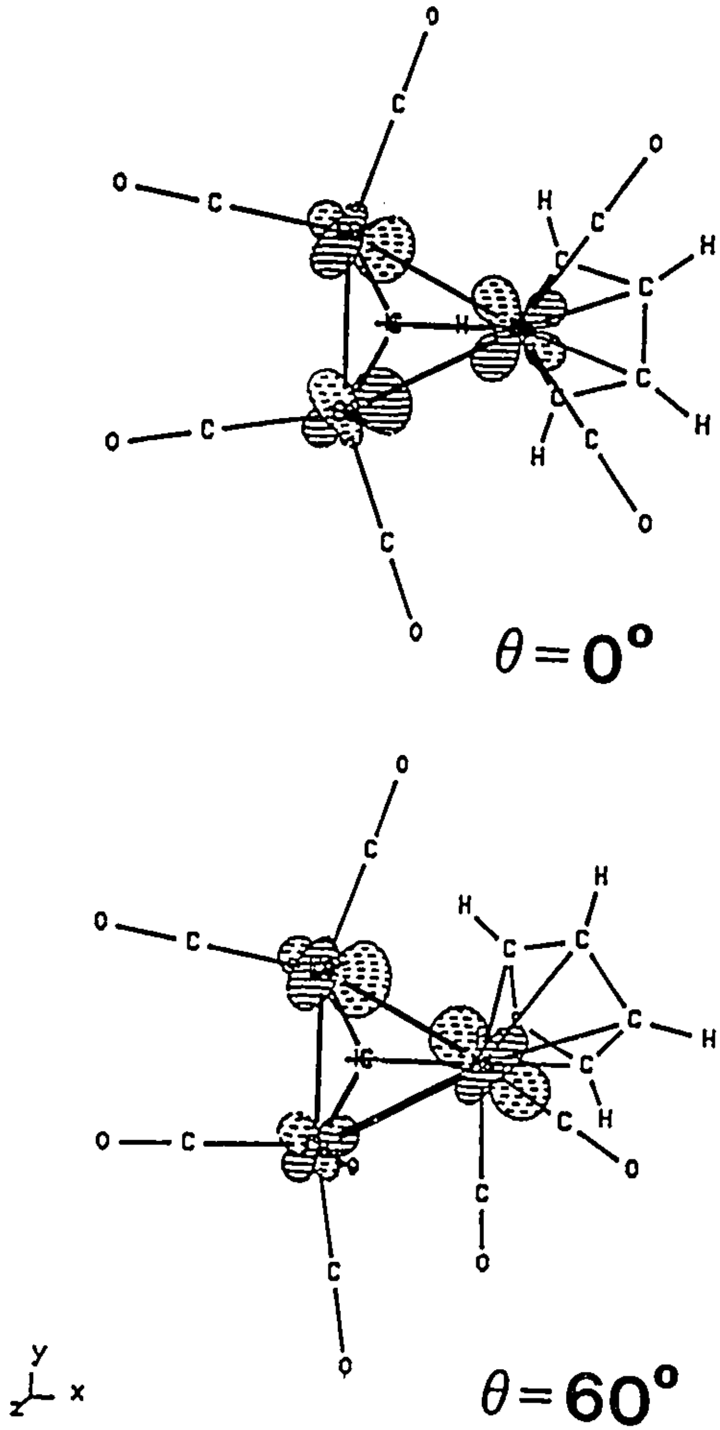

Figure 3.7 The effect on the *1a* frontier orbital in $CpMo(CO)_2Co_2(CO)_6CH$ of rotating the $CpMo(CO)_2$ group.

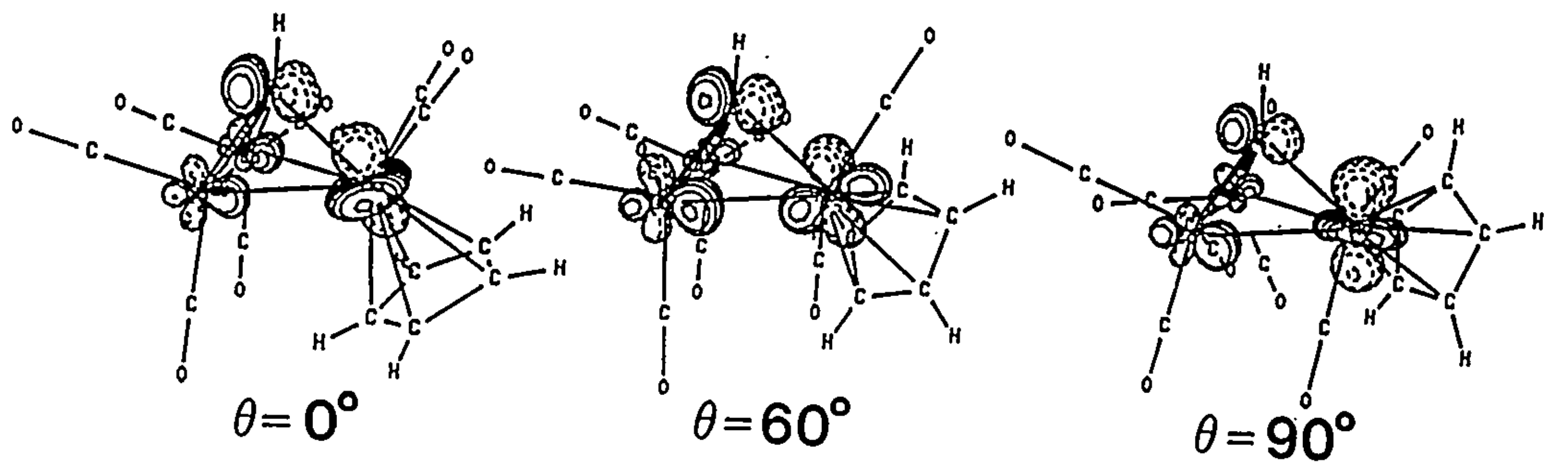

Figure 3.8 The effect on the *1s* frontier orbital in $CpMo(CO)_2Co_2(CO)_6CH$ of rotating the $CpMo(CO)_2$ group.

graphically characterized tetrahedral clusters of the general type $Cp_2M_2(CO)_4(AB)$, where M = Mo or W, and A and B are atoms or molecular fragments isolobal[47] with CH. These include systems containing such vertices as P,[153] As,[154] S^+,[155] N,[156] $Co(CO)_3$,[157] $Ir(CO)_3$,[158] etc. The NMR fluxionality of the alkyne complexes, *i.e.* where A≡B is RC≡CR, was first elucidated by Cotton who noted that two different processes were operative; these were already shown in Scheme 2.3. The lower energy process involved a pair-wise interchange of a terminal carbonyl ligand environment on one molybdenum with a semi-bridging CO on the other metal. The second, and higher energy, process equilibrated the environments of the two cyclopentadienyl groups by a mechanism which must involve some degree of $CpMo(CO)_2$ vertex rotation.[51]

The dimolybdenum-alkyne clusters originally discussed by Cotton possess a semi-bridging carbonyl ligand and this, together with the twisting of the cyclopentadienyl groups renders the clusters asymmetric.[145] In contrast, Rheingold has shown that the diarsenic cluster $[(C_5H_5)Mo(CO)_2]_2As_2$, **31**, adopts C_2 symmetry in the solid state.[154] Thus the two carbonyl ligands on each molybdenum in **31** are non-equivalent and so the barrier to oscillation of the two $(C_5H_5)Mo(CO)_2$ vertices should be measurable by using variable-temperature ^{13}C NMR techniques.

As with the molybdenum—dicobalt tetrahedral clusters discussed above, the $(C_5H_5)Mo(CO)_2$ vertices can be considered to oscillate *via* rotation about a line joining the molybdenum to a point "X" within the tetrahedron. This point **X** is positioned approximately 0.83 Å above the midpoint of the Mo-Mo bond along the pseudo-C_2 axis of the molecule. Location of the point **X** was a non-trivial exercise and required a Bürgi-Dunitz analysis of the trajectory of the ring-centroid of the cyclopentadienyl fragment. This examination of a series of tetrahedral clusters containing two $CpMo(CO)_2$ fragments is deferred until later in this chapter.

One can propose that racemization of the alkyne cluster **32** can occur either (a) by synchronous swivelling of both molybdenum vertices to generate a molecule of pseudo-C_{2v} symmetry, **39**, or (b) by rotating only one vertex so as to produce a pseudo-C_s cluster, **40**, in which the cyclopentadienyl rings are oriented in a *cis* manner. In the latter case, the other vertex must now swivel to generate the enantiomer of the original molecule. These processes were shown previously in Scheme 2.3.

EHMO calculations of the energy barriers in $[(C_5H_5)Mo(CO)_2]_2(HC{\equiv}CH)$ for process (a) are summarized in Figure 3.9. These calculations reveal that the proposed pseudo-C_{2v} structure, **39**, is apparently attainable only with considerable difficulty because of severe steric constraints. Moreover, there is a plateau on which the favoured rotamers are those of C_2 symmetry; in these systems the cyclopentadienyl groups each make a torsion angle in the range 70°—140° with a line joining the midpoints of the carbon-carbon and molybdenum-molybdenum bonds. At dihedral angles less than 60°, the energy rises sharply again as the result of steric interactions between carbonyl ligands; these unfavorable conformations are not alleviated even by bending the carbonyls as is found in semi-bridging systems. These C_2 structures correspond to numerous molecules which have been characterized crystallographically; these are typified by $[(C_5H_5)Mo(CO)_2]_2As_2$, **31**, in which the cyclopentadienyl groups both make torsion angles of 138°.[154]

The energetically most favoured process is (b) in which one $CpMo(CO)_2$ vertex maintains its orientation with respect to the alkyne and the other molybdenum vertex rotates so as to produce a molecule possessing approximate mirror symmetry. The calculated energy profile shown in Figure 3.10 was obtained by fixing one $(C_5H_5)Mo(CO)_2$ vertex such that the Mo-Cp(centroid) vector makes a torsion angle of ϕ with the line joining the centers of the C-C and Mo-Mo bonds. The other vertex was then rotated from +40° to 320°. The energy minima are found when the molecule has either approximate C_2 or C_S symmetry. These calculations yield an activation energy barrier of ≈ 25 kcal mol^{-1}, a value in reasonable accord with the experimental data.[51,52] We note that the height of the barrier is extremely sensitive to minor geometric perturbations; it is necessary to rotate the cyclopentadienyl rings about their Cp-Mo axes so as to minimize their steric interactions at each point of the calculated pathway. We reiterate that these calculations use a simple "ball-and-socket" model whereby a rigid $(C_5H_5)Mo(CO)_2$ vertex rotates about a clearly defined axis.

One is then left with the conclusion that it is better for the molecule to

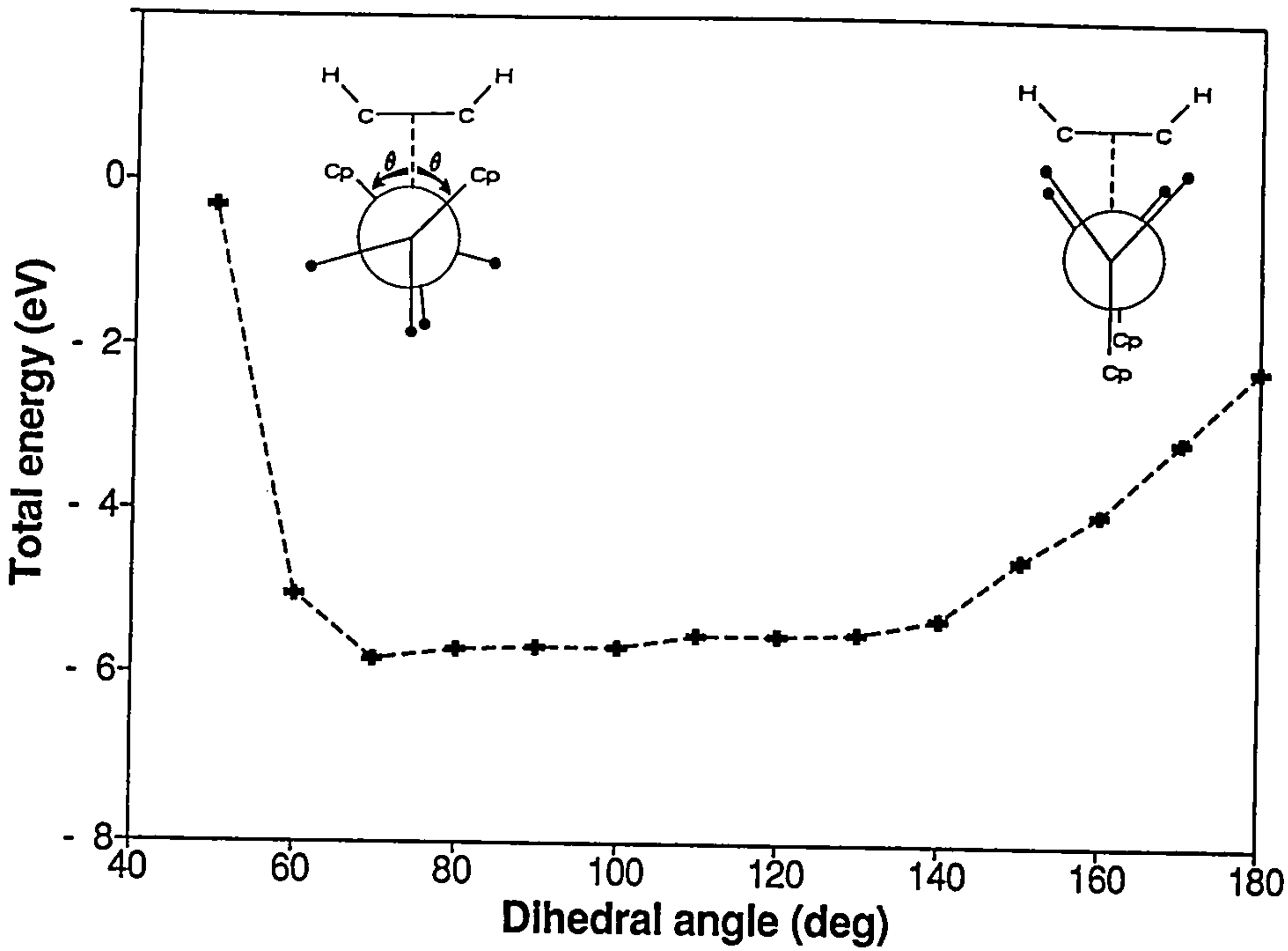

Figure 3.9 Calculated energy profile resulting from synchronous swivelling of both molybdenum vertices to generate ultimately a molecule of pseudo-C_{2v} symmetry.

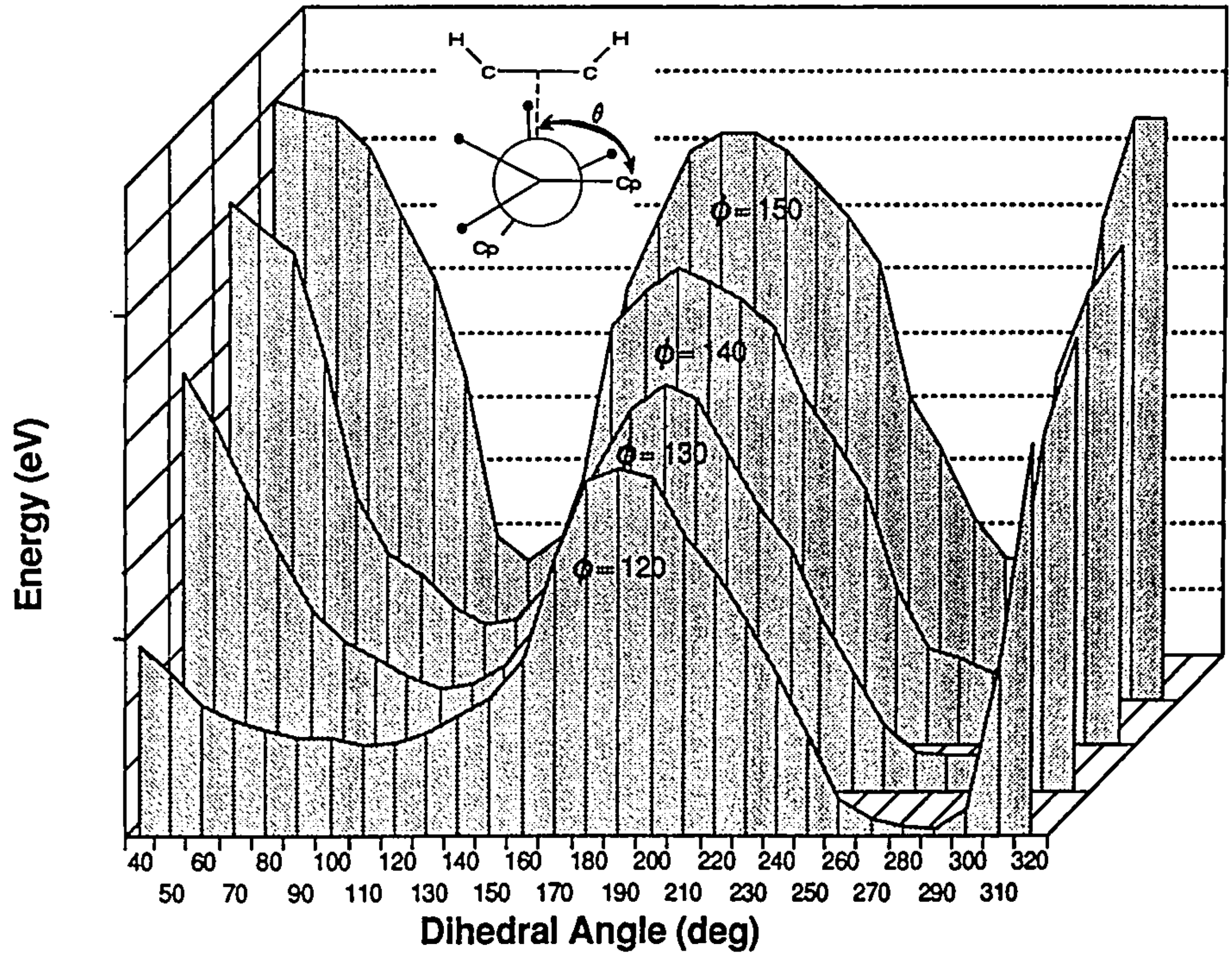

Figure 3.10 Calculated energy profiles corresponding to rotation through θ of only 1 molybdenum vertex while the other is kept constant with ϕ = 120, 130, 140, 150°.

surmount a small barrier twice rather than try to climb a single large hill. Similar considerations presumably apply to the analogous dimolybdenum-As_2 clusters for which the barriers to $CpMo(CO)_2$ oscillation have not yet been reported.

In conclusion we note that the barriers to rotation of organometallic vertices in clusters, which can be detected by using variable-temperature NMR methods, are rationalizable in terms of the energies and symmetries of their frontier orbitals. In particular, the variations between clusters containing homometallic and heterometallic triangular faces can be traced to the degree of localization of the frontier orbitals on the different metallic vertices. Furthermore, it is shown that use of the Bürgi-Dunitz trajectory approach allows the selection of reasonable pathways for fluxional processes.

3.3.4 The Structural Dynamics of $[(C_5H_5)Mo(CO)_2]_2(A{\equiv}B)$ Systems: A Bürgi-Dunitz Approach.

For decades X-ray crystallography has been recognized as the method *par excellence* for the determination of molecular structures. In recent years, however, the powerful concepts developed by J. D. Dunitz, H-B. Bürgi and their co-workers have shown us how to extract dynamic information by careful scrutiny of a series of related crystal structures.[135] The classic work on the trajectory of nucleophilic attack at carbonyl centres has already been alluded to. The significance of these observations for mechanistic organic chemistry is profound, and it was soon exploited by Baldwin to rationalize the favourable or unfavourable nature of many ring-closure processes.[146]

Furthermore, Dunitz[147] also showed how the distribution of crystal structures of more than 60 $(C_6H_5)_3P$-X fragments in many different environments can be related to the "two-ring flip" mechanism by which these chiral propeller-like moieties can undergo racemization.[147] We shall return to this particular problem in Chapter 5 when we consider the conformations of a series of organometallic derivatives of triphenylsilanol.

Initially, our own involvement with the Bürgi-Dunitz approach arose as the result of attempts to understand the fluxional character of molecules of the type $[(C_5H_5)Mo(CO)_2]_2(RC{\equiv}CR)$, **32**. In the case of $(C_5H_5)MoCo_2(CO)_8CH$ and related trimetallic clusters the axis of rotation of the $CpMo(CO)_2$ vertex is relatively straightforward to visualize. As described previously, we can readily find the point **X**, which defines the **X**—Mo axis about which vertex rotation may occur. As depicted in Figure 3.5, the locus of the centroid of the cyclopentadienyl ring attached to molybdenum defines a circle as the vertex rotates. Since we have X-ray crystallographic data for the two extreme structures **30a** and **30b**, both of which have C_S symmetry, the angles Cp_a(centroid)-Mo-**Y** and Cp_b(centroid)-Mo-**Y** (where **Y** is at the midpoint of the Co-Co bond) are known. In the case of $(C_5H_5)MoCo_2(CO)_8CH$, already discussed, the angle θ is readily evaluated as

15.25°.

For molecules possessing an alkyne bonded transverse to the Mo-Mo vector, we need X-ray crystal structures for which the centroid of the cyclopentadienyl ring lies in the plane defined by the two molybdenum atoms and the midpoint of the C≡C bond. However, all the crystallographic data available are for molecules in which the cyclopentadienyl group has been twisted out of this plane. The problem then becomes one of taking the coordinates of the Cp centroids in the numerous structures of the type $[(C_5H_5)Mo(CO)_2]_2(A{\equiv}B)$ and defining the best circle which passes through, or close to, these points.

To this end, the structures of 11 tetrahedral clusters of the type $[(C_5H_5)M(CO)_2]_2(A{\equiv}B)$, where M = Mo or W were selected which closely fit the following criteria: (a) the dihedral angle between the (M≡M) and (A≡B) vectors was ≈ 90° (b) there were no obvious perturbing effects such as the strong bonding interaction of a molybdenum carbonyl with another vertex. This latter criterion eliminated $Cp_2Mo_2(CO)_4Ir_2(CO)_6$. Thus the molecules where (A≡B) is (RC≡CR), (RC≡P), (RC≡BR) (RC≡Co$(CO)_3$), (P≡P), (As≡As), (O≡Fe$(CO)_3$) or (S≡Ru$(CO)_3$), were put into the molecular modelling program CHEM-X[148] and the following geometric parameters were evaluated for both $CpM(CO)_2$ vertices in each molecule: (i) the angles Cp(centroid)-M-M and the angles Cp(centroid)-M-C(=O), (ii) the torsion angles **Q**-**R**-M-Cp(centroid) and Cp-M-M-Cp. These data are collected in Table 3.1. As shown in Figure 3.11, the dummies **Q** and **R** are the midpoints of the A-B and Mo-Mo bonds, respectively.

As is evident from Table 3.1, the angles Cp(centroid)-M-C(=O) average 114.3° ± 3.7° for 22 different $CpM(CO)_2$ vertices. This consistency bears witness to the fact that the $(C_5H_5)Mo(CO)_2$ or $(C_5H_5)W(CO)_2$ moiety has a remarkably well-defined geometry and may be regarded as a transferable fragment between clusters, just like the regular functional groups of organic chemistry. These molecules were selected as being reasonably representative of tetrahedral clusters in that the tetrahedral angle between the Mo-Mo and A-B bond vectors was in all cases 90° ± 5.8°.

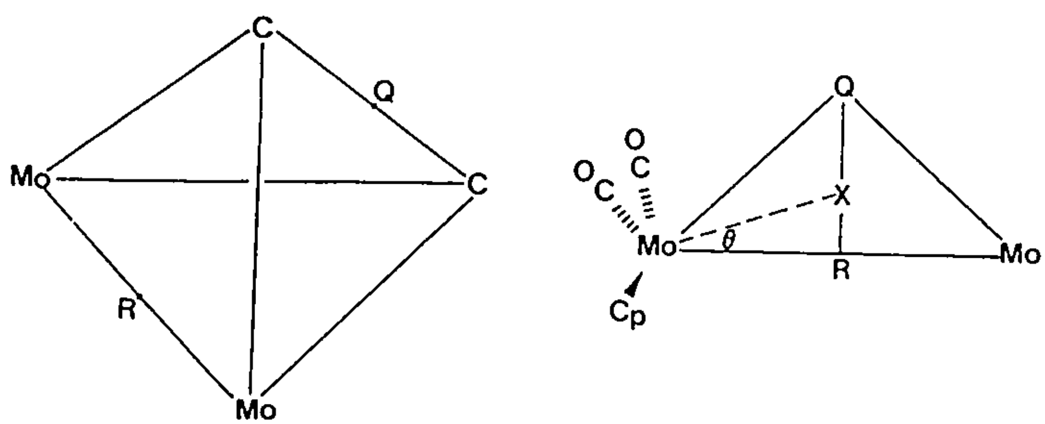

Figure 3.11 Calculation of the point "**X**" in $[CpMo(CO)_2]_2(A{\equiv}B)$ systems.

In the absence of structurally characterized rotamers in which the Cp(centroid) lies in the same plane as the two molybdenum (or tungsten) atoms and the bond midpoints **Q** and **R**, it is necessary to extrapolate from the experimentally available data and then estimate a value for θ, *i.e.* the angle Mo-

Mo-**X**, as illustrated in Figure 3.11. The original choice of $\theta = 25°$ was then refined by use of a molecular modelling program to correlate the Mo-Mo-Cp(centroid) angle with each value of the torsion angle **Q**-**R**-Mo-Cp(centroid). Figure 3.12 shows the comparison of these calculated angles, when $\theta = 29°$, with the data for the 11 $[(C_5H_5)M(CO)_2]_2(A{\equiv}B)$ crystallographically characterized molecules which are listed in Table 3.1.

The level of agreement between the idealized trajectory of $CpM(CO)_2$ vertex rotation and the X-ray crystallographically observed structures is manifest evidence of the power of the Bürgi-Dunitz approach for our understanding of molecular dynamics. According to the basic assumptions of the structure correlation method,[135,142] there should be a concentration of sample points (*i.e.* crystal structures) in the low-energy regions of three-dimensional space. Moreover, there should be a gradual thinning-out of sample points along the reaction path as the energy rises. One may thus identify the transition state as lying in the least densely populated stretch of the reaction path. In the present case, this is the region in which the torsion angle between the Mo-Cp(centroid) vector and the pseudo-C_2 axis approaches 0° or 180°. Figure 3.13 shows how the crystallographically determined structures do indeed lie primarily in the low energy regions of the favored pathway found as a result of the EHMO analysis. Once again, it is an impressive confirmation of the Bürgi-Dunitz concept.

It is interesting that the location of the axis of rotation in the di-molybdenum

Cp(centroid)-M-C(=O)	**Q**-**R**-M-Cp(cent)	M-M-Cp	Cp-M-M-Cp	M, A, B
111.2, 116.0, 115.8, 111.4	138.0, 137.7	117.8, 117.8	84.3	Mo, P, P
118.6, 119.9, 110.5, 110.8	125.3, 150.0	122.5, 118.2	84.7	W, Me-C, Et-B
115.5, 122.0, 112.9, 114.2	129.4, 147.2	123.5, 120.4	83.5	W, Me-C, B(H)Et
117.2, 113.8, 113.5, 116.8	140.0, 139.7	113.8, 114.1	80.3	W, As, As
116.3, 110.5, 112.7, 114.6	139.8, 56.6	121.4, 160.3	163.5	Mo, P, Me-C
116.4, 113.0, 113.2, 116.8	141.1, 140.9	114.3, 114.7	78.1	Mo, As, As
121.1, 109.6, 125.2, 109.7	129.1, 87.5	121.9, 150.3	143.4	Mo, Me-C, norbornene-C
109.3, 117.6, 114.2, 111.0	131.2, 82.7	124.1, 157.9	146.1	Mo, Co, Me-C
113.5, 111.8, 115.8, 109.3	-140.2, 111.4	144.1, 118.1	28.8	Mo, Ru, S
113.1, 111.9, 109.0, 114.1	120.8, -96.4	131.0, 151.0	24.4	Mo, Fe, O
118.1, 110.9, 119.9, 112.4	125.8, 75.0	121.9, 153.9	159.2	Mo, Ph-C, cyclopentene-C

Table 3.1: Selected bond angles from a number of X-ray crystal structures of the type $[C_5H_5M(CO)_2]_2(A{\equiv}B)$.

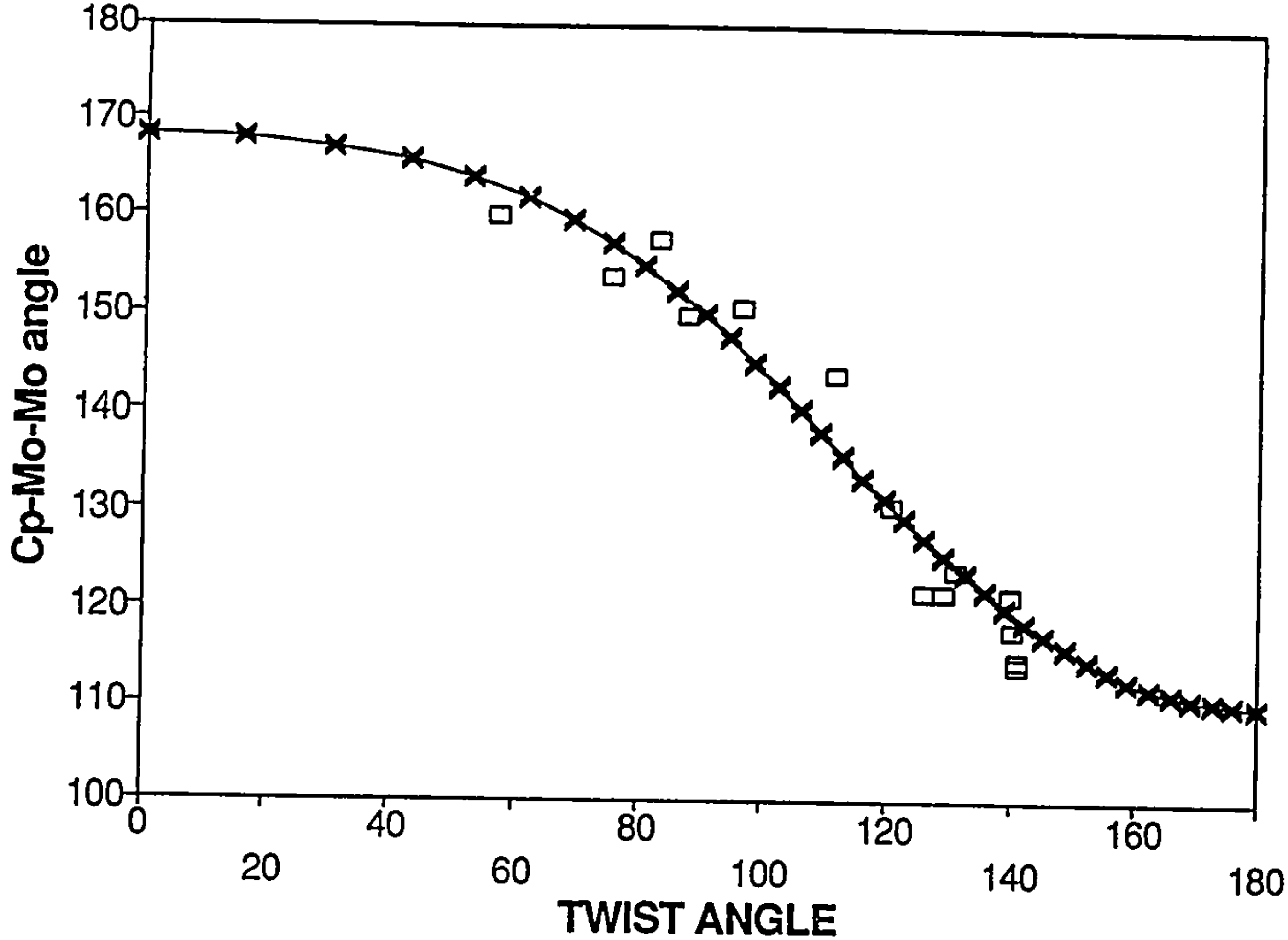

Figure 3.12 Comparison of calculated Cp-Mo-Mo angles vs twist angles with data from Table 3.1. [X - calculated; □ - X-ray crystal structures].

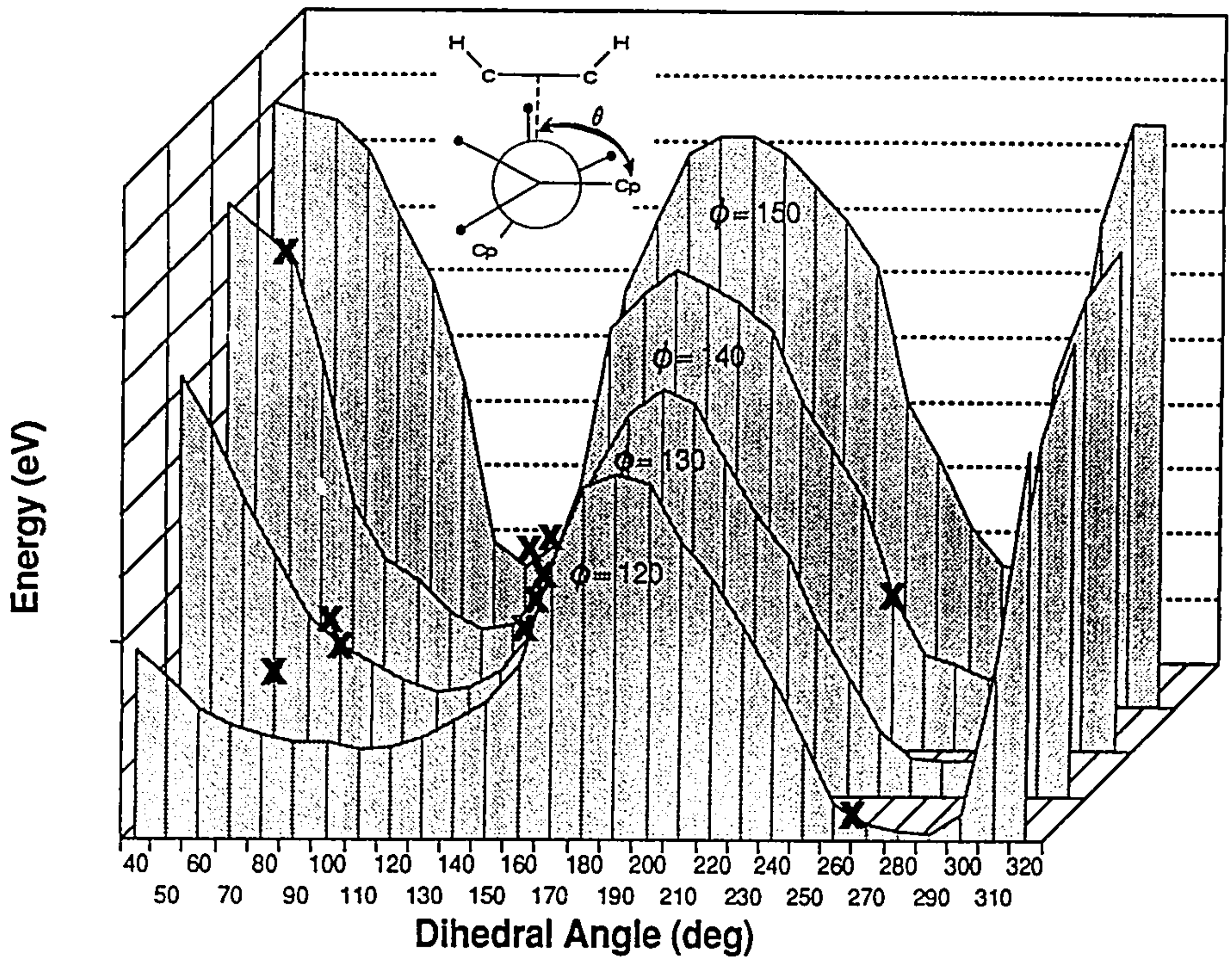

Figure 3.13 Comparison of X-ray structures with energy profile shown in Figure 3.10.

complexes, typified by **31** and **32**, yields a value of 139° for the angle **X**-Mo-Cp(centroid). We note that the corresponding angle in the $CpMo(CO)_2$-$Co_2(CO)_6CH$ system is 141°; this again supports the idea of transferability of organometallic vertices between different clusters.

3.4 Future Work.

The correlation of crystallographic data for a series of related organometallic clusters could be applied to many other situations. An example which could well be worth pursuing is the $RCCo_3(CO)_9$ series of which many have been crystallographically characterized. The rotation angles of the $Co(CO)_3$ tripod may tell us whether the intermetallic scrambling of the CO ligands over all the metal sites is correlated with rotation of the $Co(CO)_3$ vertices.

CHAPTER 4

A MODEL FOR THE STEROIDAL D-RING OF MESTRANOL

4.1 Introduction.

The syntheses and high field NMR spectra of organometallic derivatives of 17α-ethynylestradiol were reported several years ago, and metal complexes of hormonal steroids continue to attract attention. As mentioned in chapter 1, these molecules are of current interest not merely because they are close analogues of widely used contraceptives or abortifactants,[32] but they also hold considerable promise of providing a method of assaying hormonal receptor sites whilst avoiding the inconveniences associated with radiolabelling techniques.[29] These molecules are also of considerable interest to the NMR spectroscopist since they contain a rich array of functional groups whose diamagnetic anisotropies markedly affect the chemical shifts of neighboring protons. The initial interest of McGlinchey in this area involved calculations of the chemical shifts of protons in the region of molybdenum-molybdenum triple-bonded systems,[159] and these ideas have subsequently been extended by Cotton[160] and by Chisholm.[161] Burns et al.[162] have already presented chemical shift contour maps for such organometallic moieties as $Cr(CO)_3$, $Fe(C_5H_5)$ and our original goal was to investigate the diamagnetic

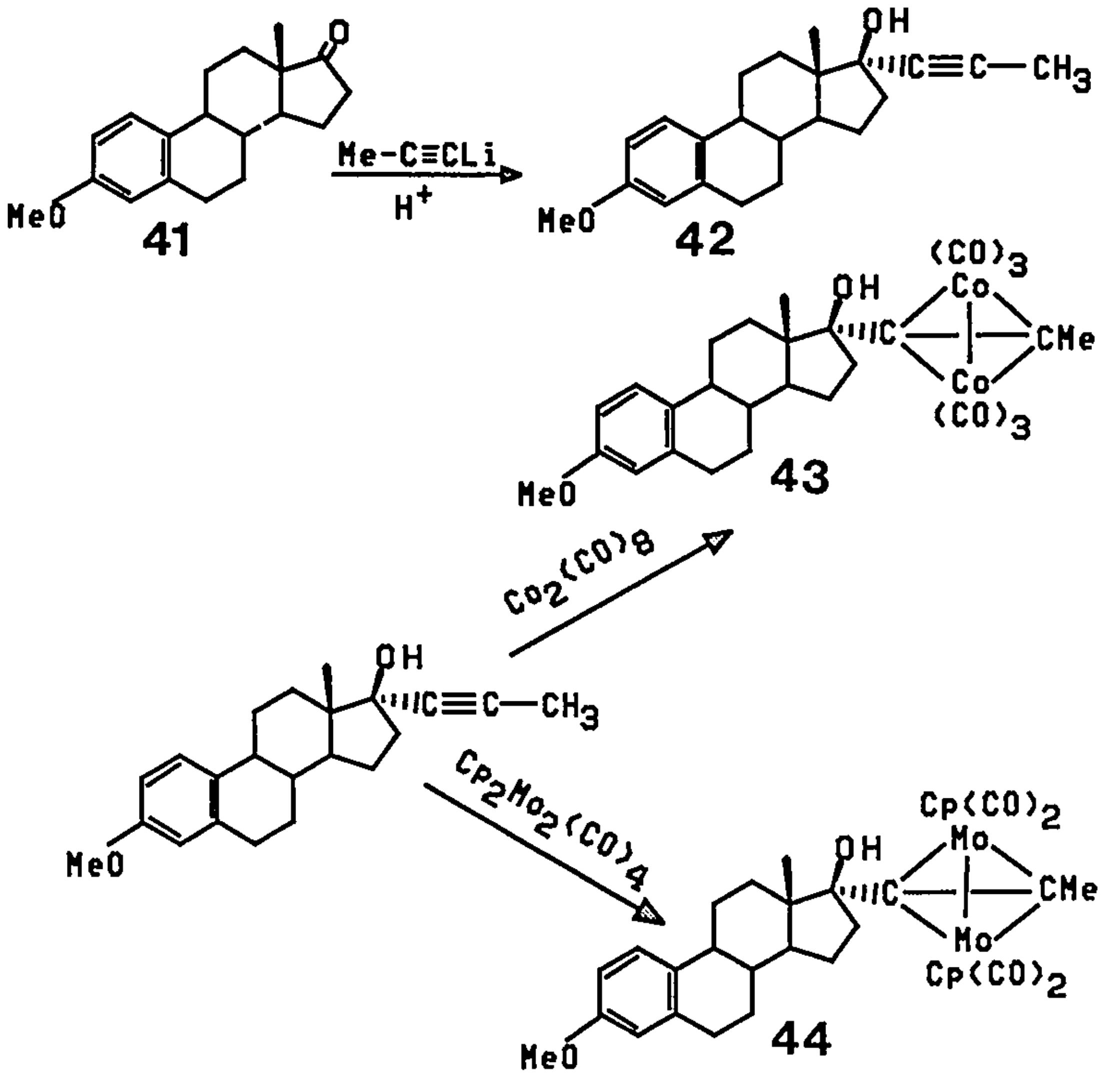

Scheme 4.1 Synthesis and complexation of the 17α-ethynyl derivative of 3-methoxyestrone.

anisotropy of the $(OC)_3Co$-$Co(CO)_3$ fragment.

The conversion of 3-methoxyestrone, **41**, to the 17α-alkynyl derivative **42** proceeds via nucleophilic attack exclusively on the α-face of the D-ring presumably so as to avoid steric interactions with the β-methyl group bonded to C(13) of the steroidal skeleton. Subsequent reaction with the appropriate organometallic precursors leads to the tetrahedral clusters **43** and **44**. Analogous behaviour has been reported for the attack of alkynyl anions on camphor; the product, **45**, again arises via attack on the less hindered face of the ketone.[133]

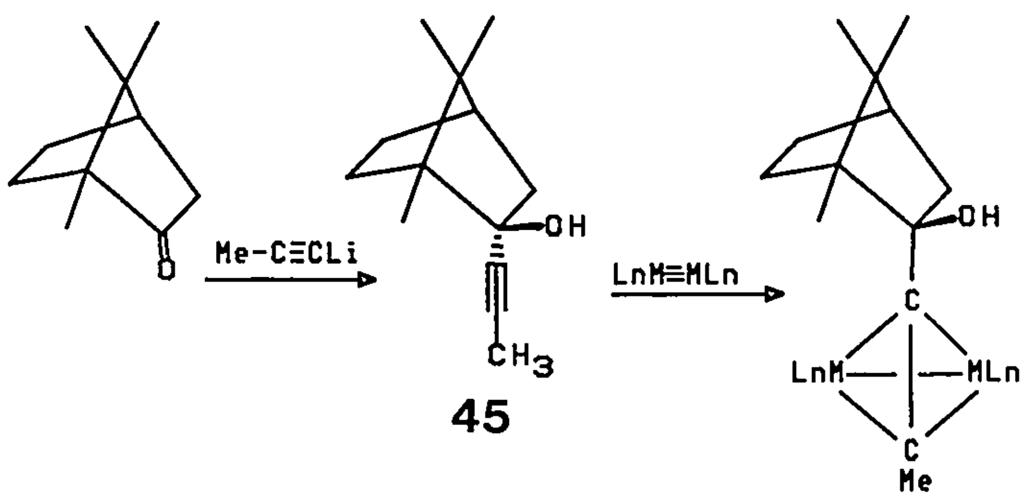

In seeking a model for the D-ring in the cobalt complex, **43**, 2-methylcyclopentanone was treated with phenylethynyl magnesium bromide in the expectation of obtaining molecule **46** as the major product, in which the methyl and the hydroxyl groups are oriented *cis* to each other. The synthesis of **46**, however, turns out to be less trivial than was originally anticipated and this chemistry is described in this chapter.

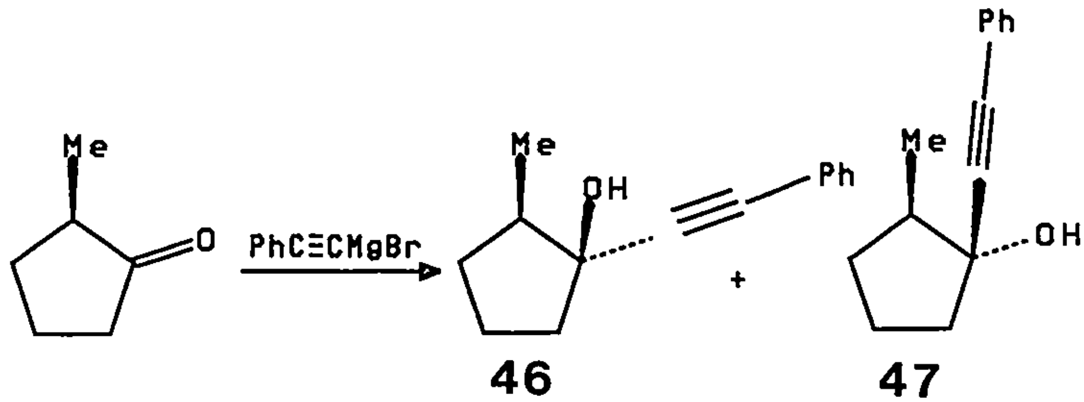

4.2 Synthesis and Reactions of 2-methyl-1-phenylethynylcyclopentanol,47.

In the course of their studies on alkynes, Cadiot and Chodkiewicz et al. found that the ratio of *cis* to *trans* attack by Grignard reagents or organo-lithiums on alkyl-substituted cyclopentanones and cyclohexanones did not simply follow Cram's rule[163] but that it varied with ring size, solvent, counter-ion, temperature and, of course, identity of the nucleophile.[164] Thus, bulky alkyl or aryl Grignard or lithium reagents attack predominantly (80-95%) on the face opposite to that occupied by the substituent already present. In contrast, alkynyl nucleophiles preferentially entered *cis* to the substituent. Moreover, in the presence of base, equilibration of the isomeric 2-methyl-1-phenylethynylcyclopentanols led to the thermodynamically controlled ratio whereby the product in which the methyl and hydroxyl groups are *trans* is favoured by a factor of 55:45. In this study, the assignment of stereochemistry was based on the assumption that the protons of a methyl group *cis* to the neighbouring hydroxyl substituent would be shielded relative to the resonance position of the corresponding *trans* isomer. These assignments were buttressed by NMR data on related diphenylphosphine oxide derivatives of the analogous allenyl systems.[165] Subsequent work by Felkin[166] and by Nguyen Trong Anh and Eisenstein[167] showed that the direction of attack by a nucleophile on a cyclic ketone is influenced not only by the steric bulk of the incoming reagent but also by the torsion angle strain imposed on the system as the sp^2 carbon is transformed into a sp^3 centre. That is, attack on the lower face of 2-methylcyclopentanone not only brings about twisting of the two axial hydrogens at C(2) and C(5) but also causes the C(1)-O(1) bond to eclipse the C(2)-C(Me) bond; this is an unfavourable conformational change.

Slow addition of 2-methylcyclopentanone to phenylethynyl magnesium bromide at 0°C yielded a 91:9 mixture of cyclopentanols; the major isomer, **47**, was indicated by 2D NMR and NOE measurements to be one in which the methyl and hydroxyl substituents were disposed in a *trans* manner. In particular, an analysis of the vicinal coupling constants suggested that the methyne hydrogen at C(2) was in a pseudo-axial position thus placing the methyl equatorially. Furthermore, the hydroxyl proton exhibited a strong NOE enhancement when the pseudo-axial hydrogen at C(5) was irradiated. These data, together with the other information provided by the ^1H-^1H COSY (see Figure 4.1) and ^1H-^{13}C shift-correlated (see Figure 4.2) spectra, suggested a structure **47** in which the phenylalkynyl fragment occupied an axial position. That is, the product obtained was not the one required to model the D-ring of the 17α-ethynyl steroid complexes **43**, and **44**. Of particular interest is the rather large chemical shift difference between the methylene protons attached to C(4). The hydrogen sited *proximal* to the alkyne linkage is markedly deshielded relative to its partner; in contrast, the resonances attributable to the methylene pair at C(3) overlap substantially.

This structural assignment by use of NMR techniques was corroborated by an X-ray crystallographic study of **47** which yielded the structure shown in Figures 4.3 and 4.4. The alkyne crystallizes as large clear prisms from which a small chip was taken. It crystallizes in the orthorhombic space group Pbcn and there are eight molecules in the unit cell. The crystal quality was poor and also showed disorder in the five membered ring, and this is reflected in the relatively high thermal parameters. Nevertheless, the main structural features are clear; the alkyne is disposed axially and the methyl and hydroxyl are both equatorial. The unit cell diagram (Figure 4.5) depicts the crystal packing viewed along the c-axis. Finally, Figure 4.6 clearly illustrates the zig-zag pattern involving hydrogen bonding of the hydroxyl groups. The structure determination summary along with tables of atomic coordinates, bond lengths, bond angles, anisotropic displacement coefficients and

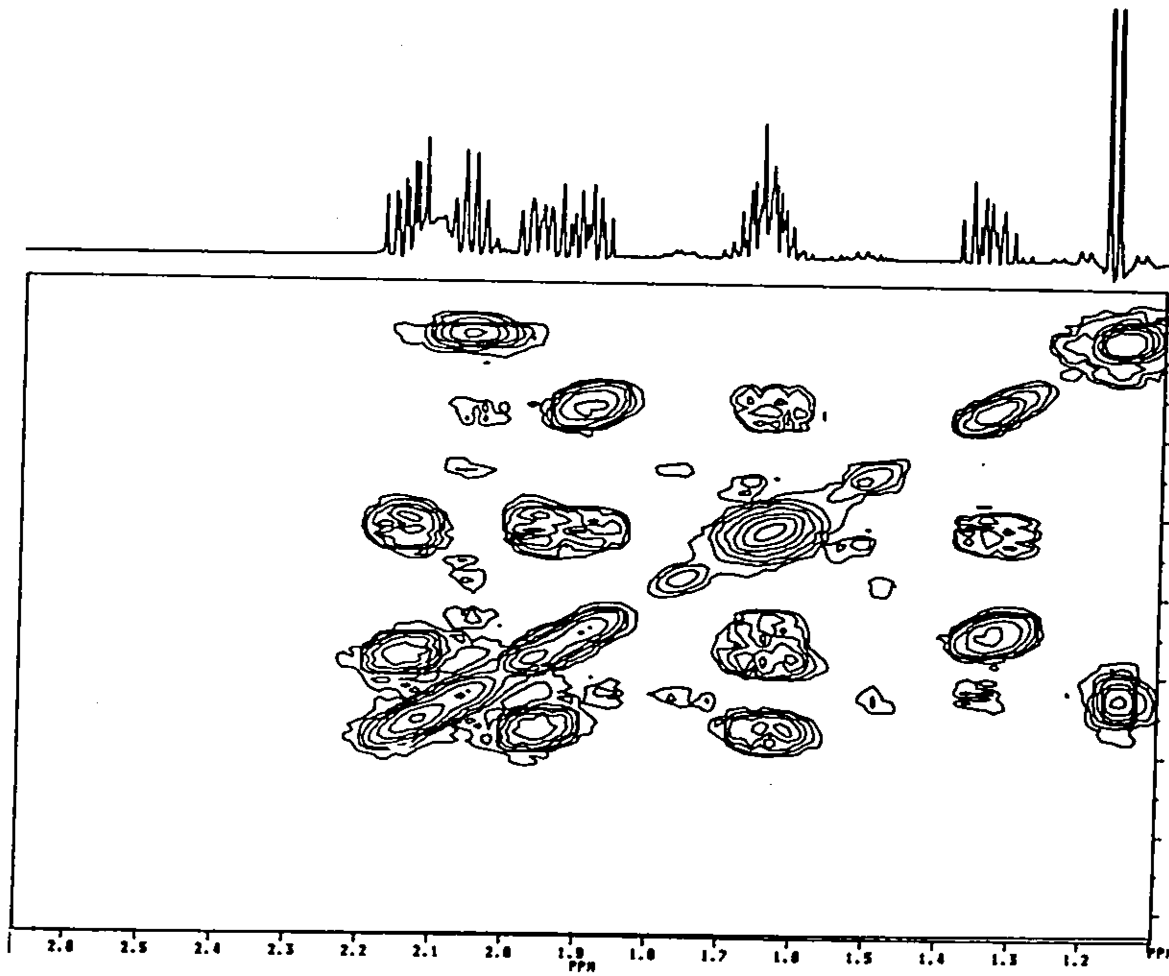

Figure 4.1 ^{1}H-^{1}H COSY spectrum of **47**.

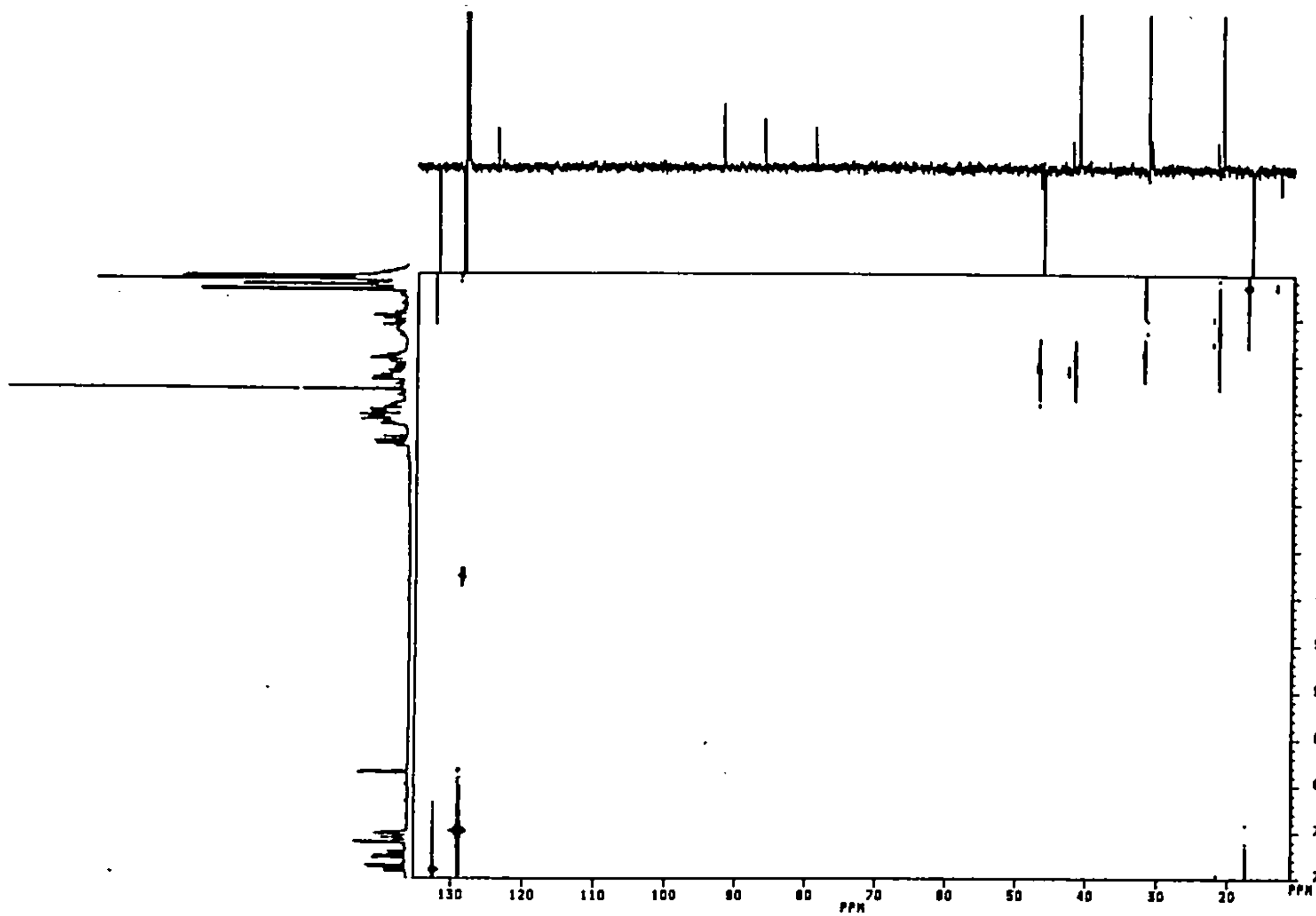

Figure 4.2 ^1H-^{13}C shift-correlated spectrum of **47**.

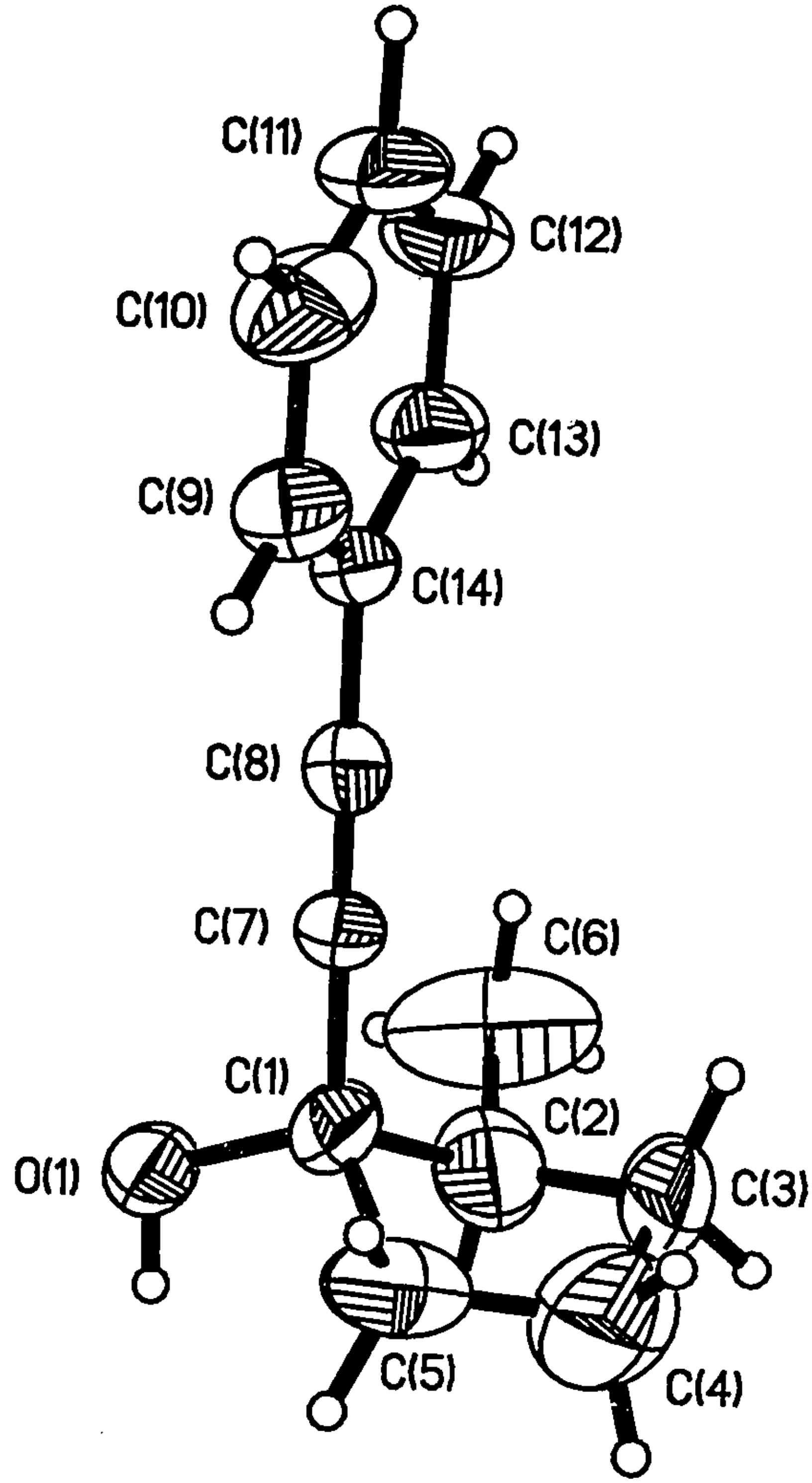

Figure 4.3 View of 2-methyl-1-phenylethynylcyclopentanol, **47**.

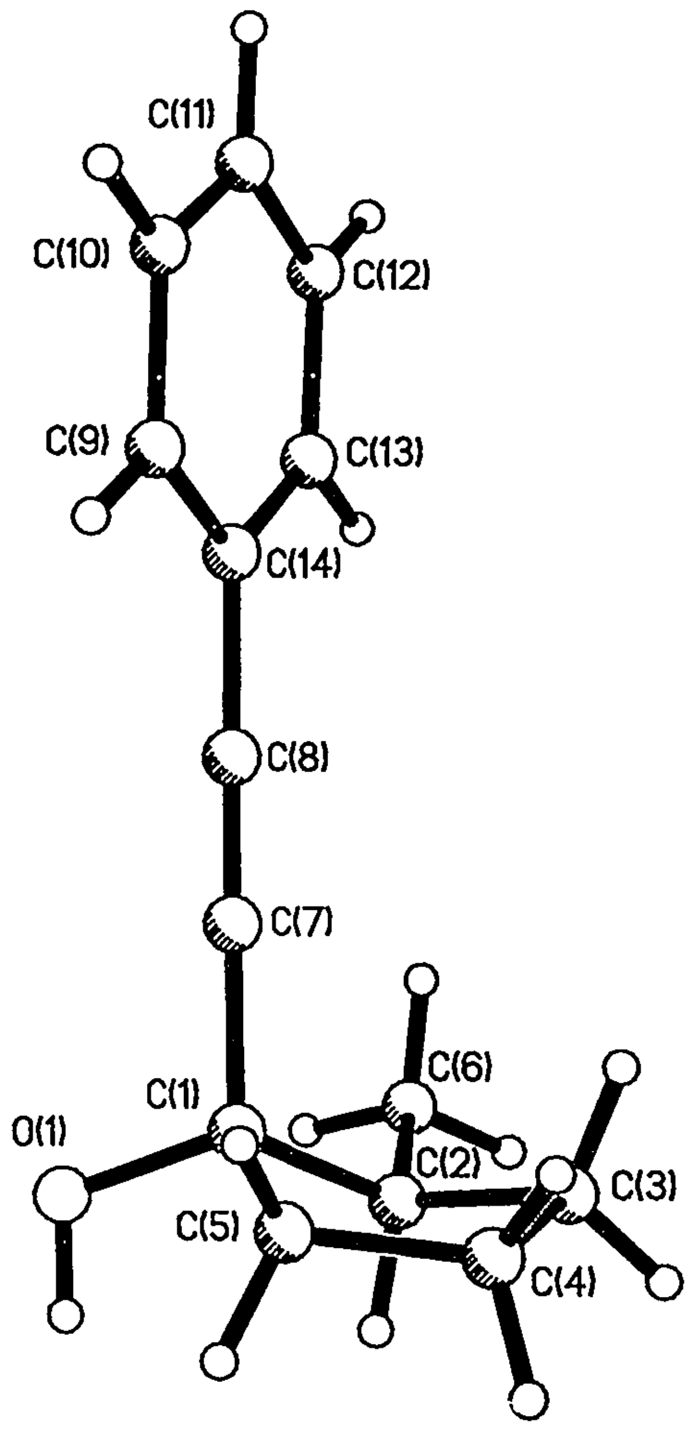

Figure 4.4 View of **47**.

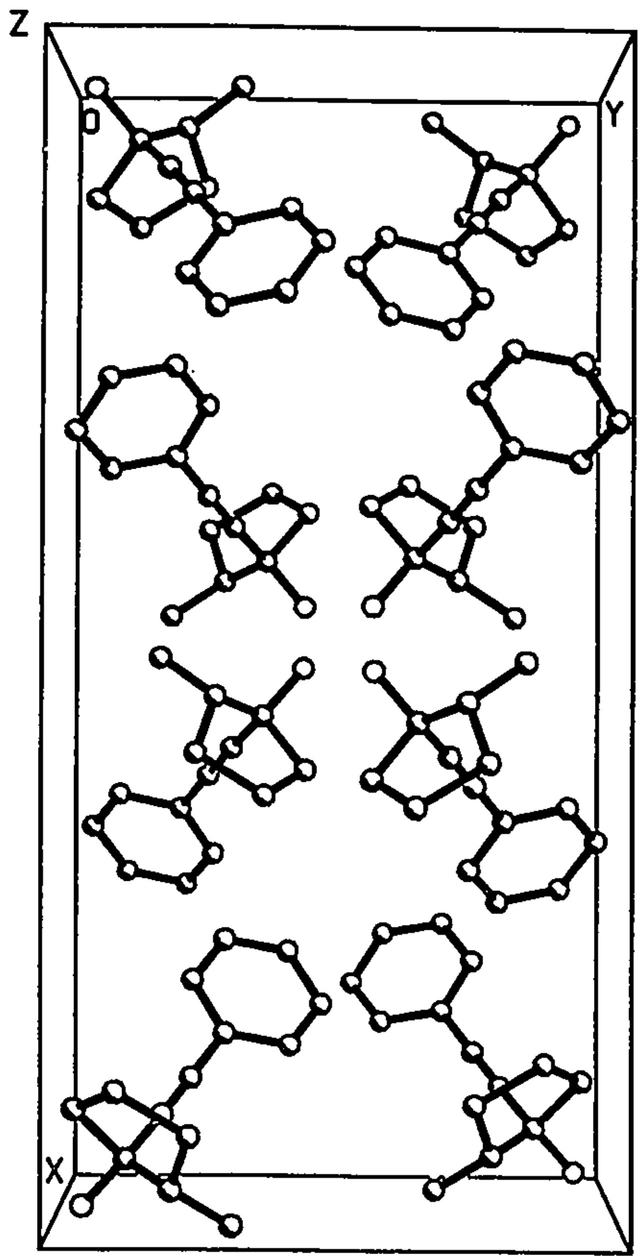

Figure 4.5 Unit cell diagram of **47**.

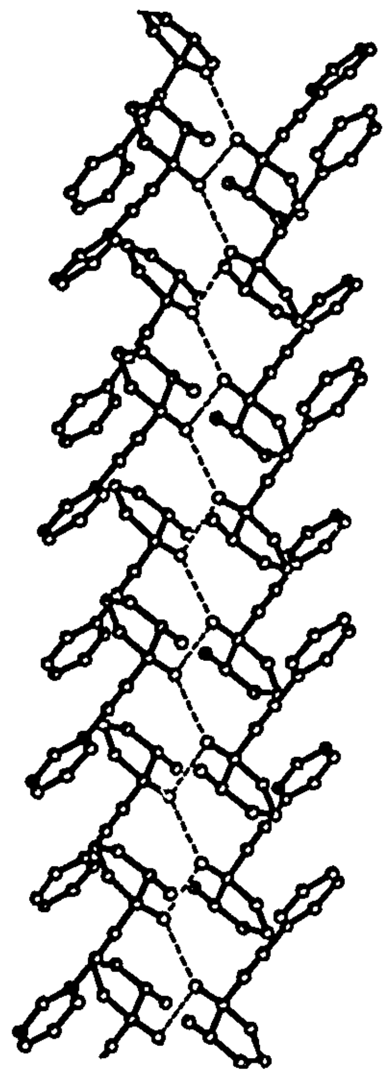

Figure 4.6 Hydrogen bonding of the hydroxy groups in **47**.

H atom coordinates may be found at the end of this chapter in Tables 4.2 - 4.7. The molecule adopts a conformation similar to a half-chair such that C(1) is above and C(2) lies below the plane defined by the methylene carbons C(3), C(4) and C(5). The positioning of the phenylethynyl moiety in the axial position at C(1) is evident and the hydroxyl and methyl substituents occupy the equatorial sites at C(1) and C(2), respectively.

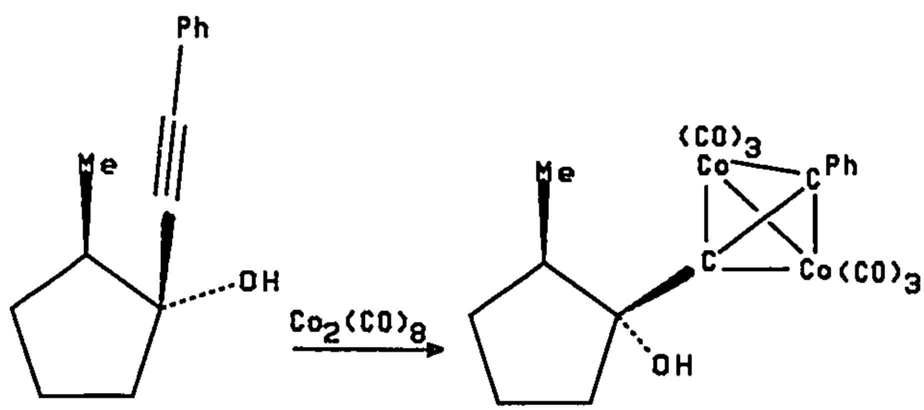

48

The alkyne **47**, when treated with dicobalt octacarbonyl, yielded the cluster, **48**, which crystallizes as purple-black plates suitable for an X-ray diffraction study. The relative orientations of the methyl and hydroxyl groups must, of course, be maintained. This assumption was verified X-ray crystallographically but, as shown in Figures 4.7 and 4.8, we see that the envelope is now folded such that the very bulky dicobalt cluster occupies an equatorial site. This has the effect of moving both the methyl and the hydroxy groups into axial positions. The cobalt-cobalt

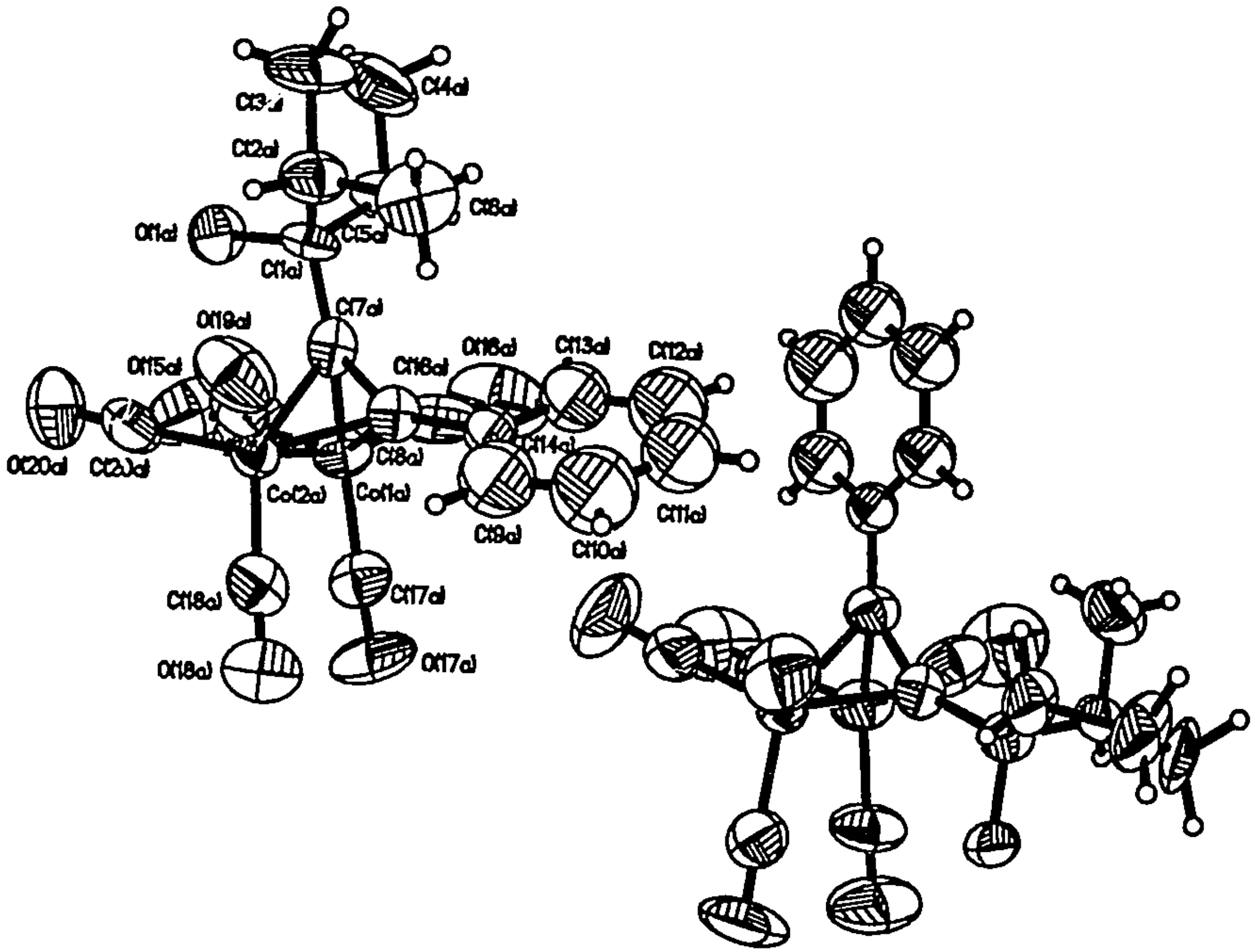

Figure 4.7 View of the cobalt complex, **48**.

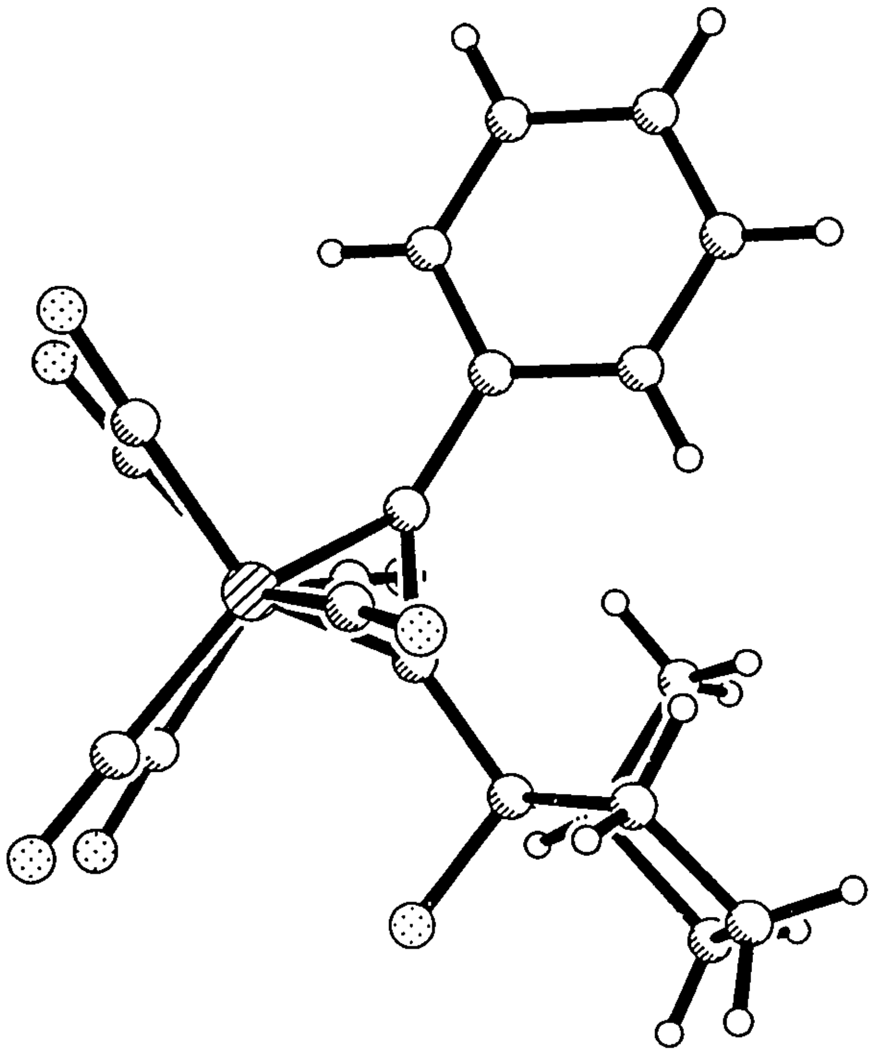

Figure 4.8 View of **48**.

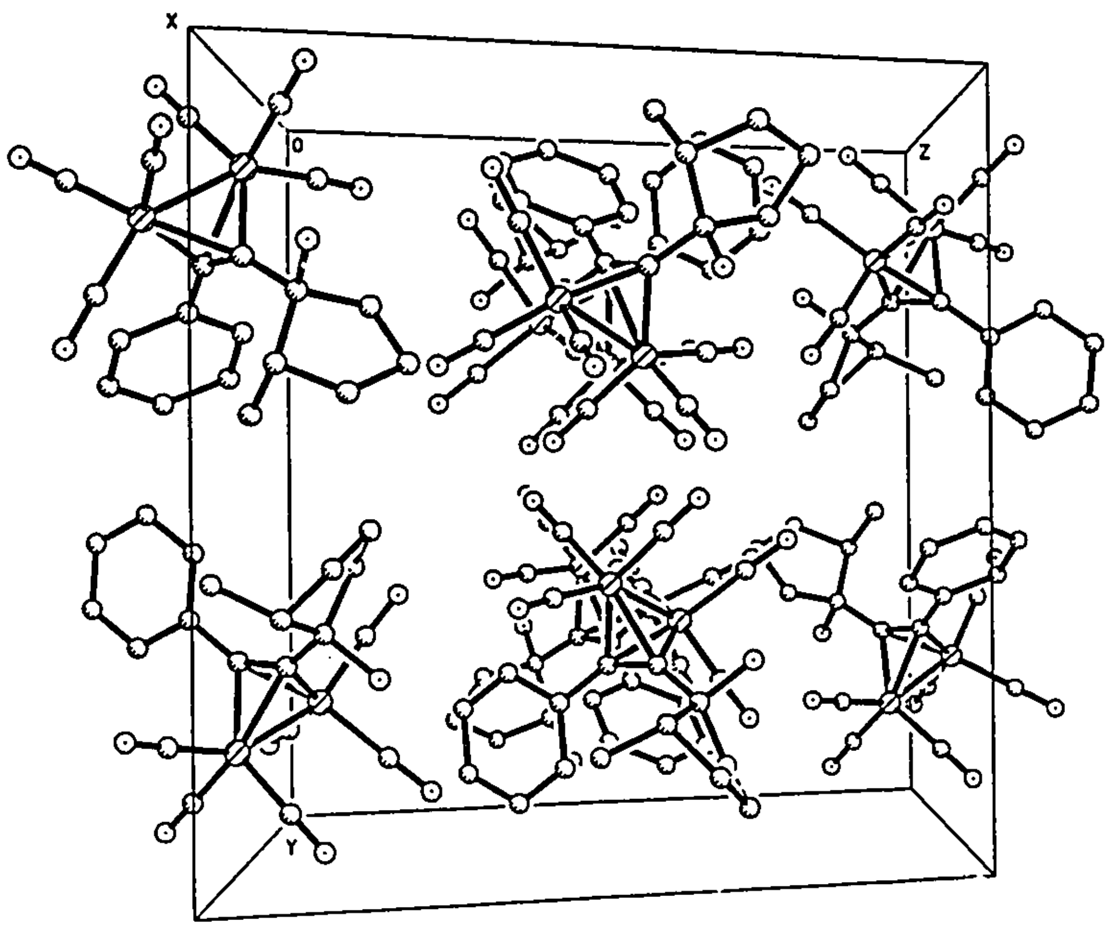

Figure 4.9 Unit cell diagram of **48**.

bond distance 2.465(3) Å and the cobalt-carbon bond lengths within the tetrahedron (average 1.972(13) Å) are within normal range for such systems. As is generally found in such clusters, the R-C≡C-R linkage is no longer linear and in **48** the substituents are bent back by ≈ 35°. Again, the bond lengths within the five-membered ring are slightly long due to a disorder in the crystal packing.

The cobalt cluster, **48**, crystallizes in the monoclinic space group $P2_1/c$ with 8 molecules in the unit cell. The unit cell diagram viewed along the a-axis is shown in Figure 4.9. The structure determination summary along with tables of atomic coordinates, bond lengths, bond angles, anisotropic displacement coefficients and H atom coordinates may be found at the end of this chapter in Tables 4.8 - 4.13.

It has been well established by Nicholas that clusters such as **48**, in which a hydroxy group is sited α to a cluster, upon protonation yield stable cations which undergo facile reactions with a variety of nucleophiles.[168] It has also been unequivocally demonstrated that these carbocationic species owe their stability to the fact that the α-carbon leans over so as to interact with a metal vertex, as in **49**.[43,55,56,169] Moreover, analogous to the behaviour of the comprehensively studied trimetallic species $[Co_3(CO)_9C\text{-}CR_2]^+$, the alkylidene capping moiety migrates from one metal vertex to the other via an antarafacial shift process, as shown in Figure 4.10. Schreiber[170] has turned these observations to synthetic advantage by changing the size of the R groups so as to favour one of the diastereomers; this

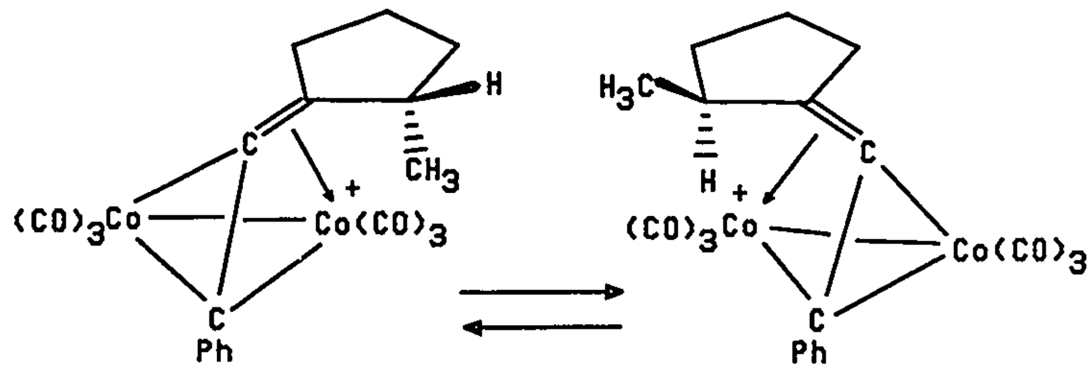

49a 49b

Figure 4.10 Antarafacial shift process.

in turn leads to product selectivity since the attacking nucleophile must approach from the non-hindered face. Since these cations are strongly stabilized via a direct interaction to a metal, one might envisage that the initially formed cation would be one in which the metal can provide anchimeric assistance to the developing trigonal centre. In the case of **48**, protonation would be expected to generate initially the sterically disfavoured isomer **49a** in which the axial methyl group is *proximal* to a bulky $Co(CO)_3$ vertex. The antarafacial migration process, however, can take the molecule into the favoured isomer **49b** in which the methyl group is now *distal* with respect to the metal vertex. Moreover, a minor conformational change can place this methyl substituent in an equatorial site which upon quenching with water it was hoped to yield the cluster in which both the very bulky alkyne cluster and the methyl substituents occupy favoured equatorial positions.

Unfortunately, instead of this rearrangement taking place, this reaction mainly yielded the elimination product **50**, in which water was eliminated. This entire process can be conveniently monitored by ^{13}C NMR spectroscopy. In particular, we note that the methyl carbon and C(1) - the carbinol carbon - in **48** resonate at δ 18.9 and δ 87.0, respectively; in the cation **49** these now appear at δ 21 and δ 168, respectively. The latter value is typical of a metal-complexed carbocationic centre. Addition of the nucleophile (water or methanol) yielded the dehydrated alkene complex **50** which exhibits a ^{13}C NMR methyl resonance at δ 14. The NMR data for these and other related molecules are collected in Table 4.1.

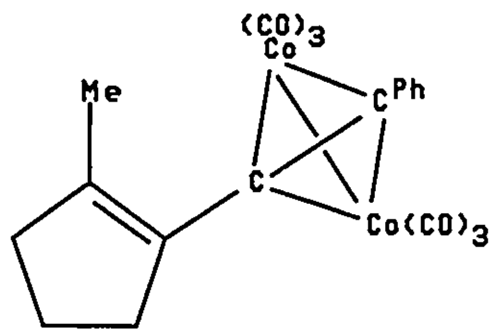

50

The alkene elimination product is also produced upon treatment of the alkynol with $Cp_2Mo_2(CO)_4$ which affords the cyclopentene complex **51** as dark red crystalline plates. X-ray crystallographic analysis of **51** showed that it crystallizes in the monoclinic space group $P2_1/n$ with four molecules in the unit cell (see Figures 4.11 and 4.12). The structure determination summary along with tables of atomic coordinates, bond lengths, bond angles, anisotropic displacement coefficients and H atom coordinates may be found at the end of this chapter in Tables 4.14 - 4.19. The bond length and bond angle data are typical for such systems. As is normal for dimolybdenum—alkyne clusters, one of the carbonyl ligands is found in a semi-bridging environment. The Mo-C-O angle for this bridging carbonyl ligand is 167.2(16)°. The molybdenum-molybdenum bond length 2.947(3) Å and molybdenum-carbon bond length in the tetrahedron (average, 2.206(13) Å) are in the normal range for these systems. The substituents in the R-C≡C-R linkage are bent back by ≈ 43°. The Mo-Mo-Cp angles have been included in the crystallographic data used in chapter 3. The cell diagram for complex **51** viewed down the b-axis is illustrated in Figure 4.13, and NMR data are included in Table 4.1.

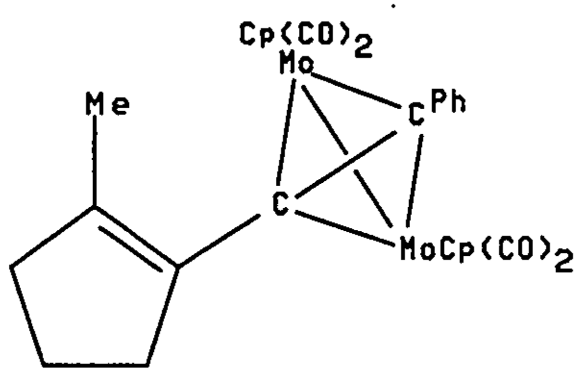

51

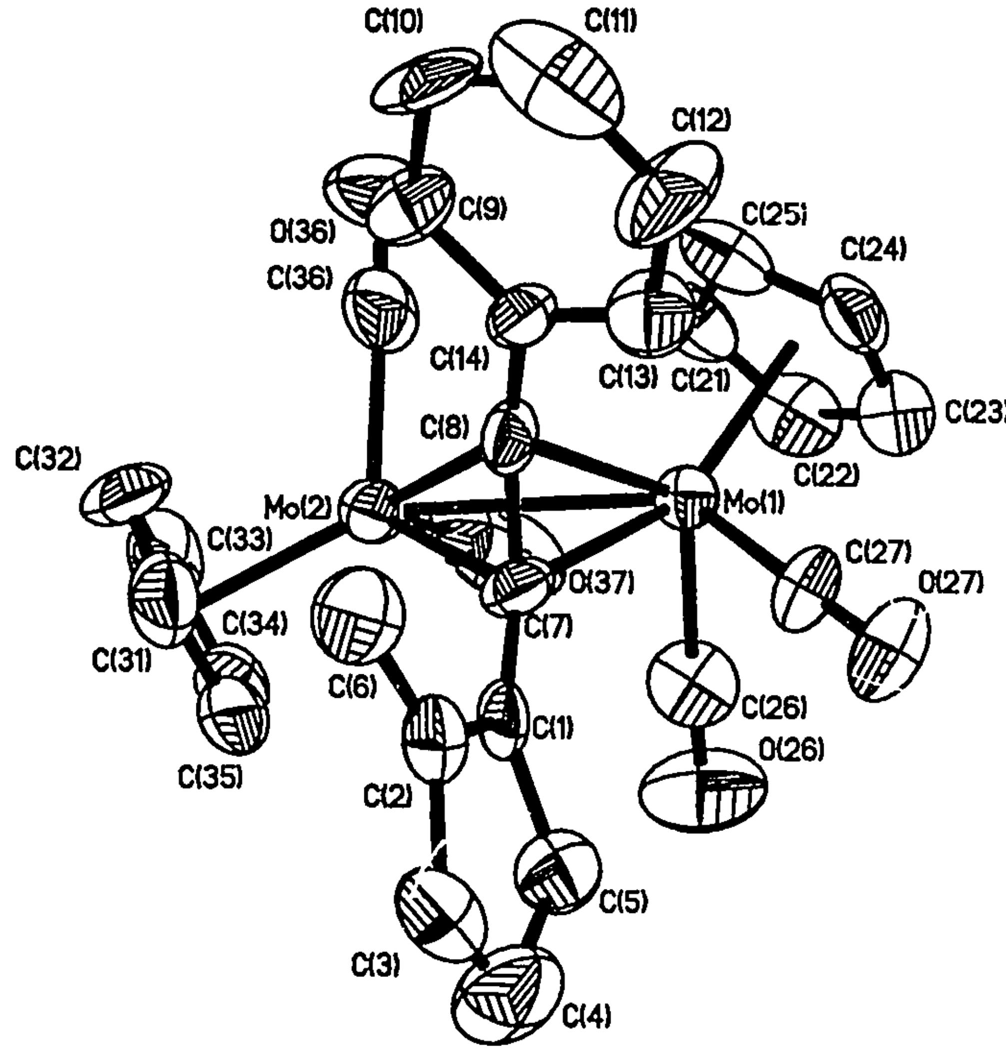

Figure 4.11 View of the molybdenum complex **51**.

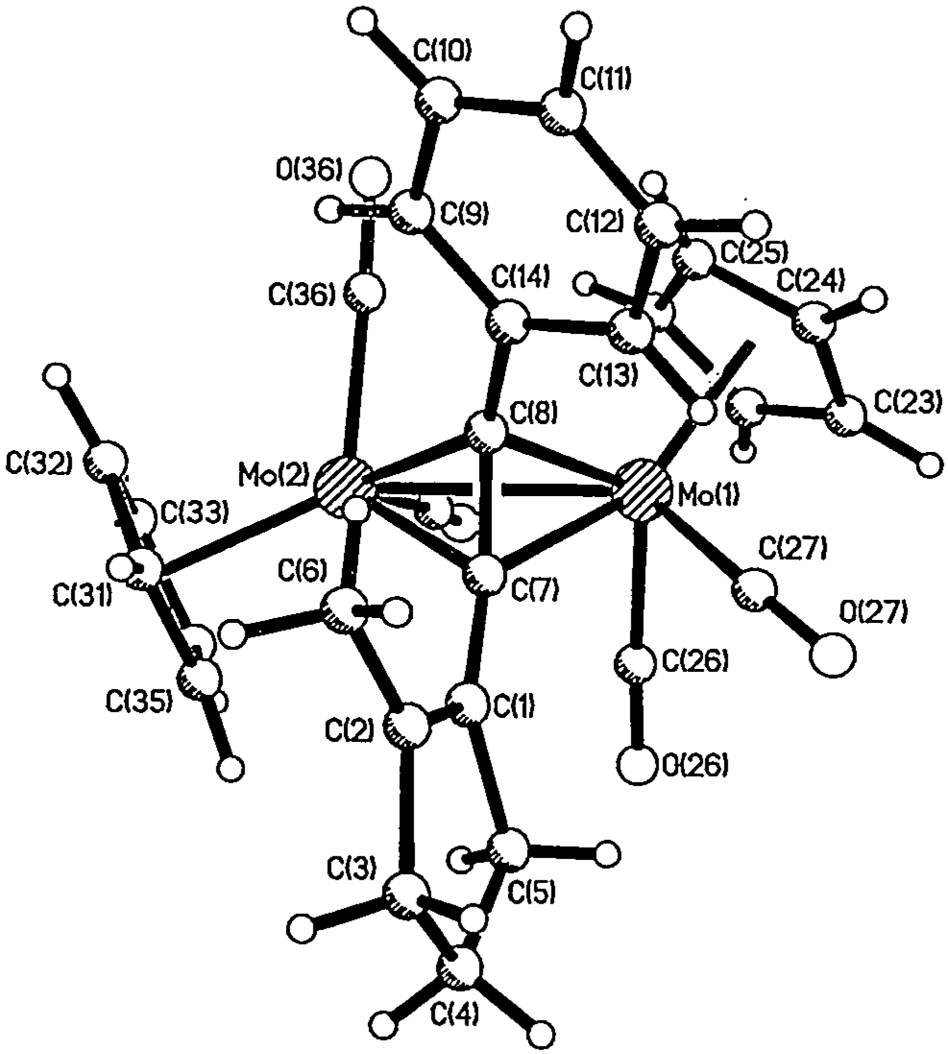

Figure 4.12 View of **51**.

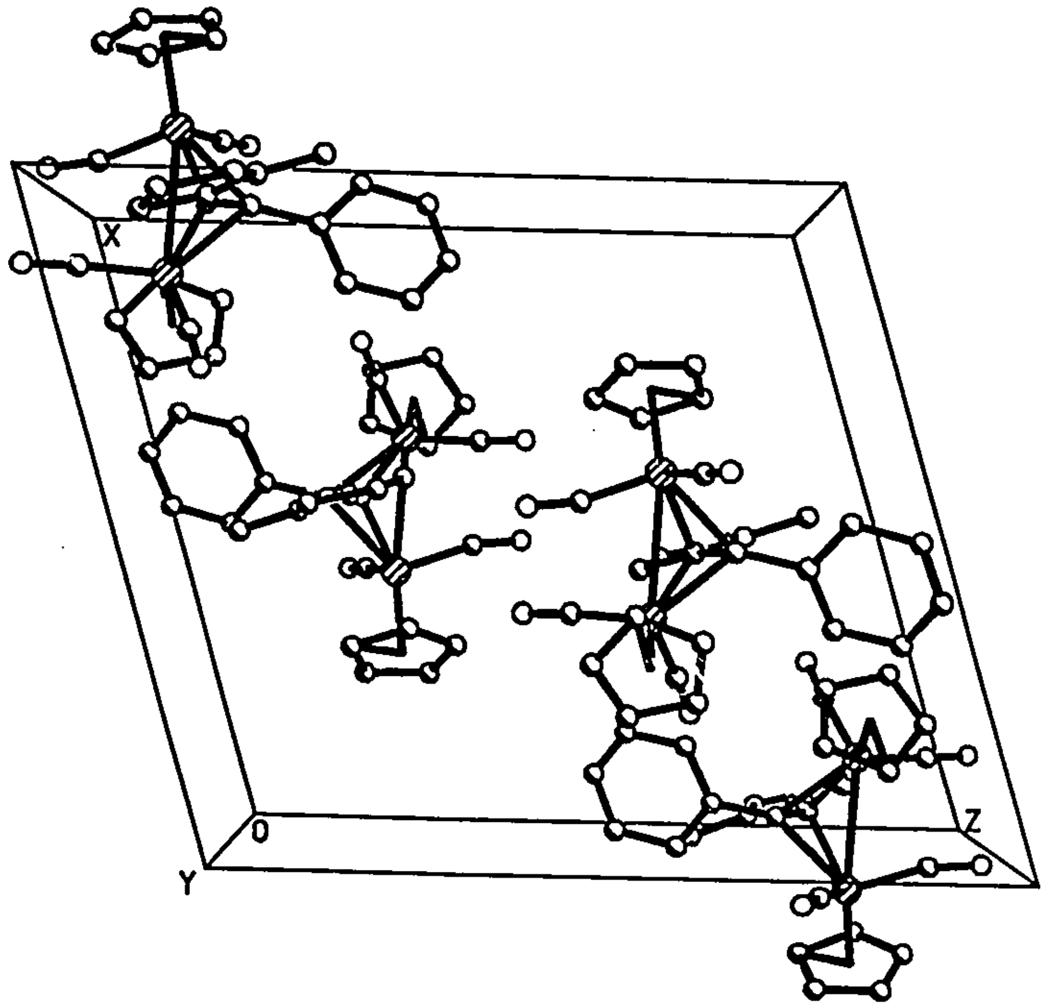

Figure 4.13 Unit cell diagram of **51**.

Table 4.1 ^{13}C NMR data for methylcyclopentanols and related metal complexes.

Molecule	C1	C2	C3	C4	C5	Me	ALKYNE C'S	CO
cis-2-methyl-1-cyclopentanol (a)	76.4	41.0	35.7	23.3	32.2	14.9	-----	-----
trans-2-methyl-1-cyclopentanol (a)	81.0	43.4	35.1	22.7	33.0	19.5	-----	-----
2-methyl-1-cyclopentene (a)(b)	124.8	140.2	37.3	24.3	33.2	16.6	-----	-----
cis-2-methyl-1-phenylethynyl-cyclopentanol, **46**	(c)	46.7	31.2	21.9	42.3	12.9	(c)	-----
trans-2-methyl-1-phenylethynyl-cyclopentanol, **47**	79.0	46.4	31.5	21.1	41.3	16.9	92.6, 86.8	-----
(**46**)-$Co_2(CO)_6$, **48**	87.0	48.5	32.2	21.2	41.5	18.9	92.9, 104.3	200.05
(cation)-$Co_2(CO)_6$, **49**	168	51	35	25	43	21.0	100, 104.2	193.1
2-methyl-1-phenylethynyl-1-cyclo-pentene-$Co_2(CO)_6$, **50**	139.5 (d)	142.1 (d)	40.8	22.4	39.8	17.0	94, 104	200.5
2-methyl-1-phenylethynyl-1-cyclo-pentene-$Cp_2Mo_2(CO)_4$, **51** (e)	134.8 (d)	137.2 (d)	40.2	22.7	34.0	16.4	(c)	233

(a) Data from "Carbon-13 NMR Spectroscopy", H.O. Kalinowski, S. Berger and S. Braun, John Wiley & Sons Ltd., 1988, p. 264, Salisbury, U.K. (b) Unconventional numbering for ease of comparison of shifts. (c) Signal not observed. (d) Assignments maybe interchanged. (e) Cyclopentadienyl resonance at 93.0.

These results must be placed in the context of other recent reports on metal-stabilized propargyl cations. Nicholas and Siegel have protonated the dicobalt hexacarbonyl complex of mestranol, **43**, and also of (*epi*-mestranol)-$Co_2(CO)_6$, **52**.[171] It was found that sodium borohydride treatment of the protonated product in each case yielded the same β-ethynyl derivative **53**. These authors proposed that the reaction proceeds via a common cationic intermediate which undergoes nucleophilic attack on the less hindered α-face. Further support is

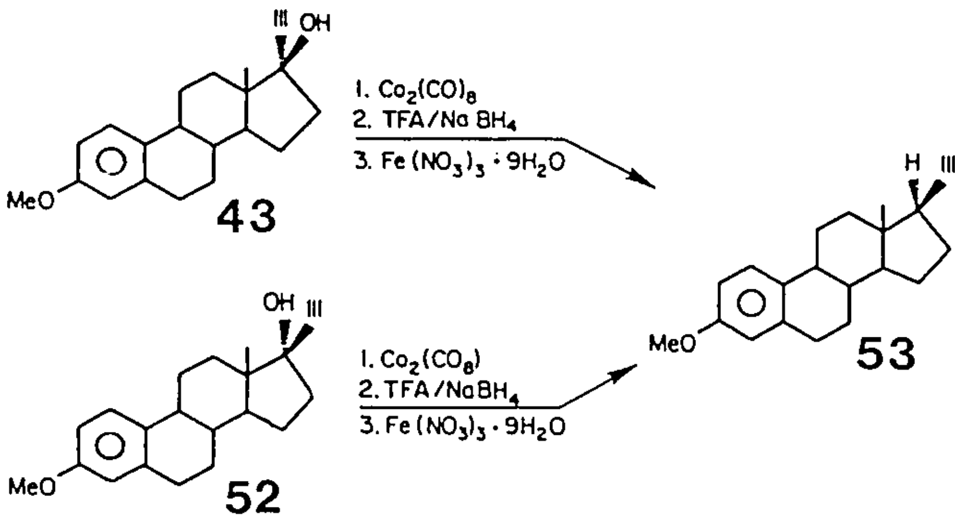

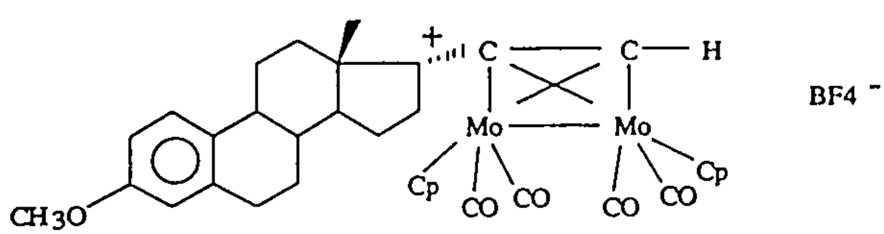

54

offered by the closely analogous cationic dimolybdenum cluster **54** in which the β-face of the steroid leans towards one of the molybdenum vertices. In this structure C(17) lies only 2.74 Å from the molybdenum atom. However, variable-temperature NMR data reveal that **54** is in equilibrium with **55** in which the α-face of the steroid interacts with the other molybdenum centre, (see scheme 4.2*).[131] The barrier to interconversion of these two isomers is ≈ 17 kcal mol^{-1}. It should be noted that the molybdenum clusters **54** and **55** are precisely those which would arise if the development of the cationic centre receives anchimeric assistance from the metal vertex. Cation **55** can form directly from protonated **44** by loss of water *trans* to the molybdenum vertex, while **54** results from the antarafacial migration of the steroidal vinylidene capping group. Such a process leaves the bond C(16)-C(15) as the *endo* edge in the transition state. In contrast, if the cationic centre were to be generated at the other molybdenum vertex (and so produce diastereomer **56**) its conversion to **57** would require that the antarafacial migration proceed via a sterically unfavourable transition state which places the steroidal C ring in the *endo* position.

The final product of borohydride attack of a metal-stabilized cation such as **54** allows the bulky dimetalla-tetrahedrane to occupy the C(17) pseudo-equatorial position, as in **55**.

---

* Taken with permission from Ph.D. thesis of C. Cordier, University of Paris, 1991.

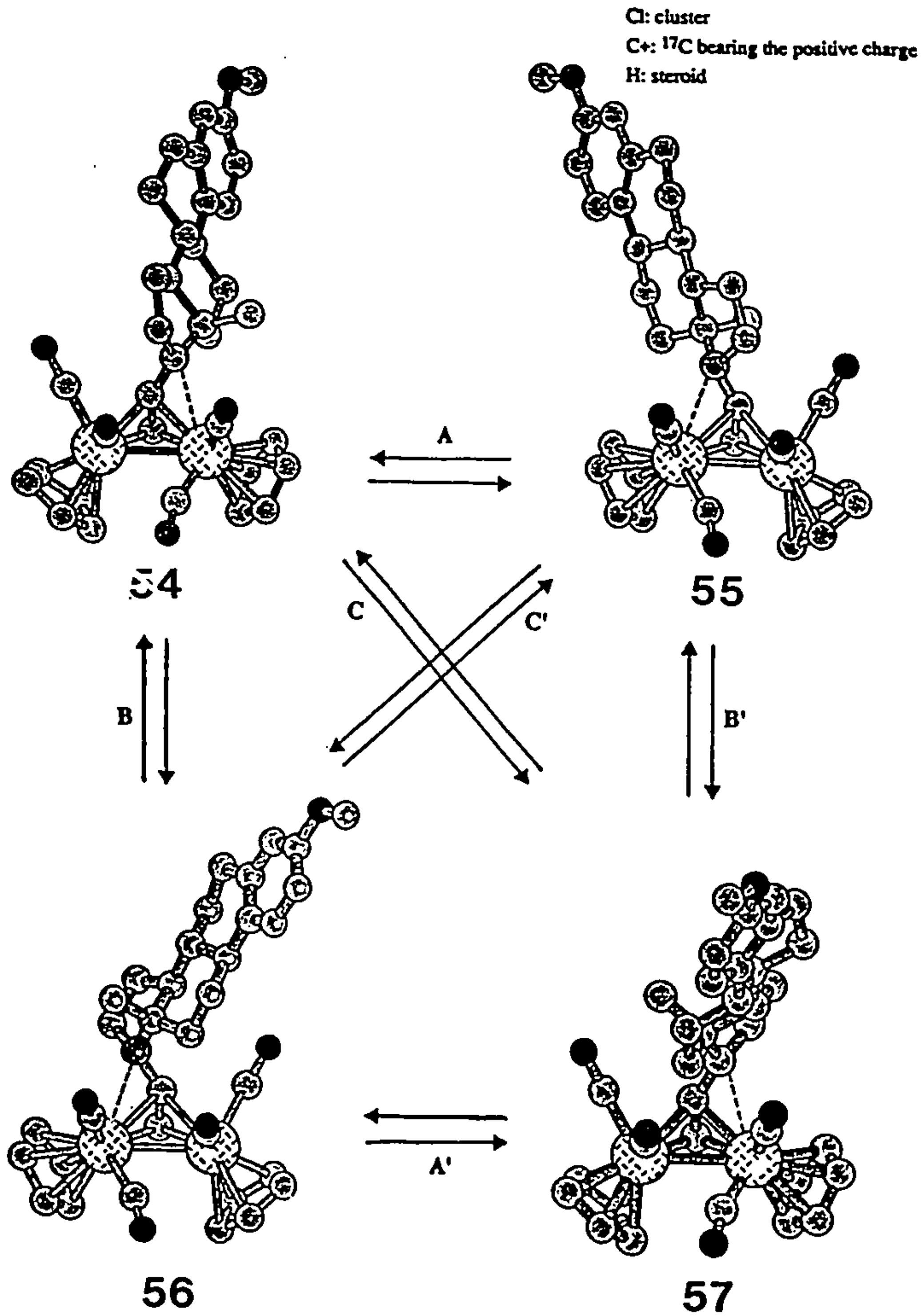

Scheme 4.2 Fluxional processes illustrating interconversion of stereoisomers.

4.3 Future Work.

Using a model analogous to that invoked for aromatic ring currents, McGlinchey and co-workers have previously presented a chemical shift contour map for protons sited close to a carbon-carbon triple bond.[172] Now, using the x-ray structural data on **47** to evaluate the geometric terms, one can readily calculate the effect of the alkyne on the chemical shifts of the methylene protons at positions C(3) and C(4).

Very recently (August 1992) Nicholas has reported[173] that although $Co_2(CO)_6$ complexes of propargyl cations readily undergo elimination to yield alkenes, the analogous clusters containing a triphenylphosphine ligand can be successfully treated with oxygen nucleophiles such as water or alcohols, as shown below:

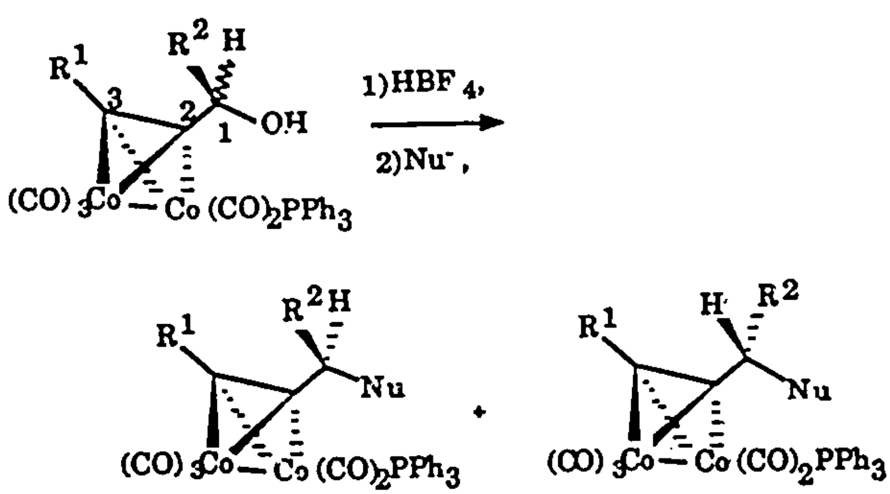

1R*, 2S*,3R*   1S*, 2S*,3R*

In the light of these recent results, it would be appropriate to continue to study the reactions of the cyclopentyl cationic cluster complexes in which one of the cobalt carbonyls had been replaced by a phosphine ligand. In this way, it should be possible to determine which epimeric cyclopentanol cobalt complex (i.e. methyl and OH cis or trans) is the more favored.

Table 4.2 STRUCTURE DETERMINATION SUMMARY FOR COMPLEX **47**

Crystal Data

Empirical Formula	$C_{14}H_{16}O$
Color; Habit	colourless chip
Crystal size (mm)	0.111 x 0.200 x 0.400
Crystal System	Orthorhombic
Space Group	Pbcn
Unit Cell Dimensions	$\underline{a}$ = 23.493(4) Å $\underline{b}$ = 11.357(4) Å $\underline{c}$ = 8.816(2) Å
Volume	2352.2(12) $Å^3$
Z	8
Formula weight	200.3
Density(calc.)	1.131 Mg/m^3
Absorption Coefficient	0.535 mm^{-1}
F(000)	864

Data Collection (COMPLEX **47**)

Diffractometer Used	Siemens P4, rotating anode
Radiation	CuKα (λ = 1.54178 Å)
Temperature (K)	296
Monochromator	Highly oriented graphite crystal
2θ Range	7.0 to 45.0°
Scan Type	ω
Scan Speed	Variable; 2.0 to 29.3°/min. in ω
Scan Range (ω)	1.20° plus Kα-separation
Background Measurement	Stationary crystal and stationary counter at beginning and end of scan, each for 0.5% of total scan time
Standard Reflections	3 measured every 100 reflections
Index Ranges	$0 \le h \le 24$, $0 \le k \le 12$ $-9 \le l \le 0$
Reflections Collected	1791
Independent Reflections	1749 (no equivalent reflections measured)
Observed Reflections	1006 ($F \geq 6.0\sigma(F)$)
Absorption Correction	DIFABS

Solution and Refinement (COMPLEX **47**)

System Used	Siemens SHELXTL PLUS (PC Version)
Solution	Direct Methods
Refinement Method	Full-Matrix Least-Squares
Quantity Minimized	$\Sigma w(\lvert F_o\rvert - \lvert F_c\rvert)^2$
Absolute Structure	N/A
Extinction Correction	N/A
Hydrogen Atoms	Riding model, fixed isotropic U
Weighting Scheme	$w^{-1} = \sigma^2(F) + 0.0007F^2$
Number of Parameters Refined	136
Final R Indices (obs. data)	R =8.77 %, wR = 13.51 %
R Indices (all data)	R = 11.76 %, wR = 13.88 %
Goodness-of-Fit	3.18
Largest and Mean Δ/σ	0.244,0.019
Data-to-Parameter Ratio	7.4:1
Largest Difference Peak	0.66 eÅ^{-3}
Largest Difference Hole	-0.30 eÅ^{-3}

Table 4.3 Atomic coordinates ($x10^4$) and equivalent isotropic displacement coefficients ($Å^2x10^3$) (COMPLEX **47**)

	x	y	z	U(eq)
C(1)	4301(3)	3609(6)	540(6)	66(2)
C(2)	4481(3)	2793(7)	-669(8)	89(3)
C(3)	3998(4)	2468(7)	-1577(8)	90(3)
C(4)	3640(4)	3685(9)	-1650(11)	112(4)
C(5)	3840(3)	4408(7)	-459(9)	83(3)
C(6)	4810(4)	1790(8)	-25(10)	131(4)
C(7)	4001(2)	3028(5)	1776(6)	48(2)
C(8)	3739(2)	2571(5)	2764(6)	44(2)
C(9)	2984(3)	2606(5)	4699(6)	53(2)
C(10)	2675(3)	2057(7)	5827(7)	72(3)
C(11)	2784(3)	914(7)	6202(7)	75(3)
C(12)	3221(3)	290(5)	5483(8)	73(3)
C(13)	3533(3)	851(5)	4373(7)	57(2)
C(14)	3418(2)	2012(4)	3970(6)	40(2)
O(1)	4722(2)	4362(3)	1145(4)	59(1)

* Equivalent isotropic U defined as one third of the trace of the orthogonalized U_{ij} tensor.

Table 4.4 Bond lengths (Å) (COMPLEX **47**).

C(1)-C(2)	1.474 (10)	C(1)-C(5)	1.665 (10)
C(1)-C(7)	1.456 (8)	C(1)-O(1)	1.412 (8)
C(2)-C(3)	1.436 (11)	C(2)-C(6)	1.489 (12)
C(3)-C(4)	1.621 (13)	C(4)-C(5)	1.413 (12)
C(7)-C(8)	1.186 (8)	C(8)-C(14)	1.450 (7)
C(9)-C(10)	1.380 (9)	C(9)-C(14)	1.381 (8)
C(10)-C(11)	1.364 (11)	C(11)-C(12)	1.400 (10)
C(12)-C(13)	1.377 (9)	C(13)-C(14)	1.392 (8)

Table 4.5 Bond angles (°) (COMPLEX **47**).

C(2)-C(1)-C(5)	98.4(5)	C(2)-C(1)-C(7)	113.2(6)
C(5)-C(1)-C(7)	109.2(5)	C(2)-C(1)-O(1)	116.9(6)
C(5)-C(1)-O(1)	109.0(5)	C(7)-C(1)-O(1)	109.3(4)
C(1)-C(2)-C(3)	109.8(7)	C(1)-C(2)-C(6)	110.7(6)
C(3)-C(2)-C(6)	115.2(7)	C(2)-C(3)-C(4)	102.3(7)
C(3)-C(4)-C(5)	107.0(7)	C(1)-C(5)-C(4)	107.1(6)
C(1)-C(7)-C(8)	177.6(6)	C(7)-C(8)-C(14)	180.0(9)
C(10)-C(9)-C(14)	120.2(6)	C(9)-C(10)-C(11)	120.4(6)
C(10)-C(11)-C(12)	120.6(6)	C(11)-C(12)-C(13)	118.5(6)
C(12)-C(13)-C(14)	121.1(6)	C(8)-C(14)-C(9)	120.8(5)
C(8)-C(14)-C(13)	120.1(5)	C(9)-C(14)-C(13)	119.1(5)

Table 4.6 Anisotropic displacement coefficients ($Å^2 x10^3$) (COMPLEX **47**).

	U_{11}	U_{22}	U_{33}	U_{12}	U_{13}	U_{23}
C(1)	87(5)	80(5)	32(3)	-37(4)	2(3)	0(3)
C(2)	101(6)	98(6)	67(5)	-40(5)	29(5)	-15(5)
C(3)	130(7)	92(6)	49(4)	-44(6)	7(5)	-22(4)
C(4)	100(6)	131(8)	105(7)	-11(6)	-36(6)	24(7)
C(5)	91(5)	77(5)	81(5)	-5(4)	5(5)	34(5)
C(6)	120(8)	138(7)	137(8)	85(6)	75(7)	55(7)
C(7)	59(3)	51(3)	34(3)	-21(3)	4(3)	5(3)
C(8)	46(3)	44(3)	42(3)	-7(3)	-5(3)	0(3)
C(9)	53(3)	56(4)	49(4)	3(3)	7(3)	4(3)
C(10)	57(4)	107(6)	53(4)	2(4)	18(3)	0(4)
C(11)	80(5)	94(6)	52(4)	-27(4)	17(4)	19(4)
C(12)	109(6)	51(4)	60(4)	-8(4)	16(4)	18(4)
C(13)	71(4)	53(4)	48(4)	-2(3)	17(3)	5(3)
C(14)	45(3)	45(3)	30(3)	-11(3)	0(3)	5(3)
O(1)	63(2)	75(3)	41(2)	-32(2)	-1(2)	5(2)

The anisotropic displacement exponent takes the form: $-2\pi^2(h^2a^{*2}U_{11} + ... + 2hka^*b^*U_{12})$.

Table 4.7 H-Atom coordinates (x10^4) and isotropic displacement coefficients ($Å^2$x10^3) (COMPLEX **47**).

	x	y	z	U
H(2A)	4735	3222	-1318	80
H(3A)	3782	1854	-1101	80
H(3B)	4112	2215	-2571	80
H(4A)	3241	3533	-1531	80
H(4B)	3698	4067	-2609	80
H(5A)	4023	5096	-860	80
H(5B)	3529	4652	171	80
H(6A)	4924	1267	-825	80
H(6B)	5142	2093	476	80
H(6C)	4579	1371	692	80
H(9)	2905	3422	4428	80
H(10)	2366	2486	6330	80
H(11)	2563	519	6995	80
H(12)	3299	-511	5757	80
H(13)	3837	426	3855	80
H(1A)	4877	4724	408	80

Table 4.8 STRUCTURE DETERMINATION SUMMARY FOR COMPLEX **48**

Crystal Data

Empirical Formula	$C_{20}H_{15}Co_2O_7$
Color; Habit	Purple plate
Crystal Size (mm)	.06 x .08 x .30
Crystal System	Monoclinic
Space Group	$P2_1/c$
Unit Cell Dimension	$\underline{a}$ = 17.198(3) Å $\underline{b}$ = 16.224(3) Å $\underline{c}$ = 16.182(3) Å $\underline{\beta}$ = 110.89(2)°
Volume	4218.3(13) $Å^3$
Z	8
Formula Weight	485.2
Density(calc.)	1.528 Mg/m^3
Absorption Coefficient	1.610 mm^{-1}
F(000)	1960

Data Collection (COMPLEX **48**)

Diffractometer Used	Siemens P4, rotating anode
Radiation	MoKα (λ = 0.71073 Å)
Temperature (K)	295
Monochromator	Highly oriented graphite crystal
2θ Range	5.0 to 45.0°
Scan Type	2θ-θ
Scan Speed	Variable; 1.5 to 14.65°/min. in ω
Scan Range (ω)	1.00° plus Kα-separation
Background Measurement	Stationary crystal and stationary counter at beginning and end of scan, each for 25.0% of total scan time
Standard Reflections	3 measured every 100 reflections
Index Ranges	$-18 \leq h \leq 17$, $-17 \leq k \leq 0$ $0 \leq \ell \leq 17$
Reflections Collected	6015
Independent Reflections	5538 (R_{int} =2.20%)
Observed Reflections	2326 ($F \geq 2.0\sigma(F)$)
Absorption Correction	psi scan

Solution and Refinement (COMPLEX **48**)

System Used	Siemens SHELXTL PLUS (VMS)
Solution	Direct Methods
Refinement Method	Full-Matrix Least-Squares
Quantity Minimized	$\Sigma w(\lvert F_o\rvert - \lvert F_c\rvert)^2$
Hydrogen Atoms	Riding model, fixed isotropic U
Weighting Scheme	$w^{-1} = \sigma^2(F) + 0.0009F^2$
Number of Parameters Refined	446
Final R Indices (obs. data)	R = 6.29 %, wR = 5.18 %
R Indices (all data)	R = 15.52 %, wR = 6.89 %
Goodness-of-Fit	0.84
Largest and Mean Δ/σ	0.199, 0.015
Data-to-Parameter Ratio	5.3:1
Largest Difference Peak	0.74 $e\AA^{-3}$
Largest Difference Hole	-0.41 $e\AA^{-3}$
Rigid Groups	C9A to C14A, C9B to C14B

Table 4.9 Atomic coordinates (x10[4]) and equivalent isotropic displacement coefficients (Å^{2}x10^3) (COMPLEX **48**).

	x	y	z	U(eq)
Co(1A)	8890(1)	1421(1)	474(1)	54(1)
Co(2A)	9381(1)	2071(1)	-629(1)	47(1)
O(1A)	10885(6)	2395(6)	1437(6)	79(5)
O(15A)	10308(8)	364(8)	1351(8)	124(7)
O(16A)	813(1)	156(1)	1810(8)	149(9)
O(17A)	7595(7)	371(7)	-742(7)	98(6)
O(18A)	8213(7)	1312(7)	-2235(7)	90(6)
O(19A)	9713(8)	3581(7)	-1451(7)	94(6)
O(20A)	10991(7)	1215(8)	-163(8)	114(7)
C(1A)	10170(9)	2914(9)	1233(8)	48(6)
C(2A)	10377(9)	3761(9)	1009(9)	65(7)
C(3A)	1098(1)	4099(9)	189(1)	95(9)
C(4A)	1057(1)	375(1)	255(1)	12(1)
C(5A)	9974(9)	308(1)	2068(8)	75(8)
C(6A)	956(1)	4337(9)	626(9)	91(9)
C(7A)	9461(9)	2495(8)	536(8)	43(6)
C(8A)	8675(8)	2556(8)	-26(8)	45(6)
C(9A)	7622(7)	3386(7)	-1177(6)	102(6)
C(10A)	6943	3922	-1429	130(7)
C(11A)	6570	4140	-823	107(6)
C(12A)	6877	3824	34	116(6)
C(13A)	7556	3288	286	92(5)
C(14A)	7929	3070	-320	51(4)
C(15A)	976(1)	78(1)	101(1)	76(9)
C(16A)	846(1)	150(1)	131(1)	9(1)
C(17A)	810(1)	78(1)	-28(1)	63(8)
C(18A)	8680(9)	160(1)	-161(1)	64(8)
C(19A)	961(1)	298(1)	-112(1)	67(8)
C(20A)	1037(1)	152(1)	-338(9)	67(8)
Co(1B)	4496(1)	2036(1)	-988(1)	61(1)
Co(2B)	3799(1)	1498(1)	-3(1)	68(1)
O(1B)	2380(5)	2446(6)	-1950(6)	73(4)
O(15B)	3666(8)	941(8)	-2511(7)	122(7)
O(16B)	4815(8)	3387(9)	-2007(8)	101(7)
O(17B)	6176(7)	1382(9)	-122(9)	153(8)
O(18B)	514(1)	416(9)	110(1)	17(1)

O(19B)	295(1)	176(1)	126(1)	16(1)
O(20B)	2593(9)	370(8)	-1224(9)	131(8)
C(1B)	2818(8)	2987(9)	-1210(8)	52(7)
C(2B)	2205(8)	3212(9)	-76(1)	68(8)
C(3B)	1612(9)	383(1)	-145(1)	10(1)
C(4B)	214(1)	427(1)	-187(1)	10(1)
C(5B)	2977(9)	3821(9)	-1581(9)	69(7)
C(6B)	2622(9)	363(1)	15(1)	99(9)
C(7B)	3593(9)	2559(8)	-653(8)	51(7)
C(8B)	4331(9)	2592(8)	41(8)	55(7)
C(9B)	5457(6)	2738(5)	1489(7)	86(5)
C(10B)	5982	3226	2168	113(6)
C(11B)	5934	4084	2099	90(6)
C(12B)	5361	4452	1350	91(5)
C(13B)	4835	3963	670	75(5)
C(14B)	4883	3106	740	53(4)
C(15B)	3993(9)	135(1)	-193(1)	75(8)
C(16B)	473(1)	286(1)	-158(1)	8(1)
C(17B)	550(1)	163(1)	-47(1)	96(9)
C(18B)	457(1)	83(1)	66(1)	10(1)
C(19B)	328(1)	165(2)	79(1)	10(1)
C(20B)	308(1)	80(1)	-75(1)	9(1)

* Equivalent isotropic U defined as one third of the trace of the orthogonalized U_{ij} tensor.

Table 4.10 Bond lengths (Å) (COMPLEX **48**).

Co(1A)-Co(2A)	2.466 (3)	Co(1A)-C(7A)	1.98 (1)
Co(1A)-C(8A)	1.99 (1)	Co(1A)-C(15A)	1.77 (1)
Co(1A)-C(16A)	1.76 (2)	Co(1A)-C(17A)	1.80 (1)
Co(2A)-C(7A)	1.96 (1)	Co(2A)-C(8A)	1.97 (2)
Co(2A)-C(18A)	1.79 (1)	Co(2A)-C(19A)	1.78 (2)
Co(2A)-C(20A)	1.83 (2)	O(1A)-C(1A)	1.43 (2)
O(15A)-C(15A)	1.13 (2)	O(16A)-C(16A)	1.14 (3)
O(17A)-C(17A)	1.14 (2)	O(18A)-C(18A)	1.14 (2)
O(19A)-C(19A)	1.16 (2)	O(20A)-C(20A)	1.12 (2)
C(1A)-C(2A)	1.50 (2)	C(1A)-C(5A)	1.53 (2)
C(1A)-C(7A)	1.50 (2)	C(2A)-C(3A)	1.53 (2)
C(2A)-C(6A)	1.61 (2)	C(3A)-C(4A)	1.58 (3)
C(4A)-C(5A)	1.51 (2)	C(7A)-C(8A)	1.34 (2)
C(8A)-C(14A)	1.46 (2)	Co(1B)-Co(2B)	2.470 (3)
Co(1B)-C(7B)	2.01 (2)	Co(1B)-C(8B)	2.00 (1)
Co(1B)-C(15B)	1.83 (1)	Co(1B)-C(16B)	1.76 (2)
Co(1B)-C(17B)	1.77 (2)	Co(2B)-C(7B)	1.98 (1)
Co(2B)-C(8B)	1.99 (1)	Co(2B)-C(18B)	1.76 (2)
Co(2B)-C(19B)	1.82 (3)	Co(2B)-C(20B)	1.80 (2)
O(1B)-C(1B)	1.46 (1)	O(15B)-C(15B)	1.13 (2)
O(16B)-C(16B)	1.15 (2)	O(17B)-C(17B)	1.16 (2)
O(18B)-C(18B)	1.19 (2)	O(19B)-C(19B)	1.10 (3)
O(20B)-C(20B)	1.14 (2)	C(1B)-C(2B)	1.53 (2)
C(1B)-C(5B)	1.53 (2)	C(1B)-C(7B)	1.49 (2)
C(2B)-C(3B)	1.57 (2)	C(2B)-C(6B)	1.54 (2)
C(3B)-C(4B)	1.50 (3)	C(4B)-C(5B)	1.53 (2)
C(7B)-C(8B)	1.36 (2)	C(8B)-C(14B)	1.45 (1)

Table 4.11 Bond angles (°) (COMPLEX **48**).

Co(2A)-Co(1A)-C(7A)	51.0(4)	Co(2A)-Co(1A)-C(8A)	51.2(5)
C(7A)-Co(1A)-C(8A)	39.3(5)	Co(2A)-Co(1A)-C(15A)	98.8(6)
C(7A)-Co(1A)-C(15A)	99.8(7)	C(8A)-Co(1A)-C(15A)	137.7(7)
Co(2A)-Co(1A)-C(16A)	150.7(6)	C(7A)-Co(1A)-C(16A)	103.7(7)
C(8A)-Co(1A)-C(16A)	100.4(7)	C(15A)-Co(1A)-C(16A)	100.4(8)
Co(2A)-Co(1A)-C(17A)	97.4(6)	C(7A)-Co(1A)-C(17A)	141.6(6)
C(8A)-Co(1A)-C(17A)	106.0(6)	C(15A)-Co(1A)-C(17A)	107.1(7)
C(16A)-Co(1A)-C(17A)	97.8(8)	Co(1A)-Co(2A)-C(7A)	51.7(4)
Co(1A)-Co(2A)-C(8A)	51.9(4)	C(7A)-Co(2A)-C(8A)	39.7(5)
Co(1A)-Co(2A)-C(18A)	99.6(6)	C(7A)-Co(2A)-C(18A)	142.8(7)
C(8A)-Co(2A)-C(18A)	105.7(7)	Co(1A)-Co(2A)-C(19A)	149.9(6)
C(7A)-Co(2A)-C(19A)	101.1(7)	C(8A)-Co(2A)-C(19A)	99.7(7)
C(18A)-Co(2A)-C(19A)	97.8(7)	Co(1A)-Co(2A)-C(20A)	97.8(6)
C(7A)-Co(2A)-C(20A)	100.6(6)	C(8A)-Co(2A)-C(20A)	138.5(6)
C(18A)-Co(2A)-C(20A)	107.2(7)	C(19A)-Co(2A)-C(20A)	100.2(8)
O(1A)-C(1A)-C(2A)	109.7(12)	O(1A)-C(1A)-C(5A)	110.1(10)
C(2A)-C(1A)-C(5A)	101.5(12)	O(1A)-C(1A)-C(7A)	108.0(11)
C(2A)-C(1A)-C(7A)	115.7(10)	C(5A)-C(1A)-C(7A)	111.6(13)
C(1A)-C(2A)-C(3A)	104.0(11)	C(1A)-C(2A)-C(6A)	112.1(13)
C(3A)-C(2A)-C(6A)	110.7(12)	C(2A)-C(3A)-C(4A)	101.0(13)
C(3A)-C(4A)-C(5A)	106.9(13)	C(1A)-C(5A)-C(4A)	105.1(14)
Co(1A)-C(7A)-Co(2A)	77.3(5)	Co(1A)-C(7A)-C(1A)	133.8(9)
Co(2A)-C(7A)-C(1A)	129.9(12)	Co(1A)-C(7A)-C(8A)	70.7(8)
Co(2A)-C(7A)-C(8A)	70.5(8)	C(1A)-C(7A)-C(8A)	146.4(13)
Co(1A)-C(8A)-Co(2A)	76.9(5)	Co(1A)-C(8A)-C(7A)	70.0(8)
Co(2A)-C(8A)-C(7A)	69.8(9)	Co(1A)-C(8A)-C(14A)	132.4(10)
Co(2A)-C(8A)-C(14A)	133.7(9)	C(7A)-C(8A)-C(14A)	145.3(12)
C(8A)-C(14A)-C(9A)	120.7(7)	C(8A)-C(14A)-C(13A)	119.1(7)
Co(1A)-C(15A)-O(15A)	178.5(16)	Co(1A)-C(16A)-O(16A)	175.5(15)
Co(1A)-C(17A)-O(17A)	178.7(16)	Co(2A)-C(18A)-O(18A)	178.2(17)
Co(2A)-C(19A)-O(19A)	175.8(16)	Co(2A)-C(20A)-O(20A)	177.8(16)
Co(2B)-Co(1B)-C(7B)	51.3(4)	Co(2B)-Co(1B)-C(8B)	51.4(4)
C(7B)-Co(1B)-C(8B)	39.8(5)	Co(2B)-Co(1B)-C(15B)	97.3(6)
C(7B)-Co(1B)-C(15B)	107.4(6)	C(8B)-Co(1B)-C(15B)	143.0(7)
Co(2B)-Co(1B)-C(16B)	150.6(7)	C(7B)-Co(1B)-C(16B)	100.0(8)
C(8B)-Co(1B)-C(16B)	103.7(8)	C(15B)-Co(1B)-C(16B)	98.0(8)
Co(2B)-Co(1B)-C(17B)	100.4(6)	C(7B)-Co(1B)-C(17B)	138.9(7)
C(8B)-Co(1B)-C(17B)	100.3(7)	C(15B)-Co(1B)-C(17B)	105.2(7)
C(16B)-Co(1B)-C(17B)	99.6(8)	Co(1B)-Co(2B)-C(7B)	52.2(5)

Co(1B)-Co(2B)-C(8B)	52.0(5)	C(7B)-Co(2B)-C(8B)	40.2(5)
Co(1B)-Co(2B)-C(18B)	100.2(8)	C(7B)-Co(2B)-C(18B)	144.5(8)
C(8B)-Co(2B)-C(18B)	106.9(8)	Co(1B)-Co(2B)-C(19B)	151.6(8)
C(7B)-Co(2B)-C(19B)	102.6(9)	C(8B)-Co(2B)-C(19B)	101.0(9)
C(18B)-Co(2B)-C(19B)	96.1(10)	Co(1B)-Co(2B)-C(20B)	99.7(7)
C(7B)-Co(2B)-C(20B)	104.0(6)	C(8B)-Co(2B)-C(20B)	142.1(7)
C(18B)-Co(2B)-C(20B)	102.3(8)	C(19B)-Co(2B)-C(20B)	99.3(10)
O(1B)-C(1B)-C(2B)	107.2(11)	O(1B)-C(1B)-C(5B)	108.6(10)
C(2B)-C(1B)-C(5B)	103.0(12)	O(1B)-C(1B)-C(7B)	107.8(11)
C(2B)-C(1B)-C(7B)	116.2(12)	C(5B)-C(1B)-C(7B)	113.6(12)
C(1B)-C(2B)-C(3B)	101.0(13)	C(1B)-C(2B)-C(6B)	113.3(11)
C(3B)-C(2B)-C(6B)	111.2(13)	C(2B)-C(3B)-C(4B)	106.4(13)
C(3B)-C(4B)-C(5B)	106.8(13)	C(1B)-C(5B)-C(4B)	105.2(13)
Co(1B)-C(7B)-Co(2B)	76.5(5)	Co(1B)-C(7B)-C(1B)	130.2(10)
Co(2B)-C(7B)-C(1B)	132.7(11)	Co(1B)-C(7B)-C(8B)	69.9(9)
Co(2B)-C(7B)-C(8B)	70.0(8)	C(1B)-C(7B)-C(8B)	148.3(13)
Co(1B)-C(8B)-Co(2B)	76.5(5)	Co(1B)-C(8B)-C(7B)	70.3(9)
Co(2B)-C(8B)-C(7B)	69.8(8)	Co(1B)-C(8B)-C(14B)	131.2(11)
Co(2B)-C(8B)-C(14B)	134.9(9)	C(7B)-C(8B)-C(14B)	145.3(13)
C(8B)-C(14B)-C(9B)	119.6(6)	C(8B)-C(14B)-C(13B)	120.4(6)
Co(1B)-C(15B)-O(15B)	178.3(14)	Co(1B)-C(16B)-O(16B)	174.6(13)
Co(1B)-C(17B)-O(17B)	178.4(17)	Co(2B)-C(18B)-O(18B)	174.9(20)
Co(2B)-C(19B)-O(19B)	178.2(22)	Co(2B)-C(20B)-O(20B)	177.6(18)

Table 4.12 Anisotropic displacement coefficients ($Å^2x10^3$) (COMPLEX 48).

	U_{11}	U_{22}	U_{33}	U_{12}	U_{13}	U_{23}
Co(1A)	60(1)	41(2)	57(1)	-13(1)	16(1)	4(1)
Co(2A)	52(1)	37(1)	55(1)	-1(1)	22(1)	-4(1)
O(1A)	55(6)	49(7)	111(8)	26(6)	3(6)	-11(6)
O(15A)	96(10)	76(11)	147(11)	-3(8)	-21(9)	43(9)
O(16A)	233(16)	157(14)	95(10)	-83(12)	104(10)	-14(10)
O(17A)	85(9)	97(11)	92(9)	-58(8)	9(7)	-4(7)
O(18A)	105(10)	83(10)	76(8)	-16(8)	24(7)	-7(7)
O(19A)	144(10)	60(9)	96(9)	-10(9)	65(8)	-4(8)
O(20A)	86(10)	103(12)	152(11)	47(9)	41(9)	-14(8)
C(1A)	68(11)	33(10)	40(8)	-16(10)	17(8)	-12(8)
C(2A)	77(12)	41(11)	67(10)	-3(10)	11(9)	-2(9)
C(3A)	119(15)	37(11)	98(13)	-24(11)	2(12)	-10(10)
C(4A)	158(18)	115(19)	88(13)	-20(15)	60(13)	-52(13)
C(5A)	89(12)	74(13)	51(9)	-25(11)	11(9)	-23(9)
C(6A)	115(15)	66(13)	88(12)	-1(12)	31(11)	18(10)
C(7A)	55(10)	24(9)	54(10)	16(8)	24(8)	28(8)
C(8A)	54(10)	32(9)	50(9)	6(9)	17(8)	17(8)
C(15A)	64(13)	56(13)	87(13)	-5(11)	2(10)	34(10)
C(16A)	135(18)	60(13)	66(13)	-55(13)	23(12)	2(12)
C(17A)	66(12)	66(14)	61(11)	-16(11)	26(9)	7(10)
C(18A)	77(12)	52(12)	54(10)	24(10)	14(9)	10(9)
C(19A)	84(12)	54(13)	72(12)	3(13)	41(9)	-9(11)
C(20A)	85(13)	57(13)	64(10)	-5(12)	34(10)	-19(9)
Co(1B)	56(2)	50(2)	70(1)	6(1)	13(1)	-10(1)
Co(2B)	78(2)	44(2)	68(2)	-7(1)	7(1)	5(1)
O(1B)	55(6)	57(7)	82(7)	4(6)	-7(5)	-26(6)
O(15B)	159(12)	92(11)	86(9)	-15(9)	11(8)	-55(8)
O(16B)	92(9)	97(12)	124(11)	-23(9)	52(7)	6(9)
O(17B)	68(9)	149(14)	197(14)	37(10)	-6(9)	1(11)
O(18B)	194(17)	79(12)	173(15)	33(11)	-25(12)	12(10)
O(19B)	153(15)	197(20)	140(16)	-41(13)	70(12)	13(14)
O(20B)	150(13)	81(11)	123(11)	-44(10)	1(9)	-13(8)
C(1B)	61(10)	30(10)	54(9)	4(10)	6(8)	9(9)
C(2B)	47(10)	64(13)	94(12)	-14(9)	28(10)	-39(10)
C(3B)	35(11)	72(15)	179(18)	27(11)	7(12)	-15(13)
C(4B)	67(13)	49(13)	161(18)	19(11)	-4(12)	22(12)
C(5B)	63(11)	48(11)	83(11)	19(9)	10(8)	18(9)

C(6B)	96(13)	105(16)	108(13)	-6(13)	53(11)	-37(12)
C(7B)	59(11)	35(10)	62(10)	1(9)	25(9)	11(8)
C(8B)	57(10)	40(10)	60(10)	-6(9)	11(8)	2(8)
C(15B)	68(12)	71(14)	77(12)	1(11)	12(9)	-3(11)
C(16B)	64(12)	54(16)	113(17)	-11(12)	29(11)	-19(12)
C(17B)	76(13)	97(16)	88(12)	22(12)	-3(10)	-28(11)
C(18B)	118(18)	79(17)	87(14)	-21(14)	12(12)	-3(12)
C(19B)	94(20)	87(17)	99(20)	-16(14)	-9(14)	29(15)
C(20B)	117(17)	49(14)	77(13)	-26(12)	8(11)	-12(10)

The anisotropic displacement factor exponent takes the form: $-2\pi^2(h^2a^{*2}U_{11} + ... + 2hka^*b^*U_{12})$

Table 4.13 H-Atom coordinates ($x10^4$) and isotropic displacement coefficients ($Å^2x10^3$) (COMPLEX **48**).

	x	y	z	U
H(2AA)	10655	3719	590	186(15)
H(3AA)	10987	4690	1903	186(15)
H(3AB)	11531	3894	2025	186(15)
H(4AA)	10285	4181	2739	186(15)
H(4AB)	10988	3523	3064	186(15)
H(5AA)	10056	2583	2411	186(15)
H(5AB)	9410	3262	1925	186(15)
H(6AA)	9364	4438	1101	186(15)
H(6AB)	9136	4068	149	186(15)
H(6AC)	9704	4851	422	186(15)
H(9A)	7879	3236	-1594	186(15)
H(10A)	6732	4139	-2019	186(15)
H(11A)	6103	4509	-996	186(15)
H(12A)	6621	3974	451	186(15)
H(13A)	7768	3071	876	186(15)
H(2BA)	1909	2730	-691	186(15)
H(3BA)	1381	4222	-1157	186(15)
H(3BB)	1164	3540	-1881	186(15)
H(4BA)	2219	4840	-1689	186(15)
H(4BB)	1879	4252	-2498	186(15)
H(5BA)	3148	3725	-2076	186(15)
H(5BB)	3399	4131	-1140	186(15)
H(6BA)	2801	4117	-69	186(15)
H(6BB)	3098	3348	550	186(15)
H(6BC)	2256	3782	453	186(15)
H(9B)	5490	2148	1536	186(15)
H(10B)	6377	2973	2684	186(15)
H(11B)	6296	4420	2566	186(15)
H(12B)	5328	5041	1302	186(15)
H(13B)	4440	4216	155	186(15)

Table 4.14 STRUCTURE DETERMINATION SUMMARY FOR COMPLEX **51**

Crystal Data

Empirical Formula	$C_{28} H_{24} Mo_2 O_4$
Color; Habit	Red plate
Crystal size (mm)	0.10 x 0.19 x 0.02
Crystal System	Monoclinic
Space Group	$P2_1/n$
Unit Cell Dimensions	$\underline{a}$ = 14.070(10) Å $\underline{b}$ = 11.176(6) Å $\underline{c}$ = 16.018(9) Å $\underline{\beta}$ = 106.01(4)°
Volume	2421.1(12) $Å^3$
Z	4
Formula weight	616.4
Density(calc.)	1.691 Mg/m^3
Absorption Coefficient	1.068 mm^{-1}
F(000)	1232

Data Collection (COMPLEX **51**)

Diffractometer Used	Siemens P4, rotating anode
Radiation	MoKα (λ = 0.71073 Å)
Temperature (K)	297
Monochromator	Highly oriented graphite crystal
2θ Range	7.0 to 45.0°
Scan Type	ω
Scan Speed	Variable; 2.0 to 29.3°/min. in ω
Scan Range (ω)	1.20° plus Kα-separation
Background Measurement	Stationary crystal and stationary counter at beginning and end of scan, each for 0.5% of total scan time
Standard Reflections	3 measured every 100 reflections
Index Ranges	$0 \leq h \leq 15$, $0 \leq k \leq 12$ $-17 \leq l \leq 16$
Reflections Collected	4437
Independent Reflections	3372 (R_{int} = 6.59%)
Observed Reflections	1868 ($F \geq 4.0\sigma(F)$)
Absorption Correction	DIFABS

Solution and Refinement (COMPLEX **51**)

System Used	Siemens SHELXTL PLUS (PC Version)
Solution	Direct Methods
Refinement Method	Full-Matrix Least-Squares
Quantity Minimized	$\Sigma w(\|F_o\|-\|F_c\|)^2$
Hydrogen Atoms	Riding model, fixed isotropic U
Weighting Scheme	$w^{-1} = \sigma^2(F) + 0.0001F^2$
Number of Parameters Refined	307
Final R Indices (obs. data)	R = 5.59 %, wR = 5.18 %
R Indices (all data)	R = 11.12 %, wR = 6.28 %
Goodness-of-Fit	1.46
Largest and Mean Δ/σ	0.462, 0.017
Data-to-Parameter Ratio	6.1:1
Largest Difference Peak	0.58 eÅ^{-3}
Largest Difference Hole	-0.65 eÅ^{-3}

Table 4.15 Atomic coordinates ($x10^4$) and equivalent isotropic displacement coefficients ($Å^2x10^3$) (COMPLEX **51**).

	x	y	z	U(eq)
Mo(1)	6361(1)	2250(1)	3697(1)	34(1)
Mo(2)	4193(1)	2472(1)	3058(1)	44(1)
C(1)	5392(9)	4913(11)	2789(9)	37(5)
C(2)	5127(10)	5587(11)	2092(11)	47(6)
C(3)	5232(12)	6903(11)	2295(11)	57(7)
C(4)	5482(14)	6955(13)	3240(13)	88(10)
C(5)	5672(12)	5703(11)	3593(10)	59(7)
C(6)	4791(12)	5197(13)	1209(10)	68(7)
C(7)	5380(11)	3623(10)	2885(9)	41(6)
C(8)	5347(8)	2643(10)	2391(9)	44(5)
C(9)	4897(12)	1801(11)	909(10)	51(6)
C(10)	5159(16)	1578(12)	128(11)	68(8)
C(11)	6030(19)	1942(17)	51(14)	91(11)
C(12)	6670(13)	2513(16)	646(10)	80(8)
C(13)	6460(10)	2715(12)	1426(9)	55(6)
C(14)	5566(9)	2360(10)	1562(8)	41(5)
C(21)	6282(12)	163(12)	3926(12)	61(9)
C(22)	6995(15)	670(14)	4623(11)	66(8)
C(23)	7753(14)	1111(14)	4346(14)	69(9)
C(24)	7521(13)	920(12)	3449(14)	59(9)
C(25)	6632(13)	352(11)	3188(11)	58(8)
C(26)	6324(12)	3211(13)	4705(10)	57(7)
O(26)	6343(11)	3777(10)	5327(8)	95(7)
C(27)	7259(11)	3470(11)	3537(9)	39(6)
O(27)	7827(8)	4192(9)	3480(7)	61(5)
C(31)	3007(12)	3808(16)	2228(12)	68(8)
C(32)	2557(12)	2662(18)	2265(15)	95(10)
C(33)	2570(11)	2511(16)	3140(16)	90(10)
C(34)	3063(12)	3478(16)	3635(13)	73(8)
C(35)	3324(11)	4268(14)	3077(14)	67(8)
C(36)	4213(11)	869(14)	2595(12)	67(8)
O(36)	4185(9)	-98(10)	2308(9)	99(7)
C(37)	4645(13)	1799(12)	4205(13)	68(9)
O(37)	4733(11)	1360(10)	4897(9)	105(8)

* Equivalent isotropic U defined as one third of the trace of the orthogonalized U_{ij} tensor

Table 4.16 Bond lengths (Å) (COMPLEX **51**).

Mo(1)-Mo(2)	2.947 (3)	Mo(1)-C(7)	2.227 (12)
Mo(1)-C(8)	2.227 (12)	Mo(1)-C(21)	2.368 (14)
Mo(1)-C(22)	2.320 (16)	Mo(1)-C(23)	2.327 (17)
Mo(1)-C(24)	2.321 (18)	Mo(1)-C(25)	2.341 (14)
Mo(1)-C(26)	1.951 (17)	Mo(1)-C(27)	1.924 (15)
Mo(2)-C(7)	2.184 (15)	Mo(2)-C(8)	2.184 (14)
Mo(2)-C(31)	2.358 (16)	Mo(2)-C(32)	2.312 (16)
Mo(2)-C(33)	2.324 (17)	Mo(2)-C(34)	2.337 (20)
Mo(2)-C(35)	2.356 (16)	Mo(2)-C(36)	1.942 (16)
Mo(2)-C(37)	1.924 (19)	C(1)-C(2)	1.313 (20)
C(1)-C(5)	1.521 (20)	C(1)-C(7)	1.451 (17)
C(2)-C(3)	1.505 (18)	C(2)-C(6)	1.430 (22)
C(3)-C(4)	1.457 (27)	C(4)-C(5)	1.505 (19)
C(7)-C(8)	1.345 (18)	C(8)-C(14)	1.477 (20)
C(9)-C(10)	1.419 (26)	C(9)-C(14)	1.352 (18)
C(10)-C(11)	1.330 (35)	C(11)-C(12)	1.286 (26)
C(12)-C(13)	1.379 (24)	C(13)-C(14)	1.393 (21)
C(21)-C(22)	1.398 (22)	C(21)-C(25)	1.416 (28)
C(22)-C(23)	1.356 (30)	C(23)-C(24)	1.400 (30)
C(24)-C(25)	1.362 (23)	C(26)-O(26)	1.175 (21)
C(27)-O(27)	1.157 (19)	C(31)-C(32)	1.437 (27)
C(31)-C(35)	1.407 (28)	C(32)-C(33)	1.406 (36)
C(33)-C(34)	1.406 (25)	C(34)-C(35)	1.375 (29)
C(36)-O(36)	1.171 (20)	C(37)-O(37)	1.179 (25)

Table 4.17 Bond angles (°) (COMPLEX **51**).

Mo(2)-Mo(1)-C(7)	47.5(4)	Mo(2)-Mo(1)-C(8)	47.5(4)
C(7)-Mo(1)-C(8)	35.2(5)	Mo(2)-Mo(1)-C(21)	92.8(4)
C(7)-Mo(1)-C(21)	136.1(5)	C(8)-Mo(1)-C(21)	107.1(5)
Mo(2)-Mo(1)-C(22)	117.7(5)	C(7)-Mo(1)-C(22)	164.7(7)
C(8)-Mo(1)-C(22)	141.7(5)	C(21)-Mo(1)-C(22)	34.7(6)
Mo(2)-Mo(1)-C(23)	149.8(4)	C(7)-Mo(1)-C(23)	161.3(7)
C(8)-Mo(1)-C(23)	140.3(6)	C(21)-Mo(1)-C(23)	57.5(6)
C(22)-Mo(1)-C(23)	33.9(7)	Mo(2)-Mo(1)-C(24)	134.7(4)
C(7)-Mo(1)-C(24)	133.9(7)	C(8)-Mo(1)-C(24)	105.3(6)
C(21)-Mo(1)-C(24)	57.4(6)	C(22)-Mo(1)-C(24)	57.1(7)
C(23)-Mo(1)-C(24)	35.1(7)	Mo(2)-Mo(1)-C(25)	102.0(4)
C(7)-Mo(1)-C(25)	123.7(5)	C(8)-Mo(1)-C(25)	88.6(5)
C(21)-Mo(1)-C(25)	35.0(7)	C(22)-Mo(1)-C(25)	57.5(6)
C(23)-Mo(1)-C(25)	57.5(6)	C(24)-Mo(1)-C(25)	34.0(6)
Mo(2)-Mo(1)-C(26)	88.8(5)	C(7)-Mo(1)-C(26)	87.1(6)
C(8)-Mo(1)-C(26)	120.8(5)	C(21)-Mo(1)-C(26)	113.6(7)
C(22)-Mo(1)-C(26)	89.0(6)	C(23)-Mo(1)-C(26)	98.2(7)
C(24)-Mo(1)-C(26)	132.4(6)	C(25)-Mo(1)-C(26)	146.2(6)
Mo(2)-Mo(1)-C(27)	123.3(4)	C(7)-Mo(1)-C(27)	76.0(5)
C(8)-Mo(1)-C(27)	90.5(5)	C(21)-Mo(1)-C(27)	141.2(6)
C(22)-Mo(1)-C(27)	118.2(6)	C(23)-Mo(1)-C(27)	86.8(6)
C(24)-Mo(1)-C(27)	84.9(6)	C(25)-Mo(1)-C(27)	114.8(7)
C(26)-Mo(1)-C(27)	83.6(7)	Mo(1)-Mo(2)-C(7)	48.7(3)
Mo(1)-Mo(2)-C(8)	48.7(3)	C(7)-Mo(2)-C(8)	35.9(5)
Mo(1)-Mo(2)-C(31)	138.8(4)	C(7)-Mo(2)-C(31)	90.1(6)
C(8)-Mo(2)-C(31)	100.1(6)	Mo(1)-Mo(2)-C(32)	167.6(6)
C(7)-Mo(2)-C(32)	123.8(6)	C(8)-Mo(2)-C(32)	119.0(7)
C(31)-Mo(2)-C(32)	35.8(7)	Mo(1)-Mo(2)-C(33)	157.0(6)
C(7)-Mo(2)-C(33)	142.5(6)	C(8)-Mo(2)-C(33)	154.2(7)
C(31)-Mo(2)-C(33)	57.7(7)	C(32)-Mo(2)-C(33)	35.3(9)
Mo(1)-Mo(2)-C(34)	130.9(4)	C(7)-Mo(2)-C(34)	113.2(6)
C(8)-Mo(2)-C(34)	146.1(6)	C(31)-Mo(2)-C(34)	57.6(7)
C(32)-Mo(2)-C(34)	59.3(7)	C(33)-Mo(2)-C(34)	35.1(7)
Mo(1)-Mo(2)-C(35)	124.0(4)	C(7)-Mo(2)-C(35)	85.3(5)
C(8)-Mo(2)-C(35)	113.0(6)	C(31)-Mo(2)-C(35)	34.7(7)
C(32)-Mo(2)-C(35)	59.1(6)	C(33)-Mo(2)-C(35)	57.4(6)
C(34)-Mo(2)-C(35)	34.1(7)	Mo(1)-Mo(2)-C(36)	86.1(4)
C(7)-Mo(2)-C(36)	113.8(7)	C(8)-Mo(2)-C(36)	78.7(6)
C(31)-Mo(2)-C(36)	116.8(6)	C(32)-Mo(2)-C(36)	89.6(7)

C(33)-Mo(2)-C(36)	99.0(7)	C(34)-Mo(2)-C(36)	132.7(7)
C(35)-Mo(2)-C(36)	148.6(6)	Mo(1)-Mo(2)-C(37)	66.3(6)
C(7)-Mo(2)-C(37)	106.7(6)	C(8)-Mo(2)-C(37)	114.0(6)
C(31)-Mo(2)-C(37)	141.4(8)	C(32)-Mo(2)-C(37)	125.3(8)
C(33)-Mo(2)-C(37)	91.4(8)	C(34)-Mo(2)-C(37)	83.8(7)
C(35)-Mo(2)-C(37)	110.9(8)	C(36)-Mo(2)-C(37)	88.2(7)
C(2)-C(1)-C(5)	109.5(11)	C(2)-C(1)-C(7)	130.6(13)
C(5)-C(1)-C(7)	119.7(12)	C(1)-C(2)-C(3)	112.8(14)
C(1)-C(2)-C(6)	127.3(12)	C(3)-C(2)-C(6)	119.9(13)
C(2)-C(3)-C(4)	104.2(12)	C(3)-C(4)-C(5)	108.7(13)
C(1)-C(5)-C(4)	104.1(13)	Mo(1)-C(7)-Mo(2)	83.8(5)
Mo(1)-C(7)-C(1)	136.3(9)	Mo(2)-C(7)-C(1)	129.1(11)
Mo(1)-C(7)-C(8)	72.4(7)	Mo(2)-C(7)-C(8)	72.0(8)
C(1)-C(7)-C(8)	138.3(14)	Mo(1)-C(8)-Mo(2)	83.9(5)
Mo(1)-C(8)-C(7)	72.4(7)	Mo(2)-C(8)-C(7)	72.1(9)
Mo(1)-C(8)-C(14)	124.3(8)	Mo(2)-C(8)-C(14)	142.0(8)
C(7)-C(8)-C(14)	136.2(13)	C(10)-C(9)-C(14)	118.0(16)
C(9)-C(10)-C(11)	119.9(16)	C(10)-C(11)-C(12)	123.8(23)
C(11)-C(12)-C(13)	118.2(20)	C(12)-C(13)-C(14)	121.6(13)
C(8)-C(14)-C(9)	121.5(13)	C(8)-C(14)-C(13)	120.0(11)
C(9)-C(14)-C(13)	118.4(14)	Mo(1)-C(21)-C(22)	70.8(9)
Mo(1)-C(21)-C(25)	71.4(8)	C(22)-C(21)-C(25)	105.5(16)
Mo(1)-C(22)-C(21)	74.5(9)	Mo(1)-C(22)-C(23)	73.3(10)
C(21)-C(22)-C(23)	110.1(18)	Mo(1)-C(23)-C(22)	72.7(10)
Mo(1)-C(23)-C(24)	72.2(10)	C(22)-C(23)-C(24)	107.3(15)
Mo(1)-C(24)-C(23)	72.7(11)	Mo(1)-C(24)-C(25)	73.8(10)
C(23)-C(24)-C(25)	108.7(19)	Mo(1)-C(25)-C(21)	73.5(9)
Mo(1)-C(25)-C(24)	72.2(9)	C(21)-C(25)-C(24)	108.3(15)
Mo(1)-C(26)-O(26)	177.2(14)	Mo(1)-C(27)-O(27)	176.8(12)
Mo(2)-C(31)-C(32)	70.3(10)	Mo(2)-C(31)-C(35)	72.5(9)
C(32)-C(31)-C(35)	108.1(18)	Mo(2)-C(32)-C(31)	73.9(9)
Mo(2)-C(32)-C(33)	72.8(9)	C(31)-C(32)-C(33)	105.3(17)
Mo(2)-C(33)-C(32)	71.9(11)	Mo(2)-C(33)-C(34)	73.0(10)
C(32)-C(33)-C(34)	109.7(18)	Mo(2)-C(34)-C(33)	71.9(11)
Mo(2)-C(34)-C(35)	73.7(12)	C(33)-C(34)-C(35)	107.8(18)
Mo(2)-C(35)-C(31)	72.7(10)	Mo(2)-C(35)-C(34)	72.2(10)
C(31)-C(35)-C(34)	108.9(15)	Mo(2)-C(36)-O(36)	177.3(14)
Mo(2)-C(37)-O(37)	167.2(16)		

Table 4.18 Anisotropic displacement coefficients (Å^{2}x10^3) (COMPLEX **51**).

	U_{11}	U_{22}	U_{33}	U_{12}	U_{13}	U_{23}
Mo(1)	39(1)	35(1)	27(1)	2(1)	7(1)	4(1)
Mo(2)	37(1)	41(1)	58(1)	-6(1)	18(1)	-10(1)
C(1)	25(8)	44(8)	35(10)	7(6)	-5(7)	9(7)
C(2)	33(9)	55(9)	48(11)	6(7)	2(9)	6(8)
C(3)	54(11)	49(8)	75(13)	11(7)	29(11)	12(8)
C(4)	95(17)	53(10)	104(19)	-22(9)	6(14)	6(10)
C(5)	58(11)	55(9)	64(13)	-4(8)	15(10)	-1(8)
C(6)	66(12)	72(10)	58(13)	9(9)	1(11)	-4(9)
C(7)	48(10)	36(8)	34(10)	-5(7)	2(8)	-9(7)
C(8)	25(7)	41(7)	60(10)	-7(7)	3(7)	-2(8)
C(9)	64(11)	58(8)	27(10)	-6(8)	4(9)	-2(7)
C(10)	99(16)	58(10)	29(12)	-2(10)	-9(11)	-24(8)
C(11)	127(21)	100(14)	55(15)	58(14)	43(15)	35(12)
C(12)	75(12)	129(15)	32(10)	-32(13)	7(10)	-27(12)
C(13)	58(10)	72(9)	37(9)	0(9)	15(8)	-2(8)
C(14)	41(8)	35(7)	39(9)	-1(7)	-2(7)	-7(7)
C(21)	74(14)	34(8)	88(16)	19(8)	42(13)	26(8)
C(22)	87(16)	75(11)	34(12)	18(11)	15(12)	13(9)
C(23)	55(12)	73(10)	78(16)	2(10)	15(13)	-7(11)
C(24)	38(12)	56(9)	90(18)	6(8)	32(12)	-5(10)
C(25)	78(14)	44(8)	64(12)	20(9)	39(11)	11(8)
C(26)	77(13)	66(9)	34(11)	2(9)	26(10)	18(8)
O(26)	160(14)	89(8)	40(8)	-3(8)	34(9)	-12(7)
C(27)	40(10)	56(8)	13(9)	-8(8)	-6(8)	12(7)
O(27)	51(8)	81(7)	44(8)	-22(6)	1(6)	4(6)
C(31)	50(12)	84(12)	60(14)	16(10)	-1(11)	3(10)
C(32)	57(11)	111(16)	110(18)	-11(12)	14(13)	-86(15)
C(33)	29(9)	81(12)	164(22)	-14(10)	35(12)	-14(15)
C(34)	48(12)	97(13)	77(15)	13(10)	22(11)	-24(12)
C(35)	34(10)	68(10)	101(17)	2(8)	22(12)	-24(12)
C(36)	42(11)	63(10)	102(16)	-6(8)	31(12)	-9(10)
O(36)	99(11)	65(7)	147(13)	-19(7)	58(10)	-43(8)
C(37)	69(13)	54(9)	10[illegible](17)	-9(8)	57(13)	-14(10)
O(37)	155(15)	96(9)	102(12)	16(9)	97(12)	22(8)

The anisotropic displacement exponent takes the form: $-2\pi^2(h^2a^{*2}U_{11} + ... + 2hka^*b^*U_{12})$

Table 4.19 H-Atom coordinates ($x10^4$) and isotropic displacement coefficients ($Å^2x10^3$) (COMPLEX **51**).

	x	y	z	U
H(3A)	4615	7303	2044	80
H(3B)	5738	7265	2082	80
H(4A)	4955	7316	3426	80
H(4B)	6069	7425	3460	80
H(5A)	6351	5583	3910	80
H(5B)	5260	5522	3966	80
H(6A)	4774	4340	1166	80
H(6B)	4136	5511	979	80
H(6C)	5215	5511	883	80
H(9A)	4281	1568	1008	80
H(10A)	4660	1198	-327	80
H(11A)	6156	1765	-496	80
H(12A)	7293	2720	549	80
H(13A)	6942	3129	1875	80
H(21A)	5697	-269	3939	80
H(22A)	6950	624	5209	80
H(23A)	8374	1391	4713	80
H(24A)	7936	1096	3079	80
H(25A)	6332	67	2610	80
H(31A)	3033	4216	1707	80
H(32A)	2217	2164	1788	80
H(33A)	2255	1863	3354	80
H(34A)	3120	3621	4238	80
H(35A)	3625	5036	3236	80

CHAPTER 5

HINDERED ROTATIONS

5.1 Introduction.

The detection of hindered rotation of molecular fragments in sterically crowded molecules has attracted much attention in recent years.[174] In a now classic series of publications, Mislow *et al.* have elucidated the mechanistic pathways for many such processes. Typically, these studies have focussed on such systems as triarylboranes, triarylamines or polyaryl-benzenes in which the incorporation of bulky substituents in the *ortho* or *meta* positions raises the aryl rotation barriers into the NMR-detectable range.[175] In many of these cases, it has been shown that the motions of these aryl rings are coupled in such a way that none of the rings moves independently of the others; such processes are termed *correlated rotations.* Moreover, in an elegant extension of this concept, it has been demonstrated that molecules containing a closed cyclic array of securely meshed gears have parity constraints entirely analogous to mechanical systems.[176]

Our own contributions have been aimed not at differentiating the **edges** of aryl rings but rather on "painting the **faces** different colors" via the attachment of π-bonded organometallic moieties. Using this approach it has been shown that one can measure the rotational barriers for substituents attached to the central ring since they can adopt conformations in which they are *proximal* or *distal* with respect to the metal, as in **58** or **59**.[177] It is also possible, when the molecular symmetry is judiciously broken, to determine the steric or electronic barriers to tripodal rotation, as in **60** or **61**, respectively.[178]

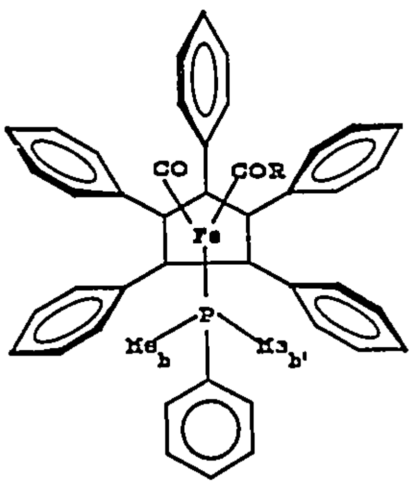

58

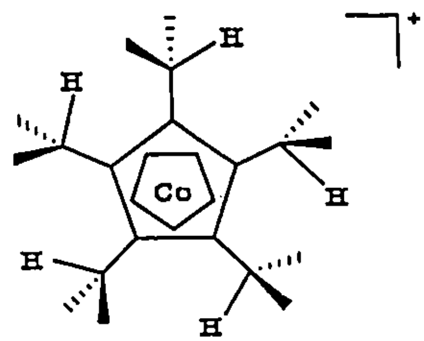

59

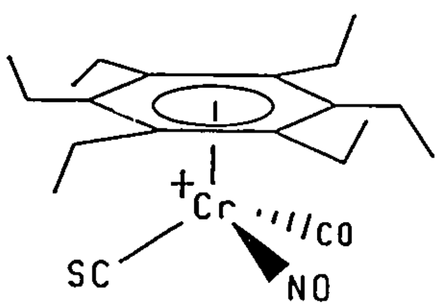

60

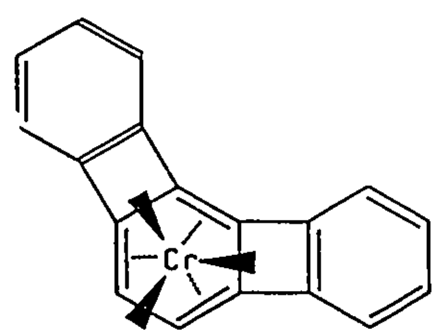

61

5.1.1 Statement of the Problem.

The syntheses, X-ray structures and variable-temperature NMR behavior of a series of tricarbonylchromium complexes of triphenylsilanol and triphenylcarbinol, and also of the triphenylmethyl cation will be described in this chapter.

5.2 Results and Discussion.

We have previously reported synthetic and variable-temperature NMR data on the mono-, bis- and tris-$Cr(CO)_3$ derivatives of 1,3,5-triphenylbenzene, **62**, **63** and **64** respectively,[179] and also on $(C_6Ph_6)Cr(CO)_3$, **65**.[180] We were unable to detect slowed rotation of the peripheral phenyl rings in **62**, **63** or **64** even at -90°C on a 500 MHz NMR spectrometer. Moreover, X-ray crystallographic data on **64** reveal[179] that no insurmountable barriers should arise so long as the molecules avoid conformations in which the metal tripods would clash. In contrast, slowed rotation of the (π-$Cr(CO)_3$-C_6H_5) ring in **65** is readily detectable by variable-temperature ^{13}C NMR spectroscopy and yields an activation energy of 12.2 kcal mol^{-1}.[180] This value may be compared to the approximately 33 kcal mol^{-1} barrier previously reported for hexaphenylbenzenes bearing methyl or methoxy substituents in *ortho* positions; the corresponding *meta*-substituted hexaphenylbenzenes yield aryl rotational barriers of $\approx$ 17 kcal mol^{-1}.[181] Apparently,

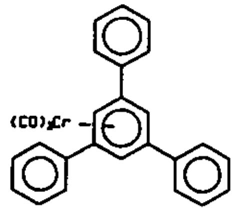

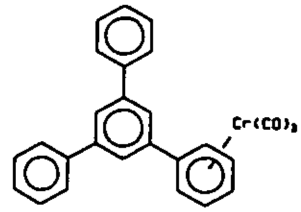

62

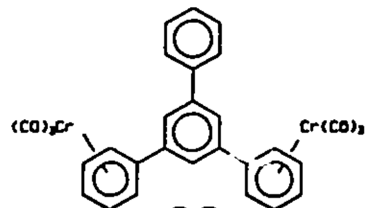

63

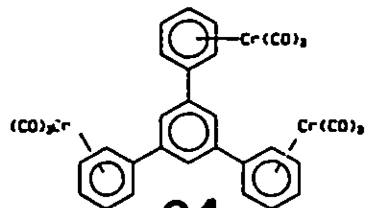

64

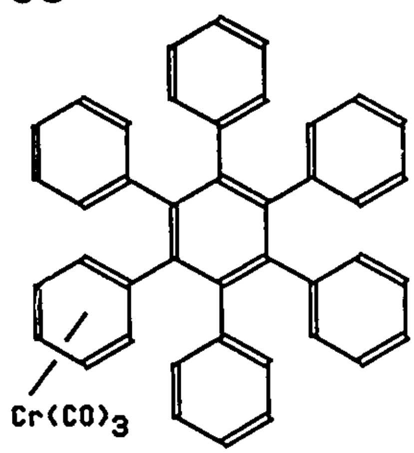

65

π-bonded addenda such as $Cr(CO)_3$ groups impose much smaller steric constraints than do *ortho*-alkyl substituents.

The molecular dynamics of triarylsilanes Ar_3SiX have been investigated and, in those molecules in which the aryl rings possess *ortho* methyl groups, the rotations of the phenyls may be slowed on the NMR time scale.[182] The $\Delta G^{\ddagger}$ values for enantiomerization of such molecules, where X is H, or Cℓ, lie in the range 11-12 kcal mol^{-1}. Furthermore, Beachley *et al.* have synthesized π-bonded triarylgallium complexes in which one or two $Mo(CO)_3$ units are bonded in an η^6 fashion to trimesitylgallium.[183] The structure is, of course, very nearly trigonal planar; the complex with one molybdenum is slightly more distorted from trigonal planar than the two-molybdenum complex. In both of these complexes, the aromatic rings are twisted in a propellor-like fashion. Interestingly, the authors stated that they also tried to prepare $Cr(CO)_3$ complexes of trimesitylgallium but were unable to obtain pure samples.[183] To study the effects of π-bonded addenda, we have prepared the mono-, bis- and tris-$Cr(CO)_3$ derivatives of triphenylsilanol, **66**, **67** and **68**, respectively.

The mono-complex, **66**, is prepared in straightforward fashion by the reaction of Ph_3SiOH with chromium hexacarbonyl in refluxing di-*n*-butyl ether and tetrahydrofuran. The bis-, **67**, and tris-, **68**, derivatives are prepared by further treatment of the mono-complexed material with excess $Cr(CO)_6$ (scheme 5.1). All three $(Ph_3SiOH)[Cr(CO)_3]_n$ complexes yield yellow crystals suitable for structural characterization by X-ray diffraction techniques. The structure determination summary of complexes of the three silanol complexes, **66**, **67** and **68**, along with the atomic positional parameters, bond lengths, bond angles, anisotropic displacement coefficients and hydrogen atom coordinates appear at the end of this chapter in Tables 5.4 to 5.9, 5.10 to 5.15, and 5.16 to 5.21 respectively.

$(Ph_3SiOH)[Cr(CO)_3]$, **66**, crystallizes in the monoclinic space group C2/c with eight molecules per unit cell. As expected the phenyls are arranged in a propellor

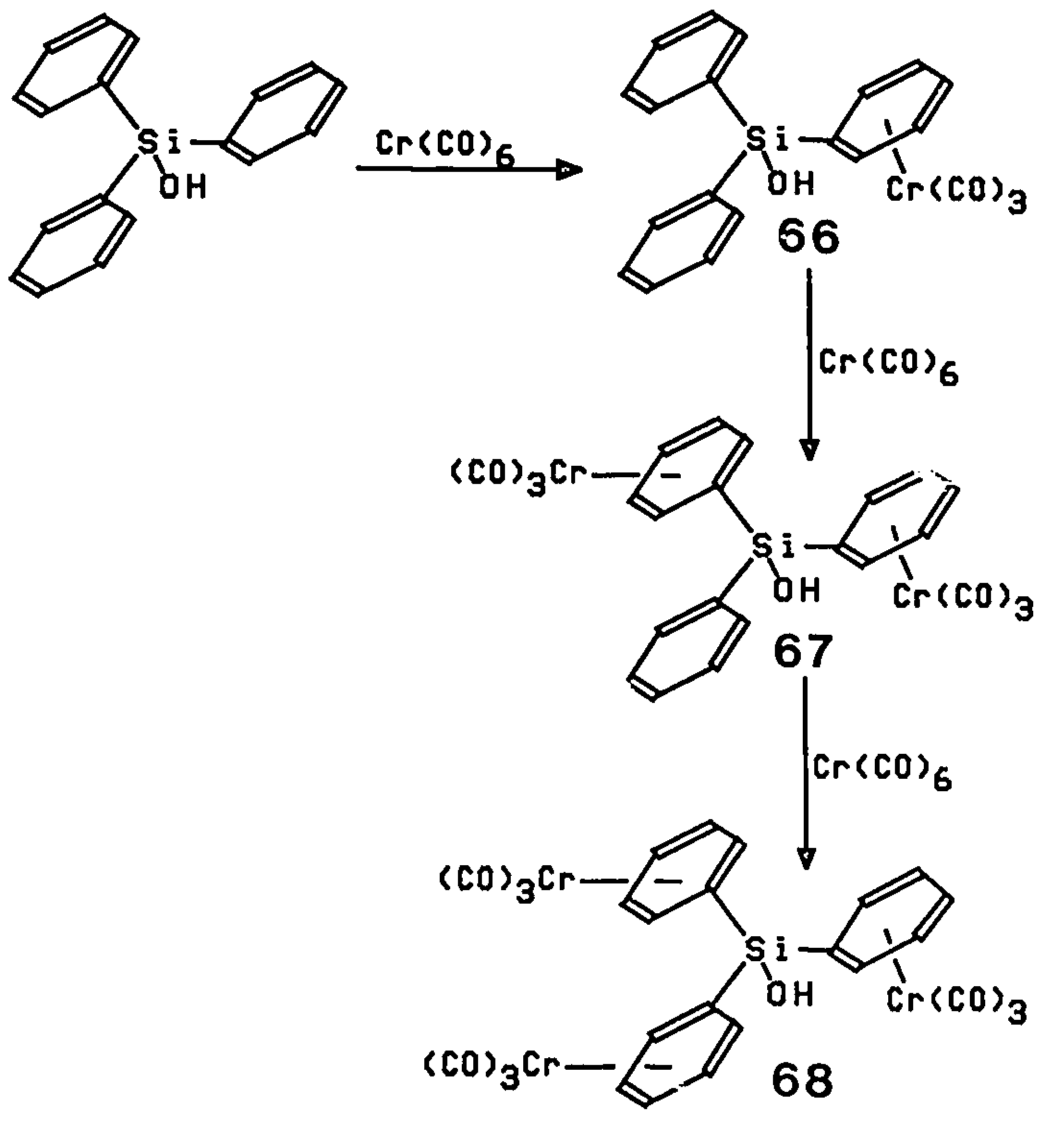

Scheme 5.1 Preparation of triphenylsilanol complexes **66**, **67** and **68**.

fashion. The dihedral angles O-Si-C_{ipso}-C_{ortho} are 45.4°, 23.3° and 73.0° for the complexed ring and the two non-complexed rings, respectively. The phenyl-silicon-phenyl angles between the complexed and non-complexed rings average 108.7° while the C_{ipso}-Si-C_{ipso} angle between the two phenyls is 109.9°; that is, the deviations from a regular tetrahedral environment around silicon are rather small. The π-complexed ring is twisted such that the tricarbonylchromium fragment is oriented towards the silanol moiety. It is the phenyl positioned closest to the $Cr(CO)_3$ tripod which adopts the smallest dihedral angle (23°) while the third phenyl ring is able to lie almost orthogonal to the silicon-oxygen bond axis. Figures 5.1 and 5.2 show an ORTEP and ball and stick view of the molecule respectively, while the unit cell is depicted in Figure 5.3.

$(Ph_3SiOH)[Cr(CO)_3]_2$, **67**, crystallizes in the triclinic space group $P\bar{1}$ with two molecules per unit cell. As with **66**, the phenyls are again arranged in a propellor fashion. The dihedral angles O-Si-C_{ipso}-C_{ortho} are 25.5°, 35.5° and 46.2° for the two complexed rings and the single non-complexed ring, respectively. The phenyl-silicon-phenyl angle between the two Cr-complexed rings is 107.2° but opens up to to 109.9° for the other two C_{ipso}-Si-C_{ipso} angles. In this case, both π-complexed rings are twisted such that the tricarbonylchromium fragments are oriented towards the silanol moiety, see figures 5.4 and 5.5. The unit cell is depicted in figure 5.6.

$(Ph_3SiOH)[Cr(CO)_3]_3$, **68**, crystallizes in the rhombohedral space group $R\bar{3}$ with two molecules per unit cell. The phenyls are again arranged in a propellor

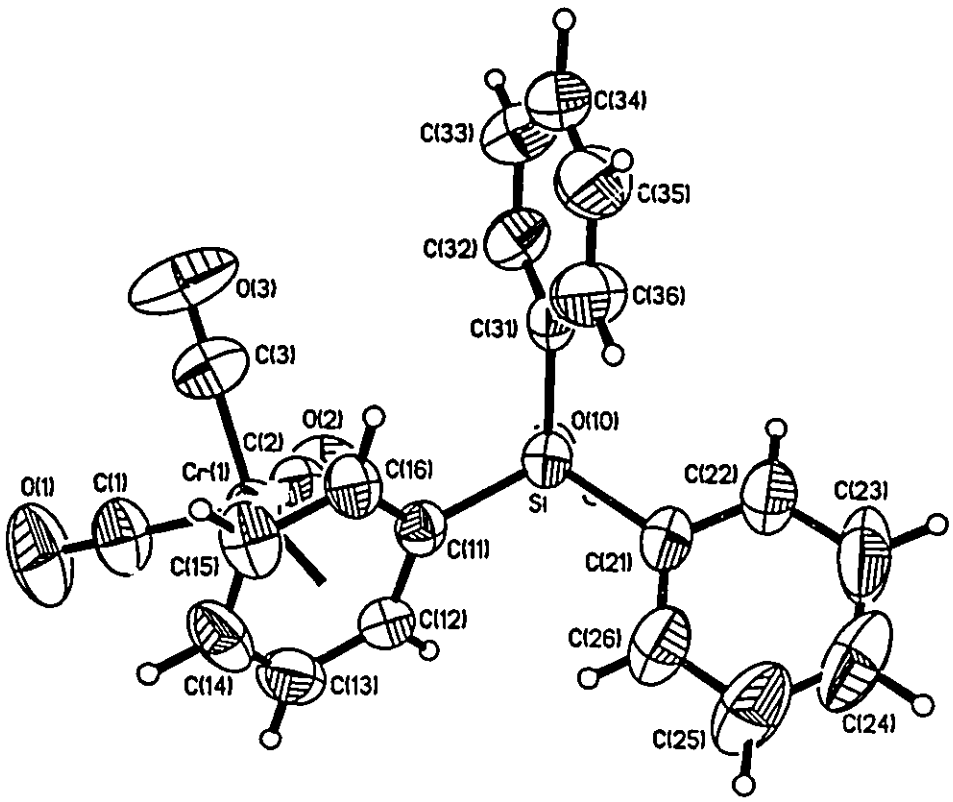

Figure 5.1 View of triphenylsilanol chromiumtricarbonyl, **66**.

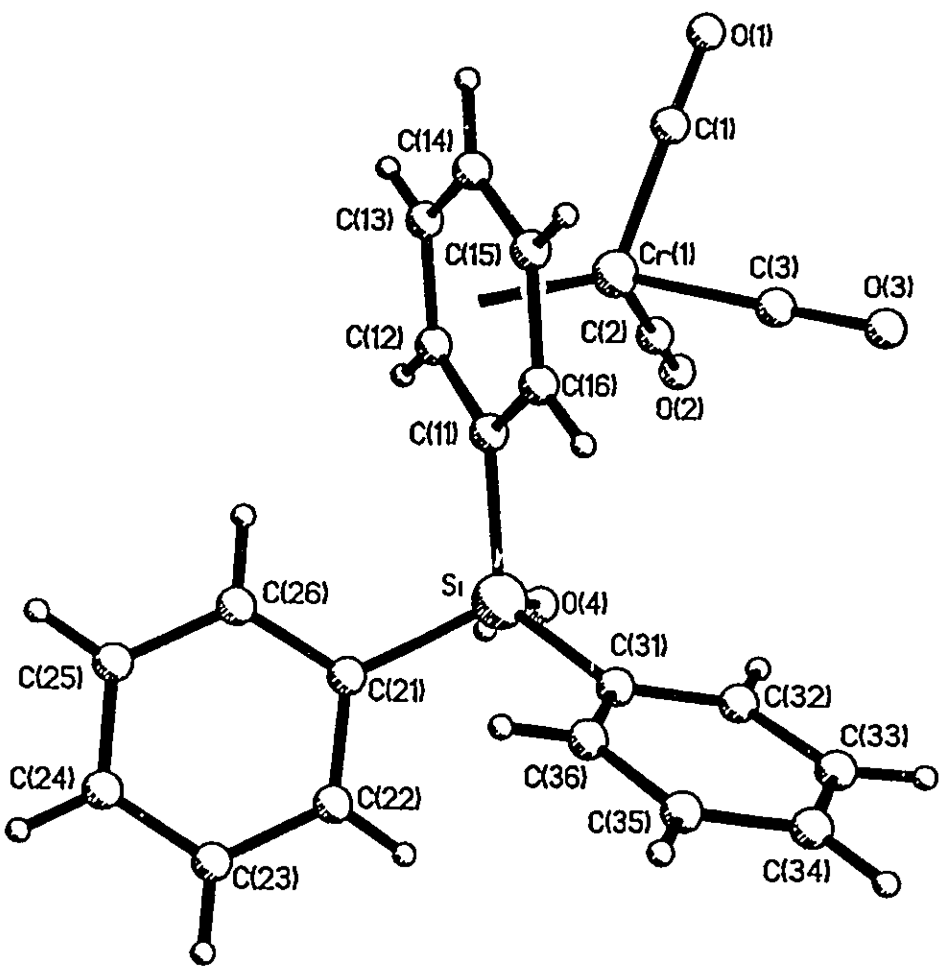

Figure 5.2 View of **66**.

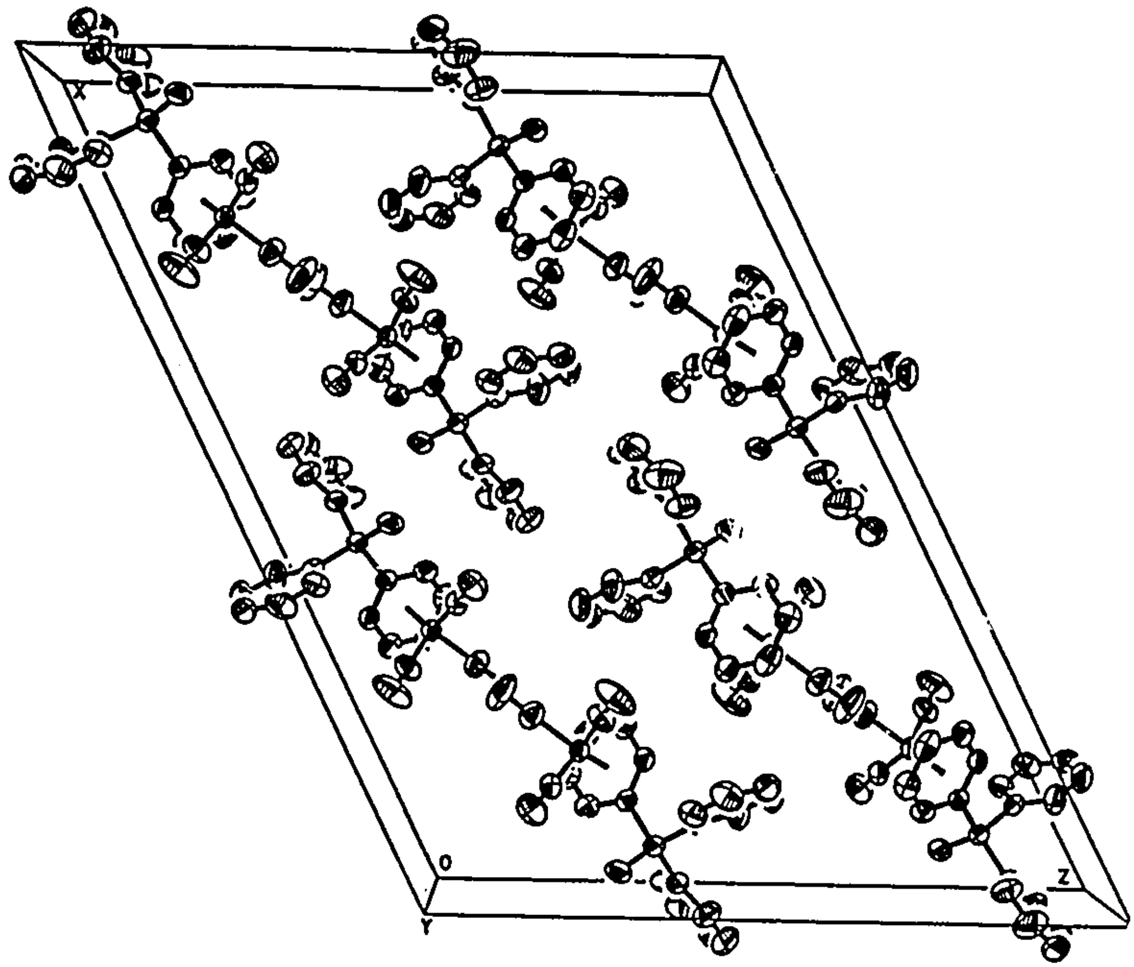

Figure 5.3 Unit cell of **66**.

fashion but, in this case, the molecule possesses a three-fold axis. The dihedral angles O-Si-C_{ipso}-C_{ortho} are 39.8° for all three complexed rings and the phenyl-silicon-phenyl angles are 108.3°. As with **66** and **67**, the π-complexed rings are twisted such that the tricarbonylchromium fragments are oriented towards the silanol moiety. Inevitably, the hydrogen of the Si-OH unit is disordered over three sites, and only one has been selected for Figure 5.7 which shows the atom numbering scheme; Figure 5.8 provides a ball and stick view of the molecule while Figure 5.9 illustrates the contents of the unit cell.

The ^{1}H and ^{13}C NMR spectra for **66**, **67** and **68** are shown in Figures 5.10 and 5.11; the shifts are collected in Table 5.1. They are unchanged over the range +30°C to -110°C and show no evidence of slowed rotation about the *ipso*-carbon—silicon bonds. Thus, in $(Ph_3SiOH)[Cr(CO)_3]$, **66**, the ^{1}H NMR spectrum exhibits a doublet for the *ortho* hydrogens and triplets for the *meta* and *para* protons in the non-complexed rings; similar patterns of half the intensity are given by the chromium-complexed ring. In accord with this picture, the ^{13}C NMR spectrum exhibits single peaks for the *ipso*, *ortho*, *meta* and *para* carbons of the two non-complexed rings at δ 132.3, 134.6, 127.8 and 130.5, respectively; corresponding resonances for the single π-complexed ring appear at δ 93.8, 100.8, 90.6 and 96.9, respectively. The differentiation of *ortho* and *meta* ^{13}C environments was made by standard two-dimensional shift-correlated techniques. If aryl rotation were to become slow on the NMR time scale, and if the spectrum

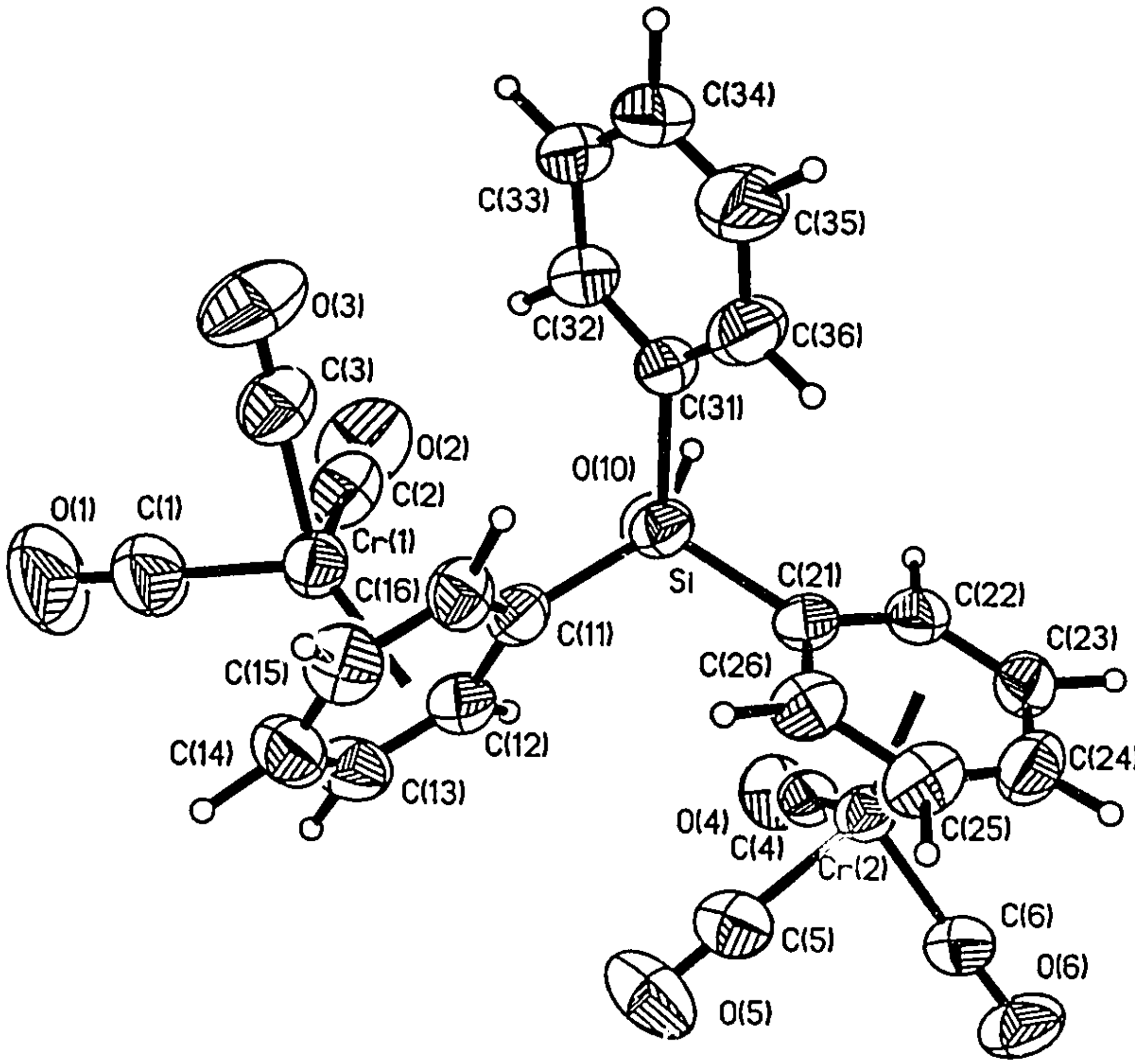

Figure 5.4 View of bis(chromiumtricarbonyl)triphenylsilanol, **67**.

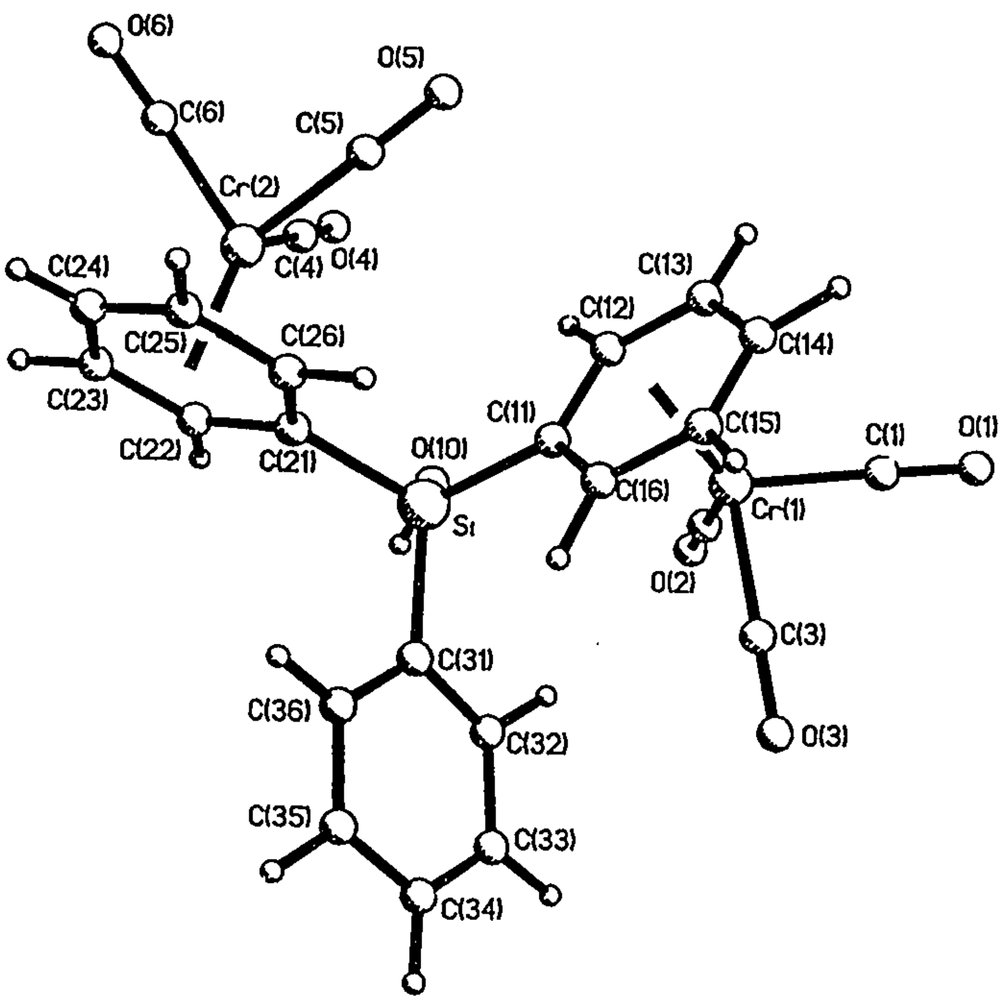

Figure 5.5 View of **67**.

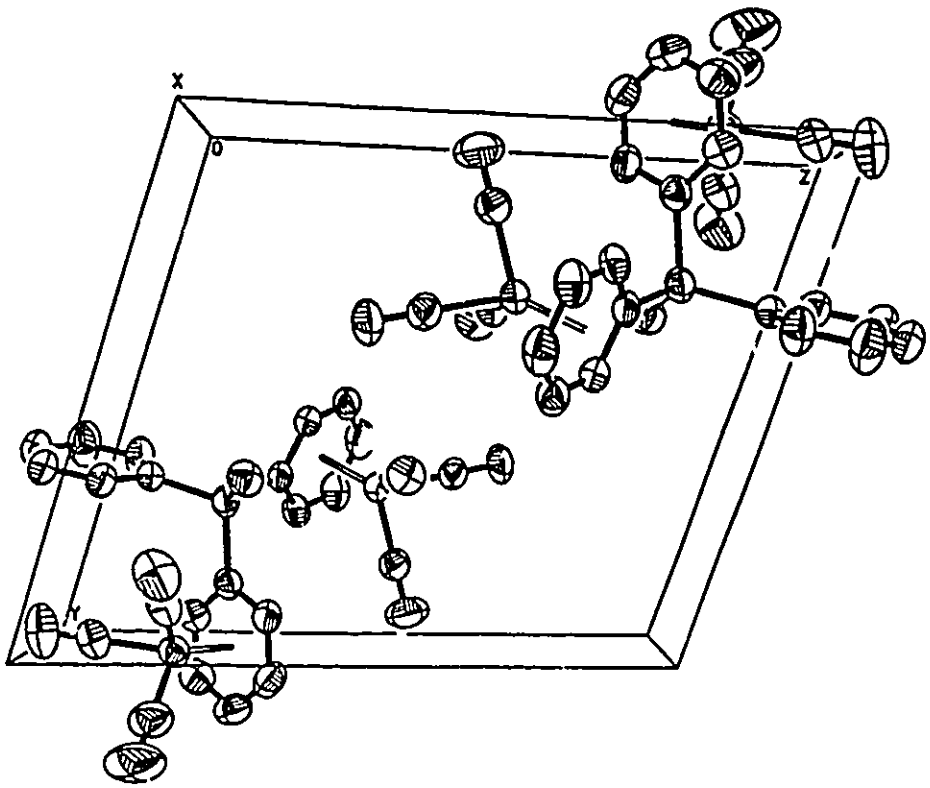

Figure 5.6 Unit cell diagram of **67**.

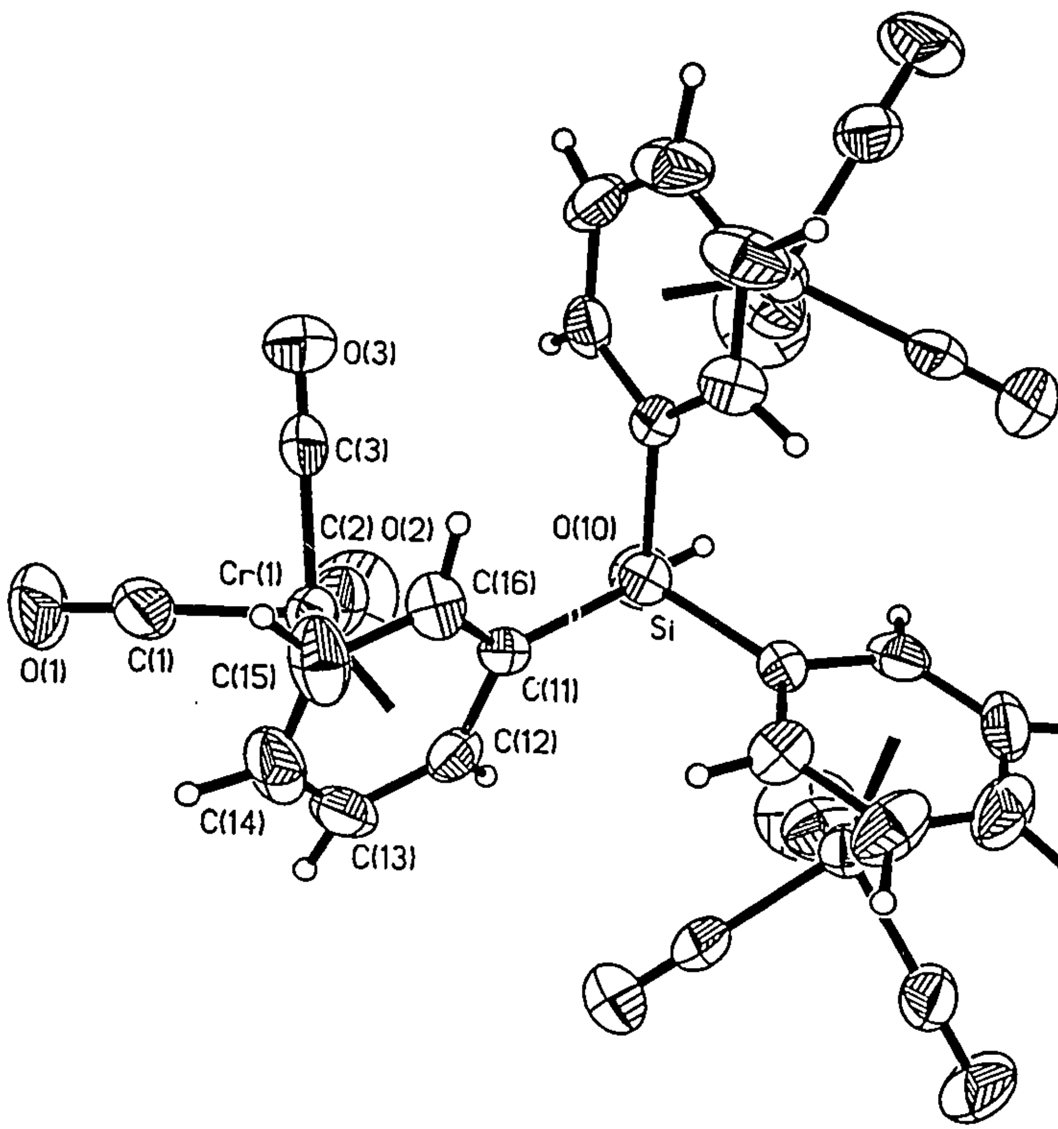

Figure 5.7 View of tris(chromiumtricarbonyl)triphenylsilanol, **68**.

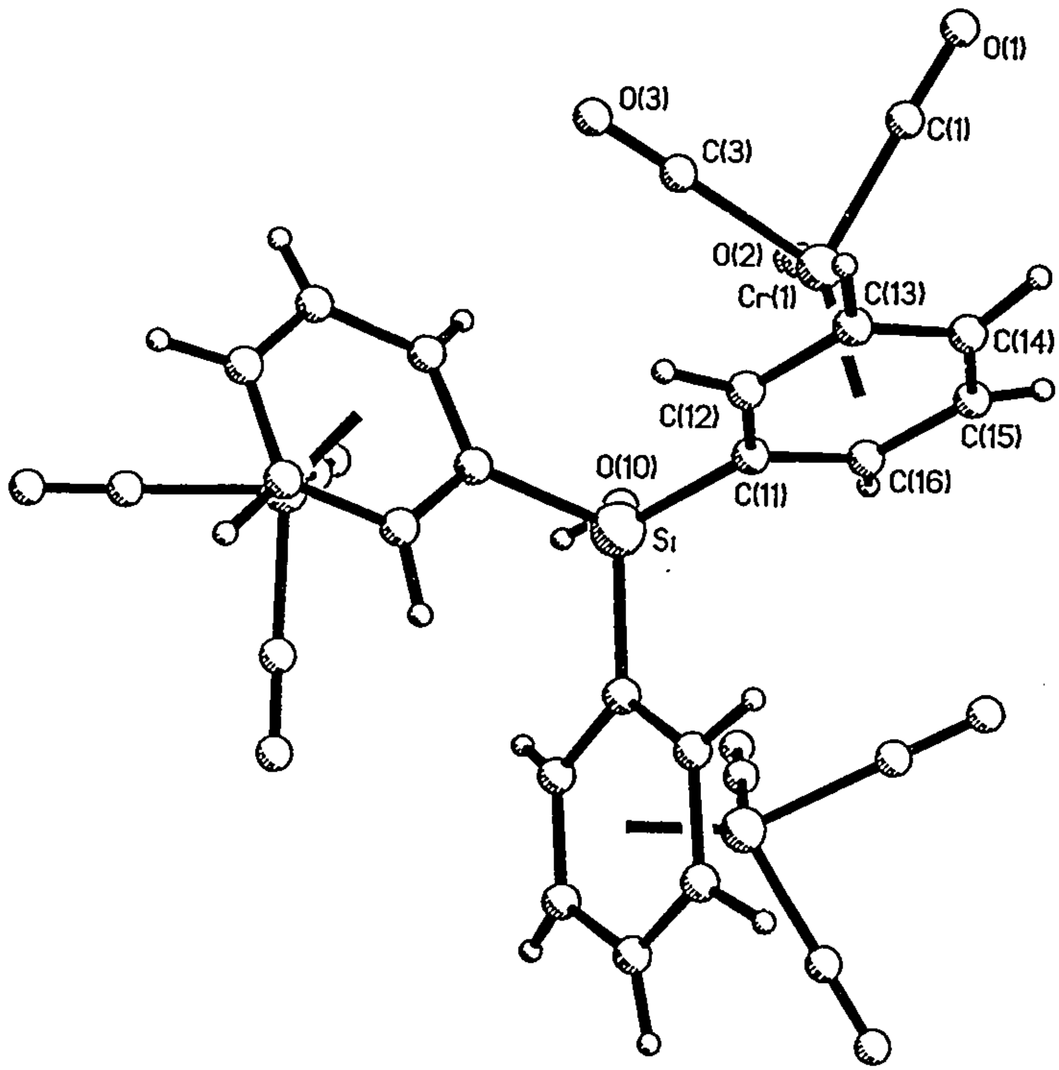

Figure 5.8 View of **68**.

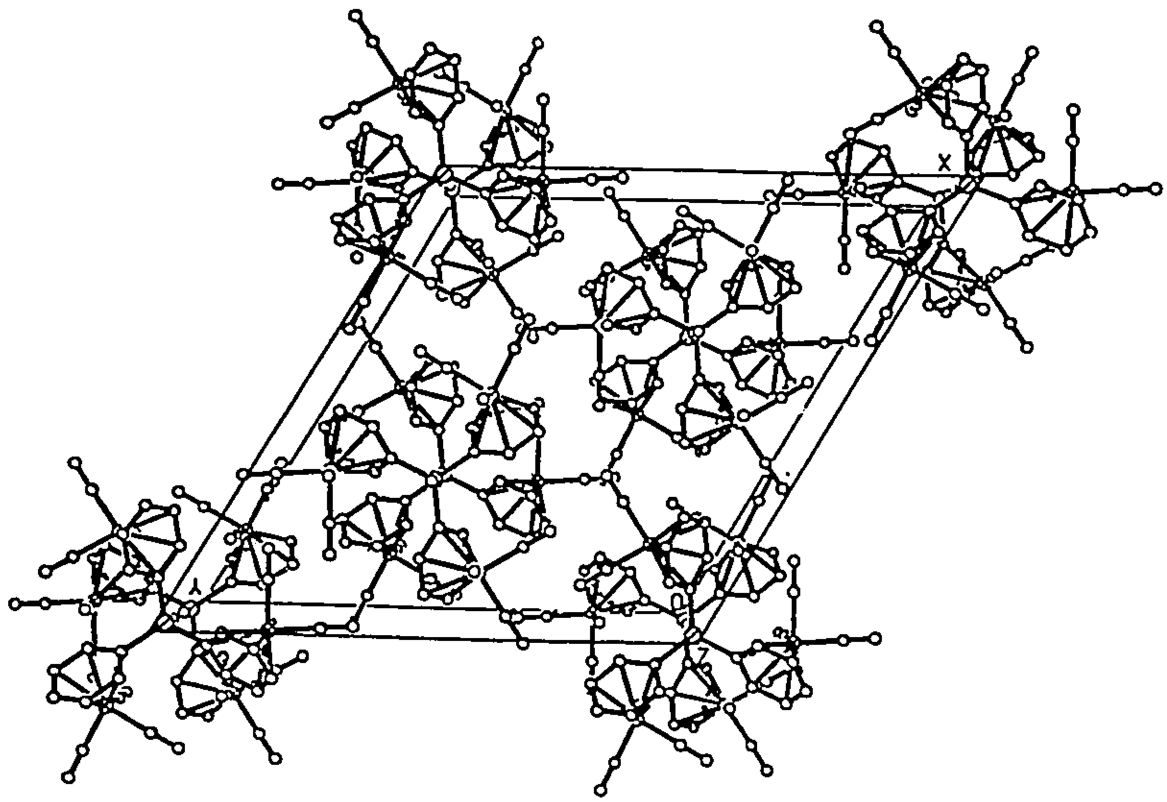

Figure 5.9 Unit cell diagram of **68**.

were to reflect the lack of molecular symmetry found in the solid state, the *ortho* and *meta* carbons and hydrogens of the phenyl rings should be split.

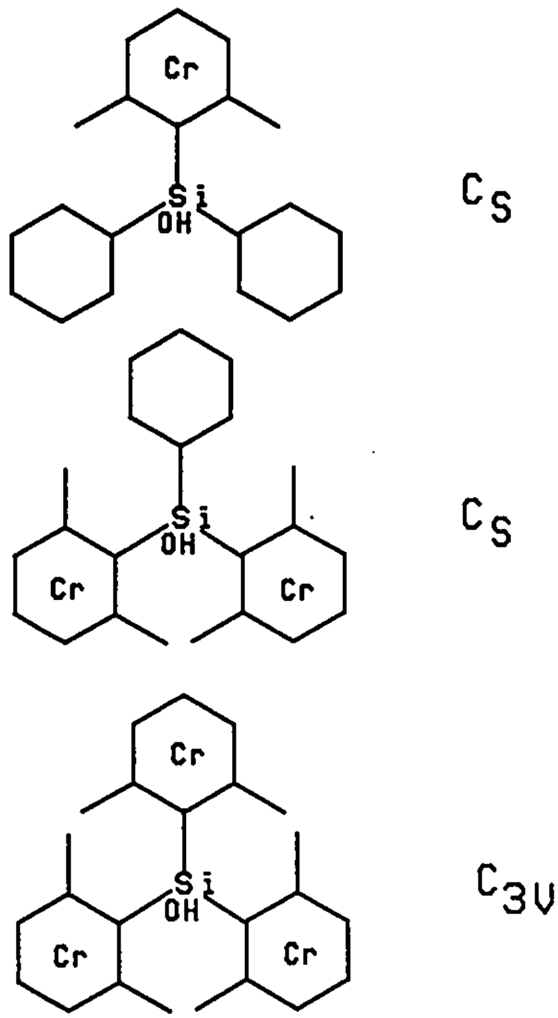

Figure 5.12 Highest available symmetry of complexes **66**, **67** and **68**.

The NMR spectra of $(Ph_3SiOH)[Cr(CO)_3]_2$, **67**, bear careful examination since it is apparent that the ^1H absorptions attributable to the two complexed rings give rise to a pair of *ortho* and a pair of *meta* resonances. At first sight, one might suspect that rotation of the (π-$Cr(CO)_3$-C_6H_5) rings has been slowed even at room temperature. Upon further reflection, however, one comes to the realization that the highest symmetry available to **67** is C_S, a single mirror plane. As shown in Figure 5.12, the "inner" and "outer" edges of the (π-$Cr(CO)_3$-C_6H_5) rings can never be equilibrated by a simple bond rotation process. Thus, each π-complexed phenyl ring will give rise to six carbon resonances even under conditions of rapid ring rotation. If rotation about the *ipso*-carbon—silicon bonds were to become slow on the NMR time scale, we would expect to see twelve resonances, six for each complexed ring. The alert reader will have already noted that $(Ph_3SiOH)[Cr(CO)_3]$, **66**, also possesses C_S symmetry at best, yet we see only four peaks for the (π-$Cr(CO)_3$-C_6H_5) ring. The explanation is simple: in **66**, the complexed ring straddles the molecular mirror plane, whereas in **67** the two rings bearing $Cr(CO)_3$ substituents are related by reflection in this mirror plane. Clearly, as we have all been cautioned by Sanders and Hunter,[184] one must take careful account of molecular symmetry before making claims about restricted rotations.

The above interpretation of the behavior of **67** is corroborated by the variable-temperature spectra of $(Ph_3SiOH)[Cr(CO)_3]_3$, **68**, which show only three proton environments and four ^{13}C resonances for the three complexed aryl rings. The molecule can adopt time-averaged C_{3v} symmetry, and the three vertical mirror planes render equivalent the edges of the phenyl rings. Clearly, since there is no evidence for slowed aryl rotation on the NMR time scale in the crowded tris-complex **68**, there is no reason to invoke it for the bis-$Cr(CO)_3$ system **67**.

Molecular modelling of the tris-complex, by starting from the X-ray structure and using the programs ALCHEMY[185] or PC-MODEL,[186] shows that it is possible to spin the rings without invoking correlated rotations. The *ipso*-carbon—silicon bonds (average length 1.86 Å) are sufficiently long to allow considerable molecular flexibility; however, these modelling studies suggested that the analogous carbinol complexes should show evidence of restricted aryl rotation.[187]

Triphenylcarbinol chromium tricarbonyl, **69**, was prepared and examined by variable-temperature ^1H and ^{13}C NMR spectroscopy; portions of these spectra are shown in Figure 5.13. One sees that, at -50°C, the *ortho* protons of the non-complexed phenyl rings have clearly split into a central peak (of intensity two H's) and two broader peaks each representing a single hydrogen. Continued cooling reveals that these two outer resonances each become 8 Hz doublets at -90°; these are clearly *ortho* hydrogens. Below this temperature, the central absorption begins to broaden and the coalescence pattern can be easily discerned from the spectra in Figure 5.13.

This fluxional behavior is rationalizable in terms of slowed rotation of the aryl rings about the central-C—*ipso*-C axes. In the absence of crystallographic data on **69**, we chose to model the system simply by taking the X-ray structure of the analogous silanol complex, **66**, and shortening the Si-C_{ipso} bonds from 1.86 Å to 1.51 Å. As was pointed out above for **66**, one of the non-complexed phenyl rings

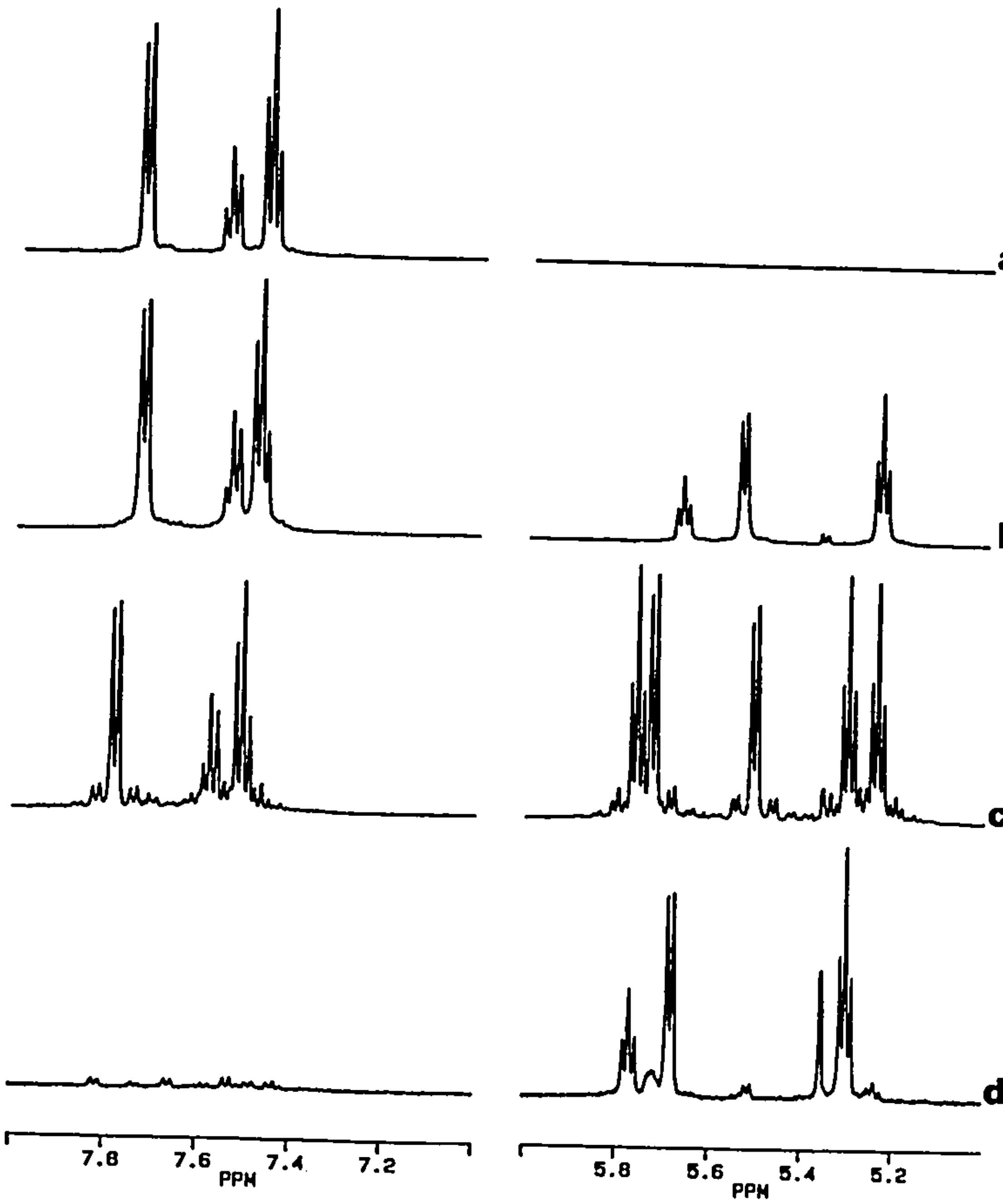

Figure 5.10 500 MHz ^{1}H NMR spectra of triphenylsilanol (a), **66** (b), **67** (c) and **68** (d).

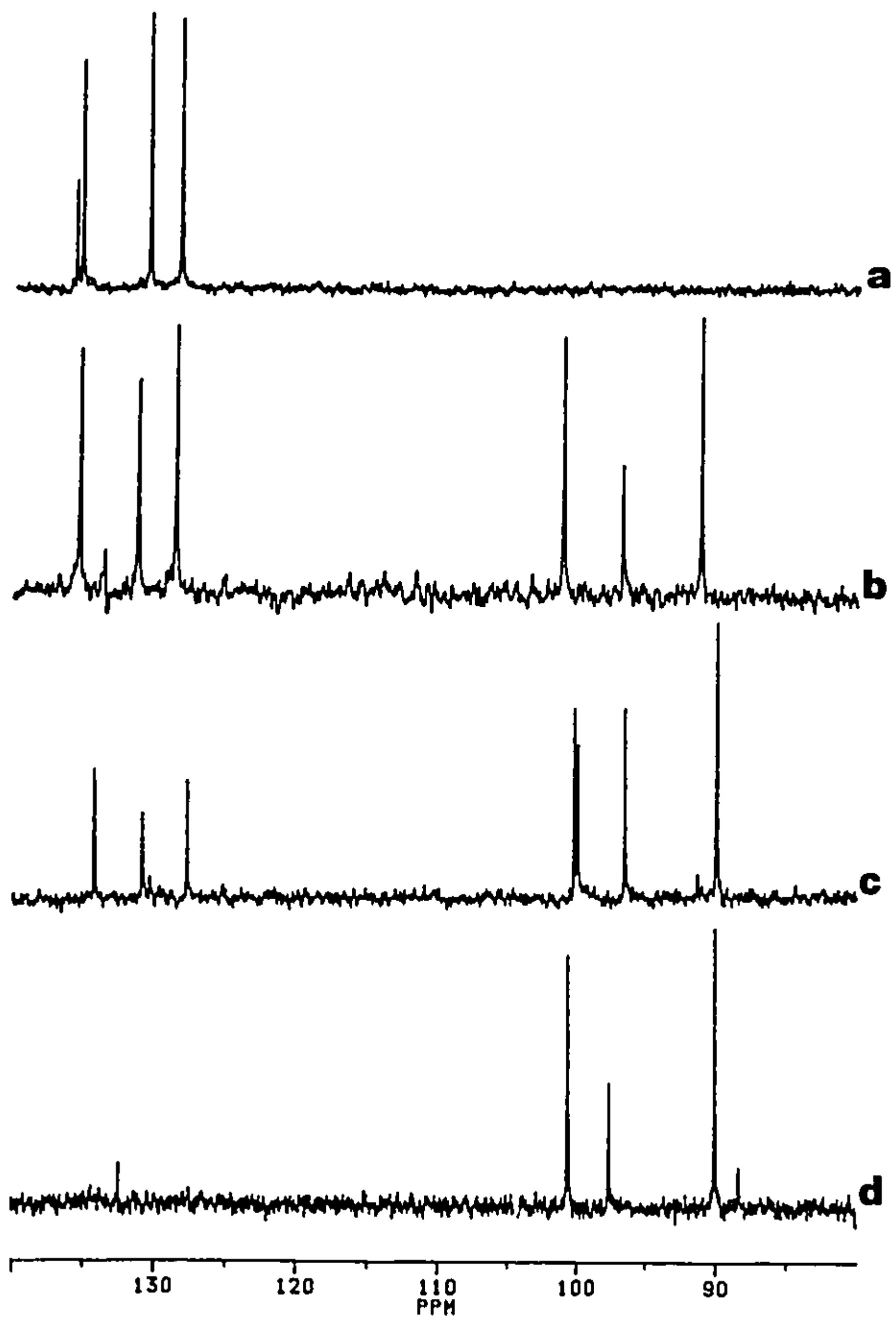

Figure 5.11 125 MHZ ^{13}C NMR spectra of triphenylsilanol (a), **66** (b), **67** (c) and **68** (d).

Table 5.1 ^{1}H and ^{13}C NMR data for Ph_3SiOH and its $Cr(CO)_3$ complexes **66**, **67** and **68**.

	Ph_3SiOH[a]	(Ph_3SiOH)-$Cr(CO)_3$, **66**.[b]	(Ph_3SiOH)-$[Cr(CO)_3]_2$, **67**.	(Ph_3SiOH)-$[Cr(CO)_3]_3$, **68**.
H-*ortho*	7.64 (d)	7.64 (d)	7.60 (d)	----
H-*meta*	7.42 (t)	7.43 (t)	7.35 (t)	----
H-*para*	7.51 (t)	7.50 (t)	7.43 (t)	----
C-*ipso*	135.1	132.33	130.48	----
C-*ortho*	135.0	134.63[c]	134.53	----
C-*meta*	127.9	127.77[c]	127.82	----
C-*para*	130.2	130.52[c]	131.07	----
H-*ortho*	----	5.51 (d)	5.50 (d) H2 5.72 (d) H6	5.64 (d)
H-*meta*	----	5.20 (t)	5.23(d,t) H3[d] 5.29(d,t) H5[d]	5.29 (t)
H-*para*	----	5.64 (t)	5.75 (t)	5.76 (t)
C-*ipso*	----	93.76	92.69	87.92
C-*ortho*	----	100.80[e]	100.63 100.84	100.60
C-*meta*	----	90.58[e]	90.27 90.33	90.02
C-*para*	----	96.88[e]	97.07	97.61
Cr-CO	----	233.2	232.7	232.0

a. ^{29}Si -12.45; b. ^{29}Si -12.96; c. J(C-H) 159 Hz; d. doublet (0.9 Hz) of triplets (6.5 Hz); e. J(C-H) 174 Hz.

is in a noticeably more crowded environment than is its partner. Initially, one can invoke slowed rotation of the relatively bulky chromium-complexed phenyl ring. (Such a scenario is in accord with the known behavior of $(C_6Ph_6)Cr(CO)_3$, **65**, in which rotation of the chromium-complexed ring is slowed but the other peripheral rings continue to spin rapidly on the NMR time scale.[180]) Thus, even though the two remaining phenyl groups in **69** may continue to spin rapidly, one of them is oriented *proximally* with respect to the chromium atom while the other is *distal*. Thus, one might expect to see two different *ortho* environments. Moreover, the non-complexed phenyl ring positioned *proximal* to the $Cr(CO)_3$ moiety will be more sterically hindered than will its partner. Slowed rotation of this more crowded phenyl ring should render non-equivalent its two *ortho* hydrogens. Subsequently, at lower temperatures, the smaller rotational barrier associated with the less hindered phenyl ring will eventually cause the ring edges to become nonequivalent. The Gutowsky-Holm approximation yields a $\Delta G^‡$ value of $\approx 11 \pm 0.5$ kcal mol^{-1} for the barrier to rotation of the more hindered phenyl ring. It is difficult to offer a $\Delta G^‡$ value for the less crowded phenyl ring since the temperature required to see the limiting spectrum is not accessible. Finally, we note that in these molecules there is no evidence for cessation of rotation of the $Cr(CO)_3$ tripod as has been noted in other sterically hindered systems.[188]

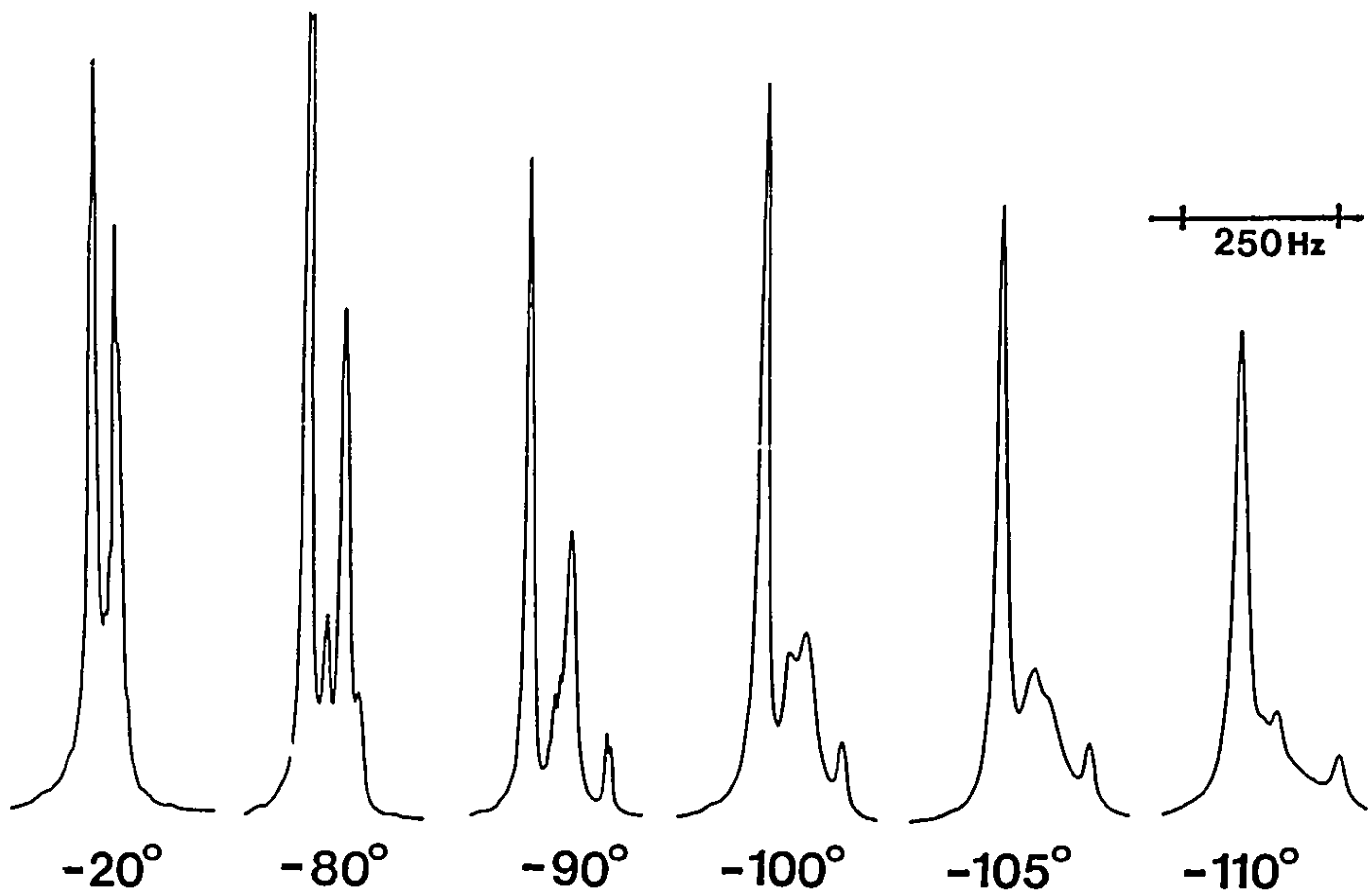

Figure 5.13 Selected variable-temperature 500 MHz ^{1}H NMR spectra of **69** in the non-complexed phenyl ring region.

5.2.1 The Significance of Torsional Angles.

To place these structural and variable-temperature NMR data in perspective we note that a number of Ph_3SiO-X molecules have been crystallographically characterized.[189] These include systems containing such X substituents as $C\ell O_3$, $SiPh_3$, C_2H_5, $U(C_5H_5)_3$, CrO_3SiPh_3 and $Si[CH{=}CH_2]_3$, (see Table 5.2). Of particular relevance is the pioneering study of Dunitz *et al.* in which it was shown that the O-P-C_{ipso}-C_{ortho} dihedral angles taken from the X-ray crystal structures of a large number of Ph_3PO-X molecules could be used to visualize the most probable pathways for stereoisomerization.[147] For these Ph_3PO-X systems, Dunitz noted that "the equilibrium structure of an isolated Ph_3P-X fragment is close to a symmetric propellor shape with all three phenyl rings rotated from the respective C-P-X planes in the same sense and by approximately the same amount, about 40°".[147] The stereoisomerization is thought to proceed by rotation of one ring towards a 90° torsion angle with concomitant rotation of the other phenyl rings in the opposite sense (*i.e.* towards 0°) so as to produce a conformation in which the torsion angles are approximately 90°, 10° and -10°. Continued rotation leads eventually to a propellor of opposite chirality. Clearly, all three rings do not rotate at the same rate and this should be reflected in the crystallographic results which capture a series of snapshots of the Ph_3P fragment in many different environments.[135] This crystallographically derived picture of the stereoisomerization pathway is complemented by force field calculations and variable-temperature NMR data on related Ar_3CH systems which also favor the "two-ring flip" mechanism.[190]

The Ph_3SiO-X systems we have found in the literature as well as the three we have reported herein, *i.e.*, **66**, **67** and **68**, all possess the propellor structure in which three rings are rotated in the same sense. Even in the cases where one phenyl group is aligned at 90° to the Si-O axis the two remaining rings are oriented in the same direction. Typically, in $Ph_3SiOC\ell O_3$, the torsion angles are 90°, 28° and 35°.[189a] When the molecules have a three-fold axis, as in the clathrate complexes of hexaphenyldisiloxane with benzene or piperidine, the dihedral angles are approximately 30°.[189b] When the phenyls each bear a relatively bulky π-bonded $Cr(CO)_3$ substituent, as in $(Ph_3SiOH)[Cr(CO)_3]_3$, **68**, these angles open up to 40°.

Interestingly, a comparison of these data for Ph_3SiO-X systems with those for Ph_3CO-X molecules reveals that, although triarylmethanes bearing bulky *ortho* sub-stituents adopt a propellor-type conformation in the solid state,[191] many trityl fragments do not.[192] Instead, a favored structure appears to be one in which one phenyl lies almost perpendicular to the pseudo three-fold axis while the remaining rings adopt small dihedral angles of opposite sign. Typically, in Ph_3C-O-CHMePh, the torsion angles are 93°, +28° and -19°.[192a] This conformation represents a relatively high-energy point approximately half way along the trajectory of the two-

Table 5.2 Phenyl torsion angles in Ph_3E-OR systems, E = Si or C.

Ring A	Ring B	Ring C	Molecule	Reference
90	28	35	$Ph_3SiO\text{-}C\ell O_3$	189a
90	28	39	$Ph_3SiO\text{-}C\ell O_3$	189a
70	70	70	$Ph_3SiO\text{-}C(vinyl)_3$	189g
63	37	18	$(Ph_3Si)_2CrO_4$	189f
56	29	50	$Ph_3SiO\text{-}U(C_5H_5)_3$	189e
56	45	36	$(Ph_3Si)_2O$	189c
31	31	31	$(Ph_3Si)_2O$ benzene clathrate	189b
29	29	29	$(Ph_3Si)_2O$ piperidine clathrate	189b
73	45	23	$(Ph_3SiOH)\text{-}[Cr(CO)_3]$	present work
46	36	26	$(Ph_3SiOH)\text{-}[Cr(CO)_3]_2$	present work
40	40	40	$(Ph_3SiOH)\text{-}[Cr(CO)_3]_3$	present work
93	28	-15	$Ph_3C\text{-}OCHC_6H_5$	192a
92	28	-19	$Ph_3C\text{-}OCHC_6H_4C\ell$	192a
89	32	23	$Ph_3C\text{-}OEt$	189d
66	30	-11	$Ph_3C\text{-}OCHC_6H_4NO_2$	192a
76	33	-1	$(Ph_3C)_2O$	192b
61	39	-17	$(Ph_3C)_2O$	192b
69	60	48	Ph_3CLi	192c

ring flip mechanism which interconverts enantiomers of Ph_3CX. Clearly, the solid-state conformations of this class of molecules merit a more comprehensive study and, to this end, we are currently compiling structures from the Cambridge Crystallographic Database.

5.2.2 Chromium-Stabilized Benzylic Cations.

It is well established that benzylic cations are noticeably stabilized by the presence of a tricarbonylchromium moiety.[124,193] Recently, Downton *et al.* have succeeded in obtaining NMR spectra of a series of primary benzylic cations each bearing a $Cr(CO)_3$ group.[194] In the present case, since the free triphenylmethyl cation is sufficiently stable to have been subjected to X-ray crystallographic structural determination,[195] one might hope to be able to isolate the corresponding $Cr(CO)_3$ complex, **70**, in crystalline form. Protonation of **69** with CF_3SO_3H or with HBF_4/ether yields immediately a green solution of the cation $[(Ph_3C)Cr(CO)_3]^+$, **70**, which can be left in air at room temperature for several hours with only minor decomposition. Interestingly, a solution which had been left overnight turned red but addition of water regenerated the yellow colour of the starting material **69**. The ^1H and ^{13}C NMR data are collected in Table 5.3 and the spectra of **70** are shown in Figure 5.14; they are entirely analogous to those chromium-stabilized cations previously reported. In particular, the benzylic carbon in **70** which formally bears

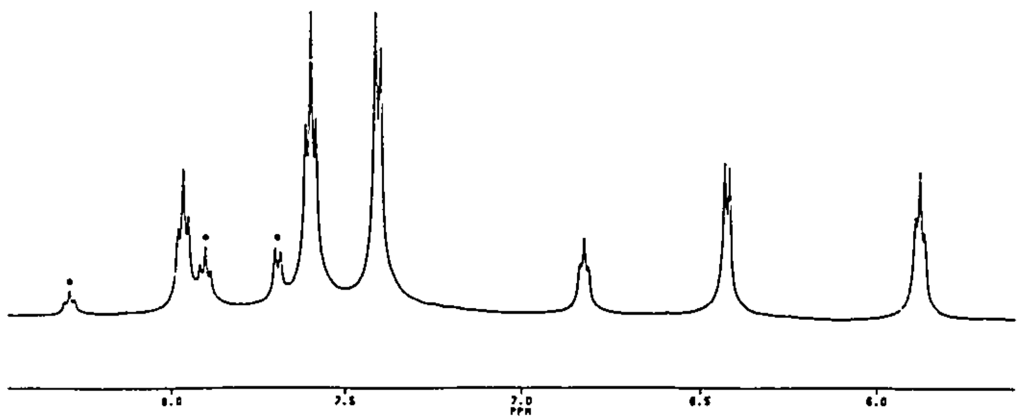

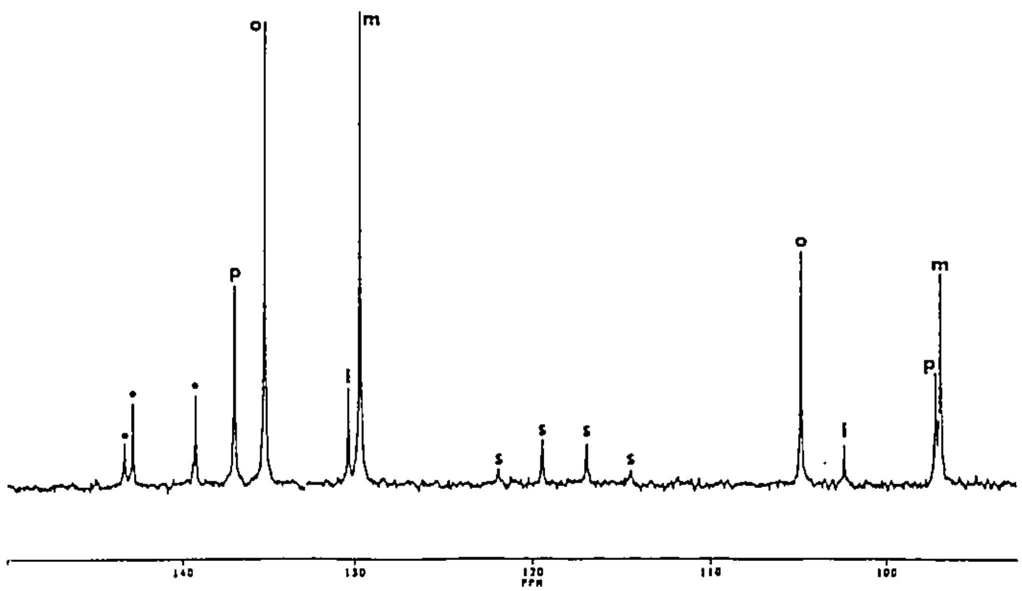

Figure 5.14 Sections of the ^{1}H and ^{13}C NMR for triphenylmethyl chromium tricarbonyl cation, **70**. The dots mark signals attributable to $[Ph_3C]^+$, and "s" is the flourine-coupled quartet from CF_3SO_3H.

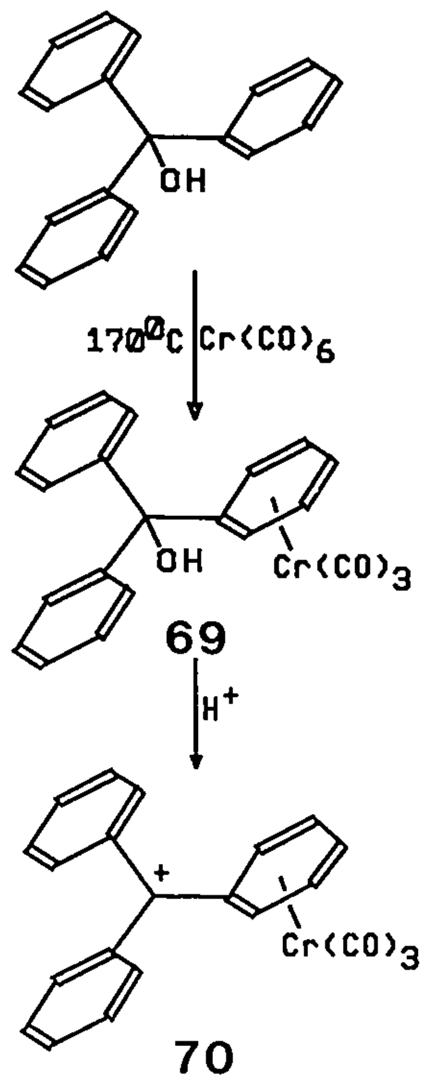

the positive charge is deshielded by 106 ppm relative to its resonance position in the alcohol **69**. This compares favorably with Olah's report that conversion of $(C_6H_5CMe_2OH)Cr(CO)_3$ to $[(C_6H_5CMe_2)Cr(CO)_3]^+$ takes the benzylic carbon ^{13}C NMR resonance from 71.4 ppm in the alcohol to 170.9 ppm in the cation.[196] It has been noted previously that both experimental data and EHMO calculations suggest

Table 5.3 ^1H and ^{13}C NMR data for Ph_3COH, for $[Ph_3C]^+$ and for the $Cr(CO)_3$ complexes **69** and **70**.

	Ph_3COH	(Ph_3COH)-$Cr(CO)_3$,**69**.	$[Ph_3C]^+$	$[(Ph_3C)$-$Cr(CO)_3]^+$, **70**.
H-*ortho*	7.49 (d)	7.49 (d)	7.69 (d)	7.40 (d)
H-*meta*	7.54 (t)	7.54 (m)	7.90 (t)	7.60 (t)
H-*para*	7.54 (t)	7.54 (m)	8.29 (t)	7.97 (t)
C-*ipso*	135.1	145.5	140.28	130.6
C-*ortho*	135.0	127.4	143.09	135.1
C-*meta*	127.9	128.2	130.89	129.9
C-*para*	130.2	127.8	143.78	137.1
H-*ortho*	----	5.65 (d)	----	6.42 (d)
H-*meta*	----	5.35 (t)	----	5.87 (t)
H-*para*	----	5.76 (t)	----	6.82 (t)
C-*ipso*	----	119.05	----	102.7
C-*ortho*	----	96.59	----	104.9
C-*meta*	----	89.39	----	97.3
C-*para*	----	96.06	----	97.4
benzylic C	82.00	79.71	211.22	185.8
Cr-CO	----	233.3	----	229.3

that for $[(benzyl)Cr(CO)_3]^+$ systems a tertiary cation requires much less anchimeric assistance from the neighboring metal than does a primary cationic center.[194] Thus a 3° cation need not bend towards the metal as is observed, for example, in ferrocenyl cations.[197] Such a concept is buttressed by X-ray crystallographic data[198,199] on the molybdenum-stabilized alkynyl cations **71** and **72** whereby the Mo-C$^+$ distance is 2.44 Å in the primary cation **71** but lengthens to 2.74 Å in the tertiary cation **72**. We are currently attempting to obtain X-ray quality crystals of **70** to clarify this point.

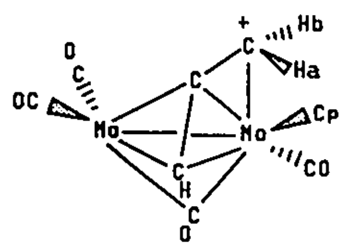

71

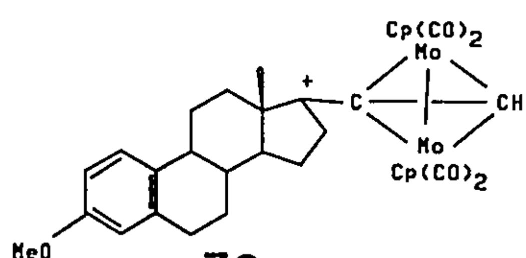

72

There has been a lively controversy[200] concerning the existence of free silicenium cations, and one might imagine that the presence of a tricarbonylchromium unit might help stabilize a positively charged silicon center. Protonation of the complexed silanols **66**, **67** or **68** brings about a small deshielding of the ring protons and carbons but we have not yet detected a ^{29}Si signal: indeed, both Olah[201] and Lambert[202] have noted difficulties in obtaining ^{29}Si data on the proposed silicenium ions which, by analogy to the ^{13}C shifts of carbenium ions, one might expect to be drastically deshielded.[203] In the present case, we believe that the chromium complexes **66**, **67** or **68** have not eliminated water and are merely protonated silanols.[204] The problem may be that the silicon-oxygen bond is too strong to be broken in these systems. It may be necessary to resort to abstraction of hydride as has been discussed extensively for the case of ferrocenyldimethylsilane.[205] Current work in this laboratory involves the preparation of $(Ph_3SiX)[Cr(CO)_3]_n$ systems, where X is H or halogen, with a view to exploring the possible generation of metal-stabilized silicenium ions.

5.3 Future Work.

While it was not possible to form a stabilized silicon cation on chromium, it may be possible to form a stabilized silicenium ion on molybdenum, as illustrated below.

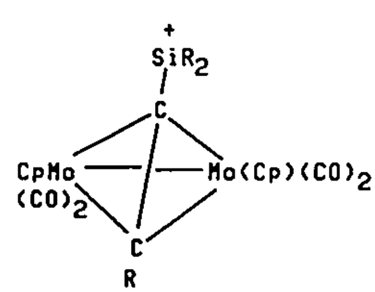

Final perspectives

The original goal was the synthesis of a cobalt complex of 2-methylcyclopentanol which could model the D ring of hormonal steroids such as estradiol or mestranol. The formation of the epimer in which the hydroxyl and methyl groups were mutually trans led to an attempt to invert the stereochemistry by use of a cobalt-stabilized cation. In turn, this prompted a more general study of metal stabilized cations, specifically sila-cations which have been the subject of much controversy. Although it was not possible to isolate a stable silicon-based cation, the corresponding carbocation was air- and thermally-stable at ambient temperature. These results suggest that the best chance of generating a sila-cation may perhaps be a cluster-stabilized one, as shown on the previous page. Such a possibility may be realized by addition of a dimetallic fragment to a silyl-alkyne; subsequent removal of a chloride ligand by means of a strong Lewis acid could lead to the desired cation.

Table 5.4 STRUCTURE DETERMINATION SUMMARY FOR COMPLEX **66**

Crystal Data

Empirical Formula	$C_{21} H_{16} Cr O_4 Si$
Color; Habit	yellow parallelepiped
Crystal Size (mm)	.22 x .25 x .28
Crystal System	Monoclinic
Space Group	C2/c
Unit Cell Dimensions	$\underline{a}$ = 29.061(3) Å $\underline{b}$ = 7.136(2) Å $\underline{c}$ = 21.331(3) Å $\underline{\beta}$ = 115.85(2)°
Volume	3980.9(8) $Å^3$
Z	8
Formula Weight	412.4
Density(calc.)	1.376 Mg/m^3
Absorption Coefficient	0.657 mm^{-1}
F(000)	1696

Data Collection (COMPLEX **66**)

Diffractometer Used	Siemens P4, rotating anode
Radiation	MoKα (λ = 0.71073 Å)
Temperature (K)	302
Monochromator	Highly oriented graphite crystal
2θ Range	3.0 to 45.0°
Scan Type	2θ-θ
Scan Speed	Variable; 1.5 to 14.65°/min. in ω
Scan Range (ω)	1.20° plus Kα-separation
Background Measurement	Stationary crystal and stationary counter at beginning and end of scan, each for 25.0% of total scan time
Standard Reflections	3 measured every 100 reflections
Index Ranges	$0 \leq h \leq 26$, $0 \leq k \leq 7$ $-22 \leq \ell \leq 20$
Reflections Collected	2808
Independent Reflections	2505 (R_{int} = 10.81%)
Observed Reflections	1811 ($F \geq 4.0\sigma(F)$)
Absorption Correction	psi scan

Solution and Refinement (COMPLEX **66**)

System Used	Siemens SHELXTL PLUS (VMS)
Solution	Direct Methods
Refinement Method	Full-Matrix Least-Squares
Quantity Minimized	$\Sigma w(\lvert F_o\rvert - \lvert F_c\rvert)^2$
Hydrogen Atoms	Riding model, fixed isotropic U
Weighting Scheme	$w^{-1} = \sigma^2(F) + 0.0006F^2$
Number of Parameters Refined	260
Final R Indices (obs. data)	R = 3.65 %, wR = 4.30 %
R Indices (all data)	R = 5.88 %, wR = 10.60 %
Goodness-of-Fit	1.25
Largest and Mean Δ/σ	0.012, 0.001
Data-to-Parameter Ratio	7.0:1
Largest Difference Peak	0.25 eÅ^{-3}
Largest Difference Hole	-0.19 eÅ^{-3}

Table 5.5 Atomic coordinates ($x10^4$) and equivalent isotropic displacement coefficients ($Å^2x10^3$) (COMPLEX **66**).

	x	y	z	U(eq)
Cr(1)	6843(1)	8129(1)	8233(1)	43(1)
Si	5764(1)	7203(2)	8689(1)	45(1)
O(1)	7514(2)	8388(6)	7504(2)	113(2)
O(2)	6239(1)	5152(5)	7222(2)	78(2)
O(3)	7546(2)	5207(6)	9153(2)	114(2)
O(10)	5507(1)	5787(4)	8017(1)	62(1)
C(1)	7249(2)	8284(7)	7783(2)	69(2)
C(2)	6475(2)	6292(6)	7614(2)	50(2)
C(3)	7274(2)	6342(7)	8796(2)	66(2)
C(11)	6241(1)	8778(5)	8578(2)	43(2)
C(12)	6128(2)	9685(6)	7938(2)	53(2)
C(13)	6474(2)	10859(6)	7850(3)	64(2)
C(14)	6955(2)	11163(6)	8412(3)	68(3)
C(15)	7082(2)	10318(6)	9049(2)	58(2)
C(16)	6726(2)	9121(6)	9123(2)	50(2)
C(21)	5260(2)	8697(6)	8755(2)	53(2)
C(22)	4919(2)	7956(10)	8976(3)	82(3)
C(23)	4556(2)	9097(14)	9058(3)	109(4)
C(24)	4536(3)	10971(13)	8906(3)	104(4)
C(25)	4855(2)	11721(10)	8670(4)	105(4)
C(26)	5215(2)	10595(8)	8599(3)	77(3)
C(31)	6093(2)	5814(6)	9496(2)	48(2)
C(32)	6264(2)	4009(7)	9495(2)	63(2)
C(33)	6508(2)	3012(8)	10099(3)	81(3)
C(34)	6589(2)	3753(9)	10718(3)	82(3)
C(35)	6443(2)	5571(10)	10754(3)	89(3)
C(36)	6199(2)	6582(7)	10148(2)	78(3)

* Equivalent isotropic U defined as one third of the trace of the orthogonalized U_{ij} tensor.

Table 5.6 Bond lengths (Å) (COMPLEX **66**).

Cr(1)-C(1)	1.819 (6)	Cr(1)-C(2)	1.837 (4)
Cr(1)-C(3)	1.824 (4)	Cr(1)-C(11)	2.222 (5)
Cr(1)-C(12)	2.191 (5)	Cr(1)-C(13)	2.201 (5)
Cr(1)-C(14)	2.198 (4)	Cr(1)-C(15)	2.213 (4)
Cr(1)-C(16)	2.189 (5)	Si-O(10)	1.644 (3)
Si-C(11)	1.879 (5)	Si-C(21)	1.866 (5)
Si-C(31)	1.850 (4)	O(1)-C(1)	1.165 (8)
O(2)-C(2)	1.154 (5)	O(3)-C(3)	1.156 (6)
C(11)-C(12)	1.414 (6)	C(11)-C(16)	1.403 (5)
C(12)-C(13)	1.382 (8)	C(13)-C(14)	1.405 (6)
C(14)-C(15)	1.381 (7)	C(15)-C(16)	1.404 (7)
C(21)-C(22)	1.376 (8)	C(21)-C(26)	1.387 (7)
C(22)-C(23)	1.403 (10)	C(23)-C(24)	1.371 (13)
C(24)-C(25)	1.344 (12)	C(25)-C(26)	1.379 (10)
C(31)-C(32)	1.381 (6)	C(31)-C(36)	1.399 (7)
C(32)-C(33)	1.368 (7)	C(33)-C(34)	1.346 (9)
C(34)-C(35)	1.377 (9)	C(35)-C(36)	1.377 (7)

Table 5.7 Bond angles (°) (COMPLEX **66**).

C(1)-Cr(1)-C(2)	88.4(2)	C(1)-Cr(1)-C(3)	88.5(2)
C(2)-Cr(1)-C(3)	89.5(2)	C(1)-Cr(1)-C(11)	161.2(2)
C(2)-Cr(1)-C(11)	95.2(2)	C(3)-Cr(1)-C(11)	109.9(2)
C(1)-Cr(1)-C(12)	124.7(2)	C(2)-Cr(1)-C(12)	88.5(2)
C(3)-Cr(1)-C(12)	146.7(2)	C(11)-Cr(1)-C(12)	37.4(2)
C(1)-Cr(1)-C(13)	94.2(2)	C(2)-Cr(1)-C(13)	109.2(2)
C(3)-Cr(1)-C(13)	161.1(2)	C(11)-Cr(1)-C(13)	67.2(2)
C(12)-Cr(1)-C(13)	36.7(2)	C(1)-Cr(1)-C(14)	87.2(2)
C(2)-Cr(1)-C(14)	145.5(2)	C(3)-Cr(1)-C(14)	124.6(2)
C(11)-Cr(1)-C(14)	79.3(2)	C(12)-Cr(1)-C(14)	66.4(2)
C(13)-Cr(1)-C(14)	37.2(2)	C(1)-Cr(1)-C(15)	108.6(2)
C(2)-Cr(1)-C(15)	162.5(2)	C(3)-Cr(1)-C(15)	94.9(2)
C(11)-Cr(1)-C(15)	67.3(2)	C(12)-Cr(1)-C(15)	78.5(2)
C(13)-Cr(1)-C(15)	66.5(2)	C(14)-Cr(1)-C(15)	36.5(2)
C(1)-Cr(1)-C(16)	145.1(2)	C(2)-Cr(1)-C(16)	126.3(2)
C(3)-Cr(1)-C(16)	88.6(2)	C(11)-Cr(1)-C(16)	37.1(1)
C(12)-Cr(1)-C(16)	66.3(2)	C(13)-Cr(1)-C(16)	78.5(2)
C(14)-Cr(1)-C(16)	66.2(2)	C(15)-Cr(1)-C(16)	37.2(2)
O(10)-Si-C(11)	109.8(2)	O(10)-Si-C(21)	110.1(2)
C(11)-Si-C(21)	108.4(2)	O(10)-Si-C(31)	109.6(2)
C(11)-Si-C(31)	109.1(2)	C(21)-Si-C(31)	109.9(2)
Cr(1)-C(1)-O(1)	179.1(4)	Cr(1)-C(2)-O(2)	179.2(4)
Cr(1)-C(3)-O(3)	180.0(7)	Cr(1)-C(11)-Si	130.4(2)
Cr(1)-C(11)-C(12)	70.1(3)	Si-C(11)-C(12)	121.5(3)
Cr(1)-C(11)-C(16)	70.2(3)	Si-C(11)-C(16)	121.9(3)
C(12)-C(11)-C(16)	116.6(4)	Cr(1)-C(12)-C(11)	72.5(2)
Cr(1)-C(12)-C(13)	72.0(3)	C(11)-C(12)-C(13)	122.1(4)
Cr(1)-C(13)-C(12)	71.3(3)	Cr(1)-C(13)-C(14)	71.3(3)
C(12)-C(13)-C(14)	119.3(5)	Cr(1)-C(14)-C(13)	71.5(3)
Cr(1)-C(14)-C(15)	72.4(3)	C(13)-C(14)-C(15)	120.8(5)
Cr(1)-C(15)-C(14)	71.2(3)	Cr(1)-C(15)-C(16)	70.5(2)
C(14)-C(15)-C(16)	118.9(4)	Cr(1)-C(16)-C(11)	72.7(3)
Cr(1)-C(16)-C(15)	72.3(3)	C(11)-C(16)-C(15)	122.4(4)
Si-C(21)-C(22)	120.9(4)	Si-C(21)-C(26)	122.3(4)
C(22)-C(21)-C(26)	116.9(5)	C(21)-C(22)-C(23)	120.9(6)
C(22)-C(23)-C(24)	119.4(7)	C(23)-C(24)-C(25)	120.9(8)
C(24)-C(25)-C(26)	119.3(7)	C(21)-C(26)-C(25)	122.6(6)
Si-C(31)-C(32)	122.6(3)	Si-C(31)-C(36)	121.0(3)
C(32)-C(31)-C(36)	116.3(4)	C(31)-C(32)-C(33)	121.5(5)

C(32)-C(33)-C(34)	121.1(6)	C(33)-C(34)-C(35)	119.9(5)
C(34)-C(35)-C(36)	119.1(5)	C(31)-C(36)-C(35)	121.9(5)

Table 5.8 Anisotropic displacement coefficients ($Å^2 x 10^3$) (COMPLEX **66**).

	U_{11}	U_{22}	U_{33}	U_{12}	U_{13}	U_{23}
Cr(1)	48(1)	45(1)	41(1)	-1(1)	22(1)	-3(1)
Si	41(1)	51(1)	46(1)	-1(1)	21(1)	-3(1)
O(1)	134(3)	124(3)	140(3)	-35(3)	113(3)	-47(3)
O(2)	91(2)	61(2)	70(2)	-12(2)	24(2)	-22(2)
O(3)	108(3)	84(3)	86(3)	37(3)	-15(2)	-3(2)
O(10)	47(2)	74(2)	58(2)	-7(2)	16(1)	-20(2)
C(1)	76(3)	74(3)	75(3)	-16(3)	49(3)	-25(3)
C(2)	59(3)	49(3)	46(2)	6(2)	26(2)	2(2)
C(3)	68(3)	62(3)	50(3)	11(3)	11(2)	-9(2)
C(11)	45(2)	42(2)	48(2)	1(2)	24(2)	-5(2)
C(12)	51(3)	48(3)	60(3)	8(2)	25(2)	10(2)
C(13)	81(4)	49(3)	71(3)	5(3)	40(3)	9(3)
C(14)	95(4)	43(3)	94(4)	-19(3)	66(4)	-11(3)
C(15)	63(3)	59(3)	61(3)	-20(2)	34(3)	-23(2)
C(16)	55(3)	58(3)	44(2)	-2(2)	28(2)	-7(2)
C(21)	43(3)	67(3)	52(2)	4(2)	22(2)	-5(2)
C(22)	64(3)	105(5)	91(4)	14(3)	48(3)	11(3)
C(23)	71(4)	184(8)	95(4)	20(5)	58(4)	8(5)
C(24)	74(4)	150(7)	85(4)	38(5)	30(3)	-34(5)
C(25)	82(4)	87(5)	145(6)	14(4)	48(4)	-38(4)
C(26)	55(3)	67(4)	108(4)	0(3)	36(3)	-22(3)
C(31)	44(2)	51(3)	56(3)	0(2)	29(2)	-3(2)
C(32)	57(3)	62(3)	61(3)	5(3)	17(2)	-5(3)
C(33)	75(3)	67(4)	85(4)	17(3)	20(3)	9(3)
C(34)	61(3)	112(5)	72(4)	20(3)	28(3)	40(3)
C(35)	101(4)	122(5)	56(3)	30(4)	45(3)	18(3)
C(36)	105(4)	77(4)	64(3)	29(3)	49(3)	9(3)

The anisotropic displacement factor exponent takes the form: $-2\pi^2(h^2a^{*2}U_{11} + ... + 2hka^*b^*U_{12})$.

Table 5.9 H-Atom coordinates ($x10^4$) and isotropic displacement coefficients ($Å^2x10^3$) (COMPLEX **66**).

	x	y	z	U
H(4)	5194	6073	7781	321(60)
H(12)	5799	9483	7555	61(12)
H(13)	6386	11446	7408	66(13)
H(14)	7200	11959	8354	64(12)
H(15)	7406	10562	9436	69(13)
H(16)	6819	8510	9563	34(9)
H(22)	4926	6638	9071	77(16)
H(23)	4321	8573	9218	123(21)
H(24)	4292	11760	8968	90(16)
H(25)	4837	13029	8557	168(32)
H(26)	5443	11135	8431	118(22)
H(32)	6207	3452	9058	100(17)
H(33)	6626	1766	10080	123(22)
H(34)	6746	3015	11135	89(16)
H(35)	6511	6126	11196	122(20)
H(36)	6098	7852	10169	82(15)

Table 5.10 STRUCTURE DETERMINATION SUMMARY FOR COMPLEX **67**

Crystal Data

Empirical Formula	$C_{24} H_{16} Cr_2 O_7 Si$
Color; Habit	yellow plate
Crystal Size (mm)	.3 x .15 x .08
Crystal System	Triclinic
Space Group	$P\bar{1}$
Unit Cell Dimensions	$\underline{a}$ = 7.731(2) Å $\underline{b}$ = 12.013(2) Å $\underline{c}$ = 13.929(3) Å $\underline{\alpha}$ = 102.89(2)° $\underline{\beta}$ = 102.34(2)° $\underline{\gamma}$ = 105.17(2)°
Volume	1165.1(3) $Å^3$
Z	2
Formula Weight	548.5
Density(calc.)	1.563 Mg/m^3
Absorption Coefficient	1.027 mm^{-1}
F(000)	556

Data Collection (COMPLEX **67**)

Diffractometer Used	Siemens P4, rotating anode
Radiation	MoKα (λ = 0.71073 Å)
Temperature (K)	302
Monochromator	Highly oriented graphite crystal
2θ Range	3.0 to 45.0°
Scan Type	2θ-θ
Scan Speed	Variable; 1.5 to 14.65°/min. in ω
Scan Range (ω)	1.20° plus Kα-separation
Background Measurement	Stationary crystal and stationary counter at beginning and end of scan, each for 25.0% of total scan time
Standard Reflections	0 measured every 100 reflections
Index Ranges	$0 \le h \le 8$, $-12 \le k \le 12$ $-15 \le \ell \le 14$
Reflections Collected	3422
Independent Reflections	3058 (R_{int} =5.05%)
Observed Reflections	2513 ($F \geq 4.0\sigma(F)$)
Absorption Correction	psi scan
Min./Max. Transmission	0.0207 / 0.0385

<u>Solution and Refinement</u> (COMPLEX **67**)

System Used	Siemens SHELXTL PLUS (VMS)
Solution	Direct Methods
Refinement Method	Full-Matrix Least-Squares
Quantity Minimized	$\Sigma w(\lvert F_o \rvert - \lvert F_c \rvert)^2$
Hydrogen Atoms	Riding model, fixed isotropic U
Weighting Scheme	$w^{-1} = \sigma^2(F) + 0.0002F^2$
Number of Parameters Refined	323
Final R Indices (obs. data)	R = 3.74 %, wR = 5.12 %
R Indices (all data)	R = 4.91 %, wR = 9.15 %
Goodness-of-Fit	2.15
Largest and Mean Δ/σ	0.004, 0.000
Data-to-Parameter Ratio	7.8:1
Largest Difference Peak	0.32 $e\text{Å}^{-3}$
Largest Difference Hole	-0.25 $e\text{Å}^{-3}$

Table 5.11 Atomic coordinates ($x10^4$) and equivalent isotropic displacement coefficients ($Å^2x10^3$) (COMPLEX **67**).

	x	y	z	U(eq)
Cr(1)	-3570(1)	-185(1)	7928(1)	52(1)
Cr(2)	660(1)	3144(1)	5582(1)	43(1)
Si	-564(2)	2797(1)	7968(1)	47(1)
O(1)	-6814(8)	-2228(5)	7860(5)	139(3)
O(2)	-5747(7)	1467(5)	8463(4)	100(3)
O(3)	-2192(8)	123(5)	10174(4)	113(3)
O(4)	-3088(5)	3490(3)	5147(3)	66(2)
O(5)	-1356(6)	545(4)	4370(3)	91(2)
O(6)	995(6)	3682(3)	3617(3)	77(2)
O(10)	-2290(5)	3328(3)	7708(3)	63(2)
C(1)	-5586(10)	-1449(6)	7874(5)	89(3)
C(2)	-4888(8)	829(6)	8256(4)	68(3)
C(3)	-2706(8)	-1(5)	9310(5)	67(3)
C(4)	-1649(7)	3361(4)	5332(3)	48(2)
C(5)	-561(7)	1534(5)	4842(4)	58(2)
C(6)	827(7)	3462(4)	4363(4)	54(2)
C(11)	-1545(6)	1118(4)	7463(3)	46(2)
C(12)	-3232(7)	531(5)	6625(3)	55(2)
C(13)	-3940(7)	-723(5)	6247(4)	65(2)
C(14)	-3042(8)	-1444(5)	6690(4)	66(3)
C(15)	-1385(8)	-891(5)	7493(4)	64(3)
C(16)	-628(6)	388(4)	7893(4)	51(2)
C(21)	1139(6)	3307(4)	7252(3)	45(2)
C(22)	1490(7)	4481(4)	7097(3)	49(2)
C(23)	2779(7)	4883(5)	6577(4)	57(2)
C(24)	3685(7)	4121(6)	6165(4)	65(3)
C(25)	3388(7)	2967(5)	6298(4)	59(2)
C(26)	2112(7)	2570(4)	6835(3)	52(2)
C(31)	663(7)	3262(4)	9367(3)	49(2)
C(32)	-356(7)	3182(5)	10078(4)	59(2)
C(33)	522(9)	3411(5)	11118(4)	71(3)
C(34)	2436(10)	3763(5)	11462(4)	77(3)
C(35)	3483(8)	3873(6)	10787(5)	87(3)
C(36)	2585(8)	3622(6)	9743(4)	71(3)

* Equivalent isotropic U defined as one third of the trace of the orthogonalized U_{ij} tensor.

Table 5.12 Bond lengths (Å) (COMPLEX **67**).

Cr(1)-C(1)	1.844(7)	Cr(1)-C(2)	1.825(7)
Cr(1)-C(3)	1.840(6)	Cr(1)-C(11)	2.220(5)
Cr(1)-C(12)	2.210(6)	Cr(1)-C(13)	2.220(5)
Cr(1)-C(14)	2.211(6)	Cr(1)-C(15)	2.213(7)
Cr(1)-C(16)	2.212(5)	Cr(2)-C(4)	1.842(6)
Cr(2)-C(5)	1.853(5)	Cr(2)-C(6)	1.844(6)
Cr(2)-C(21)	2.231(5)	Cr(2)-C(22)	2.195(4)
Cr(2)-C(23)	2.217(4)	Cr(2)-C(24)	2.199(5)
Cr(2)-C(25)	2.218(6)	Cr(2)-C(26)	2.210(5)
Si-O(10)	1.631(4)	Si-C(11)	1.864(5)
Si-C(21)	1.874(5)	Si-C(31)	1.860(4)
O(1)-C(1)	1.139(9)	O(2)-C(2)	1.167(9)
O(3)-C(3)	1.146(8)	O(4)-C(4)	1.146(7)
O(5)-C(5)	1.148(6)	O(6)-C(6)	1.153(7)
C(11)-C(12)	1.436(5)	C(11)-C(16)	1.417(8)
C(12)-C(13)	1.392(7)	C(13)-C(14)	1.408(9)
C(14)-C(15)	1.394(7)	C(15)-C(16)	1.423(7)
C(21)-C(22)	1.438(7)	C(21)-C(26)	1.413(8)
C(22)-C(23)	1.402(8)	C(23)-C(24)	1.389(9)
C(24)-C(25)	1.406(9)	C(25)-C(26)	1.409(8)
C(31)-C(32)	1.395(8)	C(31)-C(36)	1.378(7)
C(32)-C(33)	1.392(7)	C(33)-C(34)	1.370(10)
C(34)-C(35)	1.371(10)	C(35)-C(36)	1.396(8)

Table 5.13 Bond angles (°) (COMPLEX **67**).

C(1)-Cr(1)-C(2)	88.2(3)	C(1)-Cr(1)-C(3)	87.6(3)
C(2)-Cr(1)-C(3)	87.9(3)	C(1)-Cr(1)-C(11)	162.0(2)
C(2)-Cr(1)-C(11)	94.8(2)	C(3)-Cr(1)-C(11)	110.2(2)
C(1)-Cr(1)-C(12)	124.7(2)	C(2)-Cr(1)-C(12)	88.8(3)
C(3)-Cr(1)-C(12)	147.4(2)	C(11)-Cr(1)-C(12)	37.8(1)
C(1)-Cr(1)-C(13)	95.1(3)	C(2)-Cr(1)-C(13)	110.6(3)
C(3)-Cr(1)-C(13)	161.4(3)	C(11)-Cr(1)-C(13)	67.2(2)
C(12)-Cr(1)-C(13)	36.6(2)	C(1)-Cr(1)-C(14)	87.8(3)
C(2)-Cr(1)-C(14)	146.6(2)	C(3)-Cr(1)-C(14)	124.9(3)
C(11)-Cr(1)-C(14)	79.9(2)	C(12)-Cr(1)-C(14)	66.8(2)
C(13)-Cr(1)-C(14)	37.1(2)	C(1)-Cr(1)-C(15)	109.6(3)
C(2)-Cr(1)-C(15)	162.0(2)	C(3)-Cr(1)-C(15)	95.5(3)
C(11)-Cr(1)-C(15)	67.4(2)	C(12)-Cr(1)-C(15)	78.8(2)
C(13)-Cr(1)-C(15)	66.2(2)	C(14)-Cr(1)-C(15)	36.7(2)
C(1)-Cr(1)-C(16)	146.2(3)	C(2)-Cr(1)-C(16)	125.3(2)
C(3)-Cr(1)-C(16)	88.6(2)	C(11)-Cr(1)-C(16)	37.3(2)
C(12)-Cr(1)-C(16)	67.3(2)	C(13)-Cr(1)-C(16)	78.9(2)
C(14)-Cr(1)-C(16)	67.3(2)	C(15)-Cr(1)-C(16)	37.5(2)
C(4)-Cr(2)-C(5)	87.5(2)	C(4)-Cr(2)-C(6)	88.0(2)
C(5)-Cr(2)-C(6)	88.5(2)	C(4)-Cr(2)-C(21)	97.8(2)
C(5)-Cr(2)-C(21)	108.2(2)	C(6)-Cr(2)-C(21)	162.5(2)
C(4)-Cr(2)-C(22)	88.6(2)	C(5)-Cr(2)-C(22)	144.7(2)
C(6)-Cr(2)-C(22)	126.4(2)	C(21)-Cr(2)-C(22)	37.9(2)
C(4)-Cr(2)-C(23)	108.1(2)	C(5)-Cr(2)-C(23)	164.1(2)
C(6)-Cr(2)-C(23)	94.9(2)	C(21)-Cr(2)-C(23)	67.6(2)
C(22)-Cr(2)-C(23)	37.0(2)	C(4)-Cr(2)-C(24)	143.0(2)
C(5)-Cr(2)-C(24)	128.6(3)	C(6)-Cr(2)-C(24)	85.8(2)
C(21)-Cr(2)-C(24)	79.7(2)	C(22)-Cr(2)-C(24)	66.7(2)
C(23)-Cr(2)-C(24)	36.7(2)	C(4)-Cr(2)-C(25)	165.0(2)
C(5)-Cr(2)-C(25)	97.6(2)	C(6)-Cr(2)-C(25)	106.1(2)
C(21)-Cr(2)-C(25)	67.3(2)	C(22)-Cr(2)-C(25)	79.1(2)
C(23)-Cr(2)-C(25)	66.5(2)	C(24)-Cr(2)-C(25)	37.1(2)
C(4)-Cr(2)-C(26)	129.6(2)	C(5)-Cr(2)-C(26)	89.1(2)
C(6)-Cr(2)-C(26)	142.2(2)	C(21)-Cr(2)-C(26)	37.1(2)
C(22)-Cr(2)-C(26)	67.0(2)	C(23)-Cr(2)-C(26)	78.8(2)
C(24)-Cr(2)-C(26)	66.8(2)	C(25)-Cr(2)-C(26)	37.1(2)
O(10)-Si-C(11)	107.6(2)	O(10)-Si-C(21)	109.1(2)
C(11)-Si-C(21)	107.2(2)	O(10)-Si-C(31)	112.9(2)
C(11)-Si-C(31)	109.9(2)	C(21)-Si-C(31)	109.9(2)

Cr(1)-C(1)-O(1)	178.7(7)	Cr(1)-C(2)-O(2)	179.3(5)
Cr(1)-C(3)-O(3)	178.8(6)	Cr(2)-C(4)-O(4)	178.0(4)
Cr(2)-C(5)-O(5)	178.2(5)	Cr(2)-C(6)-O(6)	177.7(4)
Cr(1)-C(11)-Si	130.2(3)	Cr(1)-C(11)-C(12)	70.7(3)
Si-C(11)-C(12)	121.1(4)	Cr(1)-C(11)-C(16)	71.0(3)
Si-C(11)-C(16)	120.6(3)	C(12)-C(11)-C(16)	118.3(4)
Cr(1)-C(12)-C(11)	71.4(3)	Cr(1)-C(12)-C(13)	72.1(3)
C(11)-C(12)-C(13)	120.6(5)	Cr(1)-C(13)-C(12)	71.3(3)
Cr(1)-C(13)-C(14)	71.1(3)	C(12)-C(13)-C(14)	120.8(4)
Cr(1)-C(14)-C(13)	71.8(3)	Cr(1)-C(14)-C(15)	71.7(3)
C(13)-C(14)-C(15)	119.4(5)	Cr(1)-C(15)-C(14)	71.5(4)
Cr(1)-C(15)-C(16)	71.2(3)	C(14)-C(15)-C(16)	120.8(6)
Cr(1)-C(16)-C(11)	71.7(3)	Cr(1)-C(16)-C(15)	71.3(3)
C(11)-C(16)-C(15)	119.9(4)	Cr(2)-C(21)-Si	130.0(2)
Cr(2)-C(21)-C(22)	69.7(3)	Si-C(21)-C(22)	120.5(4)
Cr(2)-C(21)-C(26)	70.6(3)	Si-C(21)-C(26)	122.4(4)
C(22)-C(21)-C(26)	117.1(5)	Cr(2)-C(22)-C(21)	72.4(2)
Cr(2)-C(22)-C(23)	72.3(3)	C(21)-C(22)-C(23)	121.2(5)
Cr(2)-C(23)-C(22)	70.6(2)	Cr(2)-C(23)-C(24)	70.9(3)
C(22)-C(23)-C(24)	119.7(5)	Cr(2)-C(24)-C(23)	72.4(3)
Cr(2)-C(24)-C(25)	72.2(3)	C(23)-C(24)-C(25)	121.0(5)
Cr(2)-C(25)-C(24)	70.7(3)	Cr(2)-C(25)-C(26)	71.2(3)
C(24)-C(25)-C(26)	119.2(6)	Cr(2)-C(26)-C(21)	72.3(3)
Cr(2)-C(26)-C(25)	71.7(3)	C(21)-C(26)-C(25)	121.7(5)
Si-C(31)-C(32)	120.4(3)	Si-C(31)-C(36)	122.3(4)
C(32)-C(31)-C(36)	117.2(4)	C(31)-C(32)-C(33)	121.6(5)
C(32)-C(33)-C(34)	119.5(6)	C(33)-C(34)-C(35)	120.4(5)
C(34)-C(35)-C(36)	119.6(5)	C(31)-C(36)-C(35)	121.8(6)

Table 5.14 Anisotropic displacement coefficients ($Å^2x10^3$) (COMPLEX **67**).

	U_{11}	U_{22}	U_{33}	U_{12}	U_{13}	U_{23}
Cr(1)	50(1)	52(1)	51(1)	12(1)	14(1)	18(1)
Cr(2)	49(1)	46(1)	36(1)	16(1)	12(1)	15(1)
Si	52(1)	51(1)	39(1)	15(1)	14(1)	18(1)
O(1)	115(4)	92(4)	174(6)	-26(3)	77(4)	9(3)
O(2)	107(3)	118(4)	117(4)	71(3)	56(3)	54(3)
O(3)	134(4)	157(5)	67(3)	58(4)	28(3)	58(3)
C(4)	51(2)	73(3)	75(3)	22(2)	16(2)	23(2)
O(5)	109(3)	50(3)	89(3)	21(2)	1(3)	2(2)
O(6)	117(3)	83(3)	46(2)	42(2)	35(2)	31(2)
O(10)	68(2)	66(2)	64(2)	30(2)	19(2)	24(2)
C(1)	93(5)	69(4)	94(5)	5(4)	46(4)	9(4)
C(2)	69(4)	81(4)	67(4)	28(3)	25(3)	37(3)
C(3)	64(3)	79(4)	64(4)	24(3)	17(3)	32(3)
C(4)	62(3)	43(3)	39(3)	14(2)	14(2)	14(2)
C(5)	64(3)	56(4)	51(3)	26(3)	7(3)	15(3)
C(6)	69(3)	52(3)	46(3)	26(3)	21(3)	13(2)
C(11)	43(3)	53(3)	43(3)	12(2)	15(2)	18(2)
C(12)	55(3)	61(3)	42(3)	13(3)	9(2)	15(2)
C(13)	61(3)	69(4)	47(3)	10(3)	6(3)	6(3)
C(14)	78(4)	48(3)	65(4)	15(3)	24(3)	3(3)
C(15)	69(4)	62(4)	71(4)	29(3)	27(3)	23(3)
C(16)	42(3)	57(3)	57(3)	14(2)	17(2)	20(3)
C(21)	46(3)	52(3)	32(2)	13(2)	5(2)	14(2)
C(22)	58(3)	47(3)	35(3)	11(2)	6(2)	10(2)
C(23)	56(3)	56(3)	44(3)	-1(3)	8(2)	16(2)
C(24)	43(3)	92(5)	51(3)	4(3)	13(2)	25(3)
C(25)	44(3)	88(4)	54(3)	30(3)	13(2)	27(3)
C(26)	55(3)	62(3)	45(3)	27(3)	10(2)	24(2)
C(31)	64(3)	42(3)	40(3)	13(2)	18(2)	12(2)
C(32)	62(3)	62(3)	46(3)	11(3)	16(3)	10(3)
C(33)	102(5)	60(4)	44(3)	16(3)	29(3)	10(3)
C(34)	99(5)	71(4)	40(3)	7(3)	7(3)	12(3)
C(35)	61(4)	119(6)	59(4)	6(4)	-1(3)	27(4)
C(36)	67(4)	93(4)	48(3)	12(3)	18(3)	25(3)

The anisotropic displacement factor exponent takes the form: $-2\pi^2(h^2a^{*2}U_{11} + ... + 2hka^*b^*U_{12})$

Table 5.15 H-Atom coordinates ($x10^4$) and isotropic displacement coefficients ($Å^2x10^3$) (COMPLEX **67**).

	x	y	z	U
H(7)	-2120	4094	8278	162(32)
H(12)	-3888	1152	6323	80(16)
H(13)	-5225	-1156	5643	65(14)
H(14)	-3684	-2404	6340	63(14)
H(15)	-536	-1355	7834	64(14)
H(16)	710	786	8559	90(17)
H(22)	747	5051	7409	57(13)
H(23)	3269	5766	6480	87(17)
H(24)	4638	4393	5855	77(16)
H(25)	4154	2362	5968	101(19)
H(26)	2045	1667	6955	92(18)
H(32)	-1982	2868	9789	77(15)
H(33)	-585	3399	11633	173(32)
H(34)	3081	4019	12206	65(14)
H(35)	5134	4123	11096	104(19)
H(36)	3530	3634	9286	72(15)

Table 5.16 STRUCTURE DETERMINATION SUMMARY FOR COMPLEX **68**

Crystal Data

Empirical Formula	C_{27} H_{16} Cr_3 O_{10} Si
Color; Habit	Yellow fragment
Crystal size (mm)	.15 x .05 x .05
Crystal System	Rhombohedral
Space Group	$R\bar{3}$
Unit Cell Dimensions	$\underline{a}$ = 19.246(4) Å $\underline{c}$ = 12.457(6) Å
Volume	3997(3) $Å^3$
Z	6
Formula weight	684.5
Density(calc.)	1.706 Mg/m^3
Absorption Coefficient	1.305 mm^{-1}
F(000)	2064

Data Collection (COMPLEX **68**)

Diffractometer Used	Siemens P4, rotating anode
Radiation	MoKα (λ = 0.71073 Å)
Temperature (K)	297
Monochromator	Highly oriented graphite crystal
2θ Range	7.0 to 45.0°
Scan Type	ω
Scan Speed	Variable; 1.5 to 15.0°/min. in ω
Scan Range (ω)	1.20° plus Kα-separation
Background Measurement	Stationary crystal and stationary counter at beginning and end of scan, each for 0.5% of total scan time
Standard Reflections	3 measured every 100 reflections
Index Ranges	$-20 \le h \le 2$, $-1 \le k \le 20$ $-1 \le l \le 13$
Reflections Collected	1634
Independent Reflections	1157 (R_{int} =2.34%)
Observed Reflections	716 ($F \geq 4.0\sigma(F)$)
Absorption Correction	psi scan

<u>Solution and Refinement</u> (COMPLEX **68**)

System Used	Siemens SHELXTL PLUS (PC Version)
Solution	Direct Methods
Refinement Method	Full-Matrix Least-Squares
Quantity Minimized	$\Sigma w(\lvert F_o\rvert - \lvert F_c\rvert)^2$
Hydrogen Atoms	Riding model, fixed isotropic U
Weighting Scheme	$w^{-1} = \sigma^2(F) + 0.0001F^2$
Number of Parameters Refined	130
Final R Indices (obs. data)	R = 3.93 %, wR = 3.49 %
R Indices (all data)	R = 8.09 %, wR = 4.20 %
Goodness-of-Fit	1.19
Largest and Mean Δ/σ	0.016, 0.003
Data-to-Parameter Ratio	5.5:1
Largest Difference Peak	0.27 eÅ^{-3}
Largest Difference Hole	-0.27 eÅ^{-3}

Table 5.17 Atomic coordinates (x10^4) and equivalent isotropic displacement coefficients (Å^{2}x10^3) (COMPLEX **68**).

	x	y	z	U(eq)
Cr(1)	4817(1)	3453(1)	836(1)	38(1)
Si	6667	3333	744(2)	31(1)
C(1)	3826(4)	3373(4)	720(6)	57(4)
C(2)	4868(4)	3406(5)	-631(6)	60(4)
C(3)	4266(4)	2332(4)	867(6)	53(4)
C(11)	6052(3)	3757(3)	1271(4)	29(3)
C(12)	5543(4)	3429(4)	2160(5)	42(3)
C(13)	5063(4)	3727(5)	2560(5)	59(4)
C(14)	5099(5)	4384(5)	2055(7)	65(5)
C(15)	5592(4)	4742(4)	1179(7)	59(4)
C(16)	6066(3)	4433(3)	782(5)	41(3)
O(1)	3210(3)	3325(3)	649(5)	93(3)
O(2)	4913(4)	3403(4)	-1553(4)	109(4)
O(3)	3938(3)	1658(3)	873(5)	88(3)
O(10)	6667	3333	-555(5)	46(2)

* Equivalent isotropic U defined as one third of the trace of the orthogonalized U_{ij} tensor.

Table 5.18 Bond lengths (Å) (COMPLEX **68**).

Cr(1)-C(1)	1.839(9)	Cr(1)-C(2)	1.834(8)
Cr(1)-C(3)	1.868(8)	Cr(1)-C(11)	2.214(6)
Cr(1)-C(12)	2.178(7)	Cr(1)-C(13)	2.205(7)
Cr(1)-C(14)	2.200(9)	Cr(1)-C(15)	2.205(6)
Cr(1)-C(16)	2.192(5)	Si-C(11)	1.859(7)
Si-O(10)	1.619(7)	Si-C(11A)	1.859(6)
Si-C(11B)	1.859(6)	C(1)-O(1)	1.147(11)
C(2)-O(2)	1.153(9)	C(3)-O(3)	1.123(9)
C(11)-C(12)	1.402(8)	C(11)-C(16)	1.425(10)
C(12)-C(13)	1.400(14)	C(13)-C(14)	1.382(14)
C(14)-C(15)	1.383(11)	C(15)-C(16)	1.404(12)

Table 5.19 Bond angles (°) (COMPLEX **68**).

C(1)-Cr(1)-C(2)	89.8(4)	C(1)-Cr(1)-C(3)	86.5(3)
C(2)-Cr(1)-C(3)	88.7(3)	C(1)-Cr(1)-C(11)	166.6(3)
C(2)-Cr(1)-C(11)	100.4(3)	C(3)-Cr(1)-C(11)	102.4(3)
C(1)-Cr(1)-C(12)	135.0(3)	C(2)-Cr(1)-C(12)	134.6(4)
C(3)-Cr(1)-C(12)	87.7(3)	C(11)-Cr(1)-C(12)	37.2(2)
C(1)-Cr(1)-C(13)	100.7(3)	C(2)-Cr(1)-C(13)	166.2(3)
C(3)-Cr(1)-C(13)	100.7(3)	C(11)-Cr(1)-C(13)	67.9(3)
C(12)-Cr(1)-C(13)	37.3(4)	C(1)-Cr(1)-C(14)	86.9(4)
C(2)-Cr(1)-C(14)	136.9(3)	C(3)-Cr(1)-C(14)	133.8(3)
C(11)-Cr(1)-C(14)	79.7(3)	C(12)-Cr(1)-C(14)	66.1(4)
C(13)-Cr(1)-C(14)	36.6(4)	C(1)-Cr(1)-C(15)	101.5(3)
C(2)-Cr(1)-C(15)	103.1(3)	C(3)-Cr(1)-C(15)	165.7(3)
C(11)-Cr(1)-C(15)	67.8(3)	C(12)-Cr(1)-C(15)	78.3(3)
C(13)-Cr(1)-C(15)	66.3(3)	C(14)-Cr(1)-C(15)	36.6(3)
C(1)-Cr(1)-C(16)	135.6(3)	C(2)-Cr(1)-C(16)	87.1(3)
C(3)-Cr(1)-C(16)	137.6(3)	C(11)-Cr(1)-C(16)	37.7(3)
C(12)-Cr(1)-C(16)	66.5(2)	C(13)-Cr(1)-C(16)	79.2(2)
C(14)-Cr(1)-C(16)	66.6(3)	C(15)-Cr(1)-C(16)	37.2(3)
C(11)-Si-O(10)	110.7(2)	C(11)-Si-C(11A)	108.2(2)
O(10)-Si-C(11A)	110.7(2)	C(11)-Si-C(11B)	108.2(2)
O(10)-Si-C(11B)	110.7(2)	C(11A)-Si-C(11B)	108.2(2)
Cr(1)-C(1)-O(1)	179.8(8)	Cr(1)-C(2)-O(2)	177.8(7)
Cr(1)-C(3)-O(3)	179.1(7)	Cr(1)-C(11)-Si	129.2(3)
Cr(1)-C(11)-C(12)	70.0(4)	Si-C(11)-C(12)	122.4(6)
Cr(1)-C(11)-C(16)	70.3(4)	Si-C(11)-C(16)	121.6(4)
C(12)-C(11)-C(16)	116.0(7)	Cr(1)-C(12)-C(11)	72.8(4)
Cr(1)-C(12)-C(13)	72.4(4)	C(11)-C(12)-C(13)	123.5(7)
Cr(1)-C(13)-C(12)	70.3(4)	Cr(1)-C(13)-C(14)	71.5(5)
C(12)-C(13)-C(14)	118.2(7)	Cr(1)-C(14)-C(13)	71.9(5)
Cr(1)-C(14)-C(15)	71.9(5)	C(13)-C(14)-C(15)	121.5(10)
Cr(1)-C(15)-C(14)	71.5(4)	Cr(1)-C(15)-C(16)	70.9(4)
C(14)-C(15)-C(16)	119.7(8)	Cr(1)-C(16)-C(11)	71.9(3)
Cr(1)-C(16)-C(15)	71.9(3)	C(11)-C(16)-C(15)	121.1(6)

Table 5.20 Anisotropic displacement coefficients ($Å^2 x10^3$) (COMPLEX **68**).

	U_{11}	U_{22}	U_{33}	U_{12}	U_{13}	U_{23}
Cr(1)	34(1)	38(1)	43(1)	19(1)	-6(1)	-5(1)
Si	35(1)	35(1)	22(2)	18(1)	0	0
C(1)	51(5)	49(5)	77(6)	30(4)	-14(4)	-13(4)
C(2)	48(5)	73(6)	55(5)	27(4)	-19(4)	-11(5)
C(3)	33(4)	51(5)	83(6)	26(4)	-6(4)	-4(5)
C(11)	33(3)	27(3)	26(3)	14(3)	-6(3)	-1(3)
C(12)	46(4)	53(5)	32(4)	29(4)	1(4)	2(3)
C(13)	58(5)	92(6)	43(5)	50(5)	-5(4)	-19(5)
C(14)	59(5)	74(6)	79(6)	46(5)	-23(5)	-44(5)
C(15)	57(5)	34(4)	92(7)	28(4)	-33(5)	-17(4)
C(16)	29(4)	35(4)	50(4)	9(3)	-8(3)	6(4)
O(1)	49(3)	94(4)	151(6)	47(3)	-30(4)	-26(4)
O(2)	123(6)	147(6)	45(3)	59(5)	-12(4)	-15(4)
O(3)	62(4)	41(3)	153(6)	20(3)	8(4)	-9(4)
O(10)	56(3)	56(3)	26(4)	28(2)	0	0

The anisotropic displacement exponent takes the form: $-2\pi^2(h^2a^{*2}U_{11} + ... + 2hka^*b^*U_{12})$.

Table 5.21 H-Atom coordinates ($x10^4$) and isotropic displacement coefficients ($Å^2x10^3$) (COMPLEX **68**).

	x	y	z	U
H(12)	5438	2916	2421	22(14)
H(13)	4653	3431	3083	104(32)
H(14)	4701	4528	2228	67(23)
H(15)	5532	5128	762	51(19)
H(16)	6321	4617	97	28(16)
H(10)	6950	3138	-783	80(71)

CHAPTER 6

EXPERIMENTAL

6.1 General Procedures.

All syntheses were carried out under a dry nitrogen atmosphere utilizing conventional benchtop and glovebag techniques. Solvents were dried and distilled according to standard procedures.[206] Standard flash type silica gel, (particle size of 20-45 microns) was employed for flash column chromatography. Melting points were determined on a Thomas Hoover capillary melting point apparatus and are uncorrected. The 500 MHz ^{1}H and 125.7 MHz ^{13}C NMR spectra recorded on a Bruker AM-500 spectrometer were acquired using a 5 mm dual frequency $^{1}H/^{13}C$ probe. The 200 MHz ^{1}H and 50.2 MHz ^{13}C NMR spectra recorded on a Bruker AM-200 spectrometer. The 49.8 MHz ^{29}Si NMR spectra were recorded on a Bruker WM-250 spectrometer with a 10 mm probe. All chemical shifts are reported relative to tetramethylsilane using the residual C_6H_6 (7.15 ppm), $CHCl_3$ (7.24 ppm) and CH_2Cl_2 (5.35 ppm) signals as internal references. Infrared spectra were recorded on a Bio Rad FTS-40 instrument using NaCℓ plates. Fast atom bombardment mass spectra were obtained on a VG analytical ZAB-SE spectrometer. 3-Nitrobenzylalcohol was used as the sample matrix and Xe was the bombarding gas (8 keV). Microanalytical data are from Guelph Chemical Labs.

6.2 Experimental Procedures.

PREPARATION OF 2-METHYL-1-PHENYLETHYNYLCYCLOPENTANOL, **47**.

To magnesium (2.8 g, 115 mmol) in ether (65 mL) was added bromoethane (13.6 g, 9.34 mL, 125 mmol). A solution of phenylacetylene (8.89 g, 9.58 mL, 87 mmol) in ether (40 mL) was added dropwise and stirred at room temperature for 1 hour. This was then cooled in ice and 2-methylcyclopentanone (11.287 g, 12.31 mL, 115 mmol) in ether (45 mL) was added dropwise over 1.5 hours at room temperature and then heated to reflux for 0.5 hours. The solution was allowed to cool and hydrolyzed with saturated $NH_4C\ell$ solution (200 mL). The product was then extracted with ether and dried over anhydrous sodium sulfate, filtered and the solvent was removed by rotary evaporator. It was then ice cooled and recrystallized from petroleum ether. The product (6.43 g, 32 mmol, 37%) crystallized as colourless needles with a 90:10 ratio of **47** major:**46** minor isomers; m.p. 71°C. ^1H NMR (500 MHz, $CDC\ell_3$): **46**: δ 1.15 (d,3H,Me), 2.05 (1H, H-2eq), 1.55 (1H, H-3ax)[a], 1.70 (1H,H-3eq)[a], 1.50 (1H,H-4eq)[a], 1.77 (1H,H-4ax)[a], 2.10 (2H,H-5). **47**: δ 1.15 (d,3H,Me), 2.05 (1H,H-2ax), 1.87 (1H,H-3ax), 1.32 (1H,H-3eq), 1.63 (2H,H-4), 2.17 (1H,H-5ax), 1.98 (1H,H-5eq). ^{13}C NMR data are collected in Table 4.1.

---

[a] Assignments may be interchanged.

PREPARATION OF PHENYLETHYNYL-2-METHYL-CYCLOPENTANOL DICOBALT HEXACARBONYL, **48**.

A two neck 100 mL round bottom flask was charged with dicobalt octacarbonyl (0.8550 g, 2.5 mmol), THF (30 mL), magnetic stirrer, and nitrogen. This mixture was stirred for approximately 15 minutes. To this was added phenylethynyl-2-methyl-cyclopentanol (0.5 g, 2.5 mmol) and stirred at room temperature for 2 hours. The product was purified by flash column chromatography on silica gel, by using 90:10 hexane:ether as the eluent to yield dark purple crystals of **48** (1.03 g, 2.07 mmol,84 %), m.p. 49-50°C. NMR data are collected in Table 4.1. IR (cm^{-1}): carbonyl stretches at 2025.4, 2051.9 and 2089.8. Analysis: calculated for $C_{20}H_{16}O_7Co_2$, C,49.30; H, 3.52. Found, C,49.79; H, 3.55. FAB mass spectrum m/z (%): 486 (5) $(M)^+$, 458 (40) $(M\text{-}CO)^+$, 430 (80) $(M\text{-}2CO)^+$, 402 (85) $(M\text{-}3CO)^+$, 374 (53) $(M\text{-}4CO)^+$, 346 (100) $(M\text{-}5CO)^+$, 318 (35) $(M\text{-}6CO)^+$.

PROTONATION OF PHENYLETHYNYL-2-METHYL-CYCLOPENTANOL DICOBALT HEXACARBONYL, **49**.

A solution of **48** in $CD_2C\ell_2$ was placed in an NMR tube, cooled in a dry-ice/acetone bath and 4 drops of HBF_4 in ether were added. The sample was placed in the spectrometer at -10°C and the spectrum of the cation **49** was recorded: NMR data are collected in Table 4.1. The cation was then quenched with water at room temperature to yield the alkene **50**.

FAB mass spectrum m/z (%): 468 (7) $(M)^+$ = alkene, 440 (15) $(M-CO)^+$, 412 (100) $(M-2CO)^+$, 384 (53) $(M-3CO)^+$, 356 (45) $(M-4CO)^+$, 328 (22) $(M-5CO)^+$, 300 (35) $(M-6CO)^+$.

PREPARATION OF BIS(CYCLOPENTADIENYLDICARBONYL MOLYBDENUM) PHENYLETHYNYL-2-METHYLCYCLOPENTENE **51**.

A mixture of $[CpMo(CO)_3]_2$ (1.2 g, 2.6 mmol), dry toluene (90 mL) and dry THF (10 mL) was heated under strong reflux for two days. The solution was cooled and the desired alkyne, phenylethynyl-2-methyl-cyclopentanol (0.52 g, 2.6 mmol), added and then heated to reflux for two days. After cooling, filtration and removal of solvent on a rotary evaporator, the product was then purified by flash chromatography using 10 % dichloromethane in hexane. The product is a mixture of the alcohol, (trace quantities) and the alkene, **51** (1.05 g, 1.7 mmol, 67 %); m.p. 144-145°C. Analysis: calculated for $C_{28}H_{25}O_4Mo_2$, C,54.56; H, 3.92. Found, C,54.26; H, 3.93. NMR data are collected in Table 4.1.

PREPARATION OF $[(C_6H_5)_3SiOH][Cr(CO)_3]_n$, n = 1, 2; **66**, **67**.

A 250 mL round bottom flask was charged with triphenylsilanol (5.54 g, 20 mmol) and chromium hexacarbonyl (4.62 g, 21 mmol) in dry n-butyl ether (130 mL) and dry THF (15 mL). This mixture was heated to reflux for two days under nitrogen. The solution was cooled and filtered under vacuum to yield a clear yellow liquid. THF and n-butylether were removed in vacuo. The product was purified by flash column chromatography on silica gel using 1:1 ether:hexane as the eluent to give yellow crystals of $[(C_6H_5)_3SiOH]Cr(CO)_3$, **66** (1.47 g, 3.6 mmol, 18%, m.p. 115-116°C) and **67** (0.26 g, 0.5 mmol, 4.8 %, m.p. 170-171°C). Analysis: calculated for $C_{21}H_{16}O_4CrSi$, **66**, C, 61.16; H, 3.91. Found, C, 61.20; H, 3.91. Calculated for $C_{24}H_{16}O_7Cr_2Si$, **67**, C, 52.55; H, 2.94. Found, C, 52.80; H, 2.90. ^{29}Si NMR (CD_2Cl_2) for complex **66**: -12.96. ^{13}C and ^1H NMR data are collected in Table 5.1. IR (cm^{-1}): carbonyl stretches for **66**: 1896.1, 1971.3. Carbonyl stretches for **67**: 1899.9, 1972.7.

FAB mass spectrum m/z (%) **66**: 412 (8) $(M)^+$, 328 (32) $(M\text{-}3CO)^+$, 199 (45) $(M\text{-}Cr(CO)_3\text{-}Ph)^+$

FAB mass spectrum m/z (%) **67**: 548 (5) $(M)^+$, 464 (18) $(M\text{-}3CO)^+$, 436 (8) $(M\text{-}4CO)^+$, 412 (15) $(M\text{-}Cr(CO)_3)^+$, 328 (100) $(M\text{-}Cr(CO)_3\text{-}3CO)^+$, 199 (48) $(M\text{-}2Cr(CO)_3\text{-}Ph)^+$

PREPARATION OF $[(C_6H_5)_3SiOH][Cr(CO)_3]_3$, **68**.

To triphenylsilanol chromiumtricarbonyl (2.076 g, 5.04 mmol) and chromium hexacarbonyl (1.262 g, 5.74 mmol) were added dry THF (5 mL) and dry n-butyl ether (50 mL). This was heated under reflux for 2 days. The product was filtered and the solvent removed under vacuum. The mixture was subjected to flash column chromatography on silica gel and eluted with 20:80 ether:hexanes. This was re-chromatographed; elution with 50:50 ether:hexanes gave $[(C_6H_5)_3SiOH]$-$[Cr(CO)_3]_3$, **68**, (0.218 g, 0.319 mmol, 11%). This product was recrystallized from ether-hexanes to yield crystallographically pure needle-like crystals. m.p.;190-191°C. NMR data are collected in Table 5.1. IR (cm^{-1}): carbonyl stretches at 1903.6, 1974.2. Analysis: calculated for $C_{27}H_{16}O_{10}Cr_3Si$, C, 47.37; H, 2.36. Found, C, 47.19; H, 2.08.

FAB mass spectrum m/z (%): 684 (5) $(M)^+$, 600 (10) $(M\text{-}3CO)^+$, 516 (7) $(M\text{-}6CO)^+$, 488 (6) $(M\text{-}7CO)^+$, 548 (12) $(M\text{-}Cr(CO)_3)^+$, 464 (35) $(M\text{-}Cr(CO)_3\text{-}3CO)^+$, 436 (15) $(M\text{-}Cr(CO)_3\text{-}4CO)^+$, 380 (13) $(M\text{-}Cr(CO)_3\text{-}6CO)^+$, 328 (100) $(M\text{-}2Cr(CO)_3\text{-}3CO)^+$.

PROTONATION OF $[(C_6H_5)_3SiOH][Cr(CO)_3]_3$.

In an NMR tube, **68** (50 mg, 0.07 mmol) in $CD_2C\ell_2$ (2 mL) was cooled in a dry-ice/acetone bath (-70°C) and 3-4 drops of triflic acid were added. The sample was placed in the spectrometer at -70°C and the spectrum was recorded. The ^{13}C NMR spectrum exhibited a peak at 242 ppm, (CO).

PREPARATION OF $[(C_6H_5)_3COH]Cr(CO)_3$, **69**.

To triphenylcarbinol (1.224 g, 4.70 mmol) and chromium hexacarbonyl (5.171 g, 23.5 mmol) were added n-butyl ether (100 mL) and dry THF (25 mL). This was heated under reflux for three days. The product was filtered and the solvent removed under vacuum. The mixture was subjected to flash column chromatography and eluted with 5:95 ether:hexanes to yield yellow crystals of $[(C_6H_5)_3COH]Cr(CO)_3$, **69**, (1.6 g, 4.0 mmol, 85 %) m.p. NMR data are collected in Table 5.3.

PREPARATION OF $[(C_6H_5)_3COH][Cr(CO)_3]_3$.

Triphenylcarbinol (5.47 g, 20 mmol) and chromium hexacarbonyl (4.62 g, 21 mmol) were added to dry n-butylether (80 mL) and dry THF (25 mL). This mixture was allowed to stir at reflux in the absence of light for two days. The product was then filtered under vacuum and purified by flash column chromatography on silica gel by using ether:hexanes 5:95 as the eluent to yield orange crystals of $[(C_6H_5)_3COH][Cr(CO)_3]_3$. This product decomposes to yield a mixture of the mono and bis chromium complexes. The ^1H NMR spectrum exhibited peaks only in the complexed phenyl region.

X-RAY CRYSTALLOGRAPHIC DATA

X-ray crystallographic data were collected on a Siemens P4 diffractometer with a rotating anode and graphite-monochromated Mo $K\alpha$ radiation, at 298(1)K, with the exception of 2-methylphenylethynylcyclopentanol, **47**, which was collected on a Rigaku AFC6R and graphite-monochromated Cu $K\alpha$ radiation, at 298(1)K. All structures were solved by direct methods. Profile analysis and empirical absorption corrections were made with the use of *SHELXTL-Plus* (Sheldrick, 1990). Crystal data and data collection parameters are listed in the appropriate tables.

MOLECULAR ORBITAL CALCULATIONS

All calculations were carried out within the Extended Hückel formalism [207,208] using the weighted H_{ij} formula.[209] The bond lengths and angles were taken from the x-ray crystal of $Cp_2Mo_2(CO)_4(HC{\equiv}CH)$.[51] The atomic parameters used were taken from reference 210.

REFERENCES

1. L.F. Fieser and M. Fieser, "Steroids", Reinhold, New York, 1959.
2. H.L. Bradlow, Ed., "Steroids: Structure, Function and Regulation", Butterworth publishers, Stoneham.
3. H.L.J. Makin, Ed., "Biochemistry of Steroidal Hormones, 2nd Ed.", Blackwell, Oxford, 1984.
4. F. Sciarra, M. Neves, E. Castro, L. Martini and J.R. Pasqualini, Eds., "The Journal of Steroid Biochemistry", Pergamon Press, Oxford.
5. A. Nakamura and M. Tsutsui, Z. Naturforsch., 1963, 18b, 666.
6. A. Nakamura and M. Tsutsui, J. Med. Chem., 1963, 6, 796. (a) R.M. Moriarty, Y-Y. Ku, U.S. Gill, R. Gilardi, R.E. Perrier and M.J. McGlinchey, Organometallics, 1989, 8, 960. (b) A. Vessières, S. Top, A.A. Ismail, I.S. Butler, M. Louer and G. Jaouen, Biochemistry, 1988, 27, 6659.
7. D.H.R. Barton, A.A.L. Gunatilaka, T. Nakanishi, H. Patin, D.A. Widdowson and B.R. Worth, J. Chem. Soc., Perkins I., 1976, 821.
8. G. Evans, B.F.G. Johnson and J. Lewis, J. Organomet. Chem., 1975, 102, 507.
9. A.G.M. Barrett, D.H.R. Barton and G. Johnson, J. Chem. Soc., Perkins I., 1978, 1014. (a) K.M. Nicholas and R. Pettit, Tetrahedron Lett., 1971, 3475.

10. H. Alper and J.T. Edward, J. Organomet. Chem., 1968, 14, 411.

11. A. Windaus, K. Dithman, H. Murke and F. Suckfull, Leibigs. Ann. Chim., 1931, 488, 91.

12. J. Andrieux, D.H.R. Barton and H. Patin, J. Chem. Soc., Perkins I., 1977, 359.

13. D.H.R. Barton, S.G. Davies and W.B. Motherwell, Synthesis., 1979, 265.

14. S.G. Davies, "Organotransition Metal Chemistry: Applications to Organic Synthesis.", Pergamon Press, London, 1982.

15. G. Jaouen, S. Top, A. Laconi, D. Couturier and J. Brocard, J. Am. Chem. Soc., 1984, 106, 2207.

16. S. Top, A. Vessières, J.-P. Abjean and G. Jaouen, J. Chem. Soc., Chem. Comm. 1981, 428.

17. R.W. Howsam and F.J. McQuillin, Tetrahedron Lett., 1968, 3667.

18. I.T. Harrison, E. Kimura, E. Bohme and J.H. Fried, Tetrahedron Lett., 1969, 1589.

19. D.N. Jones and S.D. Knox, J. Chem. Soc., Chem. Comm., 1975, 166.

20. D.J. Collins, W.R. Jackson and R.N. Timms, Tetrahedron Lett., 1976, 495.

21. K. Henderson and F.J. McQuillin, J. Chem. Soc., Chem. Comm., 1978, 15.

22. J.Y. Satoh and C.A. Horiuchi, Bull. Chem. Soc. Jpn., 1979, 52, 2653.

23. C.A. Horiuchi and J.Y. Satoh, J. Chem. Soc., Perkins I., 1982, 2595.

24. M. Cais, S. Dani, Y. Eden, O. Gandolfi, M. Horn, E.E. Isaacs, Y. Josephy,

Y. Saar, E. Slovin and L. Snarrsky, Nature. 1977, 270, 534.

25. O. Gandolfi, M. Cais, G. Dolcetti, M. Ghedini and A. Modiano, Inorg. Chim. Acta., 1981, 56, 127.

26. O. Gandolfi, J. Blum and F. Mandelbaum-Shavit, Inorg. Chim. Acta., 1984, 91, 257.

27. M. Cais, Rec. Trav. Chim. des Pays-Bas., 1987, 106, 396.

28. M. Cais, E. Slovin and L. Snarsky, J. Organomet. Chem., 1978, 160, 223.

29. G. Jaouen, A. Vessières, S. Top, A.A. Ismail and I.S. Butler, J. Am. Chem. Soc., 1985, 107, 4778.

30. S. Top, G. Jaouen, A. Vessières, J.-P. Abjean, D. Davoust, C.A. Rodger, B.G. Sayer and M.J. McGlinchey, Organometallics, 1985, 4, 2143.

31. G. Jaouen, A. Vessières, S. Top, M. Savignas, A.A. Ismail and I.S. Butler, Organometallics, 1987, 6, 1985.

32. A. Vessières, S. Tondu, G. Jaouen, S. Top, A.A. Ismail, G. Teutsch and M. Moguilewsky, Inorg. Chem., 1988, 27, 1852.

33. M.P. Georgiadis, S.A. Haroutounian and K.P. Chondros, Inorg. Chim Acta. 1987, 178, 249.

34. J.M.G. Fernandez, M.F. Rubio-Arroyo, G. Rubio-Rao and A. de la P'na, Monatsh. Chem., 1983, 144, 535.

35. A. Saxena, F. Huber, L. Pellerito, A. Girasolo and G.C. Stocio, Inorg. Chim. Acta., 1986, 125, 197.

36. A. Saxena, F. Huber, L. Pellerito and A. Girasolo, App. Organomet. Chem., 1987, 1, 413.

37. R.H. Crabtree, "The Organometallic Chemistry of the Transition Metals", Wiley-Interscience, New York, 1988, Chapters 2 and 13.

38. F.A. Cotton and G. Wilkinson, "Advanced Inorganic Chemistry", Wiley-Interscience, New York, 1980, p. 1081.

39. J.P. Collman, L.S. Hegedus, J.R. Norton and R.G. Finke, "Principles and Applications of Organotransition Metal Chemistry", University Science Books, Mill valley, California, 1987, Chapter 2.

40. C.M. Lukehart, "Fundamental Transition Metal Organometallic Chemistry", Brooks/Cole, Monterey, California, 1985, Chapter 1.

41. F.G.A. Stone, Angew. Chem. Int. Ed. Engl., 1984, 23, 89.

42. R. Markby, I. Wender, R.A. Friedel, F.A. Cotton and H.W. Sternberg, J. Am. Chem. Soc., 1958, 80, 6529.

43. D. Seyferth, Adv. Organomet. Chem., 1976, 14, 97.

44. B.R. Penfold and B.H. Robinson, Acc. Chem. Res., 1973, 6, 73.

45. P.W. Sutton, L.F. Dahl, J. Am. Chem. Soc., 1967, 89, 261.

46. G. Jaouen, A Marinetti, B. Mentzen, R. Mutin, J.-Y. Saillard, B.G. Sayer and M.J. McGlinchey, Organometallics, 1982, 1, 753.

47. R. Hoffmann, Angew. Chem. Int. Ed. Engl., 1982, 21, 711.

48. H. Vahrenkamp, Adv. Organomet. Chem., 1983, 22, 169.

49. M.F. D'Agostino, M. Mlekuz and M.J. McGlinchey, J. Organomet. Chem., 1988, 345, 371.

50. S. Jensen, B.H. Robinson and J. Simpson, J. Chem. Soc., Chem. Comm., 1983, 1081.

51. W.I. Bailey, Jr., M.H. Chisholm, F.A. Cotton and L.A. Rankel, J Am. Chem. Soc., 1978, 100, 5764.

52. P. Bougeard, S. Peng, M. Mlekuz and M.J. McGlinchey, J. Organomet. Chem., 1985, 296, 383.

53. J.E. Huheey, "Inorganic Chemistry", 3rd Ed'n., Harper and Row, New York, 1983, pp. 239-245.

54. G.A. Carriedo, J.A.K. Howard, D.B. Lewis, G.E. Lewis and F.G.A. Stone, J. Chem. Soc., Dalton Trans., 1985, 905.

55. B.E.R. Schilling and R. Hoffmann, J. AM. Chem. Soc., 1979, 101, 3456.

56. R.T. Edidin, J.R. Norton and K. Mislow, Orgnaometallics, 1982, 1, 561.

57. M.F. D'Agostino, M. Mlekuz, J.W. Kolis, B.G. Sayer, C.A. Rodger, J.-F. Halet, J.-Y. Saillard and M.J. McGlinchey, Organometallics, 1986, 5, 2345.

58. F.A.L. Anet and E. Leblanc, J. Am. Chem. Soc., 1957, 79,2649.

59. F. Hein, Chem. Ber., 1919, 52,195.

60. H.H. Zeiss, Abstr., 126th Meet., Am. Chem. Soc., 1954, p.29-O.

61. H.H. Zeiss and M. Tsutsui, J. Am. Chem. Soc., 1957, 79,3062.

62. W. Strohmeier, Chem. Ber., 1967, 100, 265.

63. W. Herwig and H.H. Zeiss, J. Am. Chem. Soc., 1959, 81,4798.

64. H.H. Zeiss, "Organometallic Chemistry", Am. Chem. Soc. Monogr. No. 147. Van Nostrand-Reinhold, New Jersey, 1960.

65. E.O. Fischer and W. Hafner, Z. Naturforsch., 1955, B10, 655.

66. B. Nicholls and M. Whiting, J. Chem. Soc., London 1959, 551.

67. W. Strohmeier, Chem. Ber., 1961, 94, 2490.

68. S. Top and G. Jaouen, J. Organomet. Chem., 1979, 182, 381.

69. C.A.L. Mahaffy and P.L. Pauson, Inorg Synth., 1979, 19, 154.

70. G. Jaouen, L. Tchissambou and R. Dabard, C.R. Hebd. Seances Acad. Sci., Ser. C., 1972, 274, 654.

71. M.D. Rausch, Pure Appl. Chem., 1972, 30, 523.

72. K. Öfele, Chem. Ber., 1966, 99, 1372.

73. M.D. Rausch, G.A. Moser, E.J. Zaiko and A.L. Lipman Jr., J. Organomet. Chem., 1970, 23, 185.

74. H. Werner, K. Deckelmann and U. Schonenberger, Helv. Chim. Acta., 1970, 53, 2002.

75. G.R. Knox, D.G. Leppard, P.L. Pauson and W.E. Watts, J. Organomet. Chem., 1972, 34, 347.

76. P. Powell, "Principles of Organometallic Chemistry", 2nd Ed., Chapman and Hall Ltd., New York, N.Y., 1988, pp. 156, 320.

77. L.E. Orgel, Inorg. Chem., 1962, 1, 25.

78. A. Solladié-Cavallo, Polyhedron, 1985, 4, 901.

79. E.O. Fischer and S. Schreiner, Chem. Ber., 1959, 92, 938.

80. E.W. Randall and I.E. Sutton, Proc. Chem. Soc., 1959, 95.

81. R.V. Emanuel and E.W. Randall, J. Chem. Soc. A., 1969, 3002.

82. B. Debzer, H.P. Fritz, C.G. Kreiter and K. Öfele, J. Organomet. Chem., 1967, 7, 289.

83. B.E. Mann, J. Chem. Soc., Chem. Comm., 1971, 976.

84. L.F. Farnel, E.W. Randall and E. Rosenberg, J. Chem. Soc., Chem. Comm., 1971, 1078.

85. B.E. Mann, J. Chem. Soc., Dalton. Trans., 1973, 2012.

86. M.M. Maricq, J.S. Waugh, J.L. Fletcher and M.J. McGlinchey, J. Am. Chem. Soc., 1978, 100, 6092.

87. R.P.A. Sneeden, "Organochromium Compounds", Academic Press, New York, 1975.

88. J.A. Connor, J.A. Martinho-Simoes, H.A. Skinner and M.T. Zafarani-Moattar, J. Organomet. Chem., 1979, 179, 331.

89. O.S. Mills, Pure Appl. Chem., 1969, 20, 117.

90. O.L. Carter, A.T. McPhail and G.A. Sim, J. Chem. Soc. (A), 1967, 1619.

91. F. VanMeurs, J.M. van der Toorn and H. van Bekkum, J. Organomet. Chem., 1976, 113, 341.

92. W.R. Jackson, W.B. Jennings, S.C. Rennison and R.S. Pratt, J. Chem. Soc.

B., 1973, B29, 469.

93. Y. Dusausoy, J. Protas, J. Besancon and J. Tirouflet, Acta. Cryst., Ser. B., 1969, 1214.

94. A.J. Pearson, "Metallo-Organic Chemistry", John Wiley and Sons Ltd., Toronto, 1985, pp. 348-363.

95. M.F. Semmelhack, Ann. N.Y. Acad. of Sciences, 1977, 295, 37.

96. G. Jaouen, "Transition Metal Organometallics, Vol. II.", Academic Press, Inc., 1978, 65.

97. D.A. Brown and R.J. Raju, J. Chem. Soc., 1959, 551.

98. J.F. Bunnett and H. Hermann, J. Org. Chem., 1971, 36, 4081.

99. D.A. Brown and R.J. Raju, J. Chem. Soc. (A), 1966, 40.

100. L. Tchissambou, G. Jaouen and R. Dabard, C.R. Hebd. Seances Acad. Sci. Ser. C., 1972, 274, 806.

101. G. Jaouen, Ann. N.Y. Acad. of Sciences, 1977, 295, 59.

102. I.M. Palotal, G.R. Stephenson, L.A.P. Kane-Maguire, J. Organomet. Chem., 1987, 319, C5.

103. A.J. Birch, P.E. Cross, D.T. Connor, G.S.R. Subba Rao, J. Chem. Soc. (C)., 1966, 54.

104. M.F. Semmelhack, G.L. Clark, J.L. Garcia, J.J. Harrison, Y. Thebtaranonth, W. Wulff, A. Yamashita, Tetrahedron, 1981, 37, 3957.

105. M. Uemura, T. Kobayashi, K. Isobe, T. Minami, Y. Hayashi, J. Org. Chem.,

1986, 51, 2859.

106. G. Jaouen and R. Dabard, Tetrahedron Lett., 1971, 1015.

107. G. Jaouen and A. Meyer, J. Am. Chem. Soc., 1975, 97, 4667.

108. A. Meyer and G. Jaouen, J. Chem. Soc., Chem. Comm., 1974, 787.

109. W.S. Trahanovsky and R.J. Card, J. Am. Chem. Soc., 1972, 39, 3547.

110. G. Jaouen and A. Meyer, Tetrahedron Lett.,1976, 39, 3547.

111. H. Alper, "Transition Metal Organometallics in Organic Synthesis", Vol. 1., Academic Press, New York, N.Y., 1976, pp. 71-74.

112. S. Top, G. Jaouen, J. Gillois, C. Baldoli and S. Maiorana, J. Chem. Soc., Chem. Comm., 1988, 1284.

113. M.F. Semmelhack, H.T. Hall Jr., R. Farina, M. Yoshifuji, G. Clark, T. Bargar, K. Hirotsu and J. Clardy, J. Am. Chem. Soc., 1979, 101, 3536.

114. K.M. Nicholas, R.C. Kerber, E.I. Stiefel, Inorg. Chem., 1971, 10, 1515.

115. A.N. Nesmeyanov, N.A. Ustynyuk, L.G. Makarova, S. Andree, Y.A. Ustynnyuk, L.N. Novilova and Y.N. Luzikov, J. Organomet. Chem., 1978, 154, 45.

116. R.J. Card and W.S. Trahanovsky, J. Organomet. Chem., 1980, 45, 2555.

117. G. Jaouen, S. Top and M.J. McGlinchey, J. Organomet. Chem., 1980, 195, C5.

118. A. Ceccon, A. Gambaro, G. Agostini and A. Kenzo, J. Organomet. Chem., 1981, 217, 79.

119. A. Ceccon, A. Gambaro, A.M. Robinson and A. Venzo, Chem. Comm., 1982, 902.

120. S. Top, G. Jaouen, B.G. Sayer and M.J. McGlinchey, J. Am. Chem. Soc., 1983, 105, 6426.

121. M. Cais, Organomet. Chem. Rev., 1966, 1, 435.

122. L. Haynes and R. Pettit in "Carbonium Ions", G. Olah and P.V.R. Schleyer, Eds., Vol. 5, Wiley, New York, 1975.

123. D. Seyferth, J.S. Merola and C.S. Eschbach, J. Am. Chem. Soc., 1978, 100, 4124.

124. M. Acampora, A. Ceccon, M. Dal Farra, G. Giacometti and G. Riggati, J. Chem. Soc., Perkin Trans.II., 1977, 483.

125. J.D. Holmes, D.A.K. Jones and R. Pettit, J. Organomet. Chem., 1965, 4, 324.

126. S.P. Gubin, V.S. Kandkarova and A.Z. Zreindlin, J. Organomet. Chem., 1974, 64, 229.

127. S. Top, B. Caro and G. Jaouen, Tetrahedron Lett., 1978, 787.

128. S. Top and G. Jaouen, J. Chem. Soc., Chem. Comm., 1979, 224.

129. M. Savignac, G. Jaouen, C.A. Rodger, R.E. Perrier, B.G. Sayer and M.J. McGlinchey, J. Org. Chem., 1986, 51, 2328.

130. S. Tondu, Ph.D. Thesis.

131. C. Cordier, M. Gruselle, G. Jaouen, V.I. Bakhmutov, M.V. Galakhov, L.L.

Troitskaya and V.I. Sokolov, Organometallics, 1991, 10, 2303.

132. M.V. Galakhov, V.I. Bakhmutov, I.V. Barinov and O.A. Reutov, J. Organomet. Chem., 1991, 421, 65.

133. M.F. D'Agostino, C.S. Frampton and M.J. McGlinchey, Organometallics, 1990, 9, 2972.

134. M.F. D'Agostino, C.S. Frampton and M.J. McGlinchey, J. Organomet. Chem., 1990, 394, 145.

135. H.B. Bürgi and J.D. Dunitz, Accts. Chem. Res., 1983, 16, 153.

136. R.H. Crabtree and M. Lavin, Inorg. Chem., 1986, 25, 805.

137. P.W. Sutton and L.F. Dahl, J. Am. Chem. Soc., 1967, 89, 261.

138. M.J. Chetcuti, P.A.M. Chetcuti, J.C. Jeffery, R.M. Mills, P.Mitrprachachon, S.J. Pickering, F.G.A. Stone, and P. Woodward., J. Am. Chem. Soc., Dalton Trans., 1982, 699.

139. H. Beurich, H. Vahrenkamp, Chem. Ber., 1982, 115, 2385.

140. L. Busetto, J.C. Jeffery, R.M. Mills, F.G.A. Stone, M.J. Went and P. Woodward, J. Chem. Soc., Dalton Trans., 1983, 101.

141. A.A. Aitchison, L.J. Farrugia, Organometallics, 1987, 6, 819.

142. J.F. Blount, P. Finocchiaro, D. Gust and K. Mislow, J. Am. Chem. Soc., 1973, 95, 7019. (b) J.D. Andose and K. Mislow, J. Am. Chem. Soc., 1974, 96, 2168.

143. K.A. Sutin, L. Li, C.S. Frampton, B.G. Sayer and M.J. McGlinchey,

Organometallics 1991, 10, 2362.

144. CHEM-X, developed and distributed by Chemical Design Ltd., Oxford, U.K.

145. When one of the alkyne substituents is inherently chiral, such as a terpenoid or steroidal group, then the four carbonyl ligands will always yield four ^{13}CO resonances even when all fluxional processes are rapid. At lower temperatures, one sees four ^{13}CO absorptions for each diastereomer. For some recent examples, see: (a) C. Cordier, M. Gruselle, G. Jaouen, V.I. Bakhmutov, M.V. Galakhov, L.L. Troitskaya and V.I. Sokolov, Organometallics, 1991, 10, 2303. (b) S. Tondu, M.F. D'Agostino, K.L. Malisza, G. Jaouen and M.J. McGlinchey, Can. J. Chem., 1992 in press.

146. J.E. Baldwin, J. Chem. Soc., Chem. Comm., 1976,734.

147. E. Bye, W.B. Schweizer and J.D. Dunitz, J. Am. Chem. Soc., 1982, 104, 5893.

148. K. Wade, in B.F.G. Johnson Editor, "Transition Metal Clusters", Wiley-Interscience, New York, 1980, pp. 193-264.

149. D.M.P. Mingos, Adv. Organometal. Chem., 1977, 15, 1.

150. M.J. McGlinchey, M. Mlekuz, P. Bougeard, B.G. Sayer, A. Marinetti, J-Y. Saillard, G. Jaouen, Can. J. Chem., 1983, 61, 1319, and references therein.

151. S.F. Xiang, A.A. Bakke, H.W. Chen, C.J. Eyermann, J.L. Hoskins, T.H. Lee, D. Seyferth, H.P. Withers, W.L. Jolly, Organometallics, 1982, 1, 699.

152. B.E.R. Schilling, R. Hoffmann, D.L. Lichtenberger, J. Am. Chem. Soc.,

1979, 101, 585.

153. O.J. Scherer, H. Sitzmann, G. Wolmershauser, J. Organomet. Chem., 1986, 268, C9.

154. P.J. Sullivan, A.L. Rheingold, Organometallics, 1982, 1, 1547.

155. M.D. Curtis, W.M. Butler, J. Chem. Soc., Chem. Comm., 1980, 998.

156. C.P. Gibson, J. Huang, L.F. Dahl, Organometallics, 1986, 5, 1676.

157. R. Blumhofer, K. Fischer, H. Vahrenkamp, Chem. Ber., 1986, 119, 194.

158. M.R. Churchill, C. Bueno, J.P. Hutchinson, Inorg. Chem., 1982, 21, 1359.

159. M.J. McGlinchey, Inorg. Chem., 1980, 19, 1392.

160. P.A. Agaskar and F.A. Cotton, Polyhedron, 1986, 5, 899.

161. T.A. Blatchford, M.H. Chisholm and J.C. Huffman, Polyhedron, 1987, 6, 1677.

162. M.J. McGlinchey, R.C. Burns, R. Hofer, S. Top and G. Jaouen, Organometallics, 1986, 5, 104.

163. D.J. Cram and F.A. Abd Elhafez, J. Am. Chem. Soc., 1952, 74, 5828.

164. (a) J.P. Battioni, W. Chodkiewicz and P. Cadiot, C.R. Acad. Sci., 1967, 264,991. (b) J.P. Battioni, M.-L. Chapman and W. Chodkiewicz, Bull. Soc. Chim. France., 1969, 976.

165. J.P. Battioni and W. Chodkiewicz, Bull. Soc. Chim. France., 1969, 981.

166. M. Cherest, H. Felkin and N. Prudent, Tetrahedron Lett., 1968, 2201.

167. Nguyen Trong Anh and O. Eisenstein, Nouveau J. Chim., 1977, 1, 61.

168. K.M. Nicholas, Acc. Chem. Res., 1986, 20, 207.

169. M.F. D'Agostino and M.J. McGlinchey, Polyhedron, 1988, 7, 807.

170. S.L. Schreiber, M.T. Klimas and S. Sammakia, J. Am. Chem. Soc., 1987, 109, 5749.

171. K.M. Nicholas and J. Siegel, J. Am. Chem. Soc., 1985, 107, 4999.

172. (a) A. Agarwal, J.A. Barnes, J.L. Fletcher, M.J. McGlinchey and B.G. Sayer, Can. J. Chem., 1977, 55, 2575. (b) A. Agarwal and M.J. McGlinchey, Can. J. Chem., 1978, 56, 959.

173. D.H. Bradley, M.A. Kahn and K.M. Nicholas, Organometallics, 1992, 11, 2598.

174. K. Mislow, Chemtracts—Organic Chemistry, 1989, 2, 151.

175. (a) K. Mislow, D. Gust, P. Finocchiaro and R.J. Boettcher, Top. Curr. Chem., 1973, 47, 1. (b) R. Willem, M. Gielen, C. Hoogzand and H. Pepermans, Adv. Dynamic Stereochem., 1985, 1, 207. (c) K. Mislow, Acc. Chem. Res., 1980, 9, 26. (d) R. Glaser, J.F. Blount and K. Mislow, J. Am. Chem. Soc., 1980, 102, 2777.

176. (a) H. Iwamura and K. Mislow, Acc. Chem. Res., 1988, 21, 175. (b) J.M. Chance, J.H. Geiger and K. Mislow, J. Am. Chem. Soc., 1989, 111, 2326.

177. (a) D.J. Iverson, G. Hunter, J.F. Blount, J.R. Damewood Jr. and K. Mislow, J. Am. Chem. Soc., 1981, 103, 6073. (b) D. Astruc and B. Gloaguen,J. Am. Chem. Soc., 1990, 112, 4607. (c) L. Li, A. Decken, B.G. Sayer, M.J.

McGlinchey, P. Brégaint, J.-R. Hamon, C. Lapinte and L. Toupet, submitted for publication.

178. (a) B. Mailvaganam, C.S. Frampton, B.G. Sayer, S. Top and M.J. McGlinchey, J. Am. Chem. Soc., 1991, 113, 1177. (b) M. Nambu and J.S. Siegel, J. Am. Chem. Soc., 1988, 110, 3675.

179. O.T. Beachley Jr., T.L. Royster Jr., W.J. Youngs, E.A. Zarate and C.A. Tessier-Youngs, Organometallics, 1989, 8, 1679.

180. B. Mailvaganam, B.E McCarry, B.G Sayer, R.E. Perrier, R. Faggiani and M.J. McGlinchey, J. Organomet. Chem., 1987, 335, 213.

181. B. Mailvaganam, B.G Sayer and M.J. McGlinchey, J. Organomet. Chem., 1990, 395, 177.

182. D. Gust and A. Patton, J. Am. Chem. Soc., 1978, 100, 8175.

183. R.J. Boettcher, D. Gust and K. Mislow, J. Am. Chem. Soc., 1973, 95, 7157.

184. J.K.M. Sanders and B.K. Hunter, "Modern NMR Spectroscopy", Oxford University Press, Oxford, U.K., 1987, pp 299-302.

185. ALCHEMY: available from Tripos Associates, St. Louis, Missouri.

186. PCMODEL: available from Dr. K. Gilbert, Serena Software, Bloomington, Indiana.

187. We must, however, remind ourselves that steric barriers derived from rigid models (be they plastic, metallic or merely computer images) can seriously overestimate the energy requirements associated with a particular

conformation. Molecules are capable of surprising flexibility!

188. M.J. McGlinchey, Adv. Organomet. Chem., 1992, 34, 285.

189. (a) G.K.S. Prakash, S. Keyaniyan, R. Aniszfeld, L. Heiliger, G.A. Olah, R.C. Stevens, H.-K. Choi and R. Bau, J. Am. Chem. Soc., 1987, 109, 5123. (b) K. Suwińska, G.J. Palenik and R. Gerdil, Acta Cryst., 1986, C42, 615. (c) C. Glidewell and D.C. Liles, Acta Cryst., 1978, B34, 124. (d) E.V. Chuprunov, T.N. Tarkhova, T.Yu Korallova, M.A. Simonov and N.V. Belov, J. Struct. Chem., 1981, 22, 305. (e) M. Porchia, N. Brianese, U. Casellato, F. Ossola, G. Rossetto, P. Zanella and R. Graziani, J. Chem. Soc., Dalton Trans., 1989, 677. (f) B. Stensland and P. Kierkegaard, Acta Chem. Scand., 1970, 24, 211. (g) A.I. Gusev, M.G. Los, S.D. Vlasenko, V.I. Zhun and V.D. Sheludyakov, J. Struct. Chem., 1984, 25, 154.

190. (a) D. Gust and K. Mislow, J. Am. Chem. Soc., 1973, 95, 1535. (b) J.F. Blount, P. Finocchiaro, D. Gust and K. Mislow, J. Am. Chem. Soc., 1973, 95, 7019. (c) J.D. Andose and K. Mislow, J. Am. Chem. Soc., 1974, 96, 2168.

191. M.J.Sabacky, S.M. Johnson, J.C. Martin and I.C. Paul, J. Am. Chem. Soc., 1973, 95, 7542.

192. (a) P.G. Jones, G.M. Sheldrick, M.R. Edwards and A.J. Kirby, Acta Cryst., 1986, C42, 1361. (b) C. Glidewell and D.C. Liles, Acta Cryst., 1978, B34, 696. (c) H. Hope, M.M. Olmstead, P.P. Power, J. Sandell and X. Xu, J.

Am. Chem. Soc., 1985, 107, 4337.

193. (a) D. Seyferth, J.S. Merola and J.S. Eschbach, J. Am. Chem. Soc., 1978, 100, 4124. (b) T.A. Albright, R. Hoffmann and P. Hofmann, Chem. Ber., 1978, 111, 1591.

194. P.A. Downton, B.G. Sayer and M.J. McGlinchey, Organometallics, accepted for publication.

195. A.H. Gomes de Mesquita, C.H. MacGillavry and K. Eriks, Acta Cryst., 1965, 18, 437.

196. G.A. Olah and S.H. Yu, J. Org. Chem., 1976, 41, 1694.

197. (a) S. Lupon, M. Kapon, M. Cais and F.H. Herbstein, Angew. Chem., Int. Ed. Engl., 1972, 11, 1025. (b) U. Behrens, J. Organomet. Chem., 1979, 182, 89.

198. A. Meyer, D.J. McCabe and M.D. Curtis, Organometallics, 1987, 6, 1491.

199. M. Gruselle, C. Cordier, M. Salmain, H. El Amouri, C. Guérin, J. Vaissermann and G. Jaouen, Organometallics, 1990, 9, 2993.

200. P.D. Lickiss, J. Chem. Soc., Dalton Trans., 1992, 1333.

201. G.A. Olah, L. Heiliger, X.-Y. Li and G.K.S. Prakesh, J. Am. Chem. Soc., 1990, 112, 5991.

202. (a) J.B. Lambert and W.J. Schulz Jr., J. Am. Chem. Soc., 1983, 105, 1671. (b) J.B. Lambert, J.A. McConnell and W.J. Schulz Jr., J. Am. Chem. Soc., 1986, 108, 2482.

203. G.A. Olah and L. Field, Organometallics, 1982, 1, 1485.

204. Despite early claims, this system apparently does not yield a ferrocenyl-stabilized silicenium ion.[205]

205. (a) J.Y. Corey, D. Gust and K. Mislow, J. Organomet. Chem., 1975, 101, C7. (b) T.J. Barton, A.K. Hovland and C.R. Tully, J. Am. Chem. Soc., 1976, 98, 5695. (c) R.J.P. Corriu, F. Larcher and G. Royo, J. Organomet. Chem., 1976, 104, 293.

206. D.D. Perrin and D.R. Perrin, "Purification of Laboratory Chemicals", Pergamon Press, New York, 1980.

207. R. Hoffmann, J. Chem. Phys., 1963, 39, 1397.

208. R. Hoffmann and W.N.Lipscomb, J. Chem. Phys., 1962, 36, 2179 and 3489.

209. J.H. Ammeter, H.B. Burgi, J.C. Thibeault, and R. Hoffmann, J. Am. Chem. Soc., 1978, 100, 3686.

210. J.F. Halet, J.Y. Saillard, R. Lissillour, M.J. McGlinchey and G. Jaouen, Inorg. Chem., 1985, 24, 218.